

MODELLING AND CONTROL OF SUSTAINED
OSCILLATIONS IN THE CONTINUOUS EMULSION
POLYMERIZATION OF VINYL ACETATE

by
Mark James Pollock

A Thesis
Submitted to the School of Graduate Studies
in Partial Fulfilment of the Requirements
for the Degree
Doctor of Philosophy

McMaster University

© 1983

MODELLING AND CONTROL OF
SUSTAINED OSCILLATIONS IN THE
CONTINUOUS EMULSION POLYMERIZATION
OF VINYL ACETATE

To my wife, Fran
for her support and
encouragement

DOCTOR OF PHILOSOPHY
(Chemical Engineering)

McMaster University
Hamilton, Ontario

Title: Modelling and Control of Sustained Oscillations in the
Continuous Emulsion Polymerization of Vinyl Acetate

Author: Mark James Pollock, B.Eng. (McMaster University)

Supervisors: Dr. A. E. Hamielec, Dr. J. F. MacGregor

Number of Pages: xvii,258

ABSTRACT

The population balance model of Kiparissides (1978) for the continuous emulsion polymerization of vinyl acetate, has been extended to predict molecular weight moments and has been corrected for induction time and particle shrinkage due to density changes. The developed model was successfully able to simulate experimental results from Kiparissides (1978) and Greene et al. (1976) for the continuous emulsion polymerization of vinyl acetate. Application of the model to the batch data of Keung (1974) had reasonable success as well. The model was extended to the continuous emulsion polymerization of styrene which follows different nucleation kinetics and was able to predict the average conversions and particle diameters for the data of Brooks et al. (1978). Little success was achieved in predicting the small experimentally observed oscillations for the styrene system.

To eliminate the sustained property oscillations in the vinyl acetate system Linear-Quadratic stochastic optimal control theory was applied to the model. Due to extreme non-linearities inherent in the system, this approach was shown to be inadequate. Instead, the reaction system was redesigned to include a small continuous seeding reactor with monomer and water bypass. Model predictions indicated that the redesigned system eliminated the oscillations. Experimental testing of the redesigned system verified that a dramatic improvement in stability was possible. The redesigned reactor configuration was also shown to be more

flexible in controlling particle sizes and conversion through use of the ~~bypass~~.

A method for selecting the optimum sensors was developed. It was shown that the measurement combination providing the most information would be conversion (as currently available from an on-line density meter) and some measure of weight average molecular weight.

ACKNOWLEDGEMENTS

The author would like to thank the following people for their contributions:

His research directors, Drs. A. E. Hamielec and J. F. MacGregor for their direction, experience and encouragement throughout this work.

Ms. Stephanie Lowe for her patience in typing of this manuscript.

My wife, my parents and my wife's parents for their moral support and encouragement during this work.

Finally, I wish to thank the Department of Chemical Engineering and NSERC for their financial support during this research.



TABLE OF CONTENTS

	<u>Page</u>
DESCRIPTIVE NOTE	ii
ABSTRACT	iii
ACKNOWLEDGEMENTS	v
TABLE OF CONTENTS	vi
LIST OF FIGURES	xi
LIST OF TABLES	xv
CHAPTER 1: INTRODUCTION	1
CHAPTER 2: OVERVIEW OF EMULSION POLYMERIZATION THEORY	4
2.1 Introduction	4
2.2 Physical Picture	5
2.3 Emulsion Polymerization Mechanism	7
2.4 Smith-Ewart Theory	10
2.4.1 Stage I	10
2.4.2 Stage II	13
2.4.3 Modified Smith-Ewart Theory	16
2.5 Nucleation Mechanisms	18
2.6 Overall Kinetic Picture for Particle Size Development	20
2.7 Overall Kinetic Picture for Molecular Weight Development	22
CHAPTER 3: MATHEMATICAL MODELLING OF CONTINUOUS EMULSION POLYMERIZATION REACTORS	25
3.1 Introduction	25
3.2 Dynamic Phenomena in Emulsion Polymerization CSTR's	27




TABLE OF CONTENTS (CONT.)

	<u>Page</u>
3.3 Modelling of Continuous Reactors	28
3.4 Model Development for Vinyl Acetate	30
3.4.1 Balances for Initiator, Emulsifier, Monomer and Oligomeric Radicals	31
3.4.2 General Property Balances	37
3.4.3 Particle Size Development	40
3.4.4 Molecular Weight Development	47
3.4.5 Summary of Model Equations	54
3.5 Model Applications	57
3.5.1 Parameter Estimation for PSD States	57
3.5.2 Off-Line Prediction of Particle Size Distribution	65
3.5.3 Batch Reactor Operation	69
3.5.4 Reactor Start-up and Multiple Seed Reactors	75
3.6 Extension of Model to Styrene Kinetics	79
3.6.1 Introduction	79
3.6.2 Styrene CSTR Modelling	79
3.6.3 Styrene Model Development	80
3.6.4 Simulation Results for Styrene	85
CHAPTER 4: APPLICATION OF ADVANCED CONTROL THEORY TO CONTINUOUS EMULSION POLYMERIZATION	93
4.1 Introduction	93
4.2 Control of Polymerization Reactors	95
4.2.1 Batch Reactor Control	95
4.2.2 Control of Continuous Polymerization Reactors	98

6

TABLE OF CONTENTS (CONT.)

	<u>Page</u>
4.3 Application of Linear Quadratic Optimal Stochastic Control Theory	101
4.3.1 Introduction	101
4.3.2 Model Linearization and Discretization	102
4.3.3 State Estimation by Kalman Filtering	106
4.3.4 General Linear Quadratic Stochastic Optimal Control	108
4.3.5 Application of Theory to Vinyl Acetate Model	111
4.3.6 Summary	120
4.4 Simulation Results	120
4.5 Conclusions	134
CHAPTER 5: CHOICE OF OPTIMUM SENSORS	135
5.1 Introduction	135
5.2 Observability	138
5.3 Application of Kalman Filter Theory	139
5.4 Simulation Results	142
5.4.1 Individual Sensors	145
5.4.2 Sensor Combinations	151
5.4.3 Weight Average Molecular Weight Sensor	154
5.5 Conclusions	157
CHAPTER 6: REDESIGN OF LATEX REACTOR SYSTEM	159
6.1 Introduction	159
6.2 System Redesign	159
6.2.1 Problems and Goals	159
6.2.2 Literature Survey	161

TABLE OF CONTENTS (CONT.)

	<u>Page</u>
6.2.3 Reactor System Redesign for Vinyl Acetate Emulsion Polymerization	162
6.3 Simulation Results	164
6.3.1 Single CSTR vs. Redesigned System	164
6.3.2 Choice of Operating Conditions	172
6.3.3 Forced Oscillation for Broadening of PSD	188
6.4 Summary and Conclusions	193
CHAPTER 7: EXPERIMENTAL RESULTS	196
7.1 Introduction	196
7.2 Experimental Procedure	196
7.2.1 Materials	196
7.2.2 Reactor Layout	197
7.2.3 Experimental Procedure	202
7.3 Experimental Analysis	205
7.3.1 Conversion	205
7.3.2 Surface Tension	209
7.3.3 Weight Average Molecular Weight	211
7.4 Experimental Results	214
7.4.1 Control Runs	214
7.4.2 Molecular Weight Runs	224
7.5 Conclusions	229
CHAPTER 8: CONCLUSIONS AND FUTURE WORK	230
REFERENCES	234
APPENDIX 1: List of Symbols	247

TABLE OF CONTENTS (CONT.)

	<u>Page</u>
APPENDIX 2: Detailed Simulation Results	256
APPENDIX 3: Vinyl Acetate Parameter Values	257
APPENDIX 4: Styrene Parameter Values	258

LIST OF FIGURES

<u>Figure</u>	<u>Page</u>
2.1 - Harkins' (1947) View of Emulsion Polymerization Mechanism	9
3.1 - Graph of ϵ and δ' from Parameter Estimation versus Soap Concentration for Experiments of Kiparissides (1978)	60
3.2 - Graph of ϵ and δ' from Parameter Estimation versus Initiator Concentration for Experiments of Kiparissides (1978)	61
3.3 - Graph of Conversion X versus Dimensionless Time Showing Effect of Choice of D_w Parameter on Model Prediction	63
3.4 - Graph of Conversion X versus Dimensionless Time Showing Effect of Choice of ϵ Parameter on Model Prediction	64
3.5 - Graphs of Conversion X versus Dimensionless Time for Two Experiments of Kiparissides (1978) with $\theta = 30$ min. (Run 1: $[I] = .005$ mole/L, $[S] = .01$ mole/L; Run 2: $[I] = .01$ mole/L, $[S] = .06$ mole/L)	66
3.6 - Graphs of Conversion X versus Dimensionless Time for $\theta = 30$ minutes (Run 1: $[I] = .01$ mole/L $K_2S_2O_8$, $[S] = .01$ mole/L SLS, Kiparissides (1978); Run 2: $[I] = .01$ mole/L $(NH_4)_2SO_4$, $[S] = .01$ mole/L SLS, Greene, et al. (1976))	67
3.7 - Graph of Frequency f versus Particle Diameter Predicted from Model Showing Monodispersed PSD for First Particle Generation ($[I] = .01$ mole/L, $[S] = .01$ mole/L, $\theta = 30$ min., $t/\theta = 3.5$)	70
3.8 - Graph of Frequency f versus Particle Diameter Predicted from Model Showing Bimodal PSD after Second Particle Generation ($[I] = .01$ mole/L, $[S] = .01$ mole/L, $\theta = 30$ min., $t/\theta = 4.9$)	71
3.9 - Graph of Conversion X versus Time for Batch Model and Experimental Data of Keung (1979) ($[S] = 12$ gm/L SLS, $[I] = 3.33 \times 10^{-3}$ mole/L $K_2S_2O_8$)	74
4.1 - Reactor Control Scheme for Application of LQ Stochastic Optimal Control Theory	116
4.2 - Flowsheet for Application of LQ Stochastic Sub-Optimal Control	121
4.3 - LQ Control. Graph of	
A. Conversion	123
B. Number of Particles	124

LIST OF FIGURES (CONT.)

<u>Figure</u>	<u>Page</u>
C. Initiator and Emulsifier Concentrations versus Dimensionless Time for $r_I = 20,000$, $r_S = 2,000$ ($[I]_d = .01$ mole/L, $[S]_d = .01$ mole/L, $\theta = 30$ min., $x_d = .45$)	125
4.4 - LQ Control. Graph of	
A. Conversion	126
B. Number of Particles	127
C. Initiator and Emulsifier Concentrations versus Dimensionless Time for $r_I = 10,000$, $r_S = 5,000$ ($[I]_d = .01$ mole/L, $[S]_d = .01$ mole/L, $\theta = 30$ min., $x_d = .45$)	128
4.5 - LQ Control. Graph of	
A. Conversion	129
B. Number of Particles	130
C. Initiator and Emulsifier Concentrations versus Dimensionless Time for $r_I = 10,000$, $r_S = 50,000$ ($[I]_d = .01$ mole/L, $[S]_d = .01$ mole/L, $\theta = 30$ min., $x_d = .45$)	131
4.6 - Graph of Conversion versus Dimensionless Time for Single Reactor With no Control Action Taken ($[I] = .01$ mole/L, $[S] = .01$ mole/L, $\theta = 30$ min.)	133
5.1 - Graph of Percent Change of	150
A. V_2' for Alternate Sensors Compared to V_2' for X_{10}	
B. V_1' for Alternate Sensors Compared to V_1' for X_{10}	
C. V_1' Compared to V_2' for Each Sensor versus Percent Model Error of the Particle Size States	
5.1 - Comparison of Base Case Reactor Configuration with Redesigned Reactor Configuration	165
6.2 - Graph of	
A. Conversion X and Number of Particles N_p	168
B. Average Number of Branch Points per Polymer Molecule B_N , and Number Average Particle Diameter D_p versus Time for Base Case Operation	169
6.3 - Graph of	
A. Conversion X and Number of Particles N_p	170
B. Average Number of Branch Points per Polymer Molecule B_N , and Number Average Particle Diameter D_p versus Time for Redesigned Reactor Configuration	171

LIST OF FIGURES (CONT.)

<u>Figure</u>	<u>Page</u>
6.4 - Conversion X versus $[I]_w$ and Split for $V_1 = 75$ mL., $[S]_T = .01$ mole/L	175
6.5 - Conversion X versus $[I]_w$ and Split for $V_1 = 150$ mL., $[S]_T = .01$ mole/L	176
6.6 - Conversion X versus $[I]_w$ and Split for $V_1 = 225$ mL., $[S]_T = .01$ mole/L	177
6.7 - Particle Diameter D_p versus $[I]_w$ and Split for $V_1 = 75$ mL., $[S]_T = .01$ mole/L	178
6.8 - Particle Diameter D_p versus $[I]_w$ and Split for $V_1 = 150$ mL., $[S]_T = .01$ mole/L	179
6.9 - Particle Diameter D_p versus $[I]_w$ and Split for $V_1 = 225$ mL., $[S]_T = .01$ mole/L	180
6.10 - Number Average Molecular Weight M_n versus $[I]_w$ and Split for $V_1 = 75$ mL., $[S]_T = .01$ mole/L	181
6.11 - Number Average Molecular Weight M_n versus $[I]_w$ and Split for $V_1 = 150$ mL., $[S]_T = .01$ mole/L	182
6.12 - Number Average Molecular Weight M_n versus $[I]_w$ and Split for $V_1 = 225$ mL., $[S]_T = .01$ mole/L	183
6.13 - Number of Particles N_p versus $[I]_w$ and Split for $V_1 = 75$ mL., $[S]_T = .01$ mole/L	184
6.14 - Number of Particles N_p versus $[I]_w$ and Split for $V_1 = 150$ mL., $[S]_T = .01$ mole/L	185
6.15 - Number of Particles N_p versus $[I]_w$ and Split for $V_1 = 225$ mL., $[S]_T = .01$ mole/L	186
6.16 - Graph of Number Average Diameter D_p versus Dimensionless Time (t/θ_2) Showing Controlled Oscillations for Distribution Broadening	191
7.1 - Experimental Reactor System	198
7.2 - Graph of Density from Anton-Paar Digital Density Meter versus Conversion as Determined Theoretically and by Comparison to Off-Line Gravimetrically Determined Conversions	208

LIST OF FIGURES (CONT.)

<u>Figure</u>	<u>Page</u>
7.3 - Graph of Surface Tension versus Surfactant Concentration (SLS) for Literature Values (Brady (1949)) and Experimental Data from Madison-Kipp Surface Tension Meter	210
7.4 - Graph of Surface Tension γ versus Time for Run A at T = 50°C, θ = 30 min. (single reactor then two reactors)	217
7.5 - Graph of Surface Tension γ versus Time for Run B at T = 50°C, θ = 30 min. (single reactor then two reactors)	218
7.6 - Graph of Surface Tension γ versus Time for Run C at T = 50°C, θ = 30 min. (two reactors then single reactor)	219
7.7 - Graph of Density ρ (or Conversion X) versus Time for Run A at T = 50°C, θ = 30 min. (single reactor then two reactors)	220
7.8 - Graph of Density ρ (or Conversion X) versus Time for Run B at T = 50°C, θ = 30 min. (single reactor then two reactors)	221
7.9 - Graph of Density ρ (or Conversion X) versus Time for Run C at T = 50°C, θ = 30 min. (two reactors then single reactor)	222
7.10 - Experimental Illustration of Catastrophic Agglomeration	227

LIST OF TABLES

<u>Table</u>	<u>Page</u>
3.1 - Parameter Estimates from UWHAUS for Best Fit of Model to Data of Kiparissides (1978)	59
3.2 - Values of δ' and ϵ Estimated Using UWHAUS for Fitting of Model to Batch Data of Keung (1974)	75
3.3 - Simulation Results from Reactor Startup Studies	78
3.4 - Simulation Predictions for Styrene Model as Compared to Data from Brooks, et al. (1978)	87
3.5 - Comparison of Predicted Diameters from the Model Versus Experimental Diameters (Brooks, et al. (1978))	88
3.6 - Results from Simplified Styrene Model Using Particle Volume Only	91
4.1 - Final Linearized Version of the Model	118
4.2 - Penalty Matrix Values for Control Simulations	122
5.1 - Summary of Steady-State Product Property Values for Various Operating Conditions (Seed Reactor Present)	143
5.2 - V_1' , V_2' Criteria for A) 5%, B) 10%, and C) 20% Error in States for $[I] = .01$ M/L, $[S] = .01$ M/L, Split = .2	146, 147
5.3 - V_1' , V_2' Criteria for 10% State Error for $[I] = .01$ M/L, $[S] = .01$ M/L, Split = .6	147
5.4 - V_1' , V_2' Criteria for 10% State Error for $[I] = .02$ M/L, $[S] = .01$ M/L, Split = .2	148
5.5 - V_1' , V_2' Criteria for 10% State Error for $[I] = .01$ M/L, $[S] = .02$ M/L, Split = .2	148
5.6 - V_1' , V_2' Criteria for 10% Particle Size State Error for $[I] = .01$ M/L, $[S] = .01$ M/L, Split = .2 for Various Sensor Combinations	152
5.7 - V_1' , V_2' for 10% Particle Size State Error for $[I] = .01$ M/L, $[S] = .01$ M/L, Split = .2 for Molecular Weight Sensor and Sensor Combinations	155

LIST OF TABLES (CONT.)

<u>Table</u>	<u>Page</u>
6.1 - Comparison of Polymer Latex Properties of the Product for a Single CSTR (Base Case) Versus the New Reactor Configuration (Case I and Case II) where I = Potassium Persulphate and S = Sodium Lauryl Sulphate	166
6.2 - Effects of Parameter Changes on Properties as Predicted by the Model	174
6.3 - Comparison of Polymer Latex Properties from Reactor 2 when Using Different Bypass Percentages as Control Variable	187
6.4 - Simulation Results from Square Wave Variation of Split Parameter	190
7.1 - Conversion Data from Two Runs for Use in Molecular Weight Parameter Estimation	204

CHAPTER 1
INTRODUCTION

This Chapter is intended as a guide to the various topics covered by this thesis. The ultimate objective of this work was the modelling of the continuous emulsion polymerization of vinyl acetate to better understand the phenomenon of sustained property oscillations, and the subsequent use of the dynamic model to develop a stable continuous emulsion polymerization reactor system.

Continuous reactors for use in emulsion polymerization have several advantages compared to batch or semi-batch operations. High reaction rates and high molecular weight polymers can be produced at a good yield providing latexes which in many cases can be applied directly as produced. Easier operation and control, lower maintenance, consistent product quality and high throughput provide reasons for increasing interest in continuous emulsion polymerizations industrially.

One major barrier to continuous emulsion polymerization systems, however, is the phenomenon of sustained property oscillations leading to reduced product quality. A true steady-state is never achieved due to the nucleation mechanism involved in emulsion kinetics. Explosive generations of new particles can lead to inadequate coverage of the surface of the polymer particles which could result in agglomeration and fouling. Excursions to high conversion during the

oscillations can also cause excessive branching and crosslinking giving poor performance properties of the latex. For these reasons there is a great deal of interest in means of controlling the property oscillations for the continuous reactor system.

To examine and eliminate the oscillating behavior of these continuous systems, this thesis is divided into several sections.

In Chapter 2, the general mechanism of emulsion polymerization is discussed. The basic theory of emulsion polymerization kinetics is introduced and the kinetic framework for development of the particle size distribution (PSD) and molecular weight distribution (MWD) is presented.

In Chapter 3, the detailed model for the continuous emulsion polymerization of vinyl acetate is developed based on a population balance approach. The model is then applied to various problems such as off-line PSD prediction, batch reactor modelling and reactor startups to illustrate its general applicability. A final section of the chapter attempts to extend the model to styrene emulsion polymerization which follows a different kinetic scheme.

In Chapter 4 a review of past approaches to control of polymerization reactors is made. In an attempt to verify and extend the control scheme of Kiparissides (1978), linear quadratic stochastic optimal control theory was applied to the full model, and simulations of these control results are presented. Several problems with this technique caused inadequate control using this approach for the continuous emulsion polymerization of vinyl acetate.

In Chapter 5, the use of state estimation techniques for the determination of optimal sensors or sensor combinations is discussed.

In Chapter 6, the developed model was used to redesign a reactor system to eliminate the sustained oscillation phenomenon. Use of a small seed reactor with bypass provided an excellent means of controlling the latex properties.

In Chapter 7, experimental results are presented comparing the original single CSTR with sustained oscillations present, with the redesigned reactor configuration exhibiting stable operation. On-line sensor problems and attempts at obtaining kinetic parameter estimates for the molecular weight section of the model are discussed.

Chapter 8 presents the overall conclusions of this work and possible directions to be followed by future researchers.



CHAPTER 2

OVERVIEW OF EMULSION POLYMERIZATION THEORY

2.1 INTRODUCTION

Emulsion polymerization has advantages over processes such as solution and bulk polymerization. Larger heat transfer coefficients can be obtained due to lower suspension viscosity and often higher molecular weight polymer can be produced at a higher rate. Many products such as paints and adhesives employ the latex product from emulsion polymerization directly. For these reasons, emulsion polymerization has become a multi-billion dollar operation in terms of sales. In spite of the industrial impact of emulsion polymerization the complex kinetics involved in emulsion polymerization as opposed to other polymerization processes such as bulk or suspension has caused difficulty in elucidating the main mechanisms involved in the process. In the sections which follow some of the early schemes will be discussed to give an overall background as well as some of the steps considered for the model used in this thesis.

2.2 PHYSICAL PICTURE

There are four main ingredients necessary for any emulsion polymerization recipe. These are the dispersion medium, monomer, soap and initiator. The object is to convert relatively large monomer droplets which are suspended in the dispersion medium to a stable latex consisting of submicron polymer particles suspended in the dispersion medium.

A typical emulsion recipe consists of 100 parts dispersion medium, 50 parts monomer, 2 parts emulsifier and .1 part initiator. The dispersion medium typically used is water, and the monomer should be only partially soluble in the water phase. The large quantity of water phase serves to reduce the viscosity of the polymer particle suspension permitting better mixing and larger heat transfer coefficients.

For ideal emulsion polymerization, the initiator is soluble only in the continuous phase and not in the monomer droplets or polymer particles. As a result, the generation of initiator radicals takes place exclusively in the water phase. If the temperature is high enough (50°C or higher) chemical initiators such as the persulfates are used without activators. However, for polymerization at low temperatures (as in cold SBR production at 5°C) the use of redox initiation systems is required to generate radicals at a suitable rate.

Emulsifiers consist of molecules which are long chain hydrophobes with a hydrophilic end. The hydrophobe is usually a long-chain hydrocarbon while the hydrophilic end is typically a sulfate end group or the salt of a carboxylic acid. Typical emulsifiers are the sodium n-alkyl sulfates such as sodium lauryl sulfate or sodium or potassium salts of lauric acid or palmitic acid. The emulsifier plays several major roles in this system. It is first used to stabilize the monomer droplets dispersed in the aqueous phase. Secondly, the emulsifier molecules form aggregates with the hydrophobic ends pointed towards the center of the aggregate or middle when the concentration of emulsifier exceeds its solubility in water (a concentration called the critical micelle concentration, or CMC). These micelles are believed to be an integral part of the formation mechanism for new polymer particles, and the interior of these micelles also serve to solubilize a certain amount of monomer in the micellar interior. Lastly, the emulsifier is used to stabilize the polymer particles that are produced and so prevent coagulation of the latex. At any time, there will also be a small amount of free emulsifier molecules dissolved in the aqueous phase.

From the above discussion, the monomer can be seen to be present in several loci as well. The majority of the monomer at the beginning (typically 95%) is present as 1-10 μ droplets stabilized by emulsifier molecules. Also, due to solubilization, a smaller fraction of monomer is present in the interior of micelles. Finally, a small

portion of monomer is also present as an actual solution in the aqueous phase due to partial solubility of the monomer in water.

In the next few sections, various models presented to describe the behavior of an emulsion polymerization system will be discussed.

2.3 EMULSION POLYMERIZATION MECHANISM

Harkins (1947) proposed the first mechanism for emulsion polymerization systems. His assumptions were as follows:

- i) Free radicals are produced in the aqueous phase and captured by emulsifier micelles. The solubilized monomer in the "stung" micelle starts to polymerize and the micelle then becomes a polymer particle. The micelle is thus the principal component for the nucleation of polymer particles.
- ii) The majority of polymerization takes place in the monomer-swollen polymer particles due to the much larger surface area of polymer particles and micelles as compared to the monomer droplets (i.e. monomer droplets capture a negligible fraction of radicals from the water phase).
- iii) The monomer drops serve as reservoirs from which monomer diffuses through the aqueous phase into the growing polymer particles.
- iv) When all micelles disappear, further formation of new polymer particles ceases.

- v) Instantaneous termination when a radical enters a particle already containing one radical.

With these assumptions, a batch emulsion polymerization could be broken up into three stages, as shown in Fig. 2.1.

In Stage I (which is the principal particle formation stage) monomer drops, micelles and polymer particles are all present. During this stage the micelles are stung to start new particles, and also dissolve to stabilize the already existing polymer particles. At the end of Stage I, all micelles have disappeared by one of these mechanisms and all new particle formation ceases. The final number of particles produced is typically 10^{16} to 10^{18} particles per liter of latex.

During Stage II, monomer drops and polymer particles are both present. The monomer drops serve as reservoirs and the already existing polymer particles continue to grow as monomer diffuses from the drops to the particles. Usually an equilibrium is assumed such that the particles are considered saturated with monomer as long as monomer drops are still present. At the end of Stage II, the monomer droplets disappear and the residual monomer is now located in the polymer particles. This occurs at a conversion called the critical conversion x_c and is dependent on the solubility of the monomer in the polymer phase.

During Stage III, only polymer particles are present. The concentration of monomer in the polymer phase decreases steadily as conversion increases during this stage.

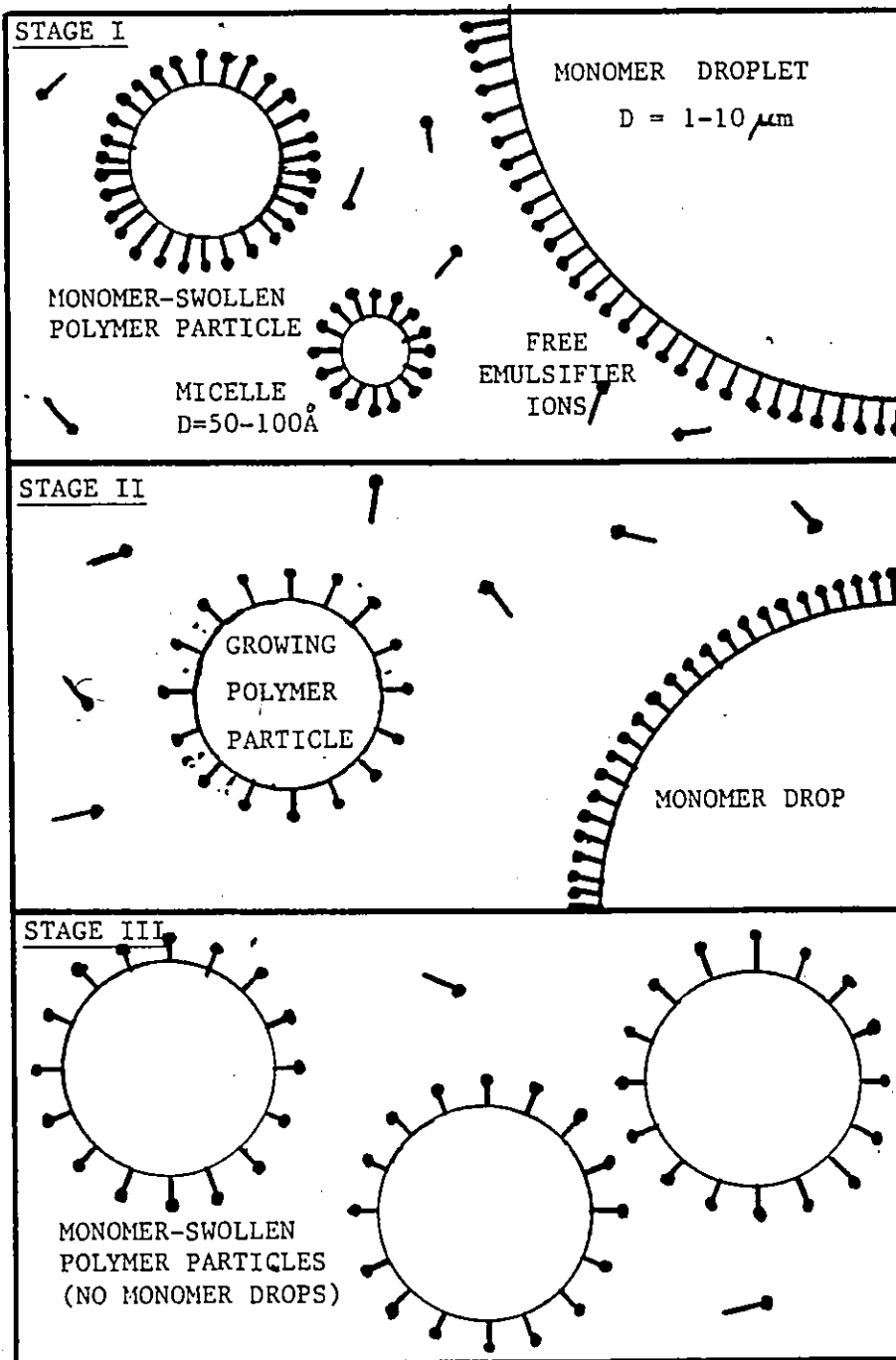


FIGURE 2.1⁶- Harkin's (1947) View of Emulsion Polymerization Mechanism

With this qualitative picture, it is worth noting that total surface area is increasing during Stage I and II due to new particle formation and polymer particle growth respectively. In Stage III, the total surface area actually decreases because of polymer particle shrinkage as conversion increases due to the density difference between monomer and polymer.

Many of the early theories which will now be discussed were based on this simple qualitative picture.

2.4 SMITH-EWART THEORY

In Stage I, the primary problem is the determination of the number of particles produced. Once all particles are formed by the end of Stage I, the primary problem becomes the determination of the average number of radicals per polymer particle. Smith-Ewart theory (1948) used the qualitative picture of Harkins (1947) to attempt to quantitatively solve for the number of particles formed and for the average number of radicals per polymer particle.

2.4.1 STAGE I

To calculate the number of particles, two limits are proposed. The upper limit for the number of particles is found by assuming only micelles capture free radicals, while the lower limit assumes that polymer particles and micelles capture free radicals in proportion to their areas. The radical capture rate proportional to area corresponds to the use of collision theory for this limit. The actual

number produced will lie somewhere between these limits since if diffusion theory is applied instead of collision theory, a unit of area in the micelles will be more effective in capturing free radicals than a unit of area on the polymer particles due to the difference in radius. This will produce more particles than shown in the lower limit but fewer than if only micelles can capture free radicals as found by the upper limit.

UPPER LIMIT

In this case, particle generation is directly proportional to radical generation by initiation, with all free radicals being captured by the soap micelles. This leads to:

$$\frac{dN_p}{dt} = \rho_i \quad (2.1)$$

where ρ_i is the radical generation rate by initiation. In its integrated form this becomes:

$$N_p = \rho_i t_f \quad (2.2)$$

where t_f is the time when all micelles disappear. This occurs when the area of the polymer particles formed A_p is equal to the area the soap can cover $a_s[S]$ where a_s is the area covered by an emulsifier molecule and $[S]$ is the soap concentration in the system.

By assuming Case II kinetics, where the volumetric growth rate is constant for all particles, the Smith-Ewart theory provided the final result:

$$N_p = .53 \left(\frac{\rho_i}{\mu} \right)^{2/5} (a_S [S])^{3/5} \quad (2.3)$$

where μ is the volume growth rate for particles. This is the upper limit on the number of polymer particles produced for a given soap and initiator concentration.

LOWER LIMIT

To achieve the lower limit, it was assumed that the rate of generation of new particles was given by the total free radical initiation rate less those free radicals captured by already existing polymer particles, where the polymer particle capture rate is based on area (hence collision theory). This led to the following expression:

$$\frac{dN_p}{dt} = \rho_i - \rho_i \frac{A_p}{A_{TOTAL}} = \rho_i \left(1 - \frac{A_p}{a_S [S]} \right) \quad (2.4)$$

In order to integrate this expression, the area of particles was calculated as:

$$A_p = \beta \int_0^t (t-t_0)^{2/3} \frac{\partial N_p}{\partial t_0} dt_0 \quad (2.5)$$

$$\beta = [(4\pi)^{1/2} 3\mu]^{2/3} \quad (2.6)$$

where β represents the area growth rate based on the constant volume growth rate μ .

By substituting (2.5) into (2.4) and integrating the resulting expression by use of infinite series expansions, Smith-Ewart theory results in the following expression for the lower limit on the number of particles:

$$N_p = .37 \left(\frac{\rho_i}{\mu} \right)^{2/5} (a_S[S])^{3/5} \quad (2.7)$$

Both the upper and lower limit have the same functional dependence and the number of particles will thus be given by:

$$N_p = K \left(\frac{\rho_i}{\mu} \right)^{2/5} (a_S[S])^{3/5} \quad (2.8)$$

where $.37 < K < .53$

This equation provides a range for the number of polymer particles produced at the end of Stage I provided that Case II kinetics apply.

2.4.2 STAGE II

In stage II, the main problem is to determine the number of radicals per polymer particle. The overall rate of polymerization is given by:

$$R_p = \frac{K_p [M]_p N_p \bar{q}}{N_A} \quad (2.9)$$

where $[M]_p$ is the concentration of monomer in the polymer phase, N_A is Avagadro's number, K_p is the propogation rate constant and \bar{q} is the average number of radicals per polymer particle which is to be determined.

By considering a steady-state balance of the number of particles containing q free radicals, Smith and Ewart (1947) obtained a recursion relationship:

$$\begin{aligned} N_{q-1} \left(\frac{\rho_A}{N} \right) + N_{q+1} k_{de} (q+1) + N_{q+2} k_{tp} \left(\frac{(q+2)(q+1)}{V} \right) \\ = N_q \left[\left(\frac{\rho_A}{N} \right) + k_{de} q + k_{tp} \left(\frac{q(q-1)}{V} \right) \right] \end{aligned} \quad (2.10)$$

where N is the total number of particles.

The terms on the left hand side represent the appearance of particles containing q free radicals by radical capture, desorption and termination while the terms on the right hand side represent disappearance by the same mechanisms of particles with q free radicals. In this equation, ρ_A is the radical capture rate, k_{de} is the desorption rate constant for the polymerization, and V is the volume of the particle. This expression can be applied to three different limiting cases:

CASE I: $\bar{q} \ll 1$ with monodispersed polymer particle size distribution

With this condition $N_0 \gg N_1 \gg N_q$ and the recursion relationship for $q=1$ becomes:

$$\rho_A \left(\frac{N_0}{N} \right) = \rho_A \left(\frac{N_1}{N} \right) + k_{de} N_1 \quad (2.11)$$

and since $N_0/N \approx 1$, $N_1/N \approx 0$ and $\bar{q} \approx N_1/N$ it is found that:

$$\rho_A \approx k_{de} N \bar{q} \quad (2.12)$$

Also by a steady state argument on the total free radicals, the rate of initiation equals the rate of termination. However, instantaneous termination implies the rate of termination will be the same as the rate of radical entry into a particle already containing one radical. Using this idea, the following expression results:

$$\rho_i = 2\rho_A \left(\frac{N_1}{N} \right) = 2\rho_A \bar{q} \quad (2.13)$$

which when combined with equation (2.12) yields

$$\bar{q} = \left(\frac{\rho_i}{2k_{de}N} \right)^{1/2} \quad (2.14)$$

This is the simplified expression for the number of radicals per particle with instantaneous termination when $\bar{q} \ll 1$.

CASE II: $\bar{q} = .5$

This case results if there is no desorption of radicals. With this assumption, and with instantaneous termination so that $N_2 = N_q$ (for $q > 2$) = 0, the recursion relationship becomes:

$$\rho_A \left(\frac{N_0}{N} \right) = \rho_A \left(\frac{N_1}{N} \right) \quad (2.15)$$

and hence $N_0 = N_1$ and $\bar{q} = N_1/(N_0 + N_1) = .5$. By a steady state total radical balance with this result, equation (2.13) also reduces to:

$$\rho_i = \rho_A \quad (2.16)$$

These results correspond to the Smith-Ewart theory as used for calculating the number of particles formed.

CASE III: $\bar{q} \gg 1$

This is the usual case where diffusion controlled termination becomes important, and hence instantaneous termination no longer holds. If desorption is neglected, then it can be shown that $\rho_i = \rho_A$ as in (2.16) and the governing equation becomes:

$$\bar{q} = \left(\frac{\rho_i V}{2k_t N} \right)^{1/2} \quad (2.17)$$

2.4.3 MODIFIED SMITH-EWART THEORY

The recursion relationship derived by Smith-Ewart (1947) was solved by Stockmayer (1957) and modified by O'Toole (1965). The analytical expression which results is:

$$N_q = a^q 2^{(b-1-3q)/2} \frac{I_{b+q-1}(a\sqrt{2}/2)}{q I_{b-1}(a)} \quad (2.18)$$

where $I_k(x)$ is the modified Bessel function of the first kind and:

$$a = \left(\frac{8 \rho_A V}{N k_{tp}} \right)^{1/2} \quad (2.19)$$

$$b = \left(\frac{k_{de} V}{k_{tp}} \right) \quad (2.20)$$

Hence, a expresses the ratio of absorption or radical production to termination and b is the ratio of desorption to termination.

By summing over all particles the following expressions were derived for this system:

$$\begin{aligned}
 \bar{q} &= \frac{\sum_{q=0}^{\infty} qN_q}{N} = \frac{1-b}{2} + \frac{a}{4} \frac{I_{b-2}(a)}{I_{b-1}(a)} ; \quad b \geq 1 \\
 &= \frac{a}{4} \frac{I_b(a)}{I_{b-1}(a)} ; \quad 0 < b \leq 1 \quad (2.21) \\
 &= \frac{a}{4} \frac{I_0(a)}{I_1(a)} ; \quad b = 0
 \end{aligned}$$

These equations thus specify the value of \bar{q} for various degrees of importance of desorption as given by b .

By assuming a steady-state balance on the number of radicals in the water phase, the following expression was obtained by Ugelstad, et al (1967) for a monodispersed PSD:

$$\rho_A = \rho_i + k_{de}N\bar{q} - 2k_{tw}[R\cdot]_w^2 \quad (2.22)$$

which could be coupled with equation (2.21) to provide a complete solution for this problem.

Gardon (1968) used an unsteady-state approach where a derivative term, dN_q/dt , was added to the recursion relationship (2.10) but the numerical solution to this yielded the same result as the Stockmayer (1957) solution, indicating that a steady-state treatment was valid.

Katz and Sidel (1969) approached the problem from a stochastic viewpoint by postulating probability distributions for a particle containing various size polymer molecules. By using equations for

change of moments, the molecular weight averages M_n and M_w are also available from their technique. They assume that only particles having 0 or 1 radical are present; hence, Smith-Ewart case II kinetics. In addition, it is assumed that: i) particles are of uniform size, ii) there is a constant N_p , iii) the particle density is constant, iv) there is a uniform distribution of materials in a particle, and v) it is an isothermal, batch polymerization.

One further problem for the original Smith-Ewart theory is provided by high conversion data. Gardon (1968) provided data showing deviations from Smith-Ewart theory at high conversion for different sized particles. Friis and Nuyhagen (1973) and Friis and Hamielec (1973) have shown that this is probably tied into the gel effect which occurs at high conversions, which is the result of diffusion-controlled termination in the particles. Models for this effect which are tied to the reduction of (K_{tp}) with conversion were developed by Friis and Hamielec (1976) for various polymerization systems.

2.5 NUCLEATION MECHANISMS

The Smith-Ewart theory (1948) was based on the Harkins (1947) qualitative view that particle nucleation is caused by absorption of free radicals into soap micelles, which will be called the micellar nucleation theory. However, experimentally Nomura et al (1978) have shown that polymerization can occur even in the absence of micelles, such as when the soap concentration is maintained below the CMC*. To

* CMC=Critical Micelle Concentration.

handle this result, a second theory of nucleation is also available in the literature, the homogeneous nucleation theory.

Roe (1968) and Fitch and Tsai (1971) have developed a nucleation system whereby particle generation depends on three processes as follows:

$$\frac{dN}{dt} = \rho_i - \rho_C - \rho_F \quad (2.23)$$

where ρ_i is radical initiation rate, ρ_C is radical capture rate by already existing polymer particles, ρ_F is the coalescence rate of polymer particles and desorption is ignored.

If the monomer is fairly soluble in the water phase such as vinyl acetate, it is possible that the radicals propagate in the water phase up to some critical chain length whereupon they precipitate and are stabilized by soap molecules to form a primary polymer particle. Fitch and Tsai (1971) used the collision theory where radical capture rate is proportional to area. Using this, the expression for free radical capture rate by polymer particles became:

$$\rho_C = \rho_i L \left(\frac{A_p}{4} \right) \quad (2.24)$$

where L is the Einstein diffusion length given by:

$$L = \frac{2 D_w}{k_p} \left(\frac{DP_{max}}{MW} \right)^{1/2} \quad (2.25)$$

The L and D_w are for each size oligomer and since the oligomers are continually growing, an average value of D_w and L are used. This then is substituted in equation (2.23) with the assumption of little coalescence or agglomeration to yield:

$$\frac{dN}{dt} = \rho_i \left(1 - \frac{LA_p}{4} \right) \quad (2.26)$$

which is similar to equation 2.4 supplied by Smith-Ewart theory.

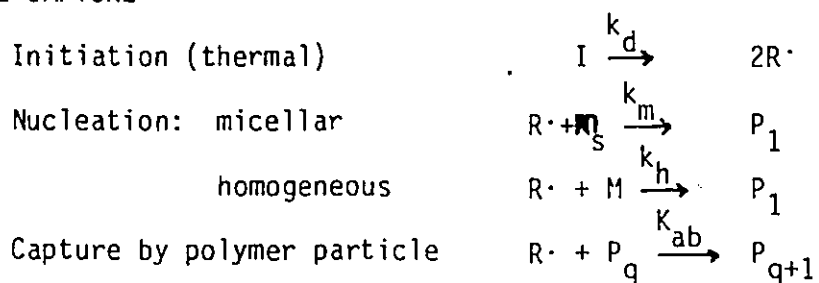
It is thus seen that both theories yield similar expressions for particle generation and it is expected that when micelles are present in the early stages of an emulsion polymerization for reasonably soluble monomers that both nucleation mechanisms are probably taking place and should be accounted for.

Hansen and Ugelstad (1978) also presented a homogeneous nucleation model where the critical length of a polymer chain is the important variable, this length being the maximum number of monomer units which could be added to the growing polymer chain in the water phase without precipitation occurring. This theory, along with those of Fitch and Tsai (1971) and Smith-Ewart (1947), will be discussed in more detail in the next chapter.

2.6 OVERALL KINETIC PICTURE FOR PARTICLE SIZE DEVELOPMENT

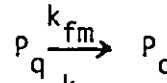
From the discussion in previous sections, a sample kinetic scheme can be developed to describe changes in the particle size distribution and number of particles. These are as follows:

RADICAL CAPTURE

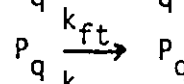


RADICAL DESORPTION

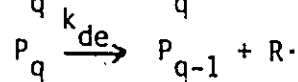
Chain transfer: monomer



chain transfer agent

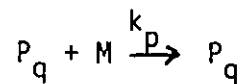


Radical desorption



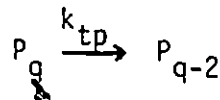
PROPAGATION

Propagation: polymer particles



TERMINATION

Termination: polymer particles



where P_q is a polymer particle containing q free radicals, $R\cdot$ is a radical in the water phase and N_q is the number of particles P_q .

Several assumptions have been made for this kinetic scheme.

These are:

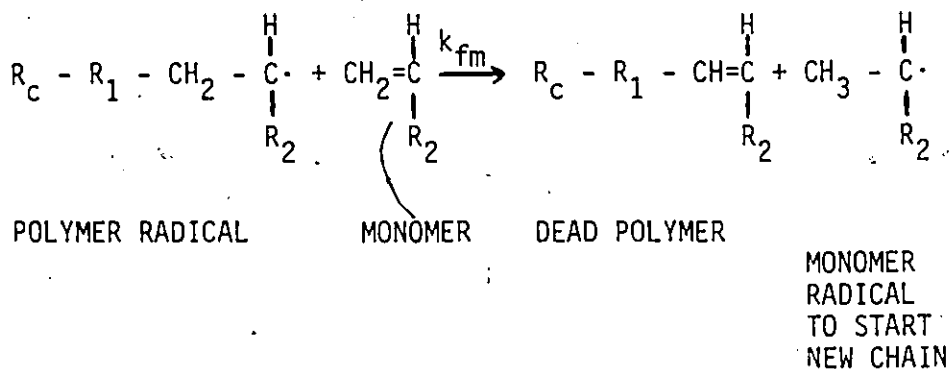
- i) there is no termination in the water phase.
- ii) coagulation of polymer particles is not considered.
- iii) impurities in water and polymer phases which can react with radicals are not considered.
- iv) both micellar and homogeneous nucleation can take place.

It is also worth noting that chain transfer and desorption are linked. Larger radicals existing in a polymer particle are entangled with polymer chains already present and are unable to diffuse out. Only small radicals may diffuse out of a polymer particle easily. As a result, unless there is a significant degree of transfer of the

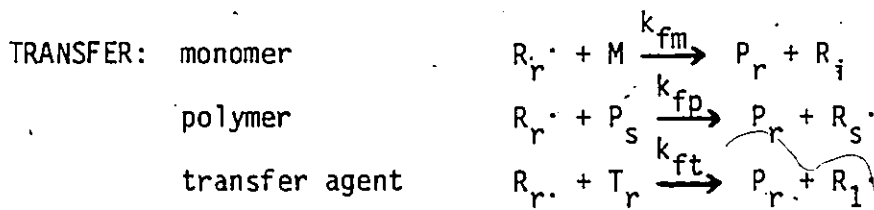
radical nature to small molecules, desorption of radicals from polymer particles is not important. Since vinyl acetate can have significant transfer rates to monomer, or chain transfer agents can be added for control of molecular weight, this reaction has been included in this model.

2.7 OVERALL KINETIC PICTURE FOR MOLECULAR WEIGHT DEVELOPMENT

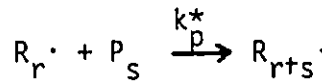
For the emulsion polymerization of vinyl acetate, the rate of transfer to monomer or other molecules is the dominant step in controlling the molecular weight development. Termination reactions play a negligible role in determining the molecular weight distributions. If there is no transfer to solvent, then essentially all polymers formed will have a terminal double bond. This is due to the fact that transfer to monomer provides much larger numbers of free radicals than the rate of initiation for this system, so that effectively all polymers will have terminal double bonds by the transfer reaction as shown below:



As a result, terminal double bond polymerization must also be included in the kinetic scheme. With these considerations, the kinetic scheme for molecular weight development is as follows:

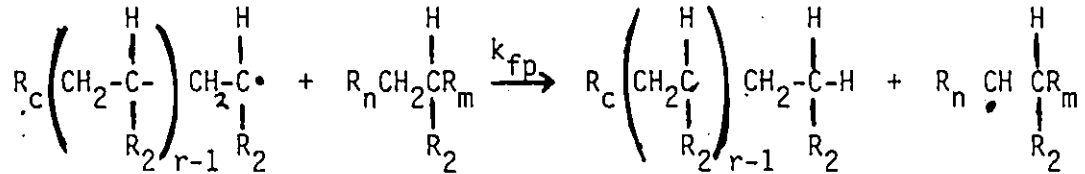


TERMINAL DOUBLE BOND POLYMERIZATION



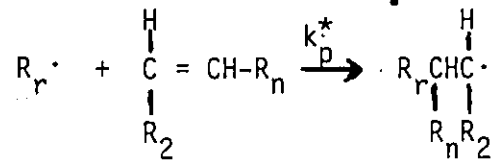
The model can also be easily generalized to include polymer chains with and without terminal double bonds (Hamielec (1976)).

It is also worth noting that long chain branching can result from transfer to polymer according to the following scheme:



where the polymeric radical removes hydrogen from any unit along the polymer chain followed by the formation of a polymer branch.

Long chain branching can also occur by the terminal double bond polymerization mechanism as follows:



Both of these mechanisms yield long chain branch points and hence branched polymers which will be included in the simulation equations of the next chapter.

CHAPTER 3

MATHEMATICAL MODELLING OF CONTINUOUS EMULSION POLYMERIZATION REACTORS

3.1 INTRODUCTION

In dealing with any complex system or piece of equipment, a question arises regarding the value of a mathematical model. There are many advantages in having a mathematical description of a process. The model provides a summary of all one's knowledge of the system. As such it highlights unknown areas and hence can direct research. If the model is accurate enough, it will provide an understanding of the underlying mechanism and interactions of the system. With this kind of information, several practical applications usually are suggested such as:

- i) Changes in operating conditions for a better product or higher production.
- ii) Extension to a new raw material is usually fairly easy.
- iii) Start-up policies may be better formulated.
- iv) Comparison of different control schemes may be attempted on the model first so the physical process does not have to be upset.

v) Effects of disturbances and operating variable interactions can be found.

A model then, if it is comprehensive enough to describe the process trends has many potential uses.

The next question that must be answered is whether the model should be steady-state or dynamic in nature. If the only result that is desired is to find what final conditions a steady-state continuous process will attain for a given set of operating conditions, a steady-state model is sufficient. However, for continuous emulsion polymerization, several dynamic phenomenon such as sustained oscillations occur. In addition, because of strong non-linearities in the model, changes from one condition to another operating point may not be straightforward. It may also be desired to apply the model to batch and semi-batch situations, and to investigate start-up policies and control strategies. All of the above require a dynamic model for the system. As a result, it was necessary to develop a dynamic model for vinyl acetate emulsion polymerization which would describe the system with reasonable accuracy.

In the next section, an examination of previous models in the literature followed by development of the dynamic model with several applications is carried out.

3.2 DYNAMIC PHENOMENA IN EMULSION POLYMERIZATION CSTR'S

There are several phenomena that occur during start-up and even steady flow operation of an emulsion polymerization CSTR^{*} which require a dynamic model to explain.

Gorber (1973) has shown experimentally that during a reactor start-up for the emulsion polymerization of styrene there is an initial overshoot of the steady-state operating conditions followed by damped oscillations which finally decay to the steady-state value. Gershberg & Longfield (1961) and Nomura, et al. (1971) while using different start-up policies also found significant overshoot.

In the literature, there are also many reports of sustained property oscillations for the emulsion polymerization of a variety of monomers. Greene, et al. (1976) and Kiparissides (1978) have shown sustained oscillations for vinyl acetate emulsion polymerization. Gerrens, et al. (1971) and Brooks, et al. (1978) showed similar oscillations for styrene, and Greene, et al. (1976) also showed sustained oscillations exist for MMA^{**} emulsion polymerization. Even when simple feedback control was attempted on Kiparissides, et al.'s simulation of a vinyl acetate emulsion polymerization CSTR, Leffew and Deshpande (1981) found that the oscillations remain.

In addition to these results, Gerrens, et al. (1971) also showed experimentally that multiple steady-states were possible for styrene emulsion polymerization due to the gel effect at high conversions.

*CSTR = Continuous Stirred Tank Reactor.

**MMA = Methyl Methacrylate.

All of these phenomena lead to the conclusion that there are genuine dynamic problems with starting and running a "steady-state" emulsion polymerization CSTR.

3.3 MODELLING OF CONTINUOUS REACTORS

Industrially, the majority of latex polymerization is carried out in a batchwise or semi-batch manner. The production of uniform latex product thus becomes a problem in scheduling additions at appropriate times and repeating these runs to achieve consistency.

Continuous stirred tank reactors have inherent advantages for large-scale commercial production of latices. Reduced maintenance, ease of operation and control, more consistent product quality and usually higher production rates are advantages of using continuous reactor systems. Latices already produced in this way are polyvinyl chloride and styrene-butadiene copolymer emulsions.

However, due to experimental difficulties in studying continuous reactors such as lack of flexibility, more complexity, larger run times and larger consumption of raw materials, past research has usually examined batch kinetics and not as much work has been carried out on continuous reactor systems.

Several publications in the literature have attacked various aspects of the modelling problem. Stevens and Funderburk (1972) developed a population balance model for predicting the particle size distribution (PSD) for the continuous emulsion polymerization of styrene based on a steady-state model. De Graaf and Poehlein (1971)

used Smith-Ewart kinetics as developed by Stockmayer (1957) coupled with a residence time distribution to predict the PSD for styrene in a continuous emulsion reactor. Predictions by this model for start-up however are not very good.

The most general model developed to date is that of Min and Ray (1974). Their model was developed based on the size distribution of polymer particles and is quite complex in scope. The resulting series of equations can be reduced to other basic theories by the appropriate assumptions, but the model requires a large number of parameters for its use. Kirillov and Ray (1978) used the model by taking moments of the distribution to predict the behavior of MMA continuous emulsion polymerization but had difficulty in estimating some of the model parameters and mechanisms. Their model however did predict the data of Greene, et al. (1976) reasonably well. The same model was also used to simulate a batch MMA reactor by Min and Ray (1978) but even with simplifications, solution times were quite large.

Gorber (1973) and Dickinson (1976) focused instead on the age distribution of particles rather than the size distribution for styrene reactors. Dickinson (1976) further simplified the model by examining only the macro-properties of the system rather than each class of particles.

Kiparissides (1978) used the same approach as Dickinson (1976) in developing a series of equations to describe the continuous emulsion polymerization of vinyl acetate. His model consisted of a series of integro-differential equations which were difficult to solve

but could predict the reactor behavior reasonably well. The fit to experimental runs of the continuous system was quite good. Chiang and Thompson (1978) made a modification of the model by Kiparissides (1978) to develop a system of ordinary differential equations for the moments of the particle size distribution. Chiang and Thompson (1978) showed that the model could fit the data of Greene, et al. (1976) reasonably if the appropriate parameters were chosen.

This final model which is complex enough to describe the system behaviors, yet simple enough to allow quick solution and possible control implementation, was used in this thesis. Derivations of the model equations for the moments of the particle size distribution, and the extension of the equations for prediction of the molecular weight distribution moments, are shown in the following section.

3.4 MODEL DEVELOPMENT FOR VINYL ACETATE

The model development follows the approach of Kiparissides (1978) and Chiang and Thompson (1978) using the age distribution analysis technique. In the next section the environmental balances are discussed followed by a discussion of the general population approach and derivation of the general macro-property equations for an emulsion polymerization CSTR system based on age distribution analysis. These are then applied to derivations of equations for the moments of the PSD and MWD. The final set of equations for this system is summarized in section 3.4.5.

3.4.1 BALANCES FOR INITIATOR, EMULSIFIER, MONOMER AND OLIGOMERIC

RADICALS:

The balances for initiator in the water phase, total emulsifier, monomer and oligomeric radicals in the water phase for a single GSTR emulsion polymerization can be written:

$$\text{Init.: } \frac{d[I]_w}{dt} = \frac{[I]_F - [I]_w}{\theta} - k_d [I]_w \quad (3.1)$$

$$\text{Emul.: } \frac{d[S]_T}{dt} = \frac{[S]_F - [S]_T}{\theta} \quad (3.2)$$

$$\text{Olig. Rad.: } \frac{d[R\cdot]_w}{dt} = \frac{1}{\theta} ([R\cdot]_{w_f} - [R\cdot]_w) + \rho_i \quad (3.3)$$

$$- k_m A_m [R\cdot]_w k_v - k_h [R\cdot]_w$$

$$- k_{ab} A_p [R\cdot]_w k_v + \rho_{DES}$$

$$- k_{tw} [R\cdot]_w^2$$

$$\text{Monomer: } \frac{\text{Total Monomer Units } d[M]_{TOT}}{dt} = \frac{[M]_F - [M]_{TOT}}{\theta} \quad (3.4)$$

$$\text{Unpolymerized Monomer: } \frac{d[M]_{FREE MON}}{dt} = \frac{d[M]_{MON}}{dt} = \frac{1}{\theta} ([M]_F - [M]_{MON}) - R_p - R_{PAQ} \quad (3.5)$$

Equation 3.4 is the balance on monomer units in the system both as free unpolymerized monomer molecules and as monomer units already part of a polymer chain. Equation 3.5 is the unpolymerized monomer balance. The two equations are required if the reactor starts up under conditions of pure water but will be combined in the final conversion equation.

INITIATOR AND EMULSIFIER BALANCES

By integrating equations 3.1 and 3.2 analytical solutions are readily obtained if desired for any given reactor start-up policy.

$$[I]_w = \frac{[I]_F}{(1+k_d\theta)} \left(1 - e^{-\left(\frac{1}{\theta}+k_d\right)t} \right) + [I]_{w_0} e^{-\left(\frac{1}{\theta}+k_d\right)t} \quad (3.6a)$$

$$\approx [I]_F (1 - e^{-t/\theta}) \quad (3.6b)$$

$$[S]_T = [S]_F(1 - e^{-t/\theta}) + [S]_{T_0} e^{-t/\theta} \quad (3.7)$$

where $[I]_{w_0}$ is usually zero since the start time of polymerization is usually when initiator addition begins, and $k_d \ll 1/\theta$ is the usual situation for residence times of the order of half an hour to an hour. If changes in operating conditions are to be studied however, the differential equations 3.1 and 3.2 are preferable.

MONOMER BALANCE

In order to take account of different start-up policies (for example, only water present initially) the conversion is defined as follows:

$$X = \frac{[M]_{TOT} - [M]_{MON}}{[M]_{TOT}} \quad (3.8)$$

where $[M]_{TOT}$ is used in place of $[M]_F$ in the usual conversion equation and is available by integrating equation 3.4 to give:

$$[M]_{TOT} = [M]_F(1 - e^{-t/\theta}) + [M]_{TOT_0} e^{-t/\theta} \quad (3.9)$$

With this definition equation 3.5 becomes by combining with equation 3.9 and some manipulation:

$$\frac{dX}{dt} = \frac{R_p}{[M]_{TOT}} - \frac{X[M]_F}{\theta[M]_{TOT}} \quad (3.10)$$

$$= \frac{R_p}{[M]_F} - \frac{X}{\theta}; [M]_{To} = [M]_F \quad (3.10a)$$

$$= \frac{1}{(1-e^{-t/\theta})} \left(\frac{R_p}{[M]_F} - \frac{X}{\theta} \right); [M]_{To} = 0 \quad (3.10b)$$

Equation 3.10 is the general expression for the monomer balance while 3.10a and 3.10b represent start-up policies where the tank contents are the same as the feed, or the contents are initially pure water respectively. R_p represents the total rate of polymerization usually assumed to be in the polymer phase only.

OLIGOMERIC RADICALS

The oligomer radical balance in equation 3.3 has assumed that the radical capture rate is proportional to area according to collision theory as used by Smith-Ewart (1948), Gardon (1968a) and Fitch and Tsai (1971). It is also possible to use diffusion theory where the capture rate is proportional to the radius as used by Ugelstad, et al. (1967) but this approach was not used in the development as the collision theory permitted accurate predictions of polymerization rate, Kiparissides (1978).

In the oligomer radical balance of equation (3.3) the terms on the right-hand side represent respectively inflow and outflow of

radicals, production of radicals by initiation in the water phase, disappearance of radicals by micellar and homogeneous nucleation mechanisms whereby radicals start new polymer particles, capture of radicals by polymer particles already existing, appearance of radicals in the water phase by desorption from particles and disappearance by termination in the water phase.

The oligomer balance is now used to derive the nucleation rate for new polymer particles. The rate of generation of new particles $f(t)$ per liter of latex is the rate of micellar nucleation plus the rate of homogeneous nucleation so that:

$$f(t) = k_m A_m [R\cdot]_w + \frac{k_h}{k_v} [R]_w \quad (3.11)$$

In order to obtain the concentration of free radicals in the water phase, the oligomer balance in equation 3.3 is simplified by the following assumptions: (i) the inflow and outflow of radicals is negligible, (ii) termination of radicals in the water phase is negligible, and (iii) the rate of change of radicals is small compared to the other terms. This corresponds to a stationary state hypothesis. With these assumptions, equation 3.3 can be rearranged to give:

$$[R]_w = \frac{\rho(t)}{k_m A_m k_v + k_h + k_{ab} A_p k_v} \quad (3.12)$$

where $\rho(t) = \rho_i + \rho_{DES} \quad (3.13)$

Equations 3.12 and 3.13 for the concentration of radicals in the water phase and rate of production of radicals in the water phase

can be substituted into equation 3.11 to yield an expression for the rate of new particle formation:

$$f(t) = \frac{p(t)}{k_v} \left(\frac{k_m A_m k_v + k_h}{k_m A_m k_v + k_h + k_{ab} A_p k_v} \right) \quad (3.14)$$

In this expression A_m is the micellar area which is given by:

$$A_m = ([S]_{TOT} - [S]_{CMC}) S_N N_A - A_p + S_p - A_d \quad (3.15)$$

where $[S]_{CMC}$ is the critical micellar concentration, A_p is the particle area, A_d is the monomer droplet area and S_p is the area of polymer particles which are stabilized by polymer end groups rather than soap. The area of monomer droplets is usually a small contribution and the area stabilized by polymer end groups is difficult to ascertain and is usually neglected in model development as being small. The contribution of polymer end groups may play a part for the vinyl acetate system but it will not be used in this development so that the expression for micellar area becomes:

$$A_m = ([S]_{TOT} - [S]_{CMC}) S_N N_A - A_p \quad (3.16)$$

In addition, the homogeneous nucleation rate constant should be allowed to tend towards zero as the area of particles increases since the capture rate by polymer particles becomes greater than the rate of initiation of new radicals. This leads to an expression of the form (Kiparissides (1978), Fitch (1981)):

$$k_h = k_{ho} (1 - LA_p/4) \quad (3.17)$$

By defining $\mu = k_{ho}/k_m$ and $\epsilon = k_{ab}/k_m$ and substituting equation 3.17

into equation 3.14, the final expression for the generation rate of new particles is given by:

$$f(t) = \frac{\rho(t)}{k_v} \left(\frac{k_v A_m + \mu (1-LA_p/4)}{k_v A_m + \mu (1-LA_p/4) + \epsilon k_v A_p} \right) \quad (3.18)$$

where A_m is defined by equation 3.16 as discussed before.

Equations 3.6, 3.7, 3.10 and 3.18 are the final results of the various balances required for the components of this system. It is also possible to use the Hansen and Ugelstad (1978) model which uses only homogeneous nucleation where r_{cA} is the critical chain length for oligomer radical precipitation and $[M]_w$ is the concentration of monomer in water phase.

$$f(t) = N_A (\rho_i + \rho_{des}) \left(\frac{1}{1 + \frac{k_m A_m + k_{ab} A_p}{k_p [M]_w}} \right)^{r_c - 1} \quad (3.18a)$$

where in our case $\rho_{des} \gg \rho_i$ (can be assumed as zero).

This approach is concerned with the probability of a chain growing in the water phase until it becomes large enough (i.e. reaches critical chain length r_c) and precipitates. This approach was not followed in this study since r_c is not well known and the experimental results of Kiparissides (1978) are fit well by the given model structures. Also, for a large number of particles the homogeneous nucleation rate plays a very minor role in the kinetics for vinyl acetate, the micellar nucleation role being the more dominant one. so that both types of nucleation must be included.

3.4.2 GENERAL PROPERTY BALANCES

Any latex particle can be characterized by a set of physical quantities which will specify a given particle or class of particles. In this way a number density function $n(z,t)$ can be used to specify the number of particles having the physical properties z at time t . By applying a continuity equation approach the population balance equation can be written:

$$\frac{\partial n}{\partial t}(z,t) + \nabla_z \cdot n(z,t) = f_{NET}(z,t) \quad (3.19)$$

where ∇_z is a $(\partial/\partial z_1, \dots, \partial/\partial z_n)$ operator for this system. $f_{NET}(z,t)$ is the net generation function for particles with the given physical properties z at time t . The generation function can be written as:

$$f_{NET}(z,t) = \frac{1}{\theta} \left(n(z,t)_{FEED} - n(z,t) \right) + f(z,t) + f_{AGG}(z,t) \quad (3.20)$$

where the first term is the net change by flow of particles, the second is the rate of generation of new particles by homogeneous and micellar nucleation of the given class, and the final term is the net rate of appearance of particles of a given class by agglomeration.

Several choices are usually available for z , the vector of physical properties. Min and Ray (1974) chose $z = (v)$ the particle volume so that $n(v,t)$ was the particle size distribution. Bivariate distributions such as $n(v,q,t)$ are also possible but this approach can be cumbersome and lead to difficult to solve partial integro-differential equations.

The approach used in this thesis is that of Kiparissides (1978), Gorber (1973) and Dickinson (1976) who followed the system using $z = (T)$ where T is the birth time of the polymer particles. The number density function $n(t, T)$ thus gives an age distribution analysis where $n(t, T)dT$ is the number of particles in the reactor at time t that were born between time T and $T+dT$. With $z = (T)$ then $z = dT/dt = 1$ becomes true since the units are the same. With this in mind, the general equation 3.19 becomes:

$$\frac{\partial n}{\partial t}(t, T) + \frac{\partial n}{\partial T}(t, T) = f_{NET}(t, T) \quad (3.21)$$

As done by Kiparissides (1978), $p(t, T)$ can be defined as some physical property associated with the class of particles $n(t, T)dT$. If in addition there are property inputs to the reactor, the total property $P(t)$, obtained by summing the property over all particles in the reactor, is given by:

$$P(t) = \int_0^t P_{GEN}(t, T) n_{GEN}(t, T) dT + \int_0^t P_{in}(t, T) n_{in}(t, T) dT \quad (3.22)$$

where $p_{GEN}(t, T) n_{GEN}(t, T)dT$ is the property of the class of particles generated within the reactor while $p_{in}(t, T) n_{in}(t, T)dT$ is the class property of the inflowing polymer particles. This distribution is required since $p_{in}(t, T) \neq p_{GEN}(t, T)$ in general.

That is, the physical property of an incoming particle which flows in at time T will not in general be the same as the property of that particle at its birth time by new nucleation at time T . By

differentiating 3.22 and applying Leibnitz rule the following result is obtained:

$$\begin{aligned} \frac{dP(t)}{dt} &= p_{GEN}(t,t)n_{GEN}(t,t) + p_{in}(t,t)n_{in}(t,t) \\ &+ \int_0^t \frac{dp_{GEN}(t,T)}{dt} n_{GEN}(t,T) dT + \int_0^t \frac{dp_{in}(t,T)}{dt} n_{in}(t,T) dT \\ &+ \int_0^t p_{GEN}(t,T) \frac{dn_{GEN}(t,T)}{dt} dT + \int_0^t p_{in}(t,T) \frac{dn_{in}(t,T)}{dt} dT \quad (3.23) \end{aligned}$$

The generating function $f_{NET}(t,T)$ in equation 3.21 for the two types of particles is:

$$f_{GEN}(t,T) = \frac{dn_{GEN}(t,T)}{dt} = -\frac{n_{GEN}(t,T)}{\theta} + f(t) \delta(t-T) \quad (3.24)$$

$$f_{in}(t,T) = \frac{dn_{in}(t,T)}{dt} = -\frac{n_{in}(t,T)}{\theta} + \frac{N_{in}(t)}{\theta} \delta(t-T) \quad (3.25)$$

where $N_{in}(t)$ is total number of particles flowing in at time t .

$$n_{GEN}(t,T) = f(T) e^{-(t-T)/\theta} \quad (3.26)$$

$$n_{in}(t,T) = \frac{N_{in}(T)}{\theta} e^{-(t-T)/\theta} \quad (3.27)$$

The values of these two functions at birth are thus given by:

$$n_{GEN}(t,t) = f(t) \quad (3.26a)$$

$$n_{in}(t,t) = \frac{N_{in}(t)}{\theta} \quad (3.27a)$$

Using these last two equations, the first two terms of the general equation 3.23 become:

$$P_{GEN}(t,t)n_{GEN}(t,t) = P_{GEN}(t,t)f(t) \quad (3.26b)$$

$$P_{in}(t,t)n_{in}(t,t) = P_{in}(t,t)\frac{N_{IN}(t)}{\theta} = \frac{P_{in}(t)}{\theta} \quad (3.27b)$$

Substitution of equations 3.24 and 3.25 into the final two terms of 3.23 yields:

$$\int_0^t P_{GEN}(t,T)\frac{dn_{GEN}(t,T)}{dT}dT + \int_0^t P_{in}(t,T)\frac{dn_{in}(t,T)}{dT}dT = -\frac{P_{GEN}(t)}{\theta} - \frac{P_{in}(t)}{\theta} = -\frac{P(t)}{\theta} \quad (3.28a)$$

Using these results the final property balance equation is given by:

$$\frac{dP(t)}{dt} = \frac{P_{in}(t)}{\theta} - \frac{P(t)}{\theta} + f(t)p(t,t) + \int_0^t \frac{dp_{GEN}(t,T)}{dT}n_{GEN}(t,T)dT + \int_0^t \frac{dp_{in}(t,T)}{dT}n_{in}(t,T)dT \quad (3.29)$$

This final equation will be used in subsequent sections.

3.4.3 PARTICLE SIZE DEVELOPMENT

The development of the particle size equations centers around the equation for volume growth rate of a polymer particle. The rate of change of polymer volume is given by the rate of polymerization as follows:

$$\frac{dv(t,T)}{dt} = R_p \frac{MW_{MON}}{d_p} \quad (3.30)$$

where R_p is the rate of polymerization in moles of monomer produced per liter latex per unit time and d_p is the polymer density, MW_{MON} is the monomer molecular weight. In this equation, $v(t,T)$ is the volume of polymer contained in a particle of class $n(t,T)dT$. The rate of polymerization from equation 2.9 (assuming one particle under consideration) can be substituted in to yield the expression:

$$\frac{dv(t,T)}{dt} = \frac{k_p [M]_p}{N_A} q(t,T) \cdot \frac{MW_{MON}}{d_p} \quad (3.31)$$

where $[M]_p$ is the concentration of monomer in the polymer particle. The usual assumption is that diffusion of monomer to the particles is fast enough that an equilibrium is attained whereby the concentration of monomer in all classes of particles is considered to be the same. The volume fraction of monomer in the polymer particles ϕ is given by (Hamielec (1976), Kiparissides (1978)):

$$\phi = \frac{1 - x_c}{1 - x_c(1 - d_m/d_p)} \quad ; x \leq x_c \quad (3.32a)$$

$$= \frac{1 - x}{1 - x(1 - d_m/d_p)} \quad ; x > x_c \quad (3.32b)$$

where x_c is the critical conversion where all the monomer drops disappear, at which point the monomer resides in the polymer particles and water phase. In these expressions, d_m is the density of pure monomer. With this definition, $[M]_p$ is given by:

$$[M]_p = \phi \frac{d_m}{MW_{MON}} \quad (3.33)$$

so that the expression for the rate of change of polymer volume (equation 3.31) is given as:

$$\frac{dv(t,T)}{dt} = \frac{k_p d_m}{d_p N_A} \Phi q(t,T) \quad (3.34)$$

With Case I kinetics, the value of $q(t,T)$ is obtained from equation 2.14 with the assumption of capture of radicals being proportional to area as:

$$q(t,T) = \left(\frac{\rho_i}{2k_{de}(t,T)n(t,T)dT} \right)^{1/2} \left(\frac{A_n(t,T)}{A_p(t)} \right)^{1/2} \quad (3.35)$$

where $A_n(t,T)$ is the total area of the class of particles $n(t,T)dT$.

Nomura, et al. (1971) have devised an expression for the desorption constant $k_{de}(t,T)$ as follows:

$$k_{de}(t,T) = \left(\bar{q} + \frac{k_p [M]_p m d^2(t,T)}{12 D_w \delta} \right)^{-1} \left(\frac{k_{fm}}{k_p} + \frac{k_{ft} [Tr]}{k_p [M]_p} + \frac{\rho_i (1-\bar{q})}{N_p k_p [M] \bar{q}} \right) k_p [M]_p \quad (3.36)$$

which if $\bar{q} \ll .5$ and for no escape of initiator radicals and no transfer agent present can be simplified to:

$$k_{de}(t,T) = \frac{12 D_w \delta k_{fm}}{m d^2(t,T) k_p} \quad (3.37)$$

where D_w is the diffusion coefficient of monomer radicals in water, m is the monomer partition coefficient, (i.e. $m = [M]_p / [M]_w$), $\delta =$ a lumped diffusion coefficient such that $\delta = (1 + D_w / m D_p)^{-1}$, k_{fm} is

the rate constant for transfer to monomer and D_p is the diffusion coefficient of monomer radicals in polymer particles.

With these expressions, the rate equation for polymer volume in a particle is:

$$\frac{dv(t,T)}{dt} = \left(\frac{k_p d_m}{N_A d_p} \right) \Phi \left(\frac{\rho_i}{2n(t,T)dT} \right)^{1/2} \left(\frac{m\pi d^2(t,T)k_p}{12\pi D_w k_{fm} \delta} \right)^{1/2} \frac{A_n(t,T)^{1/2}}{A_p(t)^{1/2}} \quad (3.38)$$

This is the same approach used by Kiparissides (1978) but Chiang and Thompson (1978) now made the following modification:

$$A_n(t,T) = a_p(t,T)n(t,T)dT \quad (3.39)$$

This slight modification simplifies the expression for rate of volume change of polymer in a particle to:

$$\frac{dv(t,T)}{dt} = \lambda \xi'(t) a_p(t,T) \quad (3.40)$$

where $\lambda = \left(\frac{k_p d_m}{N_A d_p} \right) \left(\frac{k_p m f_{eff} k_d}{12\pi D_w \delta k_{fm}} \right)^{1/2}$ (3.41)

$$\xi'(t) = \Phi(t) \left(\frac{[I]_w(t)}{A_p(t)} \right)^{1/2} \quad (3.42)$$

since $\rho_i = 2 f_{eff} k_d [I]_w$ is the rate of initiation.

To obtain the expression for particle volume, the following expression can be used:

$$v_p(t,T) = v(t,T)/(1-\Phi(t)) \quad (3.43)$$

By differentiating this expression the rate of change of polymer particle volume $v_p(t, T)$ can be shown to be:

$$\frac{dv_p(t, T)}{dt} = \lambda \xi(t) a_p(t, T) \quad ; \quad x \leq x_c \quad (3.44a)$$

$$= \lambda \xi(t) a_p(t, T) - \frac{v_p(t, T)}{(1-\Phi(t))(1-cx)^2} \frac{dx(t)}{dt} \quad ; \quad x > x_c \quad (3.44b)$$

where $\xi(t) = \zeta(t)/(1-\Phi(t))$ and $c = (1 - d_m/d_p)^2$. The second expression on the right hand side results from the differentiation of $\Phi(t)$ with respect to time. Since $x(t)$ is not considered to be dependent on the class of particles the final form of the equation is:

$$\frac{dv_p(t, T)}{dt} = \lambda \xi(t) a_p(t, T) - \mathcal{N}(t) v_p(t, T) \quad (3.45a)$$

$$\text{where } \mathcal{N}(t) = 0 \quad ; \quad x \leq x_c$$

$$= \frac{1 - c}{(1-\Phi(t))(1-cx(t))^2} \frac{dx(t)}{dt} \quad ; \quad x > x_c \quad (3.45b)$$

The final term in equation 3.45 was not included in the work by Kiparissides (1978) or Chiang and Thompson (1978). When a reactor is operated continuously, even with oscillations, $dx(t)/dt$ is usually small and so the second term is usually negligible. However, under start-up conditions or batch operation when $dx(t)/dt$ can be large, this second term is necessary. This point will be discussed further in later chapters.

The general property balance was given in equation 3.28 and is repeated below:

$$\begin{aligned} \frac{dP(t)}{dt} &= \frac{P_{in}(t) - P(t)}{\theta} + f(t)p(t,t) \\ &+ \int_0^t \frac{dp_{GEN}(t,T)}{dt} n_{GEN}(t,T) dT + \int_0^t \frac{dp_{in}(t,T)}{dt} n_{in}(t,T) dt \end{aligned} \quad (3.29)$$

If the property $P(t)$ is considered to be the total particle volume, then equation 3.44 can be substituted in the last two integrals of the general population balance to yield:

$$\begin{aligned} \frac{dV_p(t)}{dt} &= \frac{V_{pin}(t) - V_p(t)}{\theta} + f(t)V_p(t,t) \\ &+ \lambda \xi(t) \left[\int_0^t a_{pGEN}(t,T) n_{GEN}(t,T) dT + \int_0^t a_{pin}(t,T) n_{in}(t,T) dT \right] \\ &- \eta(t) \left[\int_0^t v_{pGEN}(t,T) n_{GEN}(t,T) dT + \int_0^t v_{pin}(t,T) n_{in}(t,T) dT \right] \end{aligned} \quad (3.45)$$

which by definition of the property $p(t)$ (equation 3.22) yields the final result.

$$\frac{dV_p(t)}{dt} = \frac{V_{pin}(t) - V_p(t)}{\theta} + f(t)V_p(t,t) + \lambda \xi(t) A_p(t) - \eta(t) V_p(t) \quad (3.47)$$

In order to obtain expressions for the area $A_p(t)$ and diameter $D_p(t)$ of particles, the following equations were used:

$$\frac{dV_p(t,T)}{dt} = \frac{d}{dt} \left(\frac{\pi d_p^3(t,T)}{6} \right) = \frac{\pi d_p^2(t,T)}{2} \frac{d d_p(t,T)}{dt} = \frac{a_p(t,T)}{2} \frac{d d_p(t,T)}{dt} \quad (3.48)$$

$$\frac{da_p(t,T)}{dt} = \frac{d}{dt} (\pi d_p^2(t,T)) = 2\pi d_p(t,T) \frac{d d_p(t,T)}{dt} \quad (3.49)$$

which upon rearrangement yields using equation 3.45

$$\frac{d d_p(t, T)}{dt} = 2 \lambda \xi(t) - \frac{\eta(t)}{3} d_p(t, T) \quad (3.50)$$

$$\frac{d a_p(t, T)}{dt} = 4\pi \lambda \xi(t) d_p(t, T) - \frac{2\eta(t)}{3} a_p(t, T) \quad (3.51)$$

by assuming spherical particles for the system. Following a similar development as was done for total particle volume, these expressions are used in the general property balance to yield:

$$\frac{d D_p(t)}{dt} = \frac{D_{pin}(t) - D_p(t)}{\theta} + f(t) d_p(t, t) + 2 \lambda \xi(t) N_p(t) - \frac{\eta(t)}{3} D_p(t) \quad (3.52)$$

$$\frac{d A_p(t)}{dt} = \frac{A_{pin}(t) - A_p(t)}{\theta} + f(t) a_p(t, t) + 4\pi \lambda \xi(t) D_p(t) - \frac{2}{3} \eta(t) A_p(t) \quad (3.53)$$

In addition, the general property balance for the number of particles yields:

$$\frac{d N_p(t)}{dt} = \frac{N_{pin}(t) - N_p(t)}{\theta} + f(t) \quad (3.54)$$

Equations 3.54, 3.53, 3.52 and 3.47, along with the particle nucleation function equation 3.18 provide all the information to describe the macroproperties or the moments of the particle size distribution for this system.

In order to carry out the total integration, ρ_i and ρ_{des} in equation 3.3 must be defined as well. ρ_i is the rate of initiation per liter aqueous phase:

$$\rho_i = 2 f_{\text{eff}} k_d [I]_w N_A \quad (3.55)$$

and the rate of radical desorption is given by:

$$\rho_{\text{des}} = \int_0^t k_{\text{de}}(t, T) n(t, T) q(t, T) dT \quad (3.56)$$

which by substituting in $k_{\text{de}}(t, T)$ from equation 3.37, and $q(t, T)$ and $A_n(t, T)$ from equations 3.35 and 3.39 can be integrated to yield:

$$\rho_{\text{des}} = \left(\frac{k_v^2 12\pi D_w \delta k_{\text{fm}} f_{\text{eff}} k_d N_A}{m k_p} \right)^{1/2} \left(\frac{[I]_w}{k_v A_p(t)} \right)^{1/2} N_p(t) \quad (3.57)$$

With these final two equations, the entire set of equations is specified for the particle size development. The k_v is the ratio of litre latex per liter aqueous phase and is thus a conversion factor between the two bases for this system.

3.4.4 MOLECULAR WEIGHT DEVELOPMENT

The kinetic scheme for the molecular weight development was presented in Section 2.7. One of its assumptions was that transfer reactions were the controlling factor, not termination reactions, for determining the molecular weight distribution for poly(vinyl acetate). Friis, et al. (1974) showed this to be a reasonable assumption both on theoretical grounds and by experimental evidence in this system.

Long chain branching is also important in vinyl acetate emulsion polymerization and is included in the kinetic scheme both by transfer to polymer and terminal double-bond reaction mechanisms. As

conversion increases, Friis, et al. (1974) have shown that transfer to polymer begins to dominate the molecular weight development with regards to branching so that effects of not all polymers having terminal double bonds due to transfer to a chain transfer agent or monomer molecule will not play a large role in changing the form of the model. That is, the model will not be modified to involve equations for polymers both with and without double-bonded ends.

Another problem which is mentioned in the literature (Beasley (1953), Cozewith, et al. (1979)) is the possibility of the prediction of weight average molecular weight by the simulation equations going to infinity for some conversions less than unity with reasonable degrees of branching. Jackson, et al. (1973) felt that this was due to outflow of large polymer radicals being neglected in the analysis. However, for polydispersities of 100 or less, their results indicated that the neglect of the outflow term should not introduce a large error into the solution.

The model presented by Jackson, et al. (1973) however uses the solution of a hypergeometric equation to calculate the moments of the MWD at steady-state. Since, as shown in previous sections, dynamics may be important, their approach was not used.

Instead, the development of the MWD moment differential equations is based upon work by Cozewith, et al. (1979), Friis, et al. (1974) and Hamielec (1976). The development also relies upon a similar property balance approach as done for the development of the particle size equations in Section 3.4.3.

To begin the development, equations for the moments of the MWD in a particle of a given class will first be derived. For a given class of particles $n(t,T)dT$, the class bracket will be dropped for compactness so that $R_r = R_r(t,T)$ which is the moles of radicals of length r in a particle of class $n(t,T)dT$. Similarly, $p_r = p_r(t,T)$ which is the moles of polymer of length r per particle of class $n(t,T)dT$. For a given class $n(t,T)dT$ the following definitions will hold:

$$Q_n = Q_n(t,T) = \sum_{r=1}^{\infty} r^n p_r \quad \text{DEAD POLYMER MOMENT} \quad (3.58)$$

$$Y_n = Y_n(t,T) = \sum_{r=1}^{\infty} r^n R_r \quad \text{LIVE POLYMER MOMENT} \quad (3.59)$$

By referring back to the kinetic scheme of Section 2.7, equations for the live polymer moments can be calculated by summary over all lengths r to be (Hamielec (1976)):

$$\frac{dY_0}{dt} = 0 \quad (3.50)$$

$$\begin{aligned} \frac{dY_1}{dt} = & k_p [M]_p Y_0 + (k_{fm} [M]_p + k_{ft} [Tr]) (Y_0 - Y_1) \\ & + k_{fp} \left(Y_0 \frac{Q_2}{V_p} - Y_1 \frac{Q_1}{V_p} \right) + k_p^* Y_0 \frac{Q_1}{V_p} \end{aligned} \quad (3.61)$$

$$\begin{aligned} \frac{dY_2}{dt} = & k_p [M]_p (Y_0 + 2Y_1) + (k_{fm} [M]_p + k_{ft} [Tr]) (Y_0 - Y_2) \\ & + k_{fp} \left(Y_0 \frac{Q_3}{V_p} - Y_2 \frac{Q_1}{V_p} \right) + k_p^* \left(2Y_1 \frac{Q_1}{V_p} + Y_0 \frac{Q_2}{V_p} \right) \end{aligned} \quad (3.62)$$

where $v_p = v_p(t,T)$ = the volume of a particle of class $n(t,T)dT$.

The usual assumption is that the rate of change of Y_1 and Y_2 with respect to time is negligible in comparison with the other terms, which is the steady-state hypothesis applied to equation 3.61 and 3.62. The algebraic results of these assumptions yields the following:

$$\frac{Y_1}{Y_0} = \frac{k_p[M]_p + (k_{fm}[M]_p + k_{ft}[Tr]) + k_{fp} \frac{Q_2}{V_p} + k_p^* \frac{Q_1}{V_p}}{(k_{fm}[M]_p + k_{ft}[Tr]) + k_{fp} \frac{Q_1}{V_p}} \quad (3.63)$$

$$\frac{Y_2}{Y_0} = \frac{k_p[M]_p + (k_{fm}[M]_p + k_{ft}[Tr]) + k_{fp} \frac{Q_3}{V_p} + k_p^* \frac{Q_2}{V_p} + 2(k_p[M]_p + k_p^* \frac{Q_1}{V_p})(Y_1/Y_0)}{(k_{fm}[M]_p + k_{ft}[Tr]) + k_{fp} \frac{Q_1}{V_p}} \quad (3.64)$$

These equations then describe the live polymer radical moments for the system. Referring to the kinetic scheme again, the dead polymer equations are given by:

$$\frac{dQ_0}{dt} = (k_{fm}[M]_p + k_{ft}[Tr])Y_0 - k_p^* \frac{Q_0}{V_p} Y_0 \quad (3.65)$$

$$\frac{dQ_1}{dt} = (k_{fm}[M]_p + k_{ft}[Tr] + k_{fp} \frac{Q_1}{V_p})Y_1 - (k_{fp} \frac{Q_2}{V_p} + k_p^* \frac{Q_1}{V_p})Y_0 \quad (3.66)$$

$$\frac{dQ_2}{dt} = (k_{fm}[M]_p + k_{ft}[Tr] + k_{fp} \frac{Q_1}{V_p})Y_2 - (k_{fp} \frac{Q_3}{V_p} + k_p^* \frac{Q_2}{V_p})Y_0 \quad (3.67)$$

By substituting in equations 3.63 and 3.64 for Y_1 and Y_2 respectively and simplifying, the final moment equations result:

$$\frac{dQ_0(t,T)}{dt} = (k_{fm}^*[M]_p + k_{ft}[Tr])Y_0(t,T) - k_p^* \frac{Q_0(t,T)}{V_p(t,T)} Y_0(t,T) \quad (3.68)$$

$$\frac{dQ_1(t,T)}{dt} = \frac{(k_p[M]_p + k_{fm}[M]_p + k_{ft}[Tr])Y_0(t,T)}{V_p(t,T)} \quad (3.69)$$

$$\begin{aligned} \frac{dQ_2(t,T)}{dt} &= \frac{(k_p[M]_p + k_{fm}[M]_p + k_{ft}[Tr])Y_0(t,T)}{V_p(t,T)} \\ &+ 2Y_0(t,T) \left(\frac{k_p[M]_p + k_p^* Q_1(t,T)/V_p(t,T)}{k_{fm}[M]_p + k_{ft}[Tr] + k_{fp} Q_1(t,T)/V_p(t,T)} \right) \\ &* \left(\frac{k_p[M]_p + k_{fm}[M]_p + k_{ft}[Tr] + k_{fp} Q_2(t,T)/V_p(t,T) + k_p^* Q_1(t,T)/V_p(t,T)}{V_p(t,T)} \right) \end{aligned} \quad (3.70)$$

If B_N is defined as the branch points per polymer molecule, then $Q_0 B_N$ is the branch points per polymer particle and the kinetic mechanism yields:

$$\frac{d(Q_0 B_N)(t,T)}{dt} = \left(k_{fp} \frac{Q_1(t,T)}{V(t,T)} + k_p^* \frac{Q_0(t,T)}{V(t,T)} \right) Y_0(t,T) \quad (3.71)$$

When equation 3.69 is divided by equation 3.68, and equation 3.70 by equation 3.69, it can be seen that $dQ_1(t,T)/dQ_0(t,T)$ and $dQ_2(t,T)/dQ_1(t,T)$ are independent of radical concentration $Y_0(t,T)$, hence the moments M_N and M_W will be independent of radical concentration. However, for convenience in solving the differential equations, the following approximations were used in the development:

$$\bar{Y}(t) = \frac{Y_{OT}(t)}{V_p(t)} = \frac{Y_0(t,T)}{V(t,T)} \neq g(T) \quad (3.72)$$

$$\bar{Q}_1(t) = \frac{Q_1(t)}{V_p(t)} = \frac{Q_1(t,T)}{V(t,T)} \neq g(T) \quad (3.73)$$

In addition, several dimensionless groups were defined as follows:

$$C_m = \frac{k_{fm}}{k_p} + \frac{k_{ft}[Tr]}{k_p[M]_p} \quad (3.74)$$

$$C_p = \frac{k_{fp}}{k_p} \quad (3.75)$$

$$K = \frac{k_p^*}{k_p} \quad (3.76)$$

With these assumptions and definitions, the set of equations for the molecular weight moments of a given class of particles are as follows:

$$\frac{dQ_0(t, T)}{dt} = k_p [M]_p \bar{Y}(t) \left[C_m V_p(t, T) - \frac{K Q_0(t, T)}{[M]_p} \right] \quad (3.77)$$

$$\frac{dQ_1(t, T)}{dt} = k_p [M]_p \bar{Y}(t) (1 + C_m) V_p(t, T) \quad (3.78)$$

$$\begin{aligned} \frac{dQ_2(t, T)}{dt} = & k_p [M]_p \bar{Y}(t) \left[(1 + C_m) V_p(t, T) + 2 \frac{(1 + K Q_1(t, T) / [M]_p)}{C_m + C_p Q_1(t, T) / [M]_p} \right. \\ & \left. * \left((1 + C_m) V_p(t, T) + \frac{C_p Q_2(t, T)}{[M]_p} + \frac{K Q_1(t, T)}{[M]_p} \right) \right] \quad (3.79) \end{aligned}$$

$$\frac{d(Q_0 B_N)}{dt} = k_p [M]_p \bar{Y}(t) \left(\frac{C_p Q_1(t, T)}{[M]_p} + \frac{K Q_0(t, T)}{[M]_p} \right) \quad (3.80)$$

These four equations can now be put into the general property balance equation 3.28 to yield the final equations for the total moments of the molecular weight distribution as shown below:

$$\frac{dQ_0(t)}{dt} = \frac{Q_{0in}(t) - Q_0(t)}{\theta} + k_p [M]_p \bar{Y}(t) \left(C_m V_p(t) - \frac{K Q_0(t)}{[M]_p} \right) \quad (3.81)$$

$$\frac{dQ_1(t)}{dt} = \frac{Q_{1in}(t) - Q_1(t)}{\theta} + k_p[M]_p \bar{Y}(t) (1 + C_m) v_p(t) \quad (3.82)$$

$$\frac{d(Q_0 B_N)(t)}{dt} = \frac{(Q_0 B_N)_{in}(t) - (Q_0 B_N)(t)}{\theta} + k_p[M]_p \bar{Y}(t) \left[\frac{C_p Q_1(t)}{[M]_p} + \frac{K Q_0(t)}{[M]_p} \right] \quad (3.83)$$

$$\begin{aligned} \frac{dQ_2(t)}{dt} = & \frac{Q_{2in}(t) - Q_2(t)}{\theta} + K_p[M]_p \bar{Y}(t) \left[(1 + C_m) v_p(t) \right. \\ & \left. + 2 \cdot \left(\frac{1 + K Q_1(t) / [M]_p v_p(t)}{C_m + \frac{C_p Q_1(t)}{[M]_p v_p(t)}} \right) \left((1 + C_m) v_p(t) + \frac{C_p Q_2(t)}{[M]_p} + \frac{K Q_1(t)}{[M]_p} \right) \right] \quad (3.84) \end{aligned}$$

The $(1+C_m)$ terms in these equations can usually be approximated as 1 since $C_m \approx 10^{-4} \ll 1$ is the usual situation.

With these results, the number and weight average molecular weights and average number of branch points can be calculated as:

$$M_n = \left(\frac{Q_1(t)}{Q_0(t)} \right) MW_{MON} \quad (3.85)$$

$$M_w = \left(\frac{Q_2(t)}{Q_1(t)} \right) MW_{MON} \quad (3.86)$$

$$B_N = \left(\frac{(Q_0 B_N)(t)}{Q_0(t)} \right) \quad (3.87)$$

In order to use these equations, however, the final information required is that of $Y_{OT}(t)$ in order to calculate $\bar{Y}(t)$ in the equations. This is derivable by using equations 3.35 for $q(t,T)$, 3.36 for $k_{de}(t,T)$ and 3.39 for $A_n(t,T)$ and summing over all classes of particles to give:

$$Y_{OT}(t) = \lambda \xi(t) \left(\frac{N_A d_p}{k_p d_m} \right) \left(\frac{1 - \Phi(t)}{\Phi(t)} \right) A_p(t) \quad (3.88)$$

These equations have several assumptions built into their use: i) $[M]_p$, and all rate constants are independent of the class of particles being considered, ii) polymer produced by termination is negligible, and iii) since when particles are newly formed, it is by entry of a live radical, no generation term for dead polymer is used.

Equations 3.81 to 3.84 and 3.88 along with the particle size equations allow integration of ordinary differential equations to provide information on the molecular weight averages and degree of branching in a continuous reactor system.

3.4.5 SUMMARY OF MODEL EQUATIONS

The equations summarized below are the final results from the model derived in the previous sections.

ENVIRONMENTAL BALANCE DIFF. EQ'S

$$\text{INITIATOR} \quad \frac{d[I]_w}{dt} = \frac{[I]_f - [I]_w}{\theta} - k_d [I]_w \quad (3.1)$$

$$\text{EMULSIFIER} \quad \frac{d[S]_T}{dt} = \frac{[S]_F - [S]_T}{\theta} \quad (3.2)$$

$$\text{CONVERSION} \quad \frac{dX}{dt} = \frac{R_p}{[M]_{TOT}} - \frac{X[M]_F}{\theta[M]_{TOT}} \quad (3.10)$$

$$\text{where } [M]_{TOT} = [M]_p (1 - e^{-t/\theta}) + [M]_{TOT_0} e^{-t/\theta}$$

$$\text{and } X = \frac{[M]_{TOT} - [M]_{MON}}{[M]_{TOT}}$$

PARTICLE SIZE DIFFERENTIAL EQUATIONS

NUMBER OF PARTICLES: $\frac{dN_p(t)}{dt} = \frac{N_{pin}(t) - N_p(t)}{\theta} + f(t)$ (3.54)

SUM OF PARTICLE DIAMETERS: $\frac{dD_p(t)}{dt} = \frac{D_{pin}(t) - D_p(t) + f(t)d_p(t,t)}{\theta} + 2\lambda\xi(t)N_p(t) - \frac{\mathcal{N}(t)D_p(t)}{3}$ (3.52)

TOTAL PARTICLE SURFACE AREA: $\frac{dA_p(t)}{dt} = \frac{A_{pin}(t) - A_p(t) + f(t)a_p(t,t)}{\theta} + 4\pi\lambda\xi(t)D_p(t) - \frac{2\mathcal{N}(t)A_p(t)}{3}$ (3.51)

TOTAL PARTICLE VOLUME: $\frac{dV_p(t)}{dt} = \frac{V_{pin}(t) - V_p(t) + f(t)V_p(t,t) + \lambda\xi(t)A_p(t) - \mathcal{N}(t)V_p(t)}{\theta}$ (3.46)

MOLECULAR WEIGHT DIFFERENTIAL EQUATIONS

ZEROTH MOMENT $\frac{dQ_0(t)}{dt} = \frac{Q_{0in}(t) - Q_0(t)}{\theta} + k_p[M]_p\bar{Y}(t)(C_m V_p(t) - \frac{K}{[M]_p} Q_0(t))$ (3.81)

1ST MOMENT $\frac{dQ_1(t)}{dt} = \frac{Q_{1in}(t) - Q_1(t)}{\theta} + k_p[M]_p\bar{Y}(t)(1 + C_m)V_p(t)$ (3.82)

TOTAL BRANCH POINTS $\frac{d(Q_0 B_N)(t)}{dt} = \frac{(Q_0 B_N)_{in}(t) - (Q_0 B_N)(t) + k_p[M]_p\bar{Y}(t)[\frac{C_p Q_1(t)}{[M]_p} + \frac{K}{[M]_p} Q_0(t)]}{\theta}$ (3.83)

SECOND MOMENT $\frac{dQ_2(t)}{dt} = \frac{Q_{2in}(t) - Q_2(t)}{\theta} + k_p[M]_p\bar{Y}(t) \left[(1 + C_m)V_p(t) + 2 \cdot \left(\frac{1 + KQ_1(t)/[M]_p V_p(t)}{C_m + \frac{C_p Q_1(t)}{[M]_p V_p(t)}} \right) \left((1 + C_m)V_p(t) + \frac{C_p Q_2(t) + KQ_1(t)}{[M]_p} \right) \right]$ (3.84)

ADDITIONAL FUNCTIONS

NUCLEATION FUNCTION $f(t) = \frac{\rho(t)}{k_v} \left(\frac{k_v A_m + \mu(1 - LA_p/4)}{k_v A_m + \mu(1 - LA_p/4) + k_v \epsilon A_p} \right)$ (3.18)

MICELLAR AREA $A_m = ([S]_{TOT} - [S]_{CMC}) S_{\alpha} N_A - A_p$ (3.16)

GENERATION RATE OF RADICALS IN WATER PHASE $\rho(t) = \rho_i + \rho_{DES}$ (3.13)

RATE OF INITIATION $\rho_i = 2 f_{eff} k_d [I]_w N_A$ (3.53b)

RATE OF RADICAL DESORPTION $\rho_{DES} = k_v \left(\frac{12 \pi D_w \delta K_{fm} f_{eff} k_d N_A}{m k_p} \right)^{1/2} \left(\frac{[I]_w}{k_v A_p(t)} \right)^{1/2} N_p(t)$ (3.53d)

CONSTANT $\lambda = \left(\frac{k_p d_m}{N_A d_p} \right) \left(\frac{k_p m f_{eff} k_d}{12 \pi D_w k_{fm}} \right)^{1/2}$ (3.40)

TIME DEPENDENT FUNCTION $\xi(t) = \left(\frac{\phi(t)}{1-\phi(t)} \right) \left(\frac{[I]_w}{A_p(t)} \right)^{1/2}$ (3.41)

$\eta(t) = 0 ; x \leq x_c$ (3.44b)

$= \left(\frac{(1-c)}{(1-\phi(t))} \right) \left(\frac{1}{1-cx(t)} \right)^2 \frac{dx(t)}{dt} ; x > x_c$

MONOMER VOLUME FRACTION IN POLYMER PHASE $\phi(t) = \frac{1-x_c}{1-x_c c} ; x \leq x_c$ (3.31a)

$= \frac{1-x(t)}{1-x(t)c} ; x > x_c$ (3.31a)

$c = 1 - d_m/d_p$

MONOMER CONCENTRATION IN POLYMER PARTICLES $[M]_p = \phi(t) d_m / MW_{MON}$ (3.32)

AVG. NO. OF POLYMER RADICALS PER PARTICLE $Y(t) = Y_{OT}(t) = \frac{1}{V_p(t)} \lambda \xi(t) \left(\frac{N_A d_p}{k_p d_m} \right) \left(\frac{1-\phi(t)}{\phi(t)} \right) A_p(t)$ (3.88)

3.5 MODEL APPLICATIONS

In order to use the model, it was necessary to obtain good estimates of some of the model parameters. Also, the model as shown did not provide information on the entire particle size distribution. The first two subsections that follow discuss these two problems.

In addition, to further test the model, it was applied to an examination of batch reactor operation and for determining optimal start-up policies for a continuous reactor. These topics are discussed in the final two subsections.

3.5.1 PARAMETER ESTIMATION FOR PSD STATES

Kiparissides (1978) showed that for his model, upon which the present model was based, almost all parameters were available in the literature. The only two parameters required to be estimated were $\delta^1 = \delta D_w$, and ϵ , where D_w is the diffusion coefficient of monomer in the water, δ a lumped diffusion coefficient described in Section 3.4.3 and ϵ , the ratio of the rate constant for radical capture by polymer particles over the rate constant for radical capture by micelles, k_{ab}/k_m . With these two adjustable parameters Kiparissides (1978) was able to simulate the oscillating phenomenon as well as the steady-state levels for the emulsion polymerization of vinyl acetate. The parameter $\mu = k_h/k_m$ was assumed constant at a value of .55 since the model was insensitive to changes of this parameter.

Kiparissides (1978) fit his model to ten experimental runs in order to determine model parameters, and he postulated the parameter ϵ to be a function of soap concentration and δ' to be a function of initiator concentration. However, if the model structure is correct in terms of using collision theory, then the parameter ϵ which is a ratio of rate constants should be constant at a constant temperature and not a function of soap concentration.

For emulsion polymerization, Allen (1955) showed that oxygen can act as an inhibitor for these systems. The residual oxygen at start-up in the water can act to introduce a so-called induction period during which no polymerization takes place due to radical scavenging by the residual oxygen. The data of Kiparissides (1978) show this phenomenon clearly with an induction period of 2/3 to 1 residence time being typical. The data of Keung (1974) for batch emulsion polymerization of vinyl acetate also verified the presence of an induction period.

To examine the parameter variation of ϵ and δ' and include the induction period as a parameter, this study refit the experimental runs of Kiparissides (1978) individually using a non-linear least squares routine UWHAUS to match experimental and predicted conversions. The results are shown in Table 3.1 and summarized in Figures 3.1a,b and 3.2a,b.

TABLE 3.1

PARAMETER ESTIMATES FROM UWHAUS FOR BEST FIT
OF MODEL TO DATA OF KIPARISSIDES (1978)

Residence Time (min)	[I] mole/L	[S] mole/L	S' $\times 10^7$	C.I.* For S'	ϵ	C.I.* For ϵ	T _{IND.} (sec.)	C.I.* For T _{IND.}
30	.01	.01	.77	(.56,.98)	24.4	(7.3,41.5)	720	(486,950)
	.005	.01	3.9	(2.6,5.2)	28.6	(5.4,51.8)	910	(749,1075)
	.01	.06	4.7	(4.2,5.2)	8.4	(4.7,12.1)	1500	(1322,1706)
	.005	.06	9.4	(7.9,10.9)	.9	(.43,1.37)	2870	(2380,3260)
	.01	.04	2.6	(2.3,2.9)	58.6	(2.13,85.9)	1105	(893,1317)
	.01	.02	2.3	(1.8,2.8)	2.4	(1.2,3.6)	600	(370,830)
20	.02	.01	.85	(.71,.99)	24.0	(7.3,40.7)	806	(614,998)
	.01	.01	2.65	(1.8,3.6)	26.9	(11.7,42.1)	485	(280,690)
	.02	.04	1.55	(1.04,2.06)	4.9	(1.9,7.9)	1530	(1380,1680)

* NOTE: C.I. are 95% confidence intervals based on a linear hypothesis estimates as returned from UWHAUS.

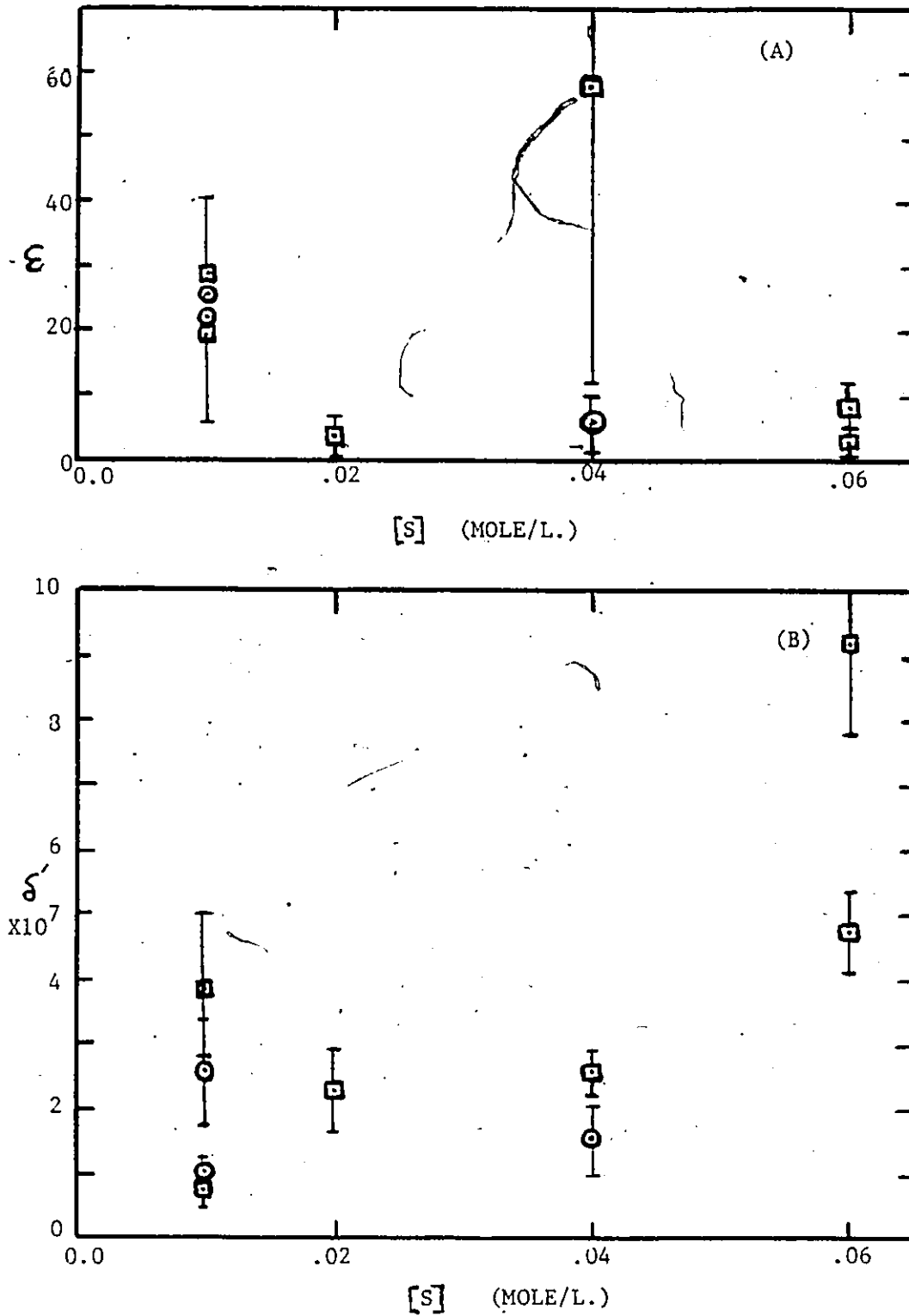


FIGURE 3.1 - Graph of ϵ and δ' from Parameter Estimation versus Soap Concentration $[S]$ for Experiments of Kiparissides (1978)
 ($\square = \theta$ of 30 min. ; $\circ = \theta$ of 20 min.)

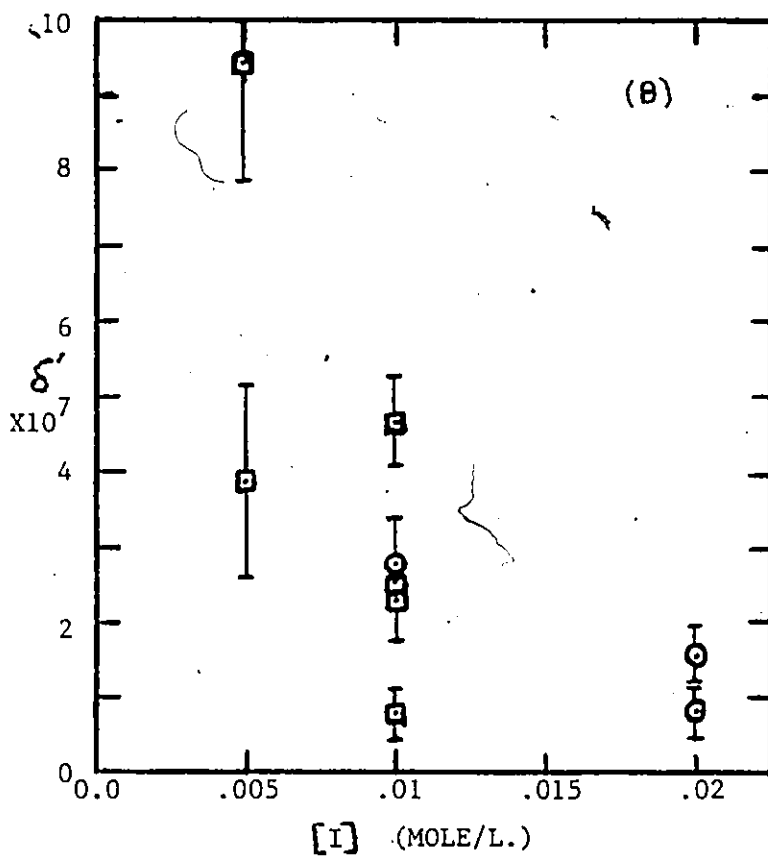
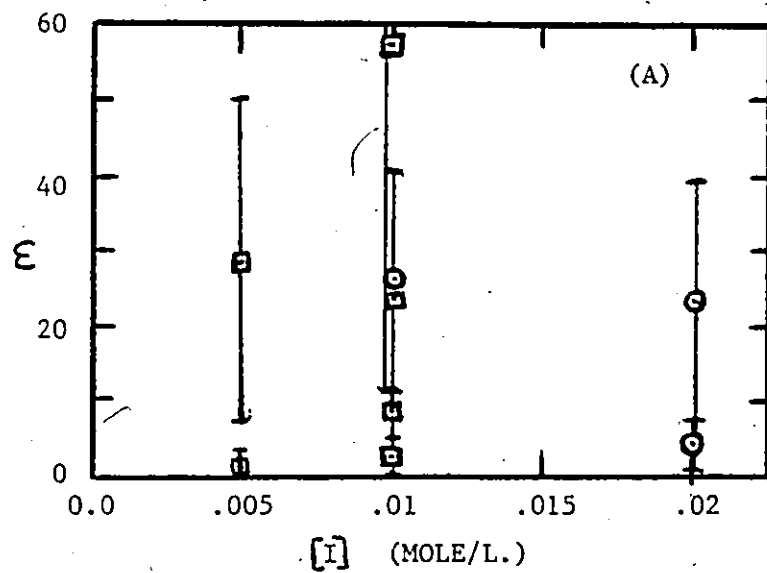


FIGURE 3.2 - Graph of ϵ and δ' from Parameter Estimation versus Initiator Concentration $[I]$ for Experiments of Kiparissides (1978) ($\square = \theta$ of 30 min. ; $\odot = \theta$ of 20 min.)

Using these results, straight lines were fitted to try and link parameters to the two concentrations as found by Kiparissides (1978). The correlation coefficient for regression of ϵ on soap was $r_{\epsilon S} = -.314$ and on initiator was $r_{\epsilon I} = -.042$ while the correlation coefficient for regression of δ' on initiator was $r_{\delta' I} = -.376$ and on emulsifier was $r_{\delta' S} = +.68$. These coefficients indicated very poor fits and were expected considering the scatter found in the data shown in Figures 3.1 and 3.2. In addition, the large variability of ϵ with soap concentration discussed by Kiparissides (1978) was not evident from these estimates.

The induction period parameter was also found to be uncorrelated with the operating conditions and was between 1/2 and 1 residence time for most runs. The reason for the difference between these results was examined by trying various choices of parameter levels in the simulation. It was found that δ' mainly altered the conversion level as shown in Figure 3.3 while ϵ was responsible for altering the period and amplitude of the oscillations as shown in Figure 3.4. The induction period was mainly responsible for start-up transients such as overshoot and time of peak conversion. Since Kiparissides (1978) did not include induction period as a parameter, this was probably responsible for his wide variability in parameters since the estimation routine would only have δ' and ϵ available to compensate for the start-up transient rather than using the correct parameter of induction period to compensate for the initial transients.

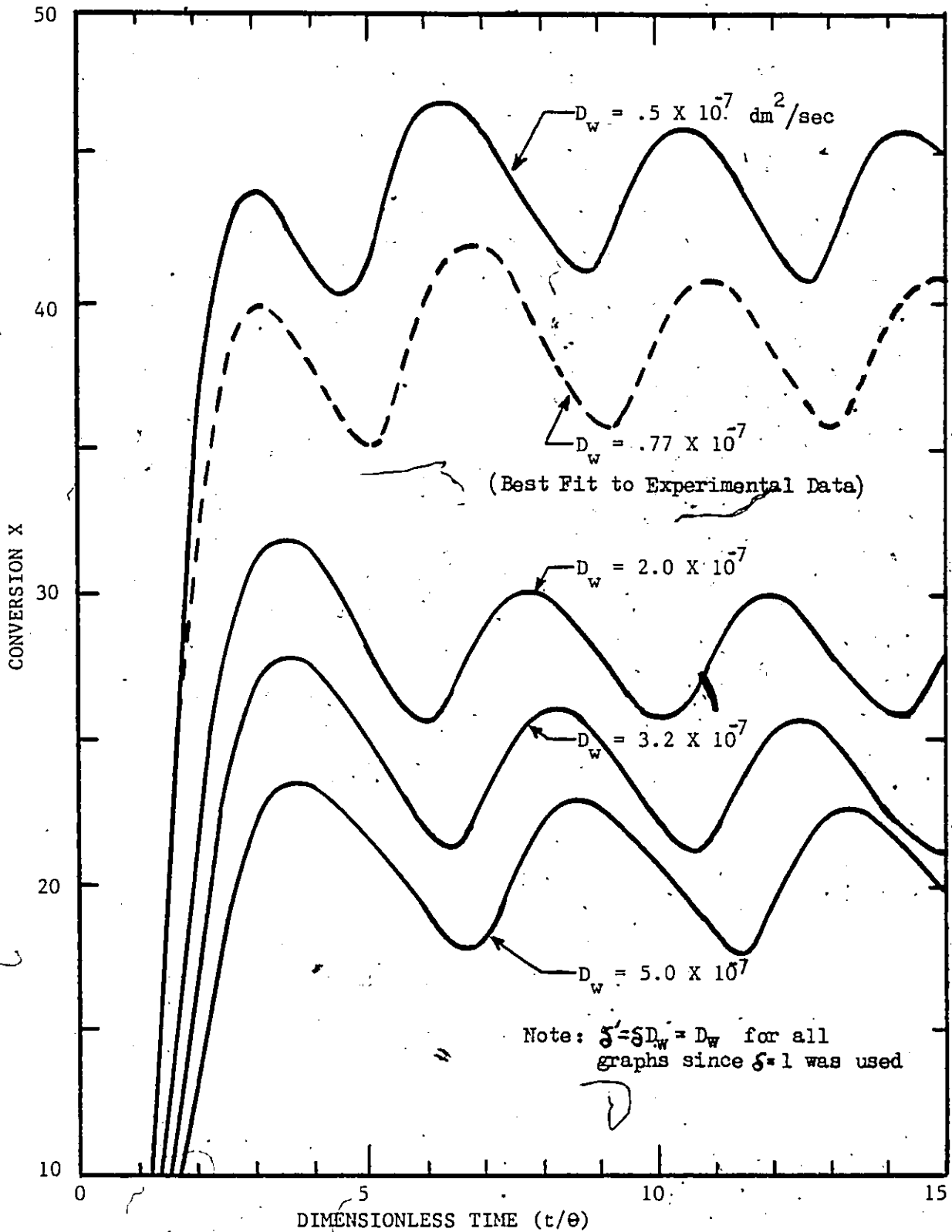


FIGURE 3.3 - Graph of Conversion X versus Dimensionless Time showing Effect of Choice of D_w Parameter on Model Prediction
 ($[I] = .01 \text{ Mole/L.}$, $\delta[S] = .01 \text{ Mole/L.}$, $\epsilon = 24.4$, and $T_{IND} = .50$ for all curves)

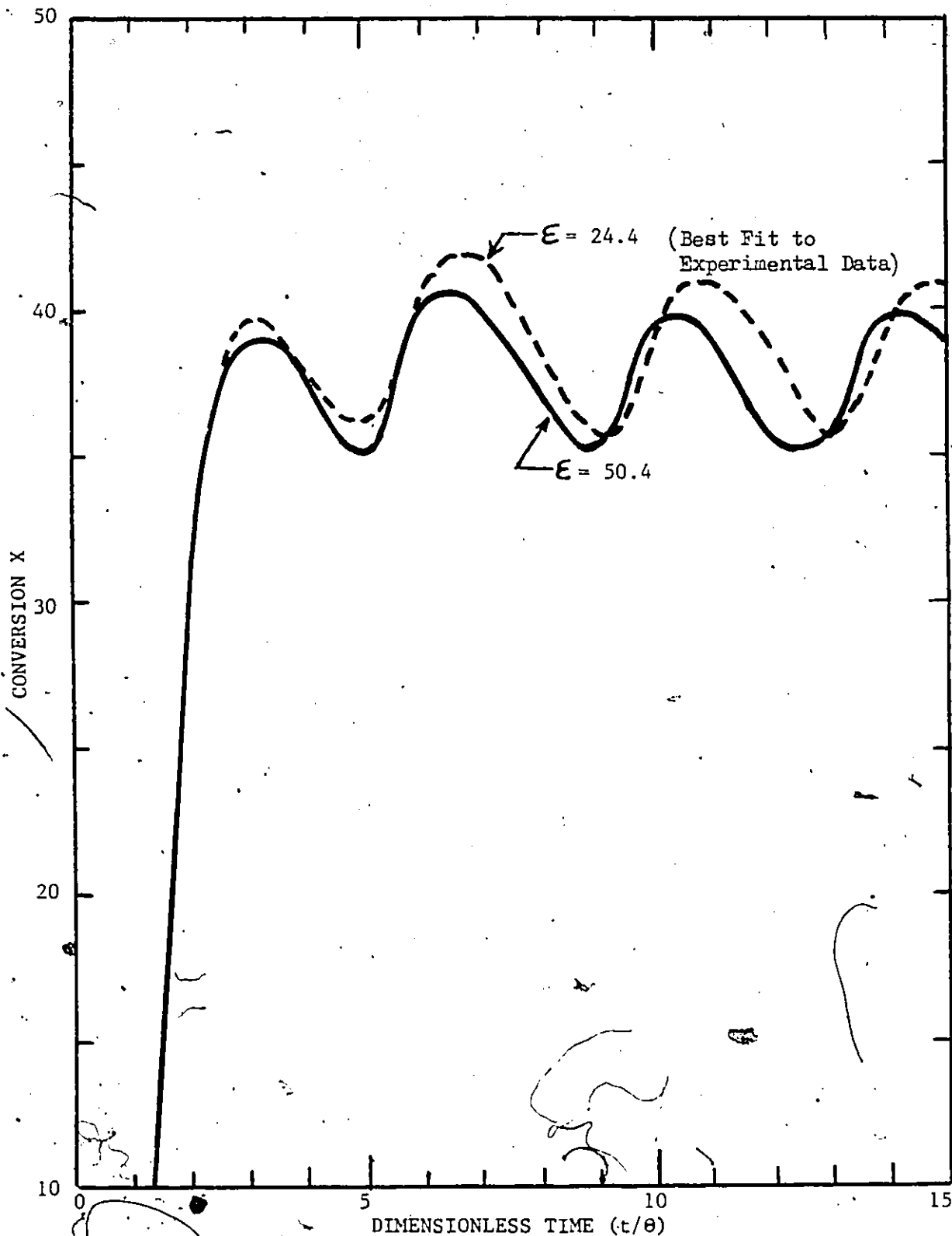


FIGURE 3.4 - Graph of Conversion X versus Dimensionless Time showing Effect of Choice of ϵ Parameter on Model Prediction
 ($[I] = .01$ Mole/L., $[S] = .01$ Mole/L., $D_w = .77 \times 10^{-7}$, and $T_{IND} = .50$ for both curves)

Typical fits by the model after parameter estimation are shown in Figures 3.5 and 3.6. The curves illustrate the excellent fit to the data of Kiparissides (1978) as well as one data set from Greene, et al. (1976). The fit was as good using the revised model including induction period as with the functional dependence form of Kiparissides (1978). The parameter estimates obtained in this section were then used in all further simulation work in this study.

3.5.2 OFF-LINE PREDICTION OF PARTICLE SIZE DISTRIBUTION

A major advantage in using the original model developed by Kiparissides (1978) involving integro-differential equations was the model's ability to calculate the entire particle size distribution at any instant in time. The present model which was developed in Section 3.4 predicts only the particle size averages of the system rather than the entire distribution and if a bimodal or trimodal distribution due to successive generations is present, or if detailed information on the distribution is required, the new model is inadequate compared to the original model. The new model is however much faster in its solution due to the use of ordinary differential equations rather than integro-differential equations. It is the purpose of this section to develop a method of predicting the entire particle size distribution at any time off-line given the history of the model states so that the speed of calculation of the new model can be taken advantage of without a loss of information.

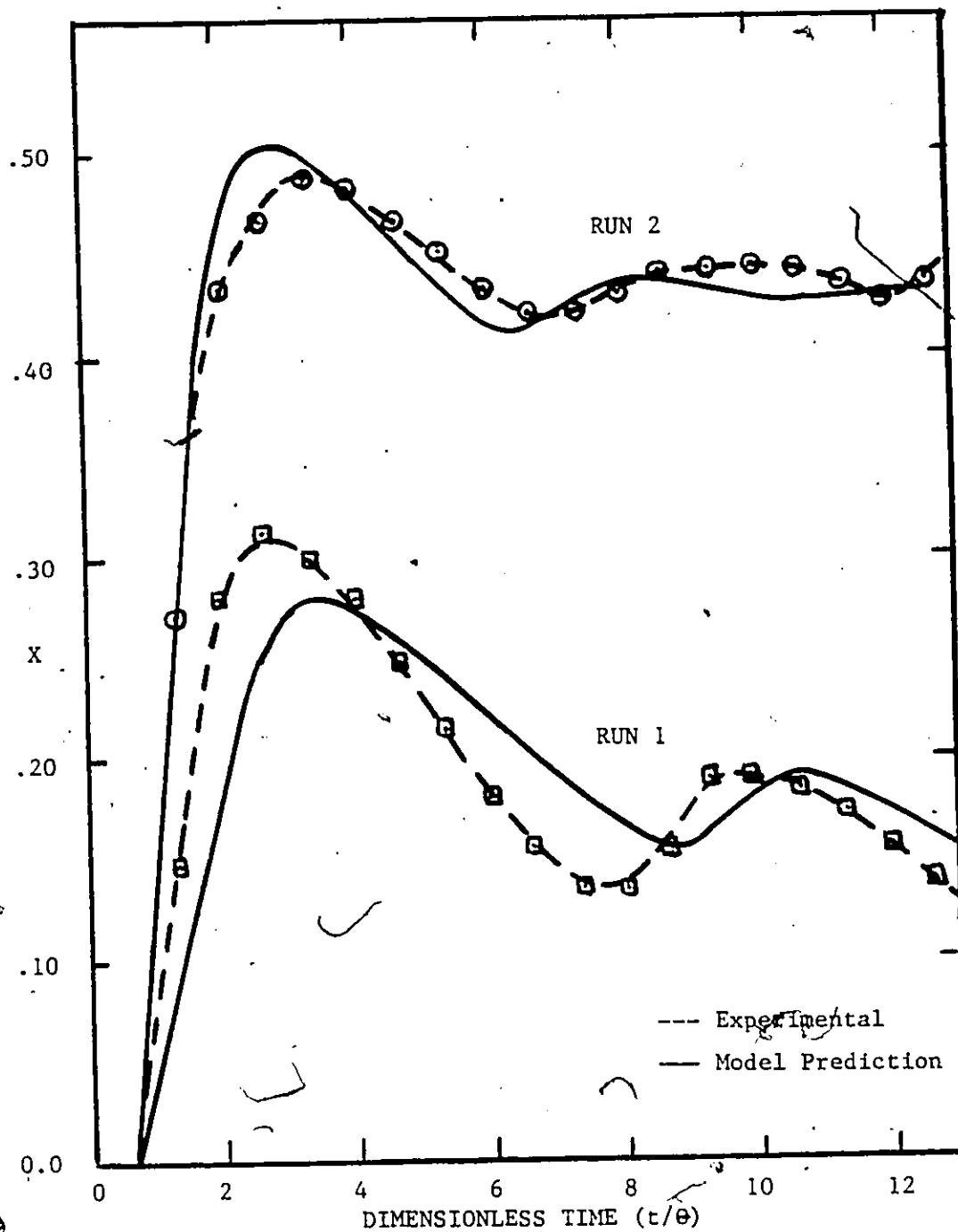


FIGURE 3.5 - Graphs of Conversion X versus Dimensionless Time for two Experiments of Kiparissides (1978) with θ of 30 minutes (Run 1: $[I] = .005$ Mole/L., $[S] = .01$ Mole/L. Run 2: $[I] = .01$ Mole/L., $[S] = .06$ Mole/L.)

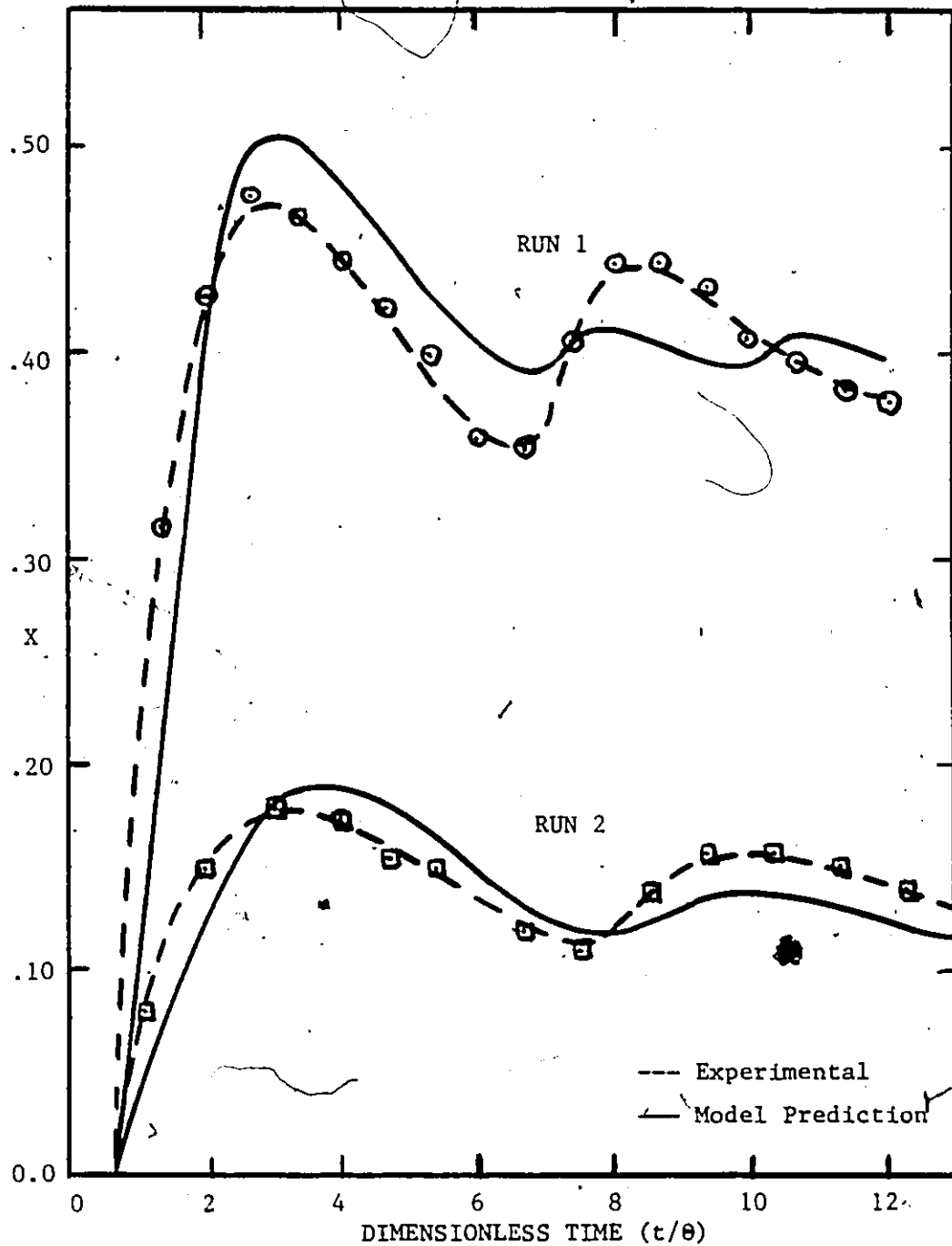


FIGURE 3.6 - Graphs of Conversion X versus Dimensionless Time for θ Of 30 Minutes (Run 1: $[I] = .01$ Mole/L. $K_2S_2O_8$, $[S] = .01$ Mole/L. SLS, Kiparissides (1978); Run 2: $[I] = .01$ Mole/L. $(NH_4)_2S_2O_8$, $[S] = .01$ Mole/L. SLS, Greene et al (1976))

The development was based on equation 3.50 for the rate of growth in diameter for an individual particle of a given class:

$$\frac{d d_p(t, T)}{dt} = 2 \lambda \xi(t) - \frac{\pi(t) d_p(t, T)}{3} \quad (3.50)$$

where $\xi(t) = f$ (conversion, particle area)

$\pi(t) = f$ (conversion)

as shown in Section 3.4.3 in equations 3.42 and 3.45b, respectively.

Using this equation, the diameter of any given particle can be calculated at any given time if the conversion and particle area histories are known for that particle.

To calculate the size distribution, it was also necessary to calculate the number of particles in a given class at its birth time. This was done by taking the difference between the total number of particles at the beginning of a class and the total particles at the end where a class was defined as those particles born during a five-minute time span which was the length of an integration step. The birth time was considered to be the time half way between the endpoints. In this way, the number of particles at birth for a class was given by:

$$n_0(T_i, T_i) = N_p(T_i + 1/2 \Delta t) - N_p(T_i - 1/2 \Delta t), \quad (3.89)$$

where Δt is the integration time step of 5 minutes. Once the number of particles at birth for a class was known, the number of particles in the reactor for that class at a given time $t \geq T_i$ was given by the decay rate for a CSTR as:

$$n(t, T_i) = n_0(T_i, T_i) e^{-(t-T_i)/\theta} \quad (3.90)$$

where θ is the reactor residence time.

Therefore, if the model states N_p , A_p and X were known from the simulations, equation 3.49 provided the diameter of all classes while equations 3.89 and 3.90 provided the number of particles present for that class. In this way the entire particle size distribution was available.

Typical results from this calculation are shown in Figures 3.7 and 3.8. It can be seen that the particle size distribution was usually fairly monodispersed with some small tail, and that when bimodal distributions occur the larger particles represent approximately 1% of the total. This result agreed closely with the model prediction of Kiparissides (1978). Hence, using this procedure, the present model can be analyzed to predict the entire particle size distribution if required.

3.5.3 BATCH REACTOR OPERATION

The model presented in Section 3.4 was also used to simulate a batch reactor for the emulsion polymerization of vinyl acetate. By neglecting the inflow and outflow terms the model was readily adapted to the batch situation.

In order to test the batch simulation, the conversion data of Keung (1974) was fit by using a non-linear least squares estimation package UWHAUS to estimate the parameters δ' and ϵ in a similar manner

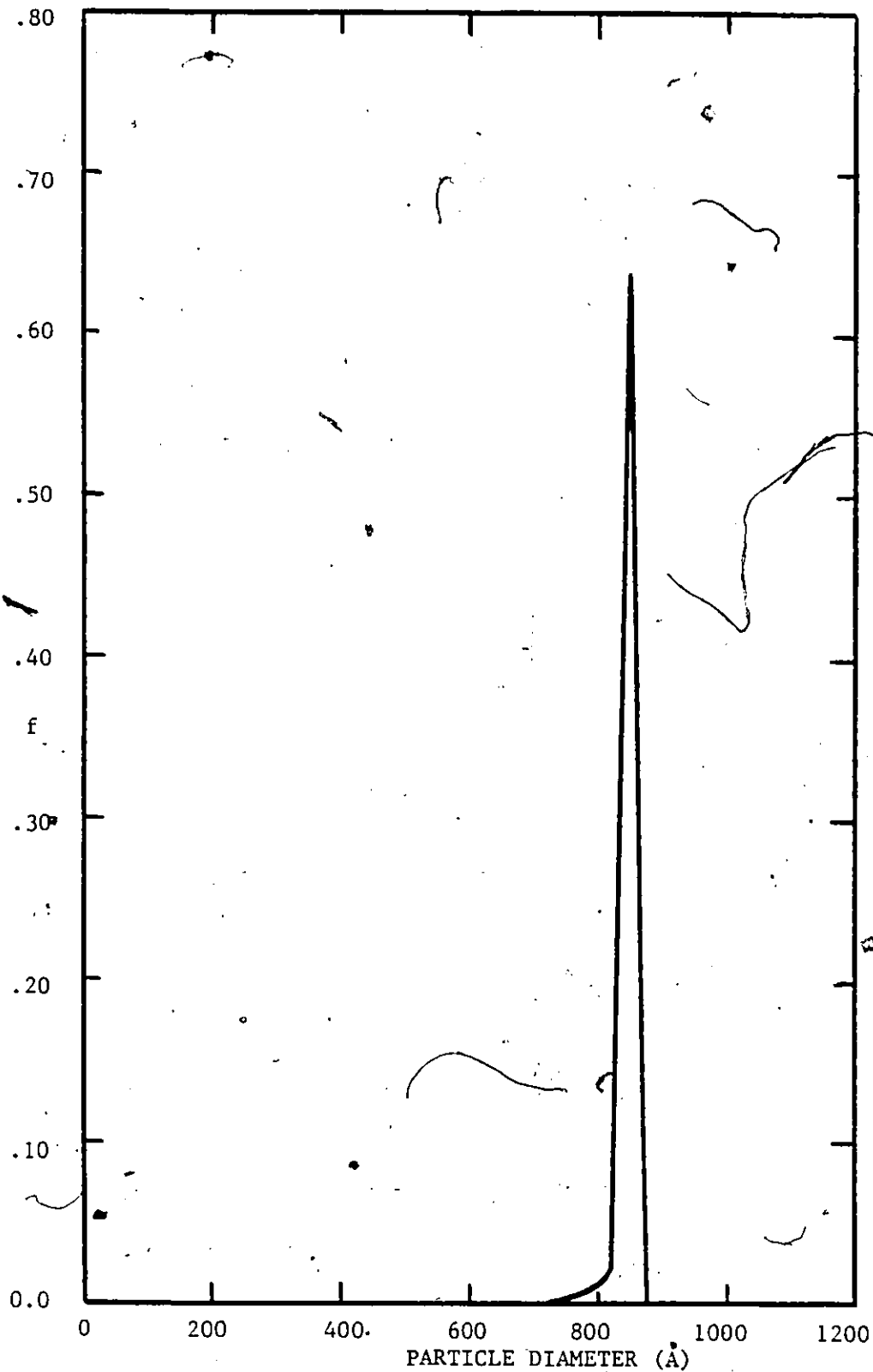


FIGURE 3.7 - Graph of Frequency f versus Predicted Particle Diameter showing Monodisperse PSD for First Particle Generation ($[I] = .01$ M, $[S] = .01$ M, $\theta = 30$ minutes, $t/\theta = 3.5$)

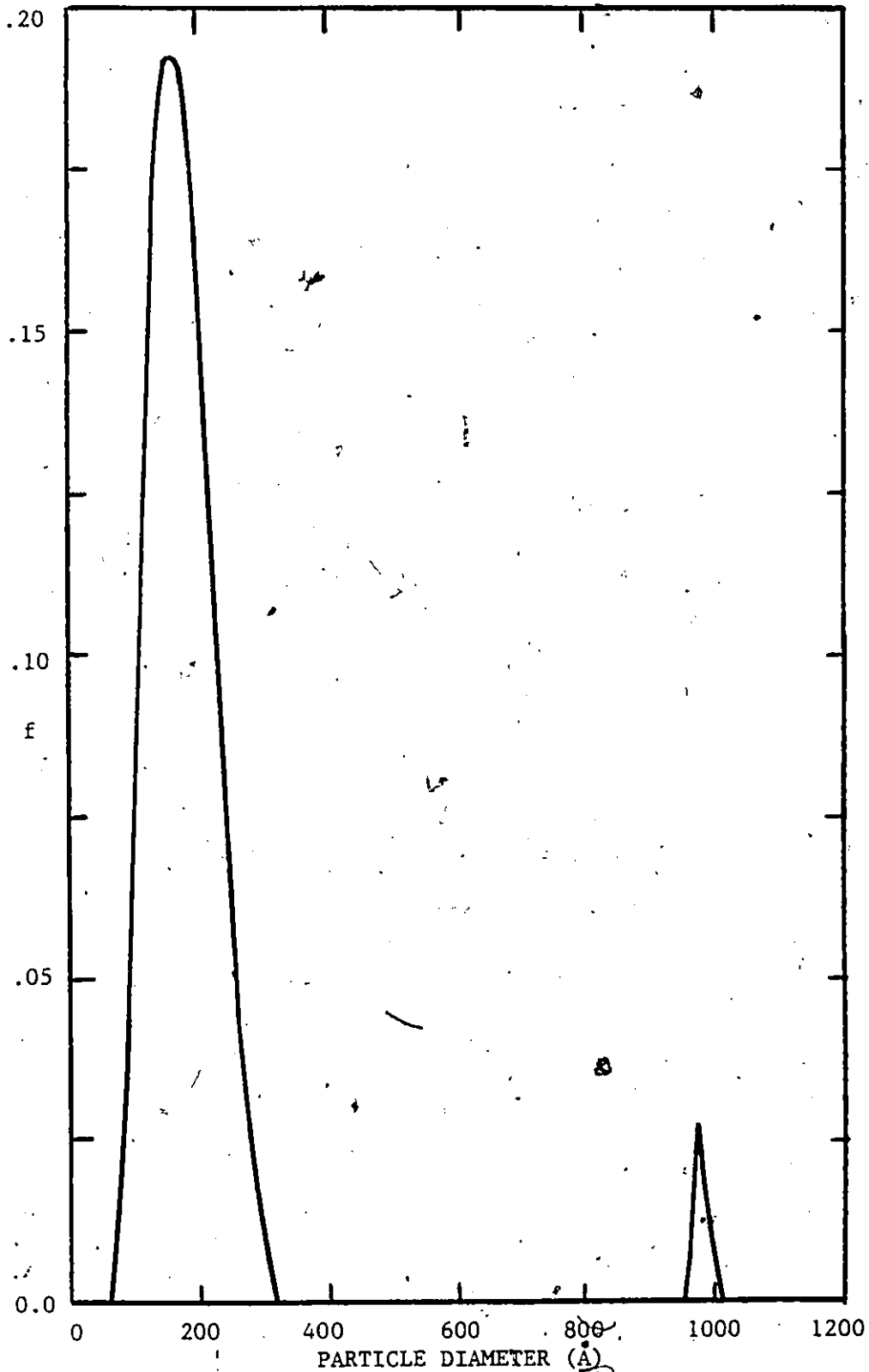


FIGURE 3.8 - Graph of Frequency f versus Predicted Particle Diameter showing Bimodal PSD after Second Particle Generation ($[I] = .01 M$, $[S] = .01 M$, $\theta = 30$ min., $\tau/\theta = 4.9$)

to the continuous case of Section 3.5.1. A typical fit to the data is shown in Figure 3.9 and the parameter estimates are shown in Table 3.2.

The average δ' for the batch case was 5.6, which was reasonably close to the value of $\delta' = 3.2$ found for the continuous reactor case. However, ϵ for the batch case was found to vary widely and were larger than values found for continuous operation. Despite the discrepancy, the model for the batch case fit the conversion data reasonably well as shown in the figure.

One discrepancy noted from the graph was that the prediction lacked the typical S-shaped conversion history which was observed experimentally. Attempts to correct this by including a gel effect were not successful. This was due to the fact that vinyl acetate, because of its high transfer to monomer rate, is not very sensitive to gel effect as shown by Hamielec (1976) and Friis & Hamielec (1974). Better parameter estimates with more data would be needed to ascertain the final reason for this difference.

One further point was noted in these simulations. The simulation of the batch case by Kiparissides (1978) yielded a particle diameter which was continuously increasing, even beyond the value x_c . In actuality, beyond x_c all monomer exists in the polymer particles and water phase and as polymerization proceeds the particles shrink in size due to the difference in density between polymer and monomer. The reason for this inaccuracy was that the simulation of Kiparissides (1978) did not include a term for $d\bar{r}/dt$ in its development as shown in

TABLE 3.2

VALUES OF δ' AND ϵ ESTIMATED USING UWHAUS FOR
FITTING OF MODEL TO BATCH DATA OF KEUNG (1974)

$\frac{[I]}{(M./L.)}$ $\times 10^3$	$\frac{[S]}{(M./L.)}$	$\frac{\delta'}{\times 10^7}$	ϵ
3.33	.04	5.6	145
2.22	.04	2.3	2400
1.65	.04	8.1	20
1.11	.04	3.9	1500
2.22	.02	7.1	24
2.22	.01	6.5	104 ^b

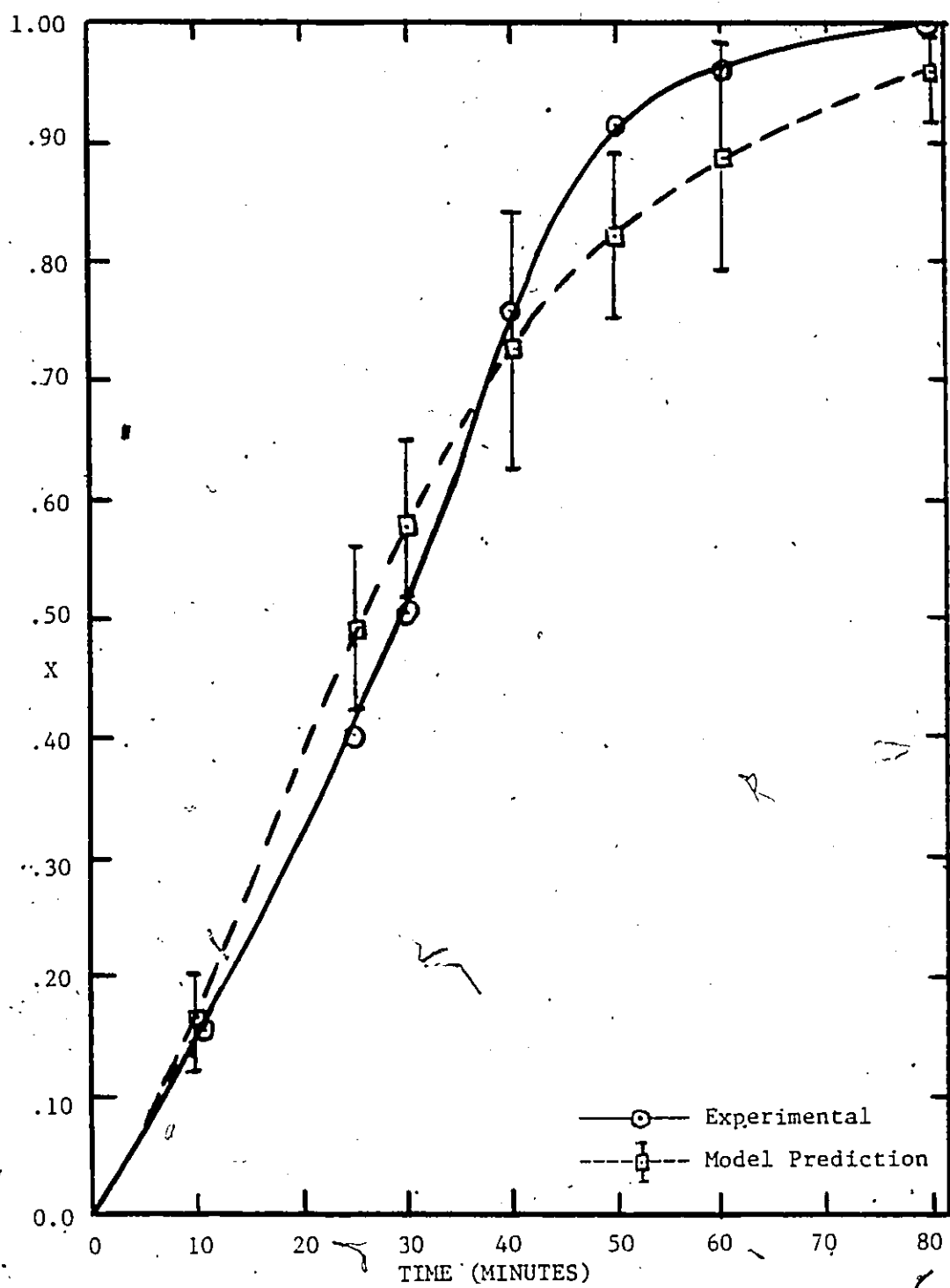


FIGURE 3.9 - Graph of Conversion X versus Time for Batch Model and Experimental Data of Keung (1974)
 ($[S] = 12 \text{ gm./L. SLS}$, $[I] = 3.33 \times 10^{-3} \text{ Mole/L. K}_2\text{S}_2\text{O}_8$)

Section 3.4.3, equation 3.44. This term was usually negligible for continuous operation as dx/dt was small, but in batch operations this term plays a large role in the determination of the states. When this term was included in the batch model, the diameters did decrease beyond x_c as required. This result verified the necessity of including the $d\bar{x}/dt$ term during periods of large conversion changes such as batch operation or during reactor startup situations.

3.5.4 REACTOR STARTUP AND MULTIPLE SEED REACTORS

As part of a fourth year chemical engineering course, several students were required to design a full scale plant for the production of poly(vinyl acetate) latex by emulsion polymerization using a continuous reactor system. While the plant was designed mainly from a steady-state viewpoint, a group of students were assigned to examine reactor operation from a dynamic viewpoint (Bergstra, et al. (1982)) using the model developed in section 3.4. This subsection shows how the model was applied to examine different start-up policies for a single CSTR for the emulsion polymerization of vinyl acetate using a dynamic executive program called DYN SYS for the solution of the equation. This could correspond to the case of startup of the first reactor in a conventional train.

The different start-up policies studied consisted of:

- a) reactor empty followed by flow of raw materials in
- b) reactor with water present (full or part full) followed by

flow

c) reactor with appropriate mix of monomer-soap-water either full or part-full with varying degrees of initial charge of initiator followed by flow

d) reactor with appropriate mix allowed to react for some time in a batchwise manner before flows started.

The determination of "optimal" policy was based on the time required to reach the normal operating levels (i.e. production of on-spec material) plus the amount of overshoot in the system. If the reactor overshoots in conversion by a significant amount, the heat generated during the overshoot may be too great for the heat removal capacity of the reactor leading to runaway conditions. For this reason, the degree of overshoot was also considered as a criterion from a safety standpoint.

The results from these simulations are summarized in Table 3.3 for a residence time of approximately 70 minutes. These results showed that even partial filling of the reactor first by ingredients in the correct ratios can be hazardous as indicated by the large overshoots observed. Also, the start-up times for these systems were at least 25% longer to produce on-spec material in terms of the desired particle diameter than the reactor empty base case. Also found was the fact that for the startup policies using mixtures the coverage by soap of the particles produced dropped from 60% for the empty case to 25-30% for these policies which could indicate agglomeration was a possibility.

The startup policy with water only in the reactor was shown to be optimal in the sense that no overshoot was observed, the time was a minimum and surface coverage remained at 60% for this system. In addition, this startup policy will discard very little raw material since much of the initial washout was water only and not ingredients of the recipe as in the other cases. Thus, the best case indicated that the reactor should be started full with water only for the optimal start-up for the policies examined.

Also studied by use of the dynamic model was the possibility of multiple seed reactors in series to determine if this configuration had any advantages. By keeping the total volume of the seeding section constant, the seeding volume was split into two or three smaller sized reactors and the results examined.

The results indicated that there was no advantage to multiple CSTR seeders for the emulsion polymerization of vinyl acetate since all particle nucleation was found to occur in the first seed reactor only. This was due to the explosive generation of particles in the vinyl acetate system as a result of the high radical desorption rates from polymer particles, and subsequent high radical entry rate into micelles. This would indicate that a PFTR seeder for this system would be small since a longer reactor would have all nucleation done in the early stages and the remaining section would be inefficient since no more nucleation would occur. Since the PFTR would be small, there would be little difference between the use of a CSTR as a small

TABLE 3.3
SIMULATION RESULTS FROM
REACTOR STARTUP STUDIES

<u>Reactor Starting Volume</u>	<u>Starting Contents</u>	<u>Percent Overshoot Based on Conversion</u>	<u>Startup Time* (Min. until On-Spec Diameter)</u>
Empty	-	10	290
40% Full	Water	-	260
60% Full	Water	-	240
Full	Water	-	225
50% Full	Mon.-Soap-Water	23	>360
Full	"	23	>360
50% Full	MSW - 50% Init.	28	>360
Full	"	28	>360
50% Full	MSW - 100% Init.	33	>360
Full	"	34	>360
**50% Full	MSW - 100% Init.	34	>360
**Full	MSW - 100% Init.	35	>360

* = Reactor has approximately 70 min. residence time
 ** = Batch operation first, then flows started

PFTR for production of seeds for the succeeding reactors, and the better mixing of the CSTR would make the CSTR reactor a better choice.

The conclusions from these simulations were that the optimal startup policy was having the initial reactor full of water only. This gave no overshoot and provided minimum time to production of on-spec material.

Also, use of multiple seed reactors was shown to have no advantage for this system due to the rapid particle generation inherent in the system.

3.6 EXTENSION OF MODEL TO STYRENE KINETICS

3.6.1 INTRODUCTION

The dynamic model developed for vinyl acetate emulsion polymerization in section 3.4 applied Case I kinetics in its derivatives. Application of the model as written to styrene was not possible since styrene follows Case II kinetics where there is no desorption of radicals from polymer particles. It is the purpose of this section to extend the model to Case II kinetics and use simulations to examine its predictive utility in applications to styrene emulsion polymerization.

3.6.2 STYRENE CSTR MODELING

Due to lower rates of polymerization and no radical desorption, the rate of production of new polymer particles is slower for styrene

than for vinyl acetate emulsion polymerization. As a result, rather than large oscillations in latex properties, styrene emulsion polymerization usually operates at a steady state. However, experimental evidence by Brooks, et al. (1978) and Gerrens, et al. (1971) and Ley and Gerrens (1968) illustrate that oscillations in latex properties are still possible for many operating conditions.

Many of the models to date such as Ueda, et al. (1971); Omi, et al. (1969), Grancio & Williams (1970) or DeGraff and Poehlein (1971) focus on steady-state models, especially concentrating on the number of particles formed. Nomura, et al. (1971) did develop a dynamic model, but were concerned primarily with the number of particles and did not include equations relating to the particle size distribution of the system.

In an attempt to model the particle size states for styrene emulsion polymerization with oscillations present, the dynamic model of section 3.4.3 was adopted and predictions from the model compared to the data from Brooks, et al. (1978). The adopted model and results are presented in the next section.

3.6.3 STYRENE MODEL DEVELOPMENT

The development for the styrene model followed in a similar way to the vinyl acetate model discussed in section 3.4. The expression for the growth rate of polymer volume in a given class of particles was still given by:

$$\frac{dv(t,T)}{dt} = \frac{k_p [M]_p}{N_A} \bar{q}(t,T) \frac{MW_{MON}}{d_p} \quad (3.31)$$

$$= \left(\frac{k_p d_m}{d_p N_A} \right) \bar{q}(t,T) \Phi \quad (3.34)$$

However, for vinyl acetate emulsion polymerization, the value of $q(t,T)$ was dependent on radical desorption from the polymer particles.

Styrene emulsion polymerization, which follows Case II kinetics rather closely and has no radical desorption due to little transfer to monomer, has a radical concentration of 1/2 for all classes, provided that the conversion is not high and the particles reasonably small (Hamielec (1976), Harris & Hamielec (1981)). This was the case for the simulations comparing Brooks, et al. (1978) data to the model predictions so that $\bar{q} = 1/2$ was used in this study. Again, the particle volume was given by equation 3.43 which upon substitution into equation 3.34 yielded:

$$\frac{dv_p(t,T)}{dt} = \left(\frac{k_p d_m \bar{q}}{N_A d_p} \right) \frac{\Phi}{1-\Phi} - \mathcal{N}(t) v_p(t,T) \quad (3.91)$$

$$\equiv \lambda' \xi'' - \mathcal{N}(t) v_p(t,T) \quad (3.92)$$

$$\text{where } \lambda' = \text{constant} = \frac{k_p d_m \bar{q}}{N_A d_p} \quad (3.93)$$

$$\text{and } \xi'' = \frac{\Phi}{1-\Phi} \quad (3.94)$$

The function $\mathcal{N}(t)$ was the same as for vinyl acetate emulsion polymerization and is given by equation 3.45b.

The general property balance was now applied in the same way as

for vinyl acetate as in section 3.4.3 with the result that the total particle volume differential equation was given by:

$$\frac{dV_p(t)}{dt} = \frac{V_{pin}(t) - V_p(t)}{\theta} + f(t)V_p(t,t) + \lambda' \xi'' N_p(t) - \mathcal{N}(t)V_p(t) \quad (3.95)$$

By following a similar development for the particle area and diameter as done for vinyl acetate, the differential equations for these macroproperties became:

$$\begin{aligned} \frac{dA_p(t)}{dt} = & \frac{A_{pin}(t) - A_p(t)}{\theta} + f(t)a_p(t,t) - \frac{2\mathcal{N}(t)A_p(t)}{3} \\ & + 4 \lambda' \xi'' \int_0^t \frac{n(t,T)}{d_p(t,T)} dt \end{aligned} \quad (3.96)$$

$$\begin{aligned} \frac{dD_p(t)}{dt} = & \frac{D_{pin}(t) - D_p(t)}{\theta} + f(t)d_p(t,t) - \frac{\mathcal{N}(t)D_p(t)}{3} \\ & + 2 \lambda' \xi'' \int_0^t \frac{n(t,T)}{a_p(t,T)} dt \end{aligned} \quad (3.97)$$

where the terms under the integral signs represent a summing over all classes formed both by inflow of material and particle generation in the reactor.

The difficulty with this set of equations was that it was not a closed set. The differential equation which described the D^N th moment (ex. $A \propto D^2$, $V \propto D^3$) had an integral which represented the D^{N-2} th moment. As such, an infinite number of equations would be required to describe the system analytically.

Attempts to solve this system numerically also caused problems. To evaluate the integrals required information about the entire particle size distribution, which as shown by Kiparissides (1978)

required time consuming and complex techniques for the solution of the integro-differential equations. Also, the lowest diameter found for a particle was considered to be micellar size since micellar nucleation was the dominant mechanism. However, this size was only an approximation and was not known accurately for this system. The integrals, though, because of the negative moments, were sensitive to the choice since the negative moments weigh the small sizes most heavily.

In order to avoid these problems, an approximation was made to solve the equations. For the integral terms, the diameter terms in the denominators were assumed independent of the class of particles being considered, that is:

$$\frac{1}{\bar{d}_p(t, T)} = 1/\bar{d}_p(t) \quad (3.98)$$

$$\frac{1}{a_p(t, T)} = \frac{1}{\pi \bar{d}_p^2(t)} \quad (3.99)$$

For a monodispersed latex, this approximation is exact since only one class of particles would be present, all with the same diameter. For a polydispersed system, however, which diameter average is used in the equations becomes important. It was found that the simulation yielded the closest fit if the number average diameter was used in the total diameter equation while the surface average diameter was used in the total area equation. In this way, the area and diameter differential equations used for the model were:

$$\frac{dA_p(t)}{dt} = \frac{A_{pin}(t) - A_p(t)}{\theta} + f(t)a_p(t,t) - \frac{2\eta(t)A_p(t)}{3} + 4\lambda'\xi'' \frac{N_p}{(\bar{d}_s)} \quad (3.100)$$

$$\frac{dD_p(t)}{dt} = \frac{D_{pin}(t) - D_p(t)}{\theta} + f(t)d_p(t,t) - \frac{\eta(t)D_p(t)}{3} + 2\lambda'\xi'' \frac{N_p}{(\pi \bar{d}_N^2)} \quad (3.101)$$

where the diameter averages were calculated as:

$$\bar{d}_N = \frac{D_p(t)}{N_p(t)} \quad (3.102)$$

$$\bar{d}_s = \sqrt{\frac{A_p}{\pi N_p}} \quad (3.103)$$

In this way a set of ordinary differential equations were obtained.

The equations for number of particles, particle generation rate, conversion and initiator and emulsifier balances were the same as for vinyl acetate emulsion polymerization except that no desorption was included in any terms. In this way, the final set of equations used for the styrene emulsion polymerization considering only particle size states were:

$$\frac{dN_p(t)}{dt} = \frac{N_{pin}(t) - N_p(t)}{\theta} + f(t) \quad (3.54)$$

$$\frac{dD_p(t)}{dt} = \frac{D_{pin}(t) - D_p(t)}{\theta} + f(t)d_p(t,t) - \frac{\eta(t)D_p(t)}{3} + 2\lambda'\xi'' \frac{N_p}{(\pi \bar{d}_N^2)} \quad (3.101)$$

$$\frac{dA_p(t)}{dt} = \frac{A_{pin}(t) - A_p(t)}{\theta} + f(t)a_p(t,t) - \frac{2\eta(t)A_p(t)}{3} + 4\lambda'\xi'' \frac{N_p}{(\bar{d}_s)} \quad (3.100)$$

$$\frac{dV_p(t)}{dt} = \frac{V_{pin}(t) - V_p(t)}{\theta} + f(t)V_p(t) + \lambda' \xi'' N_p(t) - \mathcal{R}(t)V_p(t) \quad (3.95)$$

$$\frac{dx}{dt} = \frac{R_p}{[M]_{TOT}} - \frac{X[M]_F}{\theta[M]_{TOT}} \quad (3.10)$$

$$\text{where } f(t) = \frac{\rho(t)}{k_v} \left(\frac{k_v A_m + \mu (1-LA_p/4)}{k_v A_m + \mu (1-LA_p/4) + \epsilon k_v A_p} \right) \quad (3.18)$$

$$\lambda' = \frac{k_p d_m \bar{q}}{N_A d_p} \quad (3.93)$$

$$\xi'' = \Phi(t)/(1-\Phi(t)) \quad (3.94)$$

Other equations and functions are summarized in section 3.5 and are identical for styrene and vinyl acetate.

The molecular weight equations for styrene emulsion polymerization differ greatly from vinyl acetate emulsion polymerization since styrene molecular weight is controlled by termination reactions while vinyl acetate molecular weight is controlled by transfer reactions, especially transfer to monomer (Hamielec (1976)). Due to this difference and the resulting complexity, molecular weight equations for styrene emulsion polymerization were not developed. If chain transfer agent were added in sufficient quantities to make transfer reactions dominant however, the actual model developed for vinyl acetate could thus be used.

3.6.4 SIMULATION RESULTS FOR STYRENE

In the model developed for styrene, only one adjustable parameter ϵ remained for the system. The simulation was run using

literature values for the various kinetic constants (see Appendix IV) with a range of ϵ values with the aim being to duplicate the data presented by Brooks, et al. (1978). The results are shown in Tables 3.4 and 3.5 for an ϵ value of 8×10^{-6} .

The simulation results showed good agreement with data from Brooks, et al. (1978) as far as the average conversion and peak conversions. Runs 14 and 15 showed large discrepancies but since these runs were close in operating condition to run 1 it may have been a difference in inhibitor concentration or some other factor leading to the high conversions shown in the experimental data. Diameters predicted from the model showed similar results compared to the experimental data, but the agreement was not as good as for the conversions. The differences in diameters from one experiment to another was not large and the model was unable to predict these accurately, possibly due to experimental error or the difficulty of what average to use when measuring bimodal distributions which occurred in some cases during oscillations.

One major problem with the model was the fact that no oscillations were predicted in any of the cases for any chosen value of ϵ , where the parameter $\epsilon = k_{ab}/k_m$ represents the rate of capture by polymer particle area versus capture by micellar area. Capture by micellar area should favor oscillations since large generations should be favored with micelles present, but small values of ϵ could not cause the oscillations to occur. Also, the use of $\epsilon = 8 \times 10^{-6}$ in these studies is not realistic, since $\epsilon = k_{ab}/k_m$ and

TABLE 3.4

SIMULATION PREDICTIONS FOR STYRENE MODEL
AS COMPARED TO DATA FROM BROOKS, ET AL. (1978)

Run #	[S]	[I]	EXPERIMENTAL		Oscil.?	Predicted			
	(Mol./L.)	(Mol./L.)	XPEAK	XAVE	Amplit.	Xp	XSS	Osc.?	
1	.0307	.0787	27	14	Y 2	35	15.8	N	
2	.0307	.0255	23	13.5	Y 2	28	15.9	N	
4	.0230	.0511	29	12	Y 4	26	11.5	N	
6	.0307	.042	23	12	N -	31	15.9	N	
*7	.0307	.0093	9.5	7	Y 1.5	23	15.7	N	
8	.0075	.05	11	6	N -	8	2.5	N	
9	.050	.04	38	29	N -	43	27	N	
10	.060	.10	50	45.5	Y 1	53	40.5	N	
11	.060	.05	-	42	N -	49	40.5	N	
12	.023	.025	17.5	11	Y 3	22	11.4	N	
13	.023	.075	29	13	Y 1.5	28	11.4	N	
*14	.0285	.0759	74	35	Y 10	33	14.6	N	
*15	.027	.072	73	31	N -	31	13.7	N	

TABLE 3.5

COMPARISON OF PREDICTED DIAMETERS FROM
THE MODEL VERSUS EXPERIMENTAL DIAMETERS
(BROOKS, ET AL. (1978))

<u>Run No.</u>	<u>[S]</u> mole/L	<u>[I]</u> mole/L	<u>D_{PRED.}</u>	<u>Experimental D</u>
1	.0307	.0787	700	630
2	0 .0307	.0255	700	580
4	.0230	.0511	750	
6	.0307	.042	700	-
7	.0307	.0093	700	-
8	.0075	.05	700	500
9	.050	.04	750	680
10	.060	.10	590	540
11	.060	.05	590	-
12	.023	.025	750	-
13	.023	.075	750	700
14	.0285	.0759	800	1000
15	.027	.072	750	-

should be on the order of 1.0. By setting ϵ so low, it is effectively stating that the nucleation rate equals the rate of initiating which is the maximum possible rate of nucleation for styrene particle nucleation kinetics for this model since no desorption occurs. Reducing ϵ in this system is thus an artificial means of increasing $f(t)$. For this system increasing R_I would also increase $f(t)$ so that the presence of small amounts of impurities such as reducing agents may be the cause of increasing $f(t)$ resulting in oscillations for the styrene system. If $A_m \cong A_p$, the same $f(t)$ would result by decreasing ϵ essentially to zero as done, or increasing the R_I by 10% if $\epsilon = 1.0$. As a result, the oscillations in Brooks, et al. (1978) could be caused by small impurity levels in the system giving rise to a slightly higher R_I than expected.

An alternative model could be developed whereby only the volume differential equation is used with the associated diameter $(6V/\pi)^{1/3}$ and area $(\pi(6V/\pi)^{2/3})$, and not the diameter and area differential equations. Since the deviations from steady-state were assumed to be small, an essentially steady-state particle size distribution would occur. In this way, the particle area could be estimated by a scaling factor applied to the particle volume. The volume average diameter was calculated as:

$$d_V = \left(\frac{6 V_p(t)}{\pi N_p(t)} \right)^{1/3} \quad (3.104)$$

and the polymer particle surface area was estimated as:

$$A_p(t) = \pi d_V^2 \left(\frac{d_S}{d_V} \right)_{S.S.}^2 = \pi d_V^2 f' \quad (3.105)$$

where d_S was obtained from equation 3.103 and f' , the correction factor, was found using the steady-state values of d_S and d_V even if deviations from these values occurred.

This approach corresponds to using a "lumped" model for this system whereby the volume, effectively, is distributed evenly among all particles during changes to the system. During dynamic changes, this approach will not allow the ratio of d_S to d_V to change leading to large errors in surface area calculations. For example, if a generation occurs, a large area is created but only a small volume. In this way, d_S will change dramatically but not d_V so that the true ratio of d_S/d_V also changes by a large extent. The lumped model assumes f' constant so will be in large error.

Results from this second model form are shown in Table 3.6. For larger values of ϵ (10^{-4} to 1) the results paralleled those of the full model. However, with $\epsilon \approx 10^{-5}$, oscillations did occur in the results. The magnitude of these oscillations was too large when compared to the experimental results, and since the simplified model is not accurate if it is used too far from steady-state, the results could not match the experimental data.

TABLE 3.6.

RESULTS FROM SIMPLIFIED MODEL
USING PARTICLE VOLUME ONLY

Data from Brooks, et al. (1978)

Run No.	\bar{X}_{AVE}	D	Osc.?	Amplitude of Conversion Oscillations	Oscillations Predicted with $\epsilon = 8.8-0.6$	
					X	D
1	14	630	Y	2	.18-.33	300-1300
2	13.5	580	Y	2	.17-.30	300-1200
4	12	-	Y	4	.11	700
8	6	500	N	-	.03-.2	600-1500
9	29	680	N	-	.26-.42	300-900
10	45.5	540	Y	1	.39-.57	350-700
11	42	-	N	-	.37-.46	350-700
12	11	-	Y	3	.11-.24	300-1300
13	13	700	Y	1.5	.12-.30	300-1300
14	35	1000	Y	10	.18-.38	350-1300
15	31	-	N	-	.16-.35	300-1300

In conclusion, the results from the full model predicted quite well the average conversion levels and conversion peak levels, and the simulation results were reasonably close on the diameter measurements but were unable to simulate oscillations for the case of styrene emulsion polymerization. A pseudo-steady-state type model which was developed could predict the presence of oscillations but the predicted magnitude made the model inadequate due to large deviations from steady-state.

Due to the difficulty of predicting oscillations with either of the modelling techniques, the method of artificially increasing $f(t)$ by decreasing ϵ may not be the best approach as discussed earlier. Small impurities may be changing R_I causing the oscillations. However, since the conversion predictions were relatively close to the experimental results, this may not be the best approach either.

It may be possible in the future to fine tune the developed model by including neglected terms such as termination in the water phase which may be important for styrene emulsion polymerization (Hawsett, et al. (1981)) and by a better choice of parameters. As well, the approximation made in the model to allow integration should be examined in more detail if a better model of the system is required.

CHAPTER 4
APPLICATION OF ADVANCED CONTROL THEORY
TO CONTINUOUS EMULSION POLYMERIZATION

Continuous emulsion polymerization reactors, as discussed in section 3.2, show a variety of interesting dynamic responses. On start-up, unacceptable overshoot usually results in high conversion which could lead to reactor runaway due to higher heat being generated than the reactor has been designed for at steady-state. Even with steady input conditions, many continuous emulsion polymerization reactors show sustained property oscillations in the product which lead to unacceptable product quality if a narrow distribution of particle sizes or molecular weight is desired. This chapter will investigate the possibility of using optimal control theory to control the continuous emulsion polymerization of vinyl acetate, especially as applied to the phenomenon of sustained oscillations.

4.1 INTRODUCTION

Attempts to apply modern control theory to polymerization systems have had limited success for several reasons.

- i) The complexity of the dynamic model needed to describe polymer reaction systems causes difficulty in formulating low-order dynamic models which adequately describe the system.

ii) Measurement of polymer properties on-line are often difficult to carry out as far as analysis time required, or lack of an instrumental technique for measuring the desired property. For this reason, formulation of objective functions to be minimized is usually very difficult.

iii) The model itself is often highly non-linear such as in the case of emulsion polymerization where the generation terms appear only periodically in the model. For the majority of the time, the generation term is absent from the model, but as a new particle generation begins the generation term enters the model and can dominate the equations of the system, most notably the equation describing the number of particles. This type of model or system is difficult to control by many techniques.

iv) There are often system constraints which limit one's ability to control these systems. For instance, in emulsion systems, the control of the number of particles is probably most easily attained by manipulation of soap levels. However, downstream operations such as stripping usually require that soap levels do not fluctuate very much due to coagulation and foaming problems if soap levels decrease or increase respectively. This limits the amount of control that can be applied practically for these systems.

A general critique of modern control theory has been given by Foss (1973) wherein other problems of any chemical system are also

introduced. In general, he concludes that for a number of reasons, many multi-variable control theories have had little success in actual application. Application of modern control theory to continuous emulsion polymerization reactors for the reasons given above should prove to be even more difficult than for conventional chemical systems. Previous attempts at control of polymerization reactors will be discussed in the next few sections.

4.2 CONTROL OF POLYMERIZATION REACTORS

4.2.1 BATCH REACTOR CONTROL

In the past, the bulk of the attention on controlling polymerization reactors has been on the optimization of batch reactors where the control objective has been to produce a desired product in the minimum possible time. Amrehn (1977) has recently presented a review paper which shows that process control applied to batch systems can yield marked improvements in terms of higher throughput, labor reduction and better product quality.

Past attempts at control of batch polymerization systems has usually focused on calculating an optimal temperature progression for the batch to minimize the end-time by various optimization techniques. Hoftzyer, et al. (1964), Mochizuki and Itoh (1978) and Reimscheussel and Nagasubramanian (1972) have looked at using temperature profile mainly, plus water content to minimize batch time for production of nylon by use of dynamic programming, Pontryagin's Maximum principle and a search of operating conditions while keeping the conversion and

degree of polymerization within specifications. Chen and Jeng (1978) and Sacks, et al. (1973) have also applied the Maximum Principle to the bulk polymerization of styrene to minimize the time to achieve a given conversion and molecular weight. Hicks, et al. (1969) applied the Maximum Principle to a general free radical batch polymerization in an attempt to narrow the molecular weight distribution but concluded that temperature control held little promise of achieving this objective. Osakada and Fan (1970) and Kwon and Evans (1975) used a pattern search method and coordinate transformation technique to determine an optimal temperature profile for achieving the desired conversion and molecular weights in the minimum time. The work by Osakada and Fan (1970) was unique in that the temperature profile was first expressed as a polynomial with the search being carried out for the coefficients of the polynomial for the optimum profile. Macoveneau, et al. (1977) used temperature as the manipulated variable to produce a constant desired rate of polymerization for suspension PVC, while Ray and Gall (1969) used the temperature to compensate for copolymer composition drift for a general copolymerization. In all these cases, the temperature profile was calculated to achieve a desired end point, usually in the minimum time.

Keyes and Kennedy (1974) working on suspension PVC calculated the temperature in a much different manner. They divided the batch into two sections; the first problem being start-up to a desired temperature in the minimum time with no overshoot, the second problem being to control the batch temperature at a constant value despite

state changes or time-varying parameters in the system. In this case, a nonlinear model was developed and adaptive control theory was applied to meet their objective function for the temperature profile.

As an alternative to control by temperature variation, Beste and Hall (1966), Hoffman, et al. (1964) and Osakada and Fan (1970) carried out calculations for the semi-batch case where monomer, initiator or chain transfer agent were fed in continuously over the batch in an effort to control the molecular weight in some manner. Osakada and Fan (1970) applied a temperature and initiator feed rate optimization to keep the average degree of polymerization and variance of the molecular weight distribution constant with the minimum batch time. Beste and Hall (1966) calculated monomer, initiator and chain transfer agent flow rates alone and in combinations to maintain constant degree of polymerization over the course of a batch without regard to end time. Hoffman, et al. (1964) used monomer or initiator as the control variables for the batch also without regard to minimizing the end time.

Several drawbacks can be noted for all of these attempts. First, the majority of these procedures have been carried out with the assumption of simplified kinetics which is usually sufficient for bulk or solution systems. Emulsion kinetics, being more complicated, has not been studied for batch systems in these papers. Second, and perhaps more important, is the lack of experimental work to back up many of these approaches. The majority of methods were usually shown to work in theory for the kinetic scheme assumed but were not

demonstrated experimentally to hold for these systems. Finally, for emulsion polymerization reactors, the number of particles formed is a strong function of the amount of emulsifier present. Control by emulsifier would be a way of controlling emulsion reactor systems, but as mentioned earlier would have detrimental effects on downstream operations.

4.2.2 CONTROL OF CONTINUOUS POLYMERIZATION REACTORS

Control of continuous polymerization reactor systems, especially for emulsion polymerization, has not been studied extensively to date in the literature. Much of the control work as discussed in the previous section has focused on minimizing end time in a batch reactor rather than control of continuous reactor systems. This is primarily due to the difficulty of experimental verification on continuous systems due to the large material requirements, long running times and more expensive set up required by researchers. Many continuous polymerization reactor systems have problems with dynamic phenomena, such as sustained oscillations in continuous emulsion polymerization reactor systems and property overshoot or startup which necessarily must be controlled if continuous reactors are to be used successfully in industry.

Also, in much of the literature, rather than studying dynamic models, many authors analyze continuous reactor systems from a steady-state viewpoint. Shastry, et al. (1973) have applied a system synthesis approach to a bulk styrene polymerization system at steady-state to determine the optimum reactor system configuration. Ray

(1967) has applied peak seeking methods to find the optimum conditions in a chain of CSTR's required to meet design specifications on conversion and polydispersity. Jaisinghani and Ray (1977) have studied the stability of bulk styrene and MMA reactors using bifurcation theory to detect multiple steady states, while Chiang and Thompson (1978) have studied stability for a vinyl acetate emulsion polymerization system by a deviation variable approach.

The literature on control of continuous emulsion polymerization reactors is also limited. Omi, et al. (1969) and Nomura, et al. (1981) optimized reactor train efficiency by maximizing the steady-state number of particles produced in the first reactor of an emulsion polymerization reactor train. Roquemore and Eddy (1961) and Wismer (1965) provided regulator control for a train of SBR emulsion polymerization reactors by temperature control in the reactor chain. Dickenson (1976) examined the optimal start-up of a continuous emulsion polymerization reactor in the shortest time by restriction of particle generation by an optimal soap feed profile.

Two of the more recent attempts at controlling the oscillating region in a vinyl acetate emulsion polymerization reactor were by Leffew and Deshpande (1981) and Kiparissides (1978). Leffew and Deshpande (1980) attempted to apply standard PI control with dead time compensation to the general model of Kiparissides (1978) but their results indicated they had no success with this approach. Kiparissides (1978) applied LQ optimal stochastic control theory to the same problem. His results indicated that this approach could be successful

in damping down the oscillations in the reactor to a large extent. Due to the apparent success of this approach, it was decided to try the same technique on the advanced model to determine the extent of the control which could be attained by the application of LQ optimal stochastic control for vinyl acetate emulsion polymerization.

Two final points should also be noted. In order to control a polymerization reactor, it is necessary to have on-line measurements on the system, and for polymer systems this is usually difficult. As a result, a model of the system must be used to infer states or conditions in the reactor given few measurements. Jo and Bankoff (1976) and Hyun and Bankoff (1976) have shown that by using Kalman filter theory with a model, providing the assumed errors in the model are roughly the same as the measurement error, that Kalman filters can be used successfully to track system states in a polymerization system. The last point is best illustrated in the work by Ahlberg and Cheyne (1977). They implemented an adaptive control scheme for the control of a low temperature continuous butyl rubber polymerization system. They found that 95% of the problems which occur are in the real-time applications of the control theory to the plant due to measurement problems, computer hook-up problems etc. This is a good indication that much of the optimization theory as discussed in the last two sections, even if theoretically reasonable, still should require a real time plant application before it can ever be considered successful for an industrial operation. Amrehn (1977) in his review paper indicated that successful applications have occurred

industrially but that many problems still occur in the practical application of advanced process control theory.

4.3 APPLICATION OF LINEAR QUADRATIC OPTIMAL STOCHASTIC CONTROL THEORY

4.3.1 INTRODUCTION

In order to allow the successful usage of continuous emulsion polymerization systems, a control scheme must be used which has the following capabilities:

- i) Optimal start-up of the reactor to achieve desired steady-state conditions in minimum time but with little or no overshoot to prevent reactor runaway due to excess heat generation.
- ii) Related to this is the optimal change of one production level to another.
- iii) Regulator control of steady-state levels in the face of process disturbances, and with the possibility of sustained oscillations at steady-state as well.

All of these capabilities, for an adequate and robust control system, must hold even in the presence of measurement errors and inaccuracies of the model. Due to the difficulty of on-line process measurements for polymerization systems which means few and noisy measurements, plus model inaccuracies due to the complexity of any emulsion polymerization kinetic scheme, the design of a good control scheme can be quite difficult.

Kiparissides (1978) applied LQ stochastic optimal control theory to his model in an effort to meet these control objectives. His results indicated a fair degree of success in start-up and regulator control so it was decided to repeat this technique on the model of Chapter 3 in order to further evaluate the usefulness of this approach.

By choosing a quadratic cost index with Gaussian noise in the states and measurements, then for a linear system the optimal control of the system can be broken into two parts; state estimation to obtain the best state estimate in the face of noise plus lack of direct process measurements of some states, and a linear feedback control law based on these state estimates. This result, referred to as the separation theorem, means that the estimation and control calculation can be performed independently and combined at the end to achieve the complete control strategy. Thus, the control strategy will have a state estimation followed by a control calculation using these best state estimates and these two steps can be carried out sequentially.

The state estimation and control calculation will be discussed in the next few sections.

4.3.2 MODEL LINEARIZATION AND DISCRETIZATION

The application of stochastic estimation and control theory to a non-linear model results in general in an intractable on-line estimation problem, where search techniques must be applied at each step. To counteract this problem, the model must first be linearized

in some way which allows the direct application of linear stochastic estimation and control theory which can be solved easily on-line. Since a digital computer system will usually be handling the control, often taking action only in set time periods, it is also advantageous to set up a discrete series of equations rather than the continuous form.

The general state-space form of a non-linear model can be written as:

$$\text{System} \quad \dot{\underline{x}} = \underline{f}(\underline{x}, \underline{u}, \underline{k}, t) \quad (4.1)$$

$$\text{Observation} \quad \underline{y} = \underline{h}(\underline{x}, t) \quad (4.2)$$

where \underline{x} is an $(n \times 1)$ vector of states; \underline{k} is a vector of parameters and \underline{y} is a $(m \times 1)$ vector of observations. For the control problem, \underline{u} is a $(r \times 1)$ vector of control variables chosen in such a way that some desired performance index is minimized.

In order to linearize the general equations, several approaches are possible. One of the most common is to expand the model using Taylor series expansion to yield:

$$f(\underline{x}, \underline{u}, \underline{k}, t) \doteq f(\underline{x}_0, \underline{u}_0, \underline{k}, t) + \sum_{j=1}^n \left(\frac{\partial f_i}{\partial x_j} \right) \bigg|_{\underline{x}_0, \underline{u}_0} \nabla x_j + \sum_{j=1}^r \left(\frac{\partial f_i}{\partial u_j} \right) \bigg|_{\underline{x}_0, \underline{u}_0} \nabla u_j \quad (4.3)$$

This approach has two main difficulties. Under sustained oscillations, or under reactor start-up conditions, a steady-state level about which to linearize is a difficult choice. In addition, the model as shown in Chapter 3 is highly complex, and discontinuous

as new generations occur, so that the partial derivatives required are not easily obtained.

An easier approach by factorization of the model has been introduced by Pearson (1962) and used by Weber and Lapidus (1971) and Kiparissides (1978) for his work on emulsion polymerization of vinyl acetate. In this approach, an instantaneously linearized time and state space model is obtained which is of the form:

$$\dot{\underline{x}} = \underline{A} \underline{x} + \underline{B} \underline{u} \quad (4.4)$$

where the matrices \underline{A} and \underline{B} are matrices found by linearization at a certain time. The choice of \underline{A} and \underline{B} is not unique and is carried out by factorization by assuming each derivative is a sum of functions.

$$\dot{x}_i(t) = \sum_{j=1}^n g_{ij}(\underline{x}, \underline{u}, t) + \sum_{k=1}^r p_{ik}(\underline{x}, \underline{u}, t) \quad (4.5)$$

The linearization is carried out by factoring out x_j and u_k from the general functions to yield:

$$\dot{x}_i(t) = \sum_{j=1}^n \frac{g_{ij}(\underline{x}, \underline{u}, t)}{x_j} x_j + \sum_{k=1}^r \frac{p_{ik}(\underline{x}, \underline{u}, t)}{u_k} u_k \quad (4.6)$$

where $\lim_{x_j \rightarrow 0} \left| \frac{g_{ij}(\underline{x}, \underline{u}, t)}{x_j} \right| < \infty$, $\lim_{u_k \rightarrow 0} \left| \frac{p_{ik}(\underline{x}, \underline{u}, t)}{u_k} \right| < \infty$ (4.7)

The coefficient matrices \underline{A} and \underline{B} , both of which are functions of the states, controls and time are thus given as:

$$\underline{A} = \begin{pmatrix} \frac{g_{r1}}{x_1} & \frac{g_{r2}}{x_2} & \dots & \frac{g_{rn}}{x_n} \\ \vdots & \vdots & \ddots & \vdots \\ \frac{g_{n1}}{x_1} & \dots & \dots & \frac{g_{nn}}{x_n} \end{pmatrix}, \quad \underline{B} = \begin{pmatrix} \frac{p_{11}}{u_1} & \dots & \frac{p_{1r}}{u_r} \\ \vdots & \ddots & \vdots \\ \frac{p_{r1}}{u_1} & \dots & \frac{p_{rr}}{u_r} \end{pmatrix} \quad (4.8)$$

Note that by supplying instantaneous values of states and controls, \underline{A} and \underline{B} are then functions of time only. These equations are still non-linear, but the structure gives the appearance of linearity, hence this method can be referred to as apparent linearization by factorization.

Once the linearized state equations are found, discretization is straightforward by assuming the \underline{A} and \underline{B} matrices constant over a period of discretization. Noton (1965) has solved the problem to yield:

$$\underline{x}_{k+1} = \underline{\Phi} \underline{x}_k + \underline{\Delta} u_k \quad (4.9)$$

where

$$\underline{\Phi} = \exp [\underline{A} T] \quad (4.10)$$

$$\underline{\Delta} = \underline{B} \int_0^T \exp (\underline{A}(T-t)) dt \quad (4.11)$$

where T is the discrete time interval being considered.

If the measurement equations are also linearized which is usually easily done for most systems, measurements often being linear combinations of the states, the final equations which result are:

$$\underline{x}_{k+1} = \underline{\Phi} \underline{x}_k + \underline{\Delta} \underline{u}_k + \underline{w}_k \quad (4.12)$$

$$\underline{y}_k = \underline{M} \underline{x}_k + \underline{v}_k \quad (4.13)$$

where \underline{M} is the linearized form of $h(\underline{x}, t)$ in equation 4.2. The matrices $\underline{\Phi}$ and $\underline{\Delta}$ are evaluated by assuming \underline{x} and \underline{u} constant over the discretization interval, and are evaluated through equations 4.10 and 4.11 above.

In this way, equation 4.12 is the linear model of the system with $\underline{\Phi}$ equal to the $(n \times 1)$ linear derivatives where \underline{w} takes account of any model uncertainties or inaccuracies, while equation 4.13 represents the measurements \underline{y} which are some linear combination of the states. In this sense, \underline{v} represents a vector of measurement errors in the system.

4.3.3 STATE ESTIMATION BY KALMAN FILTERING

The Kalman filter provides an optimal estimate of the state vector \underline{x}_k in the sense of minimum mean square error based on information provided by measurements at the current time \underline{y}_k . Even if some states are not directly measured, provided they are observable, the Kalman filter can provide the optimal estimates of these unmeasured states. Jazwinski (1970) has derived the extended Kalman filter so that predictions of the state one step ahead $\hat{\underline{x}}_{k+1/k}$ is calculated using the non-linear model while the filtered estimates $\hat{\underline{x}}_{k/k}$ and covariance matrices depend on the linearized model form. The linearized model can be summarized as shown in equations 4.12 and

4.13 above, and \underline{w} and \underline{v} are assumed to be independent white Gaussian noise vectors with zero mean with their covariances given by:

$$\begin{aligned} E(\underline{w}_k \underline{w}_k^T) &= \underline{R}_w \\ E(\underline{w}_k \underline{v}_k^T) &= 0 \\ E(\underline{v}_k \underline{v}_k^T) &= \underline{R}_v \end{aligned} \quad (4.14)$$

With these results, the extended Kalman filter uses the following equations to obtain a one-step ahead prediction of the states $\hat{\underline{x}}_{k+1/k}$ and the covariance matrix $\underline{P}_{k+1/k}$ for the predicted states as:

$$\hat{\underline{x}}_{k+1/k} = \underline{x}_{k/k} + \int_{t_k}^{t_{k+1}} \underline{f}(\underline{x}, \underline{u}, k, t) dt \quad (4.15)$$

$$\underline{P}_{k+1/k} = \underline{\Phi}_{k+1/k} \underline{P}_{k/k} \underline{\Phi}_{k+1/k}^T + \underline{R}_w \quad (4.16)$$

Once a set (at $k+1$) of observations \underline{y}_{k+1} becomes available, the best state estimates $\hat{\underline{x}}_{k+1/k+1}$ and covariance matrix $\underline{P}_{k+1/k+1}$ are given by:

$$\hat{\underline{x}}_{k+1/k+1} = \hat{\underline{x}}_{k+1/k} + \underline{K}_{k+1} [\underline{y}_{k+1} - \underline{M} \hat{\underline{x}}_{k+1/k}] \quad (4.17)$$

$$\underline{P}_{k+1/k+1} = [\underline{I} - \underline{K}_{k+1} \underline{M}] \underline{P}_{k+1/k} [\underline{I} - \underline{K}_{k+1} \underline{M}]^T + \underline{K}_{k+1} \underline{R}_v \underline{K}_{k+1}^T \quad (4.18)$$

where the Kalman gain \underline{K}_{k+1} is given by:

$$\underline{K}_{k+1} = \underline{P}_{k+1/k} \underline{M}^T [\underline{M} \underline{P}_{k+1/k} \underline{M}^T + \underline{R}_v]^{-1} \quad (4.19)$$

The steps involved in using the extended Kalman filter can be summarized as follows:

i) At a given time period k , use equation 4.15 to evaluate the predicted values of the states $\hat{x}_{k+1/k}$.

ii) Linearize state equations about $\hat{x}_{k+1/k}$ and u_k and discretize according to equation 4.9.

iii) Using these predictions, the Kalman gain is then calculated using equation 4.19, and the $P_{k+1/k}$ matrix by equation 4.16.

iv) As an observation becomes available, the state estimates and covariance matrix are updated using equations 4.17 and 4.18 to calculate $\hat{x}_{k+1/k+1}$ and $P_{k+1/k+1}$.

v) Time step k is incremented by 1 and steps i) to iv) repeated to achieve the full system of state estimates for all k .

4.3.4 GENERAL LINEAR-QUADRATIC STOCHASTIC OPTIMAL CONTROL

Analytical solutions are readily available (Astrom (1970), Macgregor (1973)) to evaluate the control variables for a constrained linear, discrete state space system with constant coefficient matrices and with a quadratic performance criterion. If a set of desired states \underline{x}_d and controls \underline{u}_d are available, the performance index is chosen as:

$$J = E \left(\sum_{k=1}^N [(\underline{x}-\underline{x}_d)^T \underline{Q}(\underline{x}-\underline{x}_d) + (\underline{u}-\underline{u}_d)^T \underline{R}(\underline{u}-\underline{u}_d)] \right) \quad (4.20)$$

where N control actions will be taken to achieve the desired states with the minimum value of this objective function. Q and R are positive semi-definite weighting matrices chosen to penalize state and control deviations respectively.

Kiparissides (1978) has shown that the problem can best be approached by using an augmented state vector \underline{Z} which is composed of the states, and the desired state and control levels as:

$$\underline{Z} = (\underline{x}_n, \underline{x}_n^d, \underline{u}_r^d)^T \quad (4.21)$$

where n desired state levels are set, the rest used as zeros and μ desired control levels are used ($n \leq n, \mu \leq r$). Using this convention, the full states, desired state levels and desired controller levels can be obtained as:

$$\underline{x}_n = [I_{n \times n} \quad 0_{n \times n} \quad 0_{n \times \mu}] \underline{Z} = \underline{C} \underline{Z} \quad (4.22)$$

$$\underline{x}_n^d = [0_{n \times n} \quad I_{n \times n} \quad 0_{n \times \mu}] \underline{Z} = \underline{D} \underline{Z} \quad (4.23)$$

$$\underline{u}_r^d = [0_{r \times n} \quad 0_{r \times n} \quad I_{2_{r \times \mu}}] \underline{Z} = \underline{F} \underline{Z} \quad (4.24)$$

where I_1 and I_2 are matrices having ones in the appropriate positions to obtain the desired state and control values from the \underline{Z} vector and zeros elsewhere.

The state and measurement equations are also augmented as follows:

$$\begin{aligned} \underline{z}_{k+1} &= \begin{pmatrix} \Phi_{n \times n} & 0_{n \times r} & 0_{n \times \mu} \\ 0_{r \times n} & I_{r \times r} & 0_{r \times \mu} \\ 0_{\mu \times n} & 0_{\mu \times r} & I_{\mu \times \mu} \end{pmatrix} \underline{z}_k + \begin{pmatrix} \Delta_{n \times r} \\ 0_{n \times r} \\ 0_{\mu \times r} \end{pmatrix} \underline{u}_k + \begin{pmatrix} \underline{w}_k \\ 0_{n \times 1} \\ 0_{\mu \times 1} \end{pmatrix} \\ &= \underline{\Phi}^* \underline{z}_k + \underline{\Delta}^* \underline{u}_k + \underline{w}_k^* \end{aligned} \quad (4.25)$$

$$\begin{aligned} \underline{y}_k &= [M_{m \times n} \quad 0_{m \times r} \quad 0_{m \times \mu}] \underline{z}_k + \underline{v}_k \\ &= \underline{M}^* \underline{z}_k + \underline{v}_k \end{aligned} \quad (4.26)$$

Kiparissides (1978) has shown that with these assumptions the performance index becomes:

$$J = \mathbf{E} \left(\sum_{k=1}^N (\underline{z}_k^T \underline{Q}_1 \underline{z}_k + \underline{u}_k^T \underline{R} \underline{u}_k + \underline{u}_k^T \underline{V} \underline{z}_k + \underline{z}_k^T \underline{V}^T \underline{u}_k) \right) \quad (4.27)$$

$$\text{where } \underline{Q}_1 = (\underline{C}-\underline{D})^T \underline{Q} (\underline{C}-\underline{D}) + \underline{F}^T \underline{R} \underline{F} \quad (4.28)$$

$$\underline{V} = -\underline{R} \underline{F} \quad (4.29)$$

with the additional constraint that \underline{R} must be chosen symmetric.

The optimal feedback solution to this general problem is given by:

$$\underline{u}_k = -\underline{L}_k \hat{\underline{z}}_{k/k} \quad (4.30)$$

where the \underline{L}_k controller gain matrix is obtained from the recursive set of equations:

$$\underline{L}_k = (\underline{R} + \underline{\Delta}^{*T} \underline{S}_{k+1} \underline{\Delta}^*)^{-1} (\underline{\Delta}^{*T} \underline{S}_{k+1} \underline{\Phi}^* + \underline{V}) \quad (4.31)$$

$$\underline{S}_k = \underline{\Phi}^{*T} \underline{S}_{k+1} \underline{\Phi}^* + \underline{Q}_1 - \underline{L}_k^T (\underline{R} + \underline{\Delta}^{*T} \underline{S}_{k+1} \underline{\Delta}^*) \underline{L}_k \quad (4.32a)$$


$$= \underline{\Phi}^{*T} \underline{S}_{k+1} [\underline{\Phi}^* - \underline{\Delta}^* \underline{L}_k] + \underline{Q}_1 - \underline{V}^T \underline{L}_k \quad (4.32b)$$

where $\underline{S}_N = \underline{Q}_1$ is the initial conditions and the equations are solved from $K = N$ where $N = t_f/T$ with t_f being the final control time down to $K = 1$ which is the present time.

In this way for any general optimal control problem, if N steps are allowed to move from the current state \underline{x} to the desired states \underline{x}_d , equations 4.32 and 4.31 are solved recursively to determine the series of control actions $\underline{u}_N, \dots, \underline{u}_1$ which will achieve this move with the minimum value of the objective function J in equation 4.20. The application of the controller thus uses the best state estimate $\hat{\underline{z}}_K$ provided by the Kalman filter from section 4.3.3. The relative values of the Q and R matrices in the performance index can be chosen to achieve a compromise between the tightness of control over the states and the amount of manipulation allowed to achieve the state control.

4.3.5 APPLICATION OF THEORY TO VINYL ACETATE MODEL

In applying LQ stochastic optimal control theory to the vinyl acetate model, several preliminary choices had to be made regarding controller operation. The number of control actions N allowed to achieve the desired state was chosen to be 10. Too small a value of N forces the controller to take too large an action as it moves from the current state \underline{x} to the desired state \underline{x}_d which can lead to overshoot or too drastic an action. If N is chosen too large, computation time becomes excessive to solve the equations recursively for the large number of steps since at each time step the controller solves from $k=N$ to $k=1$ to find the first control action \underline{u}_1 which is then applied. The value of 10 was thus a compromise used for this study. One other point should be noted. As N tends to infinity, if Q_1 and R are



symmetric positive semi-definite matrices as for this study, then L_k approaches a constant matrix L_∞ . The initial simulation studies indicated that $N = 10$ was a sufficient number of steps from L_k to reach the converged matrix L_∞ to a reasonable degree for this study.

The controller time interval for this study was chosen as $T = 5$ minutes. The decision was made for two reasons. First, the scan time for the UV spectrophotometer which was to be used for particle size information was 5 minutes and was thus a convenient period to assume for controller interval as well. Second, on the CDC 6400 mainframe computer the calculations for each time step were approximately 5 seconds for the controller simulations. Initial tests on the NOVA1200 minicomputer which was hooked up to the process, plus best estimates of scale-up factors in terms of computation time requirements, indicated that 5 minutes would probably be close to the minimum controller interval allowed in order to finish the computations at each time step when using the minicomputer. For these reasons the time interval used was $T = 5$ minutes for the controller time step. With $N = 10$, this meant $t_f = 50$ minutes in these studies, just under two residence times.

During initial simulations, a further problem became apparent. In his control simulations, Kiparissides (1978) used Φ and Δ matrices which were time invariant over the full N steps. These matrices were evaluated at the current conditions \underline{x} and \underline{u} and subsequently held constant. However, the model for this system can be discontinuous with the nucleation terms involving $f(t)$ appearing only for a very

short time period (approximately 5-10 minutes). In this way, if at the current \underline{x} and \underline{u} values no nucleation is occurring ($f(t) = 0$), then by assuming Φ and Δ constant no nucleation would be forecast over any of the next N steps. The controller would thus be unable to compensate at the current time t_k for any future nucleation since it would not be incorporated into the model structure at time t_k . The only time period allowing compensation would be the period during which nucleation was predicted. Since nucleation occurs over a 5-10 minute period and no nucleation occurs over the remaining cycle of 2 hours on a 30 minute reactor residence time, the period when compensation is called for by the controller is very small. During this narrow window the controller does attempt to compensate for a predicted nucleation by reducing emulsifier flow to the reactor, but this action was always too late to have any appreciable effect, and the emulsifier already present would start a massive nucleation anyway as particles were washed out reducing the surface area of the particles in the reactor. In this way, by assuming Φ and Δ constant, control action was taken only during the narrow window when generation was predicted and was insufficient to stop the massive generations which occur.

To eliminate this problem, this study integrated the state equations for N steps and linearized and discretized at each point using the new predicted states. In this way, the Φ and Δ matrices were set constant over each controller time interval but were updated over each of the N steps as the predicted states changed. If a

nucleation was predicted in the next N steps, the Φ and Δ matrices would reflect this change and should introduce a controller action in advance of the nucleation to try and decrease the extent of nucleation and provide better control of the oscillations. However, the computation time using this technique increased dramatically because of the large increase in calculation time required for integrating, linearizing and discretizing at each of the N control intervals for each time step.

The final compromise solution used for this study was a hybrid of the constant and time-varying Φ and Δ methods as follows:

- i) if the current predicted $f(t)$ is zero, assume $f(t)$ will be zero for all N control steps
- ii) integrate the A_p differential equation to determine A_p at t_{K+N} (with no $f(t)$ term, washout dominates leading to the minimum A_p occurring at t_{K+N})
- iii) evaluate A_m at t_{K+N} (maximum A_m occurs at minimum A_p)
- iv) if $A_m > 0$, micelles are present and somewhere between t_k and t_{K+N} a generation would be predicted. In this case, the time varying Φ and Δ matrices approach was used using integration, linearization and discretization at each control time step.
- v) if $A_m < 0$, no micelles are present. All the emulsifier is still being used to cover the polymer particles and insufficient is available for new nucleation. Since the model

changes only gradually if $f(t) = 0$ over the N controller steps, constant Φ and Δ matrices were used for controller computations with Φ and Δ evaluated at the current \underline{x} and \underline{u} values.

This hybrid technique yielded essentially the same result as for the complete time varying Φ and Δ method. Due to the long times between successive generations, the majority of times t_k had $f(t) = 0$ at the current time plus N steps ahead so that the use of the constant Φ and Δ matrices technique reduced the computation time significantly. This hybrid computation method was therefore used in all simulations discussed in this study.

The model used in this study was developed in section 3.4 and the required equations are summarized in section 3.4.5. This work focused on control of conversion in the reactor and since the molecular weight states were unobservable for this system (as shown in section 5.2 on observability) only the particle size states (N_p, D, A, V) conversion and initiator and emulsifier concentrations were included in the control study. The structure of the reactor control scheme is shown in Figure 4.1. Two control streams were assumed to be present, with the initiator control stream having an initiator concentration three times the concentration of the regular initiator stream and the concentrated soap stream concentration being twelve times the soap concentration in the regular monomer-water soap stream. The two

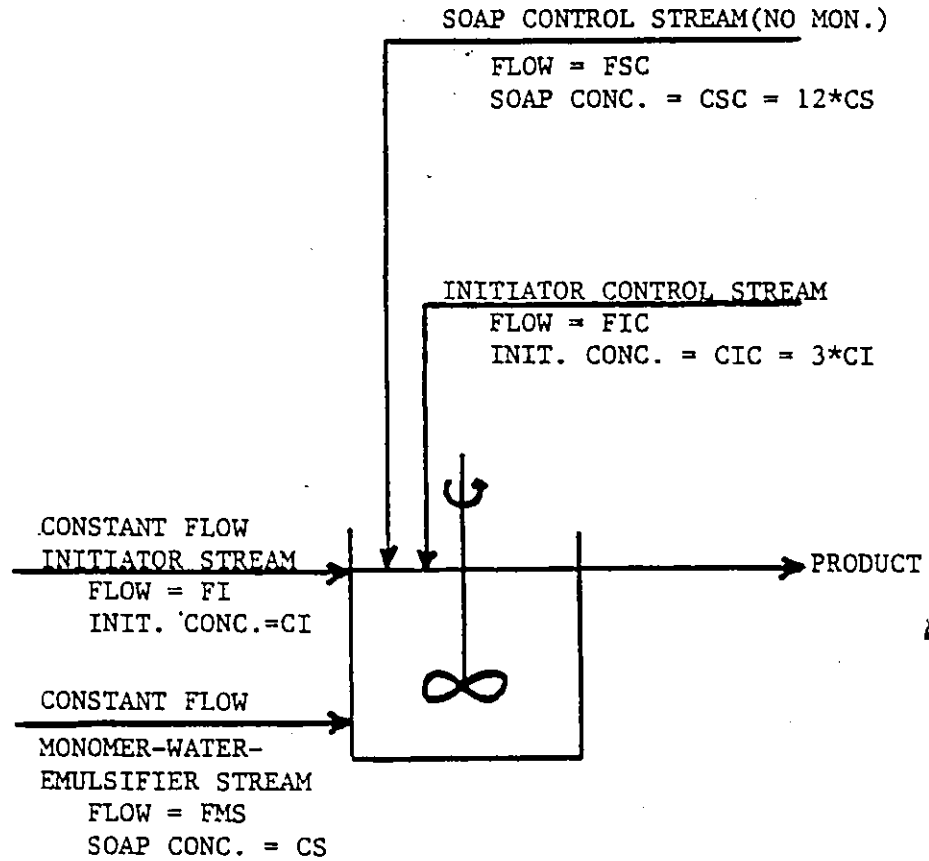


FIGURE 4.1 - Reactor Control Scheme for Application
 of LQ Stochastic Optimal Control Theory

control streams were assumed to be variable flow from zero flow up to the pump limit of 12.5 mL/min. while the regular flows were as shown in the figure and were constant. Using this structure the control variables were the initiator and soap concentration in the total feeds to the reactor as done in Kiparissides (1978) where the control stream flows were calculated to give the desired levels of the control variables.

The non-linear model structure was derived in section 3.4 for vinyl acetate emulsion polymerization. As discussed in section 4.3.2, the model must first be linearized to the form of equation 4.4.

$$\dot{\underline{x}} = \underline{A} \underline{x} + \underline{B} \underline{u} \quad (4.4)$$

Also, as discussed previously, the choice of the \underline{A} and \underline{B} matrices are not unique, and for this study were chosen to provide simplicity of calculation by including only washout terms in the \underline{A} matrix and all remaining terms were placed in the \underline{B} matrix for the control variables. As done by Kiparissides (1978), the coefficients p_{i1} and p_{i2} of equation 4.8 were obtained by halving the terms of each equation. The final result is shown in Table 4.1.

In this linearized form, no inflow of particles was assumed. This form corresponds to the structure used by Kiparissides (1978) and the discretized form of the equations was easily obtained from equations 4.10 and 4.11 as:

$$\underline{x}_{k+1} = \underline{\Phi} \underline{x}_k + \underline{\Delta} \underline{u}_k + \underline{W}_k \quad (4.12)$$

TABLE 4.1
FINAL LINEARIZED VERSION OF THE MODEL

$$\begin{bmatrix} \dot{N} \\ \dot{D} \\ \dot{A} \\ \dot{V} \\ \dot{X} \\ \dot{I}_w \\ \dot{S}_T \end{bmatrix} = \begin{bmatrix} -1/\theta & & & & & & \\ & -1/\theta & & & & & \\ & & -1/\theta & & & & \\ & & & -1/\theta & & & \\ & & & & -1/[\theta(1-\exp(-t/\theta))] & & \\ & & & & & (-1/\theta)k_d & \\ & & & & & & -1/\theta \end{bmatrix} \begin{bmatrix} N \\ D \\ A \\ V \\ X \\ I_w \\ S_T \end{bmatrix}$$

$$+ \begin{bmatrix} \frac{f(t)}{2I_F} & \frac{f(t)}{2S_F} \\ \frac{g_1}{2I_F} & \frac{g_1}{2S_F} \\ \frac{g_2}{2I_F} & \frac{g_2}{2S_F} \\ \frac{g_3}{2I_F} & \frac{g_3}{2S_F} \\ \frac{g_4}{2I_F} & \frac{g_4}{2S_F} \\ 1/\theta & 0 \\ \theta & 1/\theta \end{bmatrix} \begin{pmatrix} I_F \\ S_F \end{pmatrix} + \underline{W}$$

where $g_1 = f(t)d_p(t,t) + 2\lambda\xi N_p - \frac{2\gamma D}{3}$

$g_2 = f(t)a_p(t,t) + 4\pi\lambda\xi D - \frac{2\gamma A}{3}$

$g_3 = f(t)v_p(t,t) + \lambda\xi A - \gamma V$

$g_4 = R_p/[M_F(1-\exp(-t/\theta))]$
from section 3.4.33

$$\text{with } \underline{\Phi} = \exp[\underline{A}T] = \begin{pmatrix} \exp(-T/\theta) & & & & & & \\ & \exp(-T/\theta) & & & & & \\ & & \exp(-T/\theta) & & & & \\ & & & \exp(-T/\theta) & & & \\ & & & & \exp(-T/\theta) & & \\ & & & & & \exp(-T/\theta) & \\ & & & & & & \exp(-T/\theta) \end{pmatrix} = e^{-T/\theta} \underline{I} \quad (4.33)$$

$$\begin{aligned} \underline{\Delta} &= \underline{B} \int_0^T \exp(\underline{A}(T-t)) dt \\ &= \underline{B} \underline{I} \int_0^T \exp(-(T-t)/\theta) dt \\ &= \underline{B}(1/\theta)(1-\exp(-T/\theta))\underline{I} \end{aligned} \quad (4.34)$$

where the term $(1-e^{-T/\theta})$ in the conversion equation was negligible for reasonable time and k_d was small in comparison to $1/\theta$ in the initiator equation. The discretization in this system was thus straightforward where the \underline{B} matrix was assumed constant over the interval of integration.

The choice of \underline{R}_v and \underline{R}_w matrices also required some consideration. Kiparissides (1978) in his control studies added noise to the system so that the measurements were not the same as the states, and his studies also set the variance of the states in the \underline{R}_w matrix to non-zero levels comparable to the measurement noise variance in the \underline{R}_v matrix. However, by carrying out the study in this manner the added noise could mask out the oscillations in the system and Kalman filtering might then smooth out the variation and indicate constant levels when there were still oscillations present in significant amounts.

To separate the filtering problem and control problem in this study the model was first assumed to be completely accurate so that \underline{R}_w was set to zero while a large matrix for measurement noise (\underline{R}_v having diagonal elements of 10) was introduced. In this way the advanced control was examined as applied to a perfect model, and any inadequacies in the control section would thus be more apparent.

4.3.6 SUMMARY

From the previous sections, the flowsheet for solving the control problem using LQ stochastic optimal control theory is shown in Figure 4.2. (This work assumed a perfect model so that \underline{R}_w was a null matrix. \underline{R}_v was chosen diagonal and large in the diagonal elements so that measurements for the study were effectively ignored. The simulation results based on these structural considerations will be discussed in the following section.

4.4 SIMULATION RESULTS

The difficulty in carrying out control simulations is the knowledge of \underline{Q} and \underline{R} values in order to control the system in some optimal manner. In an effort to track only conversion correctly, at least initially, no penalties were placed on any other property deviation so that \underline{Q} only had a single value at q_{55} . For this system the q_{55} penalty or conversion was chosen as 1.0 and the r_{11} and r_{22} penalties on deviations from initiator and emulsifier setpoints were relative to this as mentioned in section 4.3.4.

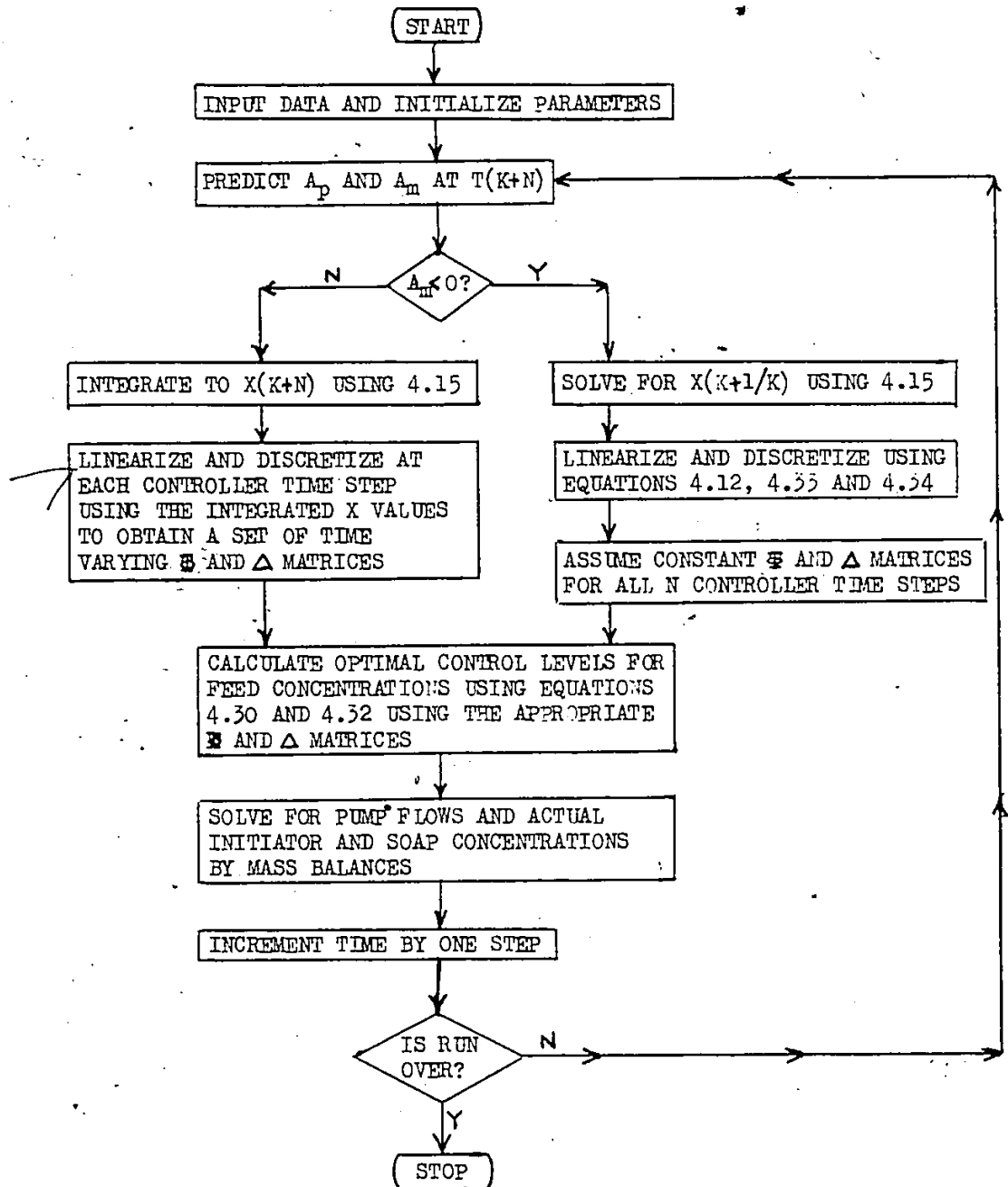


FIGURE 4.2 - Flowsheet for Application of LQ Stochastic
Sub-Optimal Control Theory

Simulations were carried out over a very wide range of r_{11} and r_{22} values and over a large range of the ratios of these quantities. The larger these values the tighter the concentrations should hold about the setpoint. If the ratio is large between the two, the control variable less tightly constrained will carry out the majority of the control action.

Some of the "best" simulation results are shown in Figures 4.3 to 4.5 where the setpoints were $x_d = .45$, $[I]_d = .01$ mole/L latex, and $[S]_d = .01$ mole/L latex. The results differed drastically from those of Kiparissides (1978). His optimal R matrix with $r_{11} = 700$ and $r_{22} = 3$ was completely unacceptable for this simulation. Penalties on the control variables were required to be much higher in these simulations than the results of Kiparissides (1978). The penalties for these simulations are summarized in Table 4.2 below.

TABLE 4.2
PENALTY MATRIX VALUES FOR CONTROL SIMULATIONS

	r_{55}	r_{11}	r_{22}
CASE I	1.0	20,000	2,000
II	1.0	20,000	5,000
III	1.0	10,000	50,000

Case I illustrated that for a high initiator penalty and lower emulsifier penalty, the initiator did the majority of fluctuating and

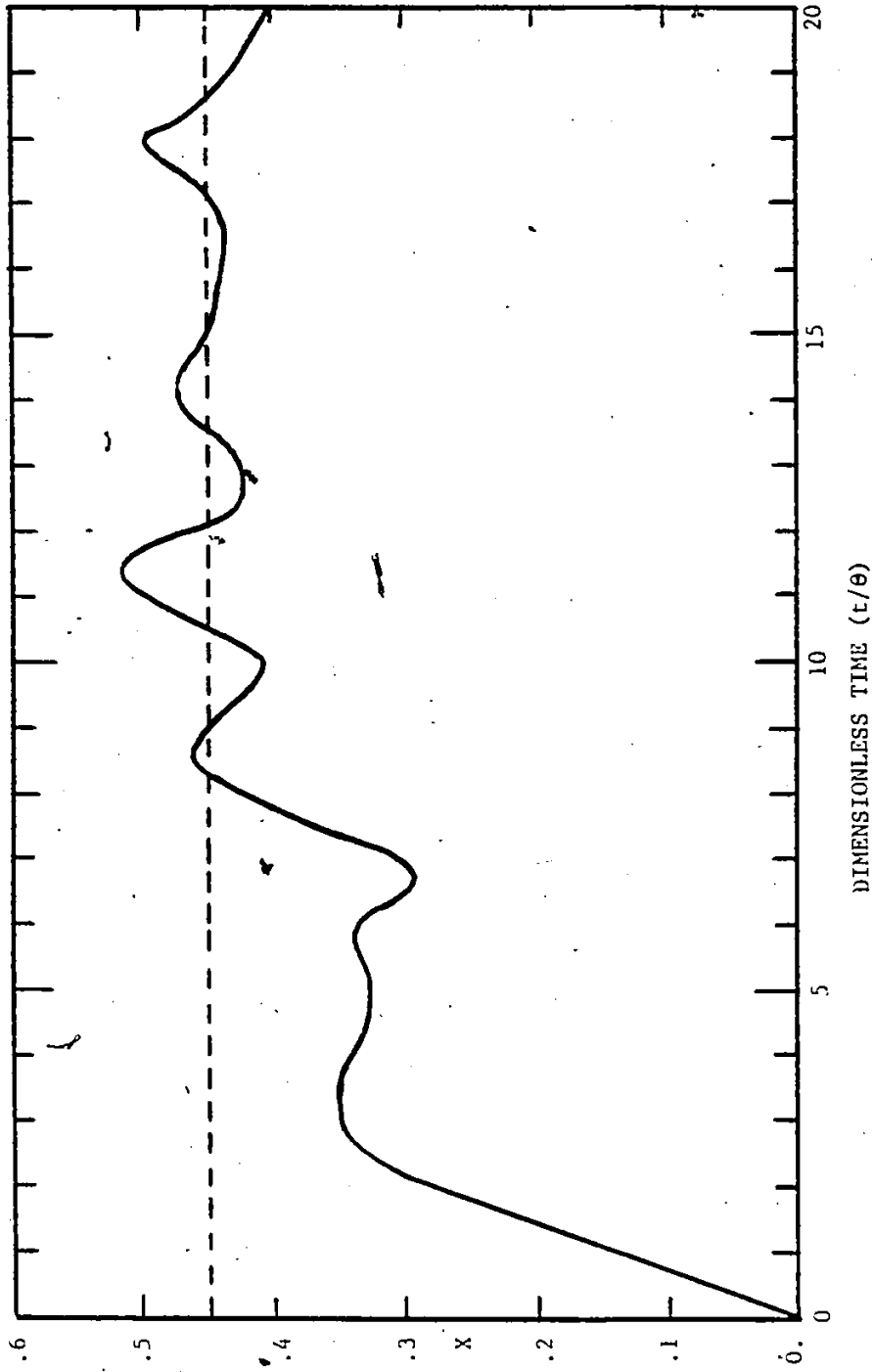


FIGURE 4.3a - Graph of Conversion X versus Dimensionless Time for $r_L=20,000$, $r_S=2,000$
 (where $[I]_d=.01$ mole/L., $[S]_d=.01$ mole/L., $\theta=30$ min., $x_d=.45$)

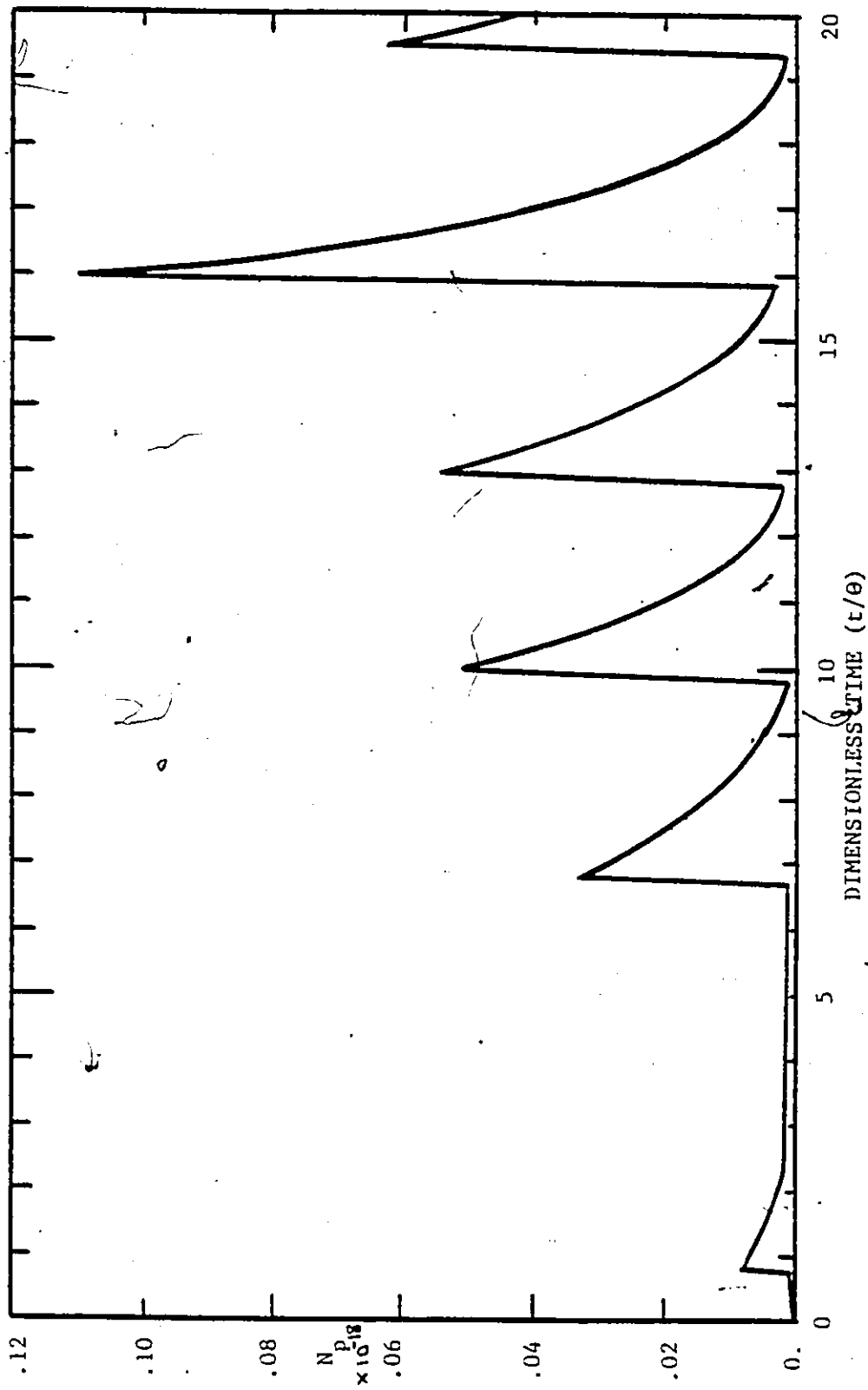


FIGURE 4.3b - Graph of Number of Particles N_p versus Dimensionless Time for $r_I=20,000$, $r_S=2,000$ (where $[I]_d = .01$ mole/L., $[S]_d = .01$ mole/L., $\theta=30$ min., $x_d = .45$)

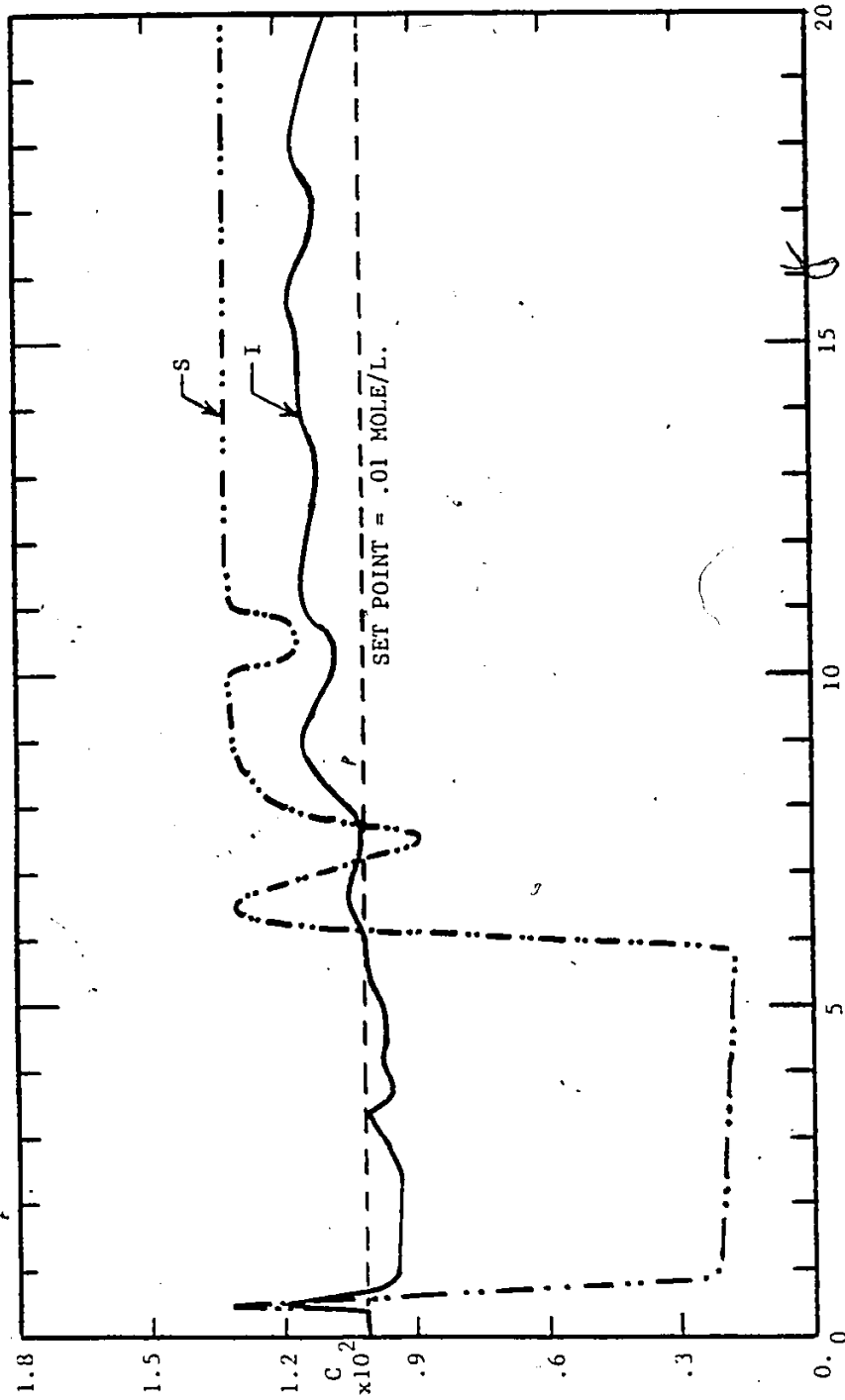


FIGURE 4.3c - Graph of Initiator and Emulsifier Concentrations C versus Dimensionless Time for $r_I = 20,000$, $r_S = 2,000$ (where $[I]_d = .01$ mole/L., $[S]_d = .01$ mole/L., $\theta = 30$ min., $x_d = .45$)

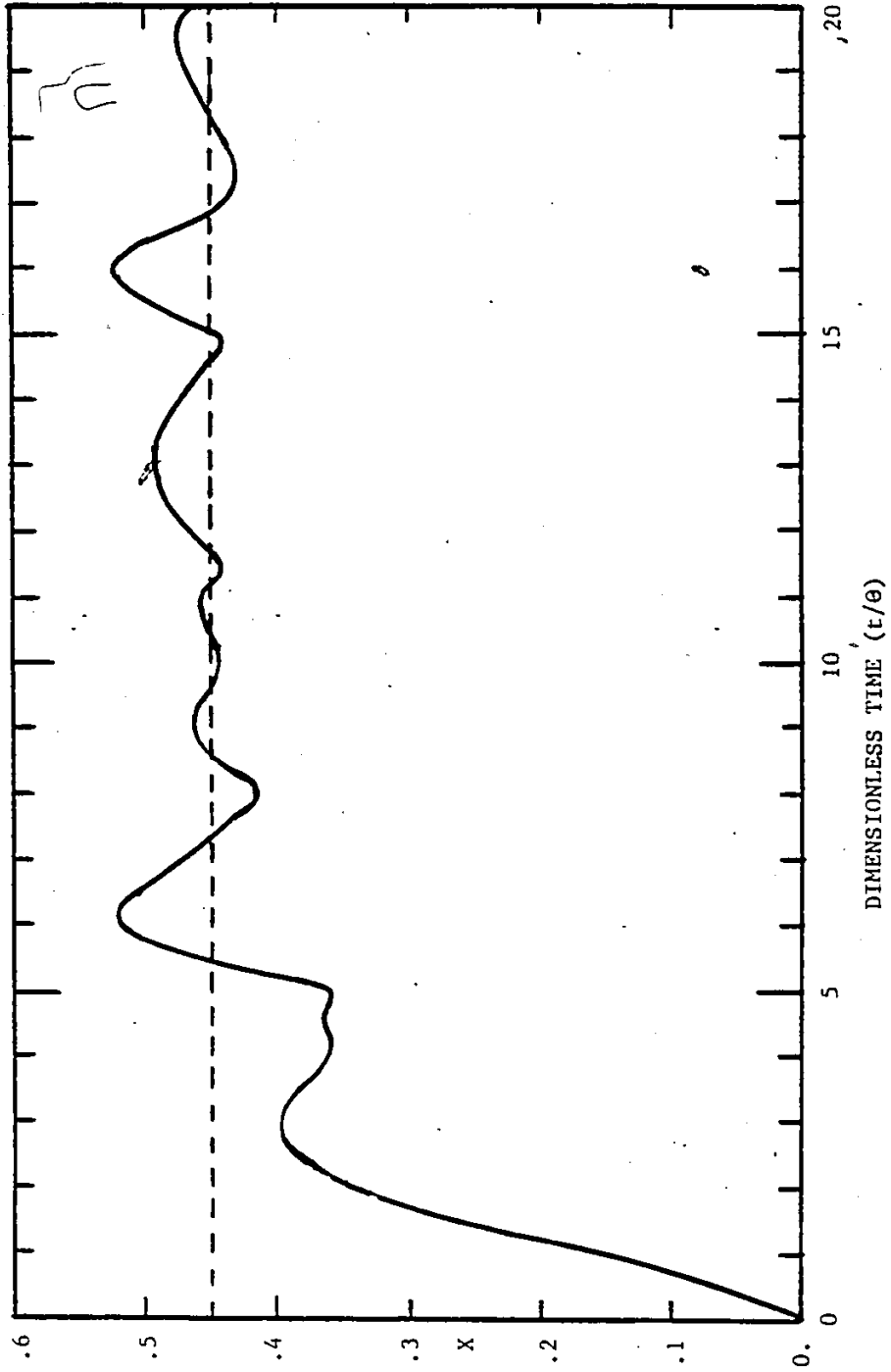


FIGURE 4.4a - Graph of Conversion X versus Dimensionless Time for $r_I = 10,000$, $r_S = 5,000$
 (where $[I]_d = .01$ mole/l., $[S]_d = .01$ mole/l., $\theta = 30$ min., $x_d = .45$)

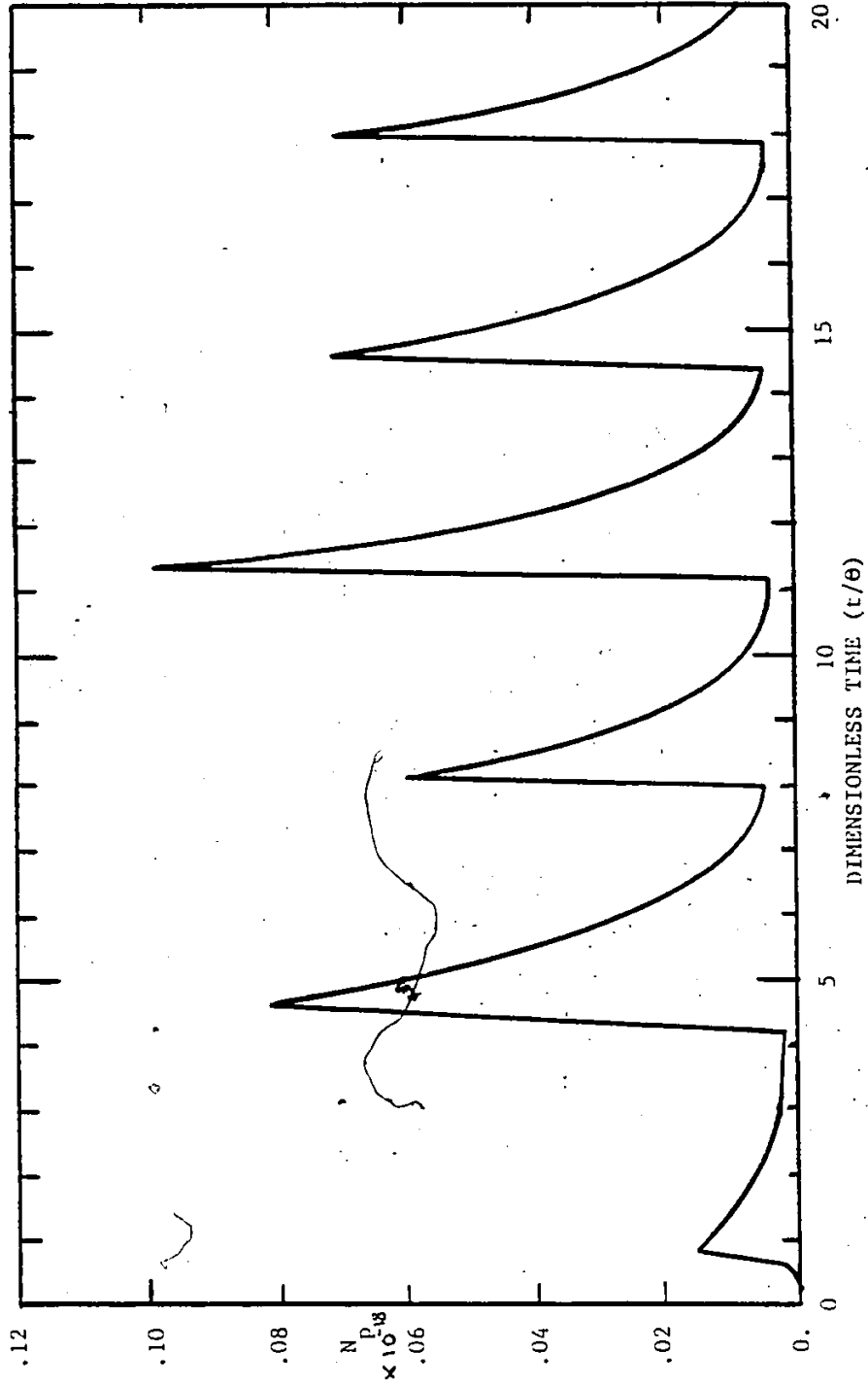


FIGURE 4.4b - Graph of Number of Particles N_p versus Dimensionless Time for $r_I=10,000$, $r_S=5,000$ (where $[I]_d=0.01$ mole/L., $[S]_d=0.01$ mole/L., $\theta=30$ min., $x_d=.45$)

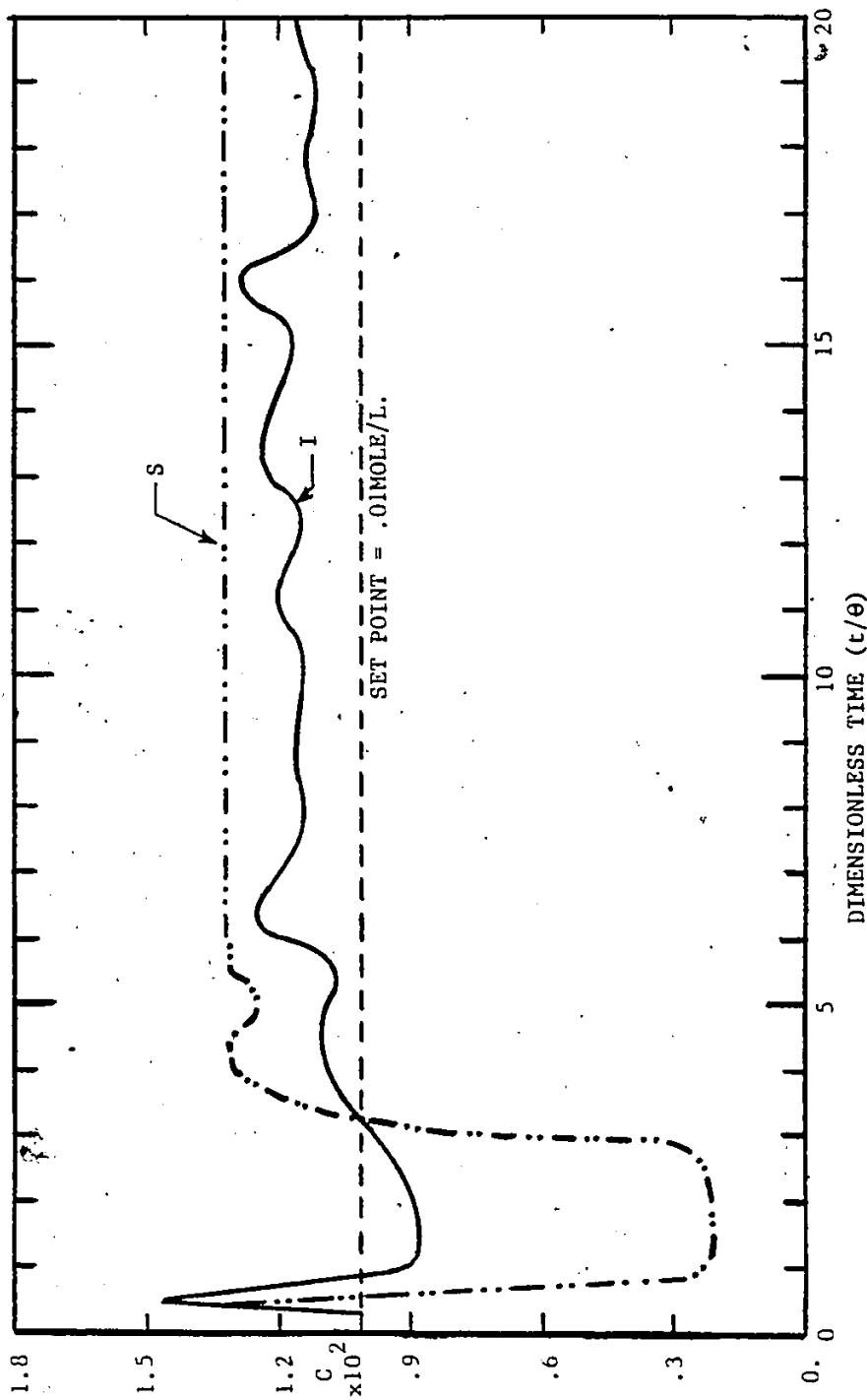


FIGURE 4.4c - Graph of Initiator and Emulsifier Concentrations C versus Dimensionless Time for $r_I = 10,000$, $r_S = 5,000$ (where $[I]_d = .01$ mole/L., $[S]_d = .01$ mole/L., $\theta = 30$ min., $x_d = .45$)

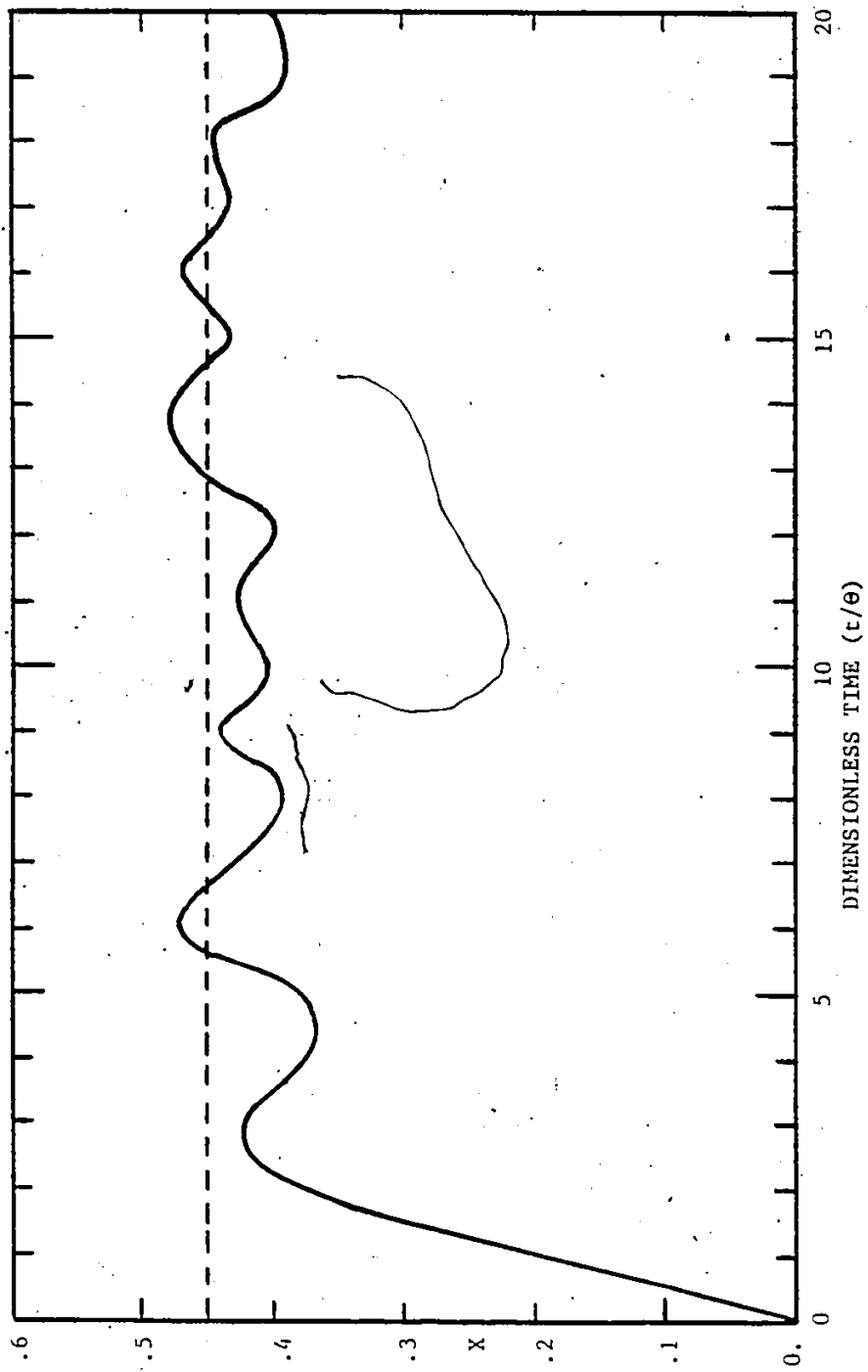


FIGURE 4.5a - Graph of Conversion X versus Dimensionless Time for $r_I=10,000$, $r_S=50,000$
 (where $[I]_d=0.1$ mole/l., $[S]_d=0.1$ mole/l., $\theta=30$ min., $x_d=.45$)

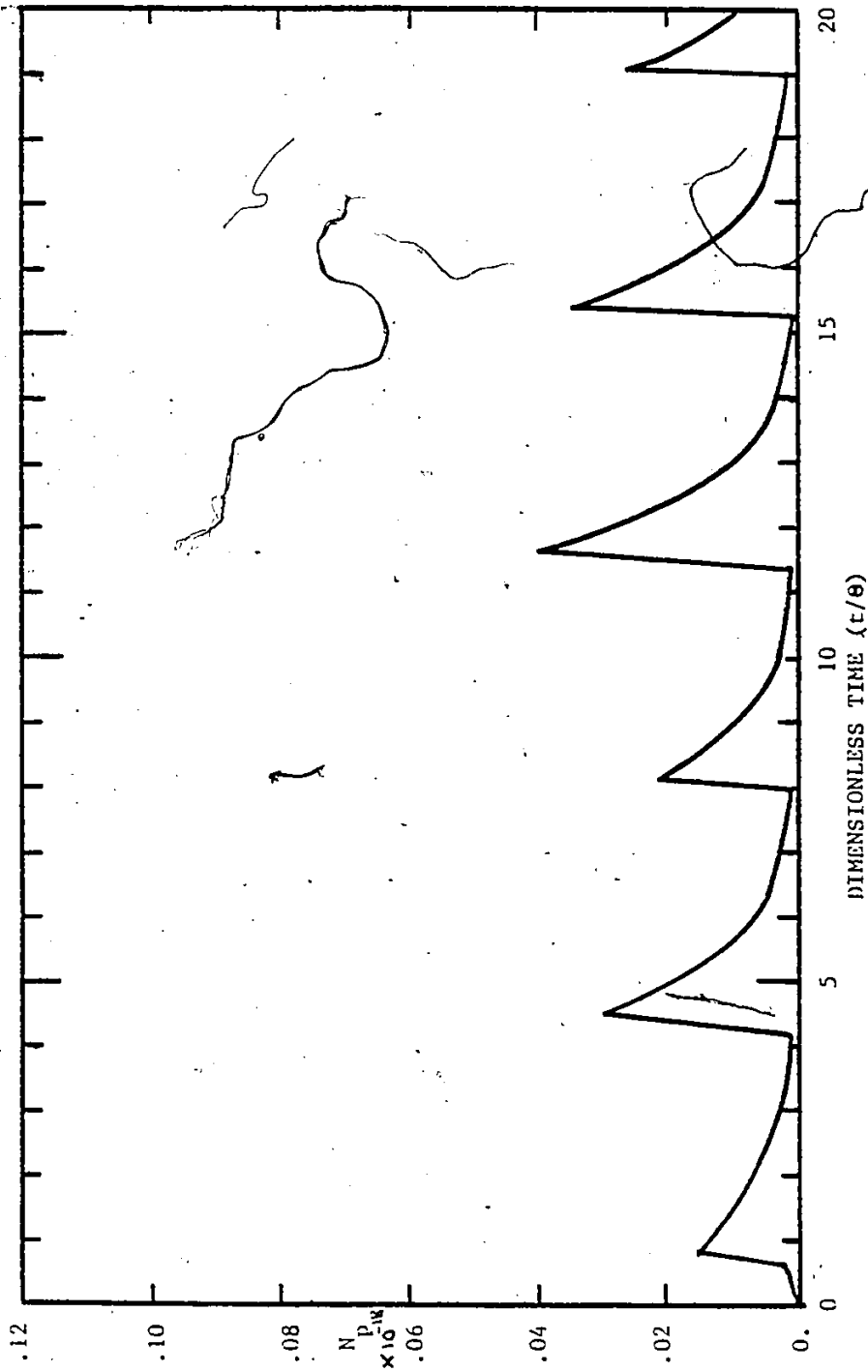


FIGURE 4.5b - Graph of Number of Particles N_p versus Dimensionless Time for $r_I=10,000$, $r_S=50,000$ (where $[I]_d=.01$ mole/L., $[S]_d=.01$ mole/L., $\theta=30$ min., $x_d=.45$)

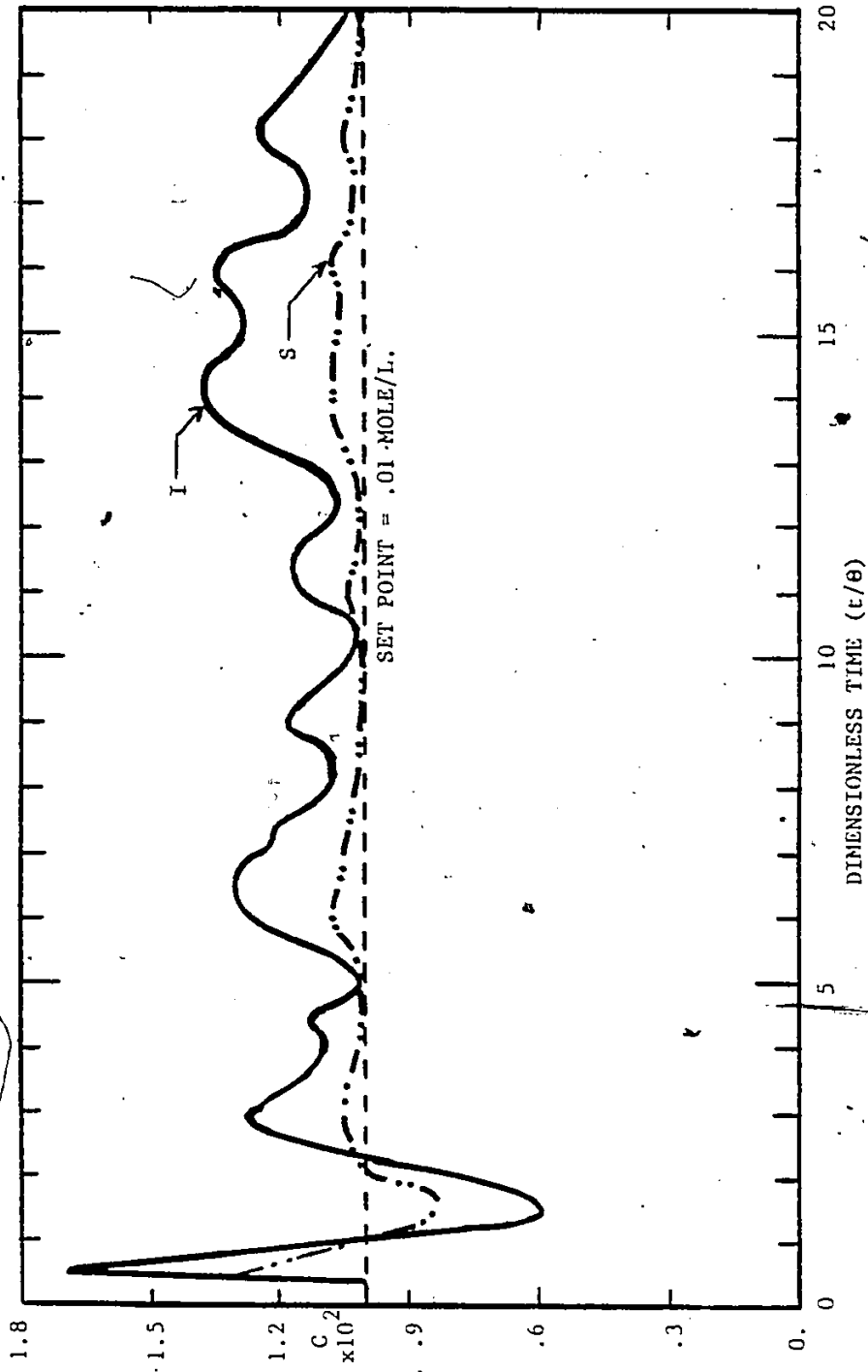


FIGURE 4.5c - Graph of Initiator and Emulsifier Concentrations C versus Dimensionless Time for $r_I=10,000$, $r_S=5,000$ (where $[I]_d=.01$ mole/L., $[S]_d=.01$ mole/L., $\theta=30$ min., $x_d=.45$)

was constrained close to the setpoint. The emulsifier level for this case went to the upper limit and eventually remained constant.

Case II with a slightly lower ratio still showed the same general effect but the initiator deviated more from its setpoint value.

Case III with high emulsifier penalty showed the emulsifier much closer to the setpoint with the initiator still free to move in a fair degree.

The emulsifier was seen to be fairly constant for all three cases presented. This was due to the fact that emulsifier changes can only have an effect during particle nucleation stages. Once the number of particles has been determined, changes in emulsifier levels have little effect on the system. By examining when the emulsifier drops in Case III it can be seen that this occurs just after or during new particle generation even with the possibility of time-varying Φ and Δ matrices used in the hybrid computation system. However, by this time the generation has essentially already finished before this decrease in soap can have an appreciable effect. As a result, the narrow window for control during the generation period using emulsifier was not adequate for good control of the system.

From the graphs, it can be seen that the initiator tries to compensate for the oscillations. However, due to the large nonlinearities due to particle generation, the initiator was unable to compensate for the generation and could not hold the conversion constant.

When the control results are compared to Figure 4.6 showing the results for the uncontrolled reactor, the conclusion was that the

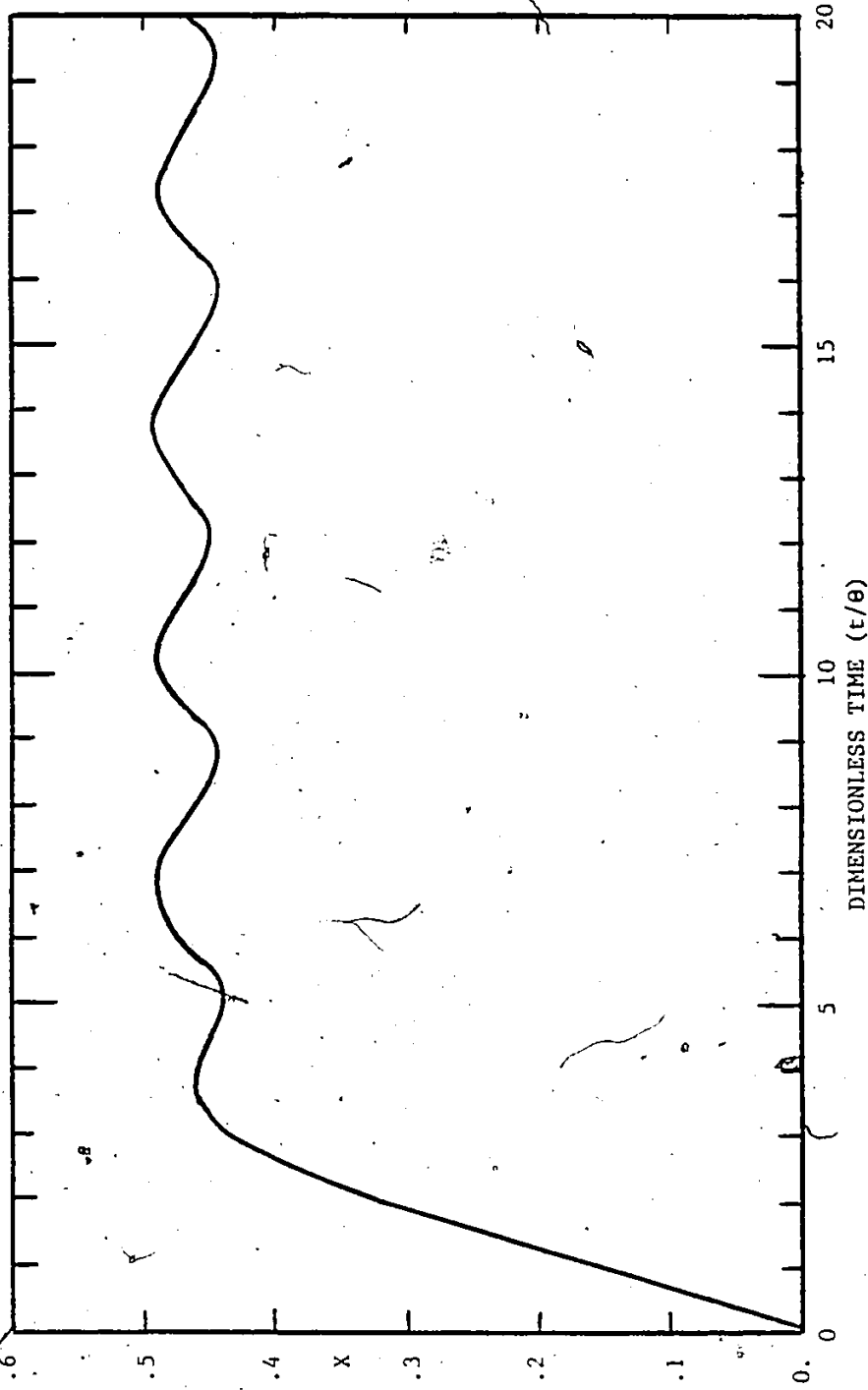


FIGURE 4.6 - Graph of Conversion versus Dimensionless Time for Single Reactor with No Control Action Taken (where $[I] = .01$ mole/L., $[S] = .01$ mole/L., $\theta = 30$ min.)

control scheme performed no better than the uncontrolled reactor. In both cases approximately a 5% range of conversions was achieved and for no values of the penalty matrices tried was the performance any better.

4.5 CONCLUSIONS

From the simulation results, the conclusion for this system would be that LQ stochastic optimal control theory applied to the continuous emulsion polymerization of vinyl acetate was not successful in maintaining reactor stability. The highly non-linear nature of this model where discontinuities are present in the model structure caused several problems in applying the control technique. To compensate for the brief bursts of nucleation which occur, it was necessary to integrate, linearize and discretize for each controller step at each time interval if nucleation was predicted in the near future, a time-consuming process. However, even this enhanced method was unable to compensate for the brief bursts of particle nucleation which occur for this system. Emulsifier changes did not prevent the oscillations due to the "window" effect and initiator changes did not correct for the large non-linearities in the system.

A different linearization method may yield better results, but was not carried out for this study. Due to the discontinuous, non-linear nature of the model, other techniques were not expected to perform any better for this system.

CHAPTER 5

CHOICE OF OPTIMUM SENSORS

5.1 INTRODUCTION

One of the main problems of studying any polymerization system, especially one as complex as emulsion polymerization, is the lack of good on-line instrumentation for determining polymer or latex properties. Good on-line measurements are necessary for any control strategies, and valuable as a source of data to allow better understanding of the polymerization system. However, on-line measurement systems are not available as yet for many properties. For example, molecular weight measurements require drying the polymer first before making accurate solutions of different concentrations for analysis by light scattering or osmometry. This is very difficult to do on-line in any reasonable time. The application of chromatograph techniques for particle size or molecular weight are lengthy and difficult on-line, and also require very accurate dilution systems.

Solution of these problems are usually possible by use of many high technology techniques which are available. However, the development of a new sensor for any property requires a great deal of time and expense before it becomes operational. A further drawback is that because of the complexity of polymerization systems, it is difficult to predict if any developed instrument will be useful in a

practical application. What is required is a means of predicting the utility of measuring any desired property or property combination before the development stage so that energy can be concentrated on the instruments that promise to be the most useful. The technique should also give an idea of how accurate the instrument has to be before it will enable useful information to be collected.

Kalman filtering as discussed in section 6.3 meets these criteria. For a given system, if a reasonable model is available, a Kalman filter provides statistical estimates of the states of the system and the covariance matrix of these states based on any given set of measurements.

By changing the choice of measurements or by combining them in various ways, the Kalman filter can be used to indicate which sensor or sensor choice will reduce some measure of the overall system variance the most and hence provide the best state estimates.

As an example, this chapter applies Kalman filter theory to the continuous emulsion polymerization of vinyl acetate at steady state with a seed reactor present as shown in Figure 5.1. The reactor system design using a seed reactor has the property of reducing or eliminating property oscillations for the continuous reactor system. A more detailed discussion of the rationale for this choice of reactor system, plus its advantages, will be presented in the next chapter. Using the reactor configuration of Figure 5.1, the best sensor choices for this system will be discussed, as well as some drawbacks to this analysis.

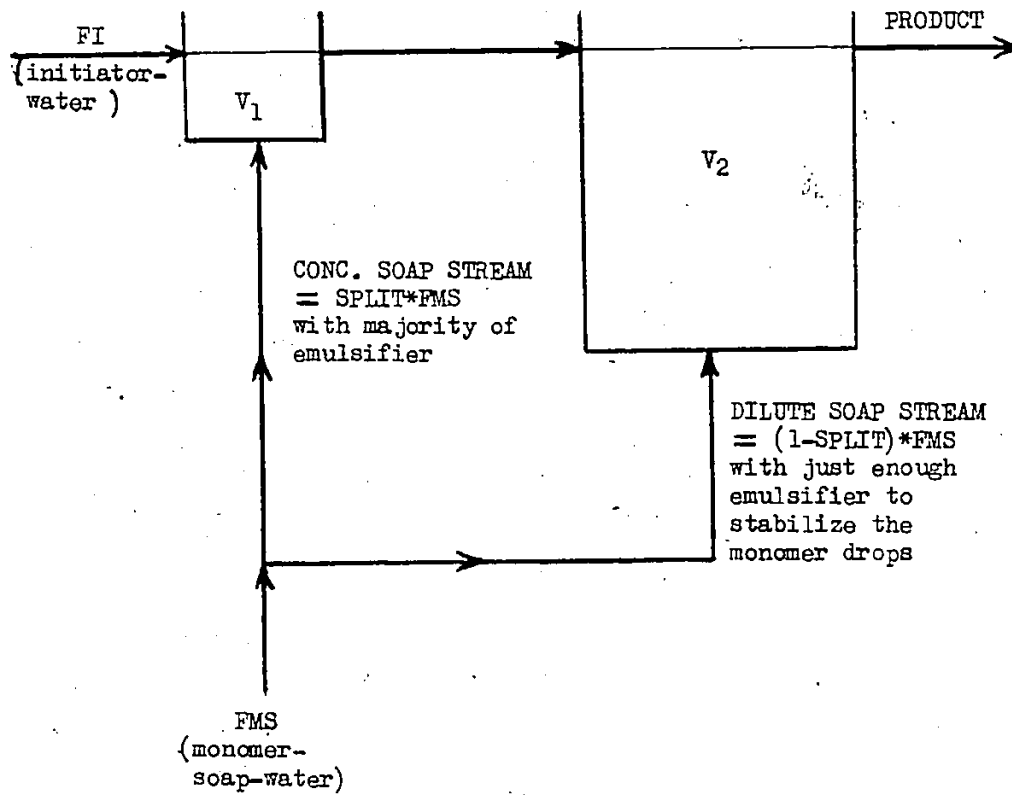


FIGURE 5.1 - Redesigned Reactor Configuration

5.2 OBSERVABILITY

A state variable in a model is said to be observable using a given property measurement if by taking the measurement it is possible to make an inference about the state level using the model. The mathematical representation of this fact is described as follows. If a state space model is written as:

$$\underline{x}_{K+1} = \underline{\Phi}^T \underline{x}_K + \underline{w}_K \quad (5.1)$$

$$\underline{y}_K = \underline{M} \underline{x}_K + \underline{v}_K \quad (5.2)$$

then the system is said to be fully observable if the observability matrix

$$P = \begin{pmatrix} \underline{M}^T & \underline{\Phi}^T \underline{M}^T & (\underline{\Phi}^T)^2 \underline{M}^T & \dots & (\underline{\Phi}^T)^n \underline{M}^T \end{pmatrix} \quad (5.3)$$

has rank n where n is the number of states in the system. Any rank less than n implies that all states are not observable, or are not able to be inferred using the model and the measurements given by equation (5.2). For the set of equations given in section 3.5 or in state space form as in section 4.3, the structure of the state space model is:

$$\begin{pmatrix} \underline{x}_{\text{PSD}} \\ \underline{x}_{\text{MWD}} \end{pmatrix} = \begin{pmatrix} A_1 & 0 \\ A_2 & A_3 \end{pmatrix} \begin{pmatrix} \underline{x}_{\text{PSD}} \\ \underline{x}_{\text{MWD}} \end{pmatrix} + \underline{w}_k \quad (5.4)$$

where $\underline{x}_{\text{PSD}}$ represents the state describing the particle size distribution (N_p, D, A, V, X) and $\underline{x}_{\text{MWD}}$ are the molecular weight states ($Q_0, Q_0 B_N, Q_1, Q_2$). It can be seen that the molecular weight states depend on the particle size states (i.e. $A_2 \neq 0$) because of the

dependence on conversion and particle volume, while the reverse is not true (i.e. top right submatrix is zero).

The usual case for on-line measurements is that measurements are available for the particle size section (such as conversion or particle area, or particle volume) but molecular weight measurements on-line are not present. This leads to a measurement equation of the form:

$$\underline{y} = [M_1^T \ 0] \begin{pmatrix} \underline{x}_{PSD} \\ \underline{x}_{MWD} \end{pmatrix} \quad (5.5)$$

The observability matrix then has the form:

$$P = \begin{pmatrix} M_1^T & A_1^T M_1^T & A_1^{T^2} M_1^T & \dots & A_1^{T^{n-1}} M_1^T \\ 0 & 0 & 0 & \dots & 0 \end{pmatrix} \quad (5.6)$$

which is non-observable in the molecular weight states. Thus, unless the measurement matrix in equation 5.5 is non-zero in the second half, the molecular weight states cannot be inferred from the model.

This result will be used in the next section to choose a criterion to be minimized to determine the optimal sensor choice for the model.

5.3 APPLICATION OF KALMAN FILTER THEORY

If the state space model is written in the general form from before:

$$\underline{x}_{K+1} = \Phi \underline{x}_K + \underline{w}_K \quad (5.1)$$

$$\underline{y}_K = \underline{M} \underline{x}_K + \underline{v}_K \quad (5.2)$$

then the Kalman filter theory presented in section 4.3 gives the following:

$$\underline{P}_{K+1/K} = \underline{\Phi}_K \underline{P}_{K/K} \underline{\Phi}_K^T + \underline{R}_w \quad (5.7)$$

$$\begin{aligned} \underline{P}_{K+1/K+1} = & [\underline{I} - \underline{K}_{K+1} \underline{M}] \underline{P}_{K+1/K} [\underline{I} - \underline{K}_{K+1} \underline{M}]^T \\ & + \underline{K}_{K+1} \underline{R}_v \underline{K}_{K+1}^T \end{aligned} \quad (5.8)$$

$$\underline{K}_{K+1} = \underline{P}_{K+1/K} \underline{M}^T [\underline{M} \underline{P}_{K+1/K} \underline{M}^T + \underline{R}_v]^{-1} \quad (5.9)$$

where $\underline{P}_{K+1/K}$ is the covariance matrix for the state prediction, $\underline{P}_{K+1/K+1}$ is the covariance matrix for the state estimates after a measurement becomes available and \underline{K}_{K+1} is the Kalman gain. \underline{R}_v represents the measurement noise and \underline{R}_w is an indicator of the noise in the states due to parameter errors or model inadequacy. The number of elements in the covariance matrices makes it difficult to compare state estimates one by one from one case to another. To circumvent this, a single scale function of the matrices is usually chosen instead.

The two commonest functions are the trace of the matrix or its determinant [see Harris (1980)]. The trace corresponds to the A-optimality criterion applied in the theory of experimental design. It has the disadvantages that it is scale dependent, and thus mixed units (such as number of particle and conversion) of different magnitudes cause stressing of the largest magnitude diagonal element rather than examining all states equally. Minimization of the determinant of these matrices corresponds to the D-optimality criteria of

experimental design. The square root of the determinant is proportional to the volume of the joint confidence region for the state estimate [Sutton and MacGregor (1977)]. Since for our example a steady-state operating condition was studied, the covariance matrices converged to a steady value and these final converged covariance matrices were then used so that the two criteria consisted of minimizing:

$$v_1 = \left| \frac{p_{-k+1/k}^{\infty}}{-k/k} \right|^{1/2} \quad (5.10)$$

$$v_2 = \left| \frac{p_{-k/k}^{\infty}}{-k/k} \right|^{1/2} \quad (5.11)$$

In this study, the interest was concentrated on the particle size data since this was of primary concern in latex production. As well, since on-line measurements of molecular weights were not available, the previous section showed that these states are non-observable and cannot be inferred by use of the model. For these reasons, only the upper left submatrix of the covariance matrices corresponding to the particle size states was examined. This yielded the following criteria:

$$v_1^1 = \left| \frac{p_{-k+1/k}^{\infty}}{-k/k} \right|_{\text{PSD}}^{1/2} \quad (5.12)$$

$$v_2^1 = \left| \frac{p_{-k/k}^{\infty}}{-k/k} \right|_{\text{PSD}}^{1/2} \quad (5.13)$$

The change in these criteria will now be examined for various choices of sensors and sensor combinations. In addition, if the molecular weight would be measured on-line, this study shows how this

information will also reduce the particle size criteria above by use of the state space model of the system.

5.4 SIMULATION RESULTS

All of the simulations for sensor choice were carried out in the same manner. The simulation of the system with one large reactor and a small seed reactor in front as discussed in Chapter 6 was run until a steady-state level was achieved for various operating conditions which are summarized in Table 5.1. This provided a constant Φ matrix in equation 5.1 for each case. Then, for each desired R_w and R_v matrix, equations 5.7 to 5.9 were iterated until convergence, which provided the converged covariance matrices $P_{-K+1/K}^{\infty}$ and $P_{-K/K}^{\infty}$ for use in the criteria of equations 5.12 and 5.13.

For the single sensor and sensor combination sections, the measurements assumed to be available on-line were the conversion x , particle surface area A ; sum of the particle diameters D and the number of particles N_p . To consider the effects of improved instrumentation, two conversion measurement errors were used, one assuming a standard deviation of 10% and one of 2% of the steady-state conversion levels. This could represent the difference between a conversion estimate by heat balance as opposed to the density meter measurement

TABLE 5.1

SUMMARY OF STEADY-STATE PRODUCT PROPERTY
VALUES FOR VARIOUS OPERATING CONDITIONS
(SEED REACTOR PRESENT)

[I] (mole/L)	[S] (mole/L)	Split	N_p $\times 10^{18}$	D $\times 10^{10}$	A $\times 10^4$	V	X	M_n $\times 10^5$	M_w $\times 10^6$	B_n	d_p (Å)
.01	.01	.2	.171	17.1	82.8	.303	.676	5.32	1.70	.559	1000
.01	.01	.6	.075	10.5	69.5	.329	.619	5.06	1.52	.472	1400
.02	.01	.2	.190	17.7	83.4	.297	.758	5.70	2.02	.690	930
.01	.02	.2	1.50	74.3	171.8	.297	.762	5.71	2.04	.695	494

discussed in chapter 7 for example. The particle surface area and diameter measurements were assumed to have standard deviations of 20% of steady-state value while the measurement of the number of particles, being more difficult to measure, was used with a standard deviation of 50% of the steady-state value.

To examine the use of an on-line molecular weight average measure in section 5.4.3, it was assumed that a measurement was available with a standard deviation of 10% of the steady-state weight average molecular weight.

The R_V matrix describing the measurement noise was assumed to be diagonal in all cases, with the diagonal elements corresponding to the variance of the appropriate measurement and it was constant for all simulation runs. This was done by choosing the number of measurements to include all required sensors for individual and

combination runs, including replicated sensors. In this way, the vector \underline{y} of measurements was used as:

$$\underline{y} = \begin{bmatrix} x_2 \\ x_2 \\ x_{10} \\ A_{10} \\ A_{10} \\ Np_{50} \\ D_{10} \\ M_{W10} \end{bmatrix} = \begin{bmatrix} 0 & 0 & 0 & 0 & 1 & 0 & 0 & 0 & 0 \\ 0 & 0 & 0 & 0 & 1 & 0 & 0 & 0 & 0 \\ 0 & 0 & 0 & 0 & 1 & 0 & 0 & 0 & 0 \\ 0 & 0 & 1 & 0 & 0 & 0 & 0 & 0 & 0 \\ 0 & 0 & 1 & 0 & 0 & 0 & 0 & 0 & 0 \\ 1 & 0 & 0 & 0 & 0 & 0 & 0 & 0 & 0 \\ 0 & 1 & 0 & 0 & 0 & 0 & 0 & 0 & 0 \\ 0 & 0 & 0 & 0 & 0 & 0 & 0 & 0 & \frac{0(MW_{MON})}{Q_{1SS}} \end{bmatrix} \begin{bmatrix} Np \\ D \\ A \\ V \\ X \\ Q_0 \\ Q_0^{BN} \\ Q_1 \\ Q_2 \end{bmatrix} = \underline{M} \underline{x} \quad (5.14)$$

where the noise matrix is given by:

$$\underline{R}_V = \begin{bmatrix} (.02x_{SS})^2 & & & & & & & & & \\ & (.02x_{SS})^2 & & & & & & & & \\ & & (.10x_{SS})^2 & & & & & & & \\ & & & (.10A_{SS})^2 & & & & & & \\ & & & & (.10A_{SS})^2 & & & & & \\ & & & & & (.50Np_{SS})^2 & & & & \\ & & & & & & (.10D_{SS})^2 & & & \\ & & & & & & & (.10M_{WSS})^2 & & \\ 0 & & & & & & & & & \end{bmatrix} \quad (5.15)$$

In this fashion the subscript on the sensors yields the percent error in the given measurement. By deleting out some of the non-zero

positions of M , single sensors or sensor combinations can be examined without changing the model structure or the R_V matrix of equation 5.15. For example, by including two measurements of conversions with 2% error (the X_2 sensors), the value of replicating the sensor rather than adding a different sensor such as surface area can be examined.

The R_W matrix describing state errors due to model inadequacies or parameter errors was also chosen to be diagonal. Since the molecular weight section is not studied by the chosen criterion, the standard deviation of the molecular weight states for each set of operating conditions was held constant at 20% of the steady-state level. For each set of operating conditions though, three different standard deviations of the particle size states were used, 5%, 10% and 20% of the steady-state values. In this way, improvement of the state estimates can be examined when measurements are available in conjunction with a good model, and a poorer model.

Examination of single sensors, sensor combinations, and molecular weight sensors will now be discussed in turn:

5.4.1 INDIVIDUAL SENSORS

The results from the simulations are summarized in Tables 5-2 through 5-5, which show the V_1^1 and V_2^1 criteria of section 5.3. The conversion measurement with 10% error was used as the base case in these tables, and the increase or decrease of the criteria from the base case is shown in the third and fourth column. The improvement in

TABLE 5.2a

V_1^1, V_2^1 CRITERIA FOR 5% ERROR IN
STATES FOR $[I]=.01$ M/L, $[S]=.01$ M/L, SPLIT=.2

Measurement	V_1^1 $\times 10^3$	V_2^1 $\times 10^3$	% Change in V_1^1 Compared to X_{10}	% Change in V_2^1 Compared to X_{10}	% Change From V_1^1 To V_2^1
Base X_{10}	.372	.299	-	-	-20
1 Np50	.563	.554	+51	+85	-2
2 D ₁₀	.374	.305	+0	+2	-18
3 A ₁₀	.330	.266	-11	-11	-19
4 X ₂	.271	.094	-27	-69	-65

TABLE 5.2b

V_1^1, V_2^1 CRITERIA FOR 10% ERROR IN
STATES FOR $[I]=.01$ M/L, $[S]=.01$ M/L, SPLIT=.2

Measurement	V_1^1 $\times 10^3$	V_2^1 $\times 10^3$	% Change in V_1^1 Compared to X_{10}	% Change in V_2^1 Compared to X_{10}	% Change From V_1^1 To V_2^1
Base X_{10}	9.92	6.23	-	-	-37
1 Np50	16.1	15.3	+62	+146	-5
2 D ₁₀	10.0	6.41	+0	+3	-36
3 A ₁₀	8.69	5.49	-12	-12	-38
4 X ₂	8.33	1.57	-16	-75	-81

TABLE 5.2c

V_1^1, V_2^1 CRITERIA FOR 20% ERROR IN
STATES FOR $[I]=.01$ M/L, $[S]=.01$ M/L, SPLIT=.2

Measurement	V_1^1 $\times 10^3$	V_2^1 $\times 10^3$	% Change in V_1^1 Compared to X_{10}	% Change in V_2^1 Compared to X_{10}	% Change From V_1^1 To V_2^1
Base X_{10}	.282	.116	-	-	-59
1 Np50	.444	.383	+57	+230	-14
2 D10	.287	.120	+2	+3	-58
3 A10	.246	.102	-13	-12	-59
4 X_2	.263	.025	-7	-78	-90

TABLE 5.3

V_1^1, V_2^1 CRITERIA FOR 10% STATE ERROR
FOR $[I]=.01$ M/L, $[S]=.01$ M/L, SPLIT=.6

Measurement	V_1^1 $\times 10^3$	V_2^1 $\times 10^3$	% Change in V_1^1 Compared to X_{10}	% Change in V_2^1 Compared to X_{10}	% Change From V_1^1 To V_2^1
Base X_{10}	1.98	1.24	-	-	-37
1 Np50	3.23	3.06	+63	+147	-5
2 D10	2.06	1.32	+4	+6	-36
3 A10	1.81	1.15	-9	-7	-36
4 X_2	1.66	.312	-16	-75	-81

TABLE 5.4

V_1^1, V_2^1 CRITERIA FOR 10% STATE ERROR
FOR $[I]=.02$ M/L, $[S]=.01$ M/L, SPLIT=.2

Measurement	V_1^1 $\times 10^3$	V_2^1 $\times 10^3$	% Change in V_1^1 Compared to X_{10}	% Change in V_2^1 Compared to X_{10}	% Change From V_1^1 To V_2^1
Base X_{10}	12.9	8.08	-	-	-37
1 Np50	20.9	19.8	+62	+145	-5
2 D ₁₀	13.0	8.29	+1	+3	-36
3 A ₁₀	11.2	7.11	-13	-12	-37
4 X_2	10.8	2.04	-16	-75	-81

TABLE 5.5

V_1^1, V_2^1 CRITERIA FOR 10% STATE ERROR
FOR $[I]=.01$ M/L, $[S]=.02$ M/L, SPLIT=.2

Measurement	V_1^1 $\times 10^3$	V_2^1 $\times 10^3$	% Change in V_1^1 Compared to X_{10}	% Change in V_2^1 Compared to X_{10}	% Change From V_1^1 To V_2^1
Base X_{10}	.926	.581	-	-	-37
1 Np50	1.47	1.40	+59	+140	-5
2 D ₁₀	.959	.613	+4	+6	-36
3 A ₁₀	.849	.539	-8	-7	-37
4 X_2	.778	.146	-16	-75	-81

state estimates when a measurement becomes available can be seen by examining the change in the covariance matrix for the predictions $\underline{P}_{k+1/k}$ versus the covariance matrix after a measurement is available $\underline{P}_{k/k}$, and the percentage change from V_1^1 to V_2^1 in the fifth column was used as a representation of this improvement.

Tables 5.2b and Tables 5.3 to 5.5 all show the results obtained when a 10% model error (i.e. R_W) in the particle size states was assumed. Despite differences in the absolute magnitudes of the V_1^1 and V_2^1 criteria for the different operating conditions, the percentage changes in columns 3 to 5 were all similar. As a result, detailed results are only presented for one operating condition and are summarized in Tables 5.2a, b and c. By comparing the criteria, the data show that doubling the percent error in the model results in approximately a thirty-fold increase in V_1^1 and approximately a twenty-fold increase in the magnitude of V_2^1 for each sensor type.

A graphical summary of the percent changes shown in Tables 5.2a, b, and c is given in Figure 5.2. The percent change from V_1^1 to V_2^1 , which yields the decrease in covariance once a measurement became available, showed that for this model, if the measurement errors were comparable, so was the increase in knowledge provided by the measurement. This could be seen by observing the closeness of the curves for X_{10} , D_{10} and A_{10} for the change of V_1^1 to V_2^1 , as well as the fact that the deviation in V_2^1 and V_1^1 from the base case was small, being 10% or less. This was primarily due to the model structure in this case, where the dominant term in the I matrix was

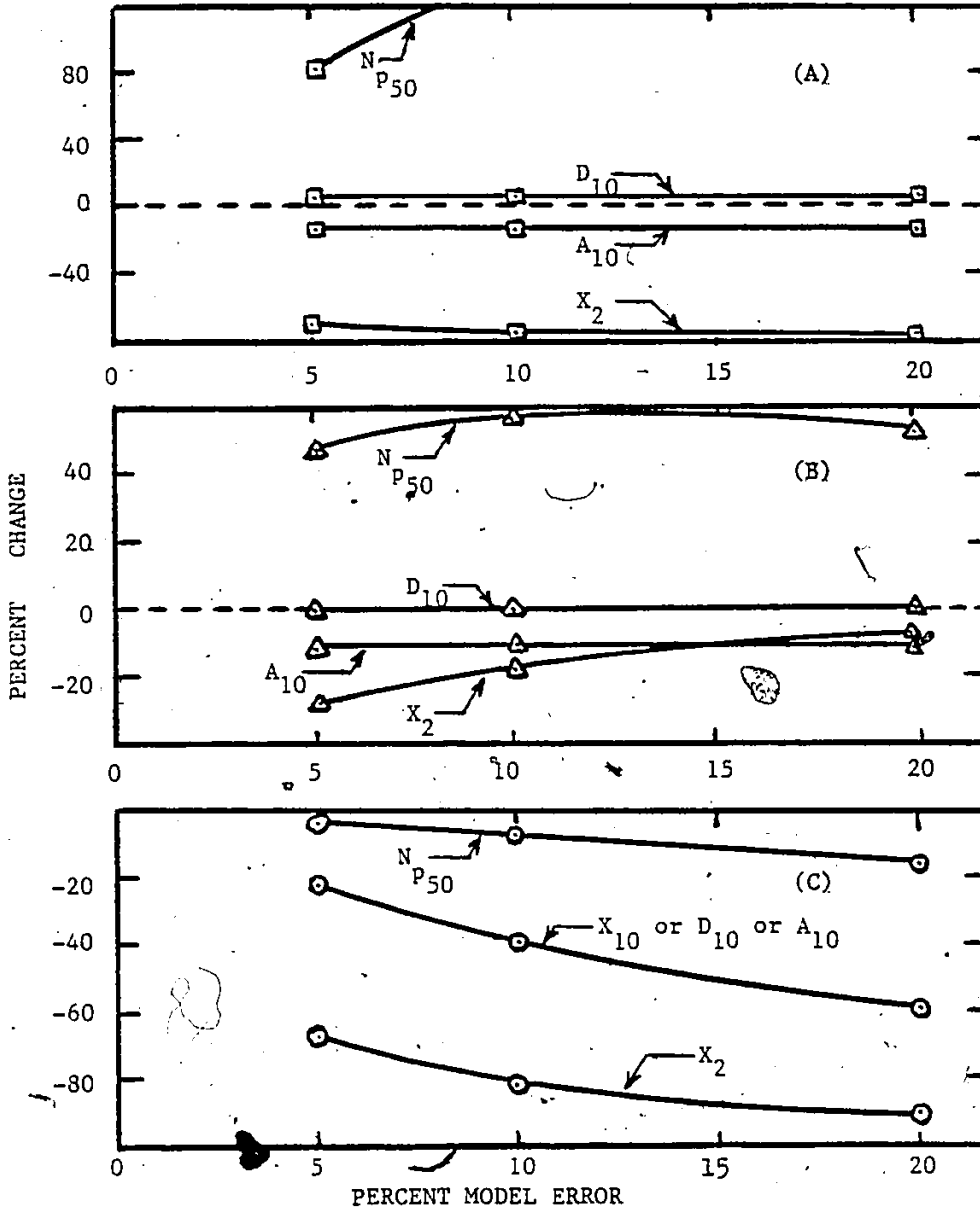


FIGURE 5.2 - Graph of Percent Change of:
 (A) v_2 for other sensors compared to v_2 for x_{10}
 (B) v_1 for other sensors compared to v_1 for x_{10}
 (C) v_1 compared to v_2 for each sensor
 versus Percent Model Error of the Particle Size States

the diagonal term relating to washout. For other models, this conclusion would not hold in general. The measurement of the number of particles to within 50% provided little information, even in the presence of a poor model since even at 20% model error, the reduction in the covariance after a measurement was only around 12%, and the deviations of V_1^1 and V_2^1 from the base case were very large and positive.

The reduction of the measurement error in the conversion from 10% to 2% did yield a substantial improvement in the covariance criteria V_2^1 and in the change from V_1^1 to V_2^1 . The change in measurement error thus represented the only way with this model to improve the state estimate for a given sensor type.

It is also worth noting that as the model became less accurate towards increasing percent model error, the importance of the measurements became greater, which was shown by the greater percent decrease from V_1^1 to V_2^1 as the model degraded.

The conclusions to be drawn are that any given sensor must have a comparable percent measurement error when compared to another sensor in order to achieve the same degree of error in the state estimates of the overall particle size properties, due to the diagonal dominance of the Φ matrix.

5.4.2 SENSOR COMBINATIONS

The results from various sensor combinations are presented in Table 5.6 for one case operating with 10% error in the prediction of

the model particle size states (i.e. in R_W). Other operating conditions yielded similar results, and the patterns found with differing model error were the same as for the single sensor section and so are not discussed further.

Several interesting points were apparent from this study. By comparing the change in V_2^1 and change from V_1^1 to V_2^1 , it could be seen that replicating a good conversion measurement using a poorer conversion measurement (as shown by the X_2 - X_{10} combination compared to the original X_2 sensor)

TABLE 5.6

V_1^1, V_2^1 CRITERIA FOR 10% PARTICLE SIZE
STATE ERROR FOR $[I]=.01$ M/L, $[S]=.01$ M/L, SPLIT=.2
FOR VARIOUS SENSOR COMBINATIONS

	V_1^1 $\times 10^3$	V_2^1 $\times 10^3$	% Change From Base For V_1^1	% Change From Base For V_2^1	% Change in V_2^1 From V_1^1
<u>Base Case 1</u>					
X_2	8.33	1.57	-	-	-81
1 X_2 - X_{10}	8.33	1.54	0	-2	-82
2 X_2 - Np_{50}	7.33	1.31	-12	-17	-84
3 X_2 - X_2	8.27	1.12	-1	-29	-87
4 X_2 - A_{10}	4.67	.57	-44	-64	-93
5 X_2 - D_{10}	4.77	.58	-43	-63	-93
<u>Base Case 2</u>					
A_{10}	8.69	5.49	-	-	-37
1 A_{10} - Np_{50}	7.69	4.61	-12	-16	-47
2 A_{10} - A_{10}	8.09	4.25	-7	-23	-51
3 A_{10} - D_{10}	5.29	2.15	-39	-61	-75

yielded no improvements in the state estimation as expected. The interesting point was that even combining a number of particles sensor with 50% error yielded better state estimation than the replication with a poor sensor.

The improvements shown in Table 5.6 for the number of particles sensor N_{p50} combined with X_2 or A_{10} are small, and replication using comparable sensors provided better state estimates than combining a sensor with the poor number of particles sensor, as shown by comparing X_2-X_2 with X_2-N_{p50} and $A_{10}-A_{10}$ with $A_{10}-N_{p50}$.

The ultimate improvement in the criteria occurred using two different sensor types such as X_2-A_{10} , X_2-D_{10} or $A_{10}-D_{10}$ due to interactions through the model.

The best overall sensor combination for this system was found to be the combination of a conversion sensor with 2% error with either a particle surface area or total particle diameter sensor with 10% measurement error. This analysis corresponds to the case where a variety of sensors are available with already calculated precision or measurement error. Given this range of sensors and some financial constraints for a system, the optimum sensor equipment for any set up would be determined with this method. For example, the study illustrated that if a conversion measurement was already available, a measure of particle surface area would be the best choice for a second sensor.

A second use of this analysis is that it could be carried out with various measurement error possibilities for the instruments in order to determine the precision required for each instrument before a

sufficient improvement in state information could be attained. For example, this study illustrated that the number of particles must have a precision of better than 50% measurement error on-line before improvement in state information is obtained when combined with another sensor. As such, a number of particles sensor with this precision would not be recommended for use with the given system.

5.4.3 WEIGHT AVERAGE MOLECULAR WEIGHT SENSOR

As discussed earlier, on-line instrumentation for measuring molecular weight averages is not available at present. Kalman filtering was used in this study to determine if development of such a sensor is worthwhile. That is, could an instrument of this type yield better state estimates and more information than sensors presently in use such as conversion monitors.

Table 5.7 summarizes the V_1^1 and V_2^1 criteria for this section. As before, only one operating condition and degree of model error is shown due to the same patterns being present as discussed for single sensors.

In this study, the weight average molecular weight was not a linear combination of the model states, but instead was a combination of the Q_2 and Q_1 model states given by:

$$\bar{M}_W = \left(\frac{Q_2}{Q_1} \right) \cdot MW_{MON} \quad (5.16)$$

where MW_{MON} is the monomer molecular weight. In order to use the Kalman filtering theory, a linearization must be used. Two linearizations were attempted.

TABLE 5.7
 V_1^1, V_2^1 CRITERIA FOR 10% PARTICLE SIZE
 STATE ERROR FOR $[I]=.01$, $[S]=.01$, SPLIT=.2
 FOR MOLECULAR WEIGHT SENSOR AND SENSOR COMBINATIONS

	V_1^1 $\times 10^3$	V_2^1 $\times 10^3$	% Change From Base in V_1^1	% Change From Base in V_2^1	% Change in V_2^1 From V_1^1
1 M_{W10}	10.3	7.60	+24	+384	-9
2 M_{W10}^{-D10}	5.85	2.76	-30	+76	-67
3 M_{W10}^{-X10}	5.84	2.72	-30	+73	-67
4 M_{W10}^{-A10}	5.53	2.62	-34	+67	-69
5 M_{W10}^{-X2}	4.91	.69	-42	-56	-92
Base X_2	8.33	1.57	-	-	-81
Best Previous X_2^{-A10}	4.67	.50	-44	-64	-93

Note! V_1^1, V_2^1 refer to particle size state information only.

$$\bar{M}_w = \left(\frac{M_{w,MON}}{Q_{1SS}} \right) \cdot Q_2 \quad (5.17)$$

$$\Delta \bar{M}_w = \left(\frac{M_{w,MON}}{Q_{1SS}} \right) \cdot Q_2 - \left(\frac{M_{w,MON} \cdot Q_{2SS}^0}{Q_{1SS}} \right) \cdot Q_1 \quad (5.18)$$

where the first linearization was obtained by holding Q_1 constant at its steady-state value Q_{1SS} . The second form was a deviation² variable form where $\Delta \bar{M}_w$ represented the deviation from the steady-state value of M_w , and the linearization was obtained by differentiation of equation 5.16. Both forms yielded the same results so the study used the simpler form of equation 5.17, as shown in the matrix of equation 5.14 in section 5.4.

As an individual sensor with 10% measurement error, the weight average molecular weight sensor was not very good as shown in Table 5.7 by comparison with the conversion sensor above. In combination with the A_{10} , D_{10} or X_{10} sensors, an improvement was noted with all combinations providing roughly the same degree of improvement, but these combinations were still not as good as the X_2 conversion measure alone. However, M_{w10} in combination with the X_2 sensor did yield a noticeable improvement and improved the criteria to approximately the same degree as the best sensor combination from the previous section, X_2 - A_{10} .

Several interesting points could be noted from these studies. Despite the fact that the molecular weight sensor did not measure any particle size state or state combinations directly, the use of the model with the molecular weight measurement in combination with the

conversion sensor yielded improved particle size state estimates as shown by the decreased criteria. An additional fact not shown was that since the M_w sensor measured properties in the molecular weight section of the model, the system was no longer unobservable in the molecular weight states as discussed in section 5.2, and the M_w sensor could then be used to yield improved state estimates for the entire model.

Also, since an on-line M_w sensor is not available at present, this approach using Kalman filtering illustrated that a potential sensor could be evaluated to determine if sufficient improvement in state estimates could be attained even before the necessary expenditure of time and money was invested for the sensor's development.

5.5 CONCLUSIONS

This study showed how the Kalman filtering theory could be used to evaluate sensors and sensor combinations for a system. Even though sensors were either not available at present, or the precision of the instruments was not known, the development in this chapter showed how to choose which instruments would best suit a given application without initiating a costly instrument development for a new sensor.

For the model of this study, it was found that combinations of different sensors rather than replication was more valuable. Due to the model structure used, this study found that all particle size sensors were roughly equivalent provided all sensors had the same

measurement error, thus indicating for this system that reduction of sensor error would be the best direction for research in order to obtain improved state estimates. Also, a molecular weight sensor for weight average molecular weight would probably be the best choice to combine with a conversion measurement as it provides almost the best particle size state estimates while at the same time making the full model observable for this system.

CHAPTER 6

REDESIGN OF LATEX REACTOR SYSTEM

6.1 INTRODUCTION

As discussed in Chapter 4, the phenomenon of sustained latex property oscillations is a major problem in attempts to carry out emulsion polymerizations in a continuous manner. Several techniques such as the use of increased emulsifier levels or the application of advanced control theory such as linear quadratic stochastic optimal control as discussed in Chapter 4 do not work well in eliminating the property oscillations for a variety of reasons which will be discussed in a later section. This chapter presents an approach to eliminating the oscillations by redesigning the reactor system so that the oscillations do not occur at all and essentially introduce latex property control at the design stage rather than applying control theory to an already existing system. The system redesign will be discussed first followed by simulation results for the redesigned system.

6.2 SYSTEM REDESIGN

6.2.1 PROBLEMS AND GOALS

As discussed in previous chapters, continuous emulsion polymerization of vinyl acetate shows the phenomenon of sustained

oscillations for many operating conditions. During the oscillations the latex properties undergo a substantial cycling behavior over the course of approximately four residence times of the reactor. This is undesirable from the viewpoint of latex-quality control, and large oscillations to high conversion levels can also lead to catastrophic agglomeration. This operating behavior is thus unacceptable for the operation of the continuous system.

Several approaches can be tried to eliminate the oscillatory behavior. First, the emulsifier level can be increased to obtain a steady-state generation of particles in the reactor. However, the increase of emulsifier causes downstream problems with foaming, and also adds additional expense to the product due to added raw material costs. If the latex is to be coagulated and used as a rubber, the extra soap presents an added contaminant in the product which must be removed. For these reasons an increase in emulsifier levels does not present a satisfactory solution in the majority of cases.

Advanced control theory can also be applied to the problem to try to eliminate the oscillations. However, as shown in Chapter 4, advanced control theory has problems in compensating for the oscillations due to large non-linearities inherent in the particle generation phenomena.

The model for particle generation developed for this system was discontinuous in the sense that generation occurred in intervals for many operating conditions so that the model structure itself did not remain constant. The generation term $f(t)$ remained zero for long

periods of time, then became exceedingly large during a short explosive generation period resulting in an effective discontinuity in the model. Control action was found to be implemented only during the brief "window" during new particle generation and any control actions were essentially useless once the particles had formed. Since the period of new particle generation was usually 5-10 minutes while the non-generating period was typically two hours for a 30 min. reactor residence time, the result was completely inadequate control on this system.

Kiparissides (1978) and this study also found that reduction of amplitude of the oscillations using advanced control theory also required going to higher emulsifier levels with the same problems as have been discussed for the high emulsifier situation.

The first approach examined by this study is the redesign of the reactor configuration in such a way that oscillations do not occur for the reactor operating conditions. The main aim of this chapter is to produce a reactor system which is stable over a wide range of operating conditions without using large emulsifier concentrations. In addition, the reactor system is redesigned so that flexibility in changing latex properties and ease of operation could be achieved.

6.2.2 LITERATURE SURVEY

In the literature few detailed studies are available for different reactor configurations. Greene, et al. (1976) showed results for methyl methacrylate emulsion polymerization where a PFTR*

* Plug Flow Tubular Reactor

was used to seed the reactor system and stable operation was shown in terms of constant conversion. Omi, et al. (1969), Ueda, et al. (1971) and Nomura and Harada (1981) studied the effects of seeders on the emulsion polymerization of styrene. Omi, et al. (1969) and Ueda, et al. (1971) examined the use of PFTR type seeders with the aim being to maximize the number of particles in the reactor. However, the results were estimated by a steady-state model and start up and change of reactor operating conditions was not considered. Nomura and Harada (1981) considered both continuous reactors and PFTR's for use as seeders with in addition a split of monomer feed between the seeder and the main reactor. Nomura and Harada (1981) concluded that the optimum configuration for styrene emulsion polymerization was a plug flow reactor with some splitting of the monomer feed. Again, the aim of this work was to maximize the particles and for all these papers the particle size and molecular weight distributions were not considered. No work to date was available for the emulsion polymerization of vinyl acetate with seeders present.

6.2.3 REACTOR SYSTEM REDESIGN FOR VINYL ACETATE EMULSION POLYMERIZATION

As the literature showed, seeding of the continuous reactor causes a substantial enhancement in stability. The choice of seeding method is either a CSTR, a PFTR, or production of seeds batchwise followed by a steady flow of the batch produced seeds into the reactor.

Batchwise production of seeds has the disadvantage that there may be batch to batch variability in the system. This method is also difficult to apply if a more polydispersed system is desired as for adhesives or for lowering the bulk viscosity. As such, the batchwise seed method is not very flexible for this system.

The seeding of a continuous reactor using a PFTR as described in the previous section can also be done. However, this system would still require a premixer for emulsifying the feeds to the system which would correspond to a CSTR.

To take advantage of the better mixing characteristics a CSTR seeder was therefore used in this study where the CSTR could also be used as an emulsifying stage as well as a seed generator.

In order to increase flexibility of the reactor system to produce latexes with different properties, a split was also used for the monomer and the water. In this way it is possible to artificially create an environment with a high emulsifier concentration in the seeding reactor thereby promoting continuous or nearly continuous particle generation. To keep emulsifier and initiator levels high in the seed reactor all initiator and the majority of emulsifier was fed to the seed reactor to maximize the particle generation in the seeder. Only enough soap to stabilize the emulsion was used in the bypass stream to the main reactor.

In this fashion the control variables can be considered as the initiator and emulsifier concentrations of the product plus the degree

of split of the monomer and water. This extra control variable allowed changes to be made in latex properties without changing emulsifier levels, thus preventing downstream problems and increasing flexibility.

The results from the simulations will now be discussed to illustrate the advantages of the new reactor configurations.

6.3 SIMULATION RESULTS

6.3.1 SINGLE CSTR VS. REDESIGNED SYSTEM

Rather than simulating an entire reactor train for continuous emulsion polymerization, this study focussed on the first reactor in the train. Any behavior which occurs in the first reactor or redesigned reactor system will appear in downstream reactors so that the study of the first main latex reactor should reveal any trends or changes due to the redesign of the reactor operation.

Figure 6.1 shows the original first latex reactor as the base case for these simulations. All feeds enter the reactor and the latex product is removed to be passed to downstream reactors. Figure 6.1 also shows the redesigned reactor configuration proposed in section 6.2. As shown for the new system, all initiator plus some fraction of the monomer-water stream was fed to the first reactor. The soap was divided such that the majority of soap was fed to the first seed reactor while just enough soap to stabilize the monomer droplets in the monomer water bypass stream was fed to the main latex reactor. The seed reactor sizes represented were approximately 1/16, 1/8 and

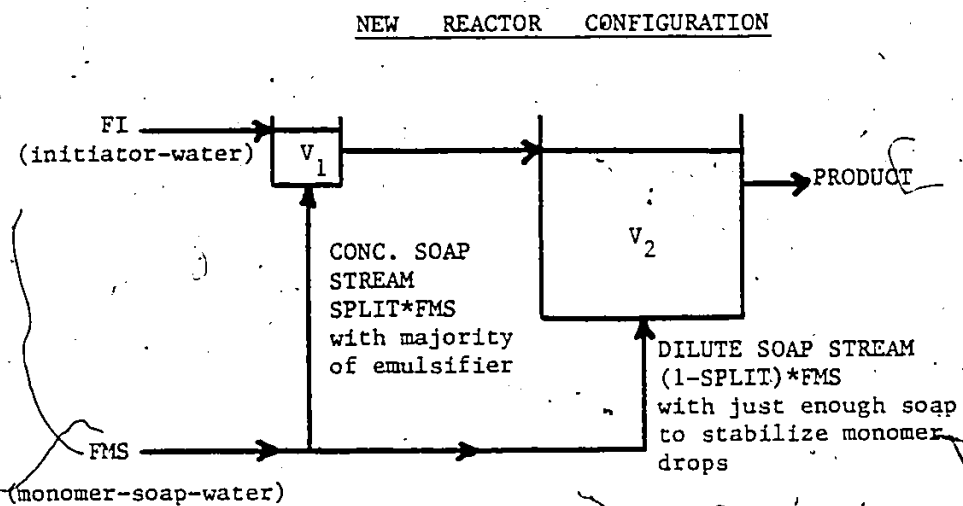
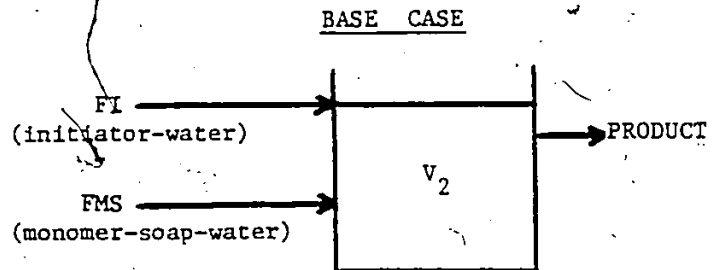


FIGURE 6.1 - Comparison of Base Case Reactor Configuration
with Redesigned Reactor Configuration

1/5 the size of the main reactor to simulate the experimental setup which was available. The overflow from the seed reactor was fed to the second main reactor, and the product from this main reactor was considered to be the input to downstream reactors as for the base case.

Due to the bypass of some of the monomer and water the seed reactor for the new configuration had a high concentration of initiator and emulsifier leading to nucleation of a sufficient number of particles for downstream reactors.

Results from the simulations for the base case and the redesigned system are shown in Figures 6.2 and 6.3 and are summarized in Table 6.1 for two runs of the redesigned system. The results shown in the figures corresponds to Case I in the table.

TABLE 6.1

COMPARISON OF POLYMER LATEX PROPERTIES OF THE PRODUCT FOR A SINGLE CSTR (BASE CASE) VERSUS THE NEW REACTOR CONFIGURATION (CASE I AND CASE II) WHERE I = POTASSIUM PERSULPHATE AND S = SODIUM LAURYL SULPHATE

	[I] (mol/l)	[S] (mol/l)	X	M_N ($\times 10^{-5}$)	M_W ($\times 10^{-6}$)	B_N	N_p ($\times 10^{-18}$)	$\frac{D_p}{A_p}$	$\frac{D_w}{D_N}$
BASE CASE (single CSTR)	.01	.01	.62 TO .67	5.89 TO 6.02	2.19 TO 2.26	.74 TO .78	.003 TO .06	400 TO 6000	1.03 TO 2.97
			(RANGE OF OSCILLATIONS)					AVE = 2700	AVE = 1.21
CASE I	.005	.0075	.66	5.58	1.91	.67	.009	2800	1.19
CASE II	.005	.01	.71	5.79	2.09	.72	.009	2700	1.18

The simulation results from the base case illustrate the phenomenon of sustained property oscillations due to periodic particle generation. Figure 6.2a shows that the number of particles undergoes a 20-fold increase during generation followed by a long washout time. Due to this, the conversion is seen to oscillate over a 5% range and from figure 6.2b the average number of branch points per polymer molecule B_N also shows a 5% oscillation. The most dramatic result however is the average particle diameter which also undergoes a 20-fold change since as a burst of new small particles occurs, the average diameter drops drastically. This leads to a very polydispersed particle size distribution being produced by the single reactor.

With a split of .2 so that only 20% of the monomer and water was being added to the seed reactor, the new reactor configuration exhibited stable operation as shown in Figures 6.3a and 6.3b. No oscillations in the number of particles were predicted and all properties maintained a constant level. From Table 6.1 for case I it can be seen that the new system was able to produce a latex with the same average diameter and conversion as the single reactor case but with fewer branches per polymer particle, and with less initiator and emulsifier requirements. In addition the particle size distribution (PSD) was narrower than the PSD during single reactor operation. The 10% reduction in the average branch points per polymer molecule observed also should yield a more processable product in terms of reduced viscosity and die swell for the system.

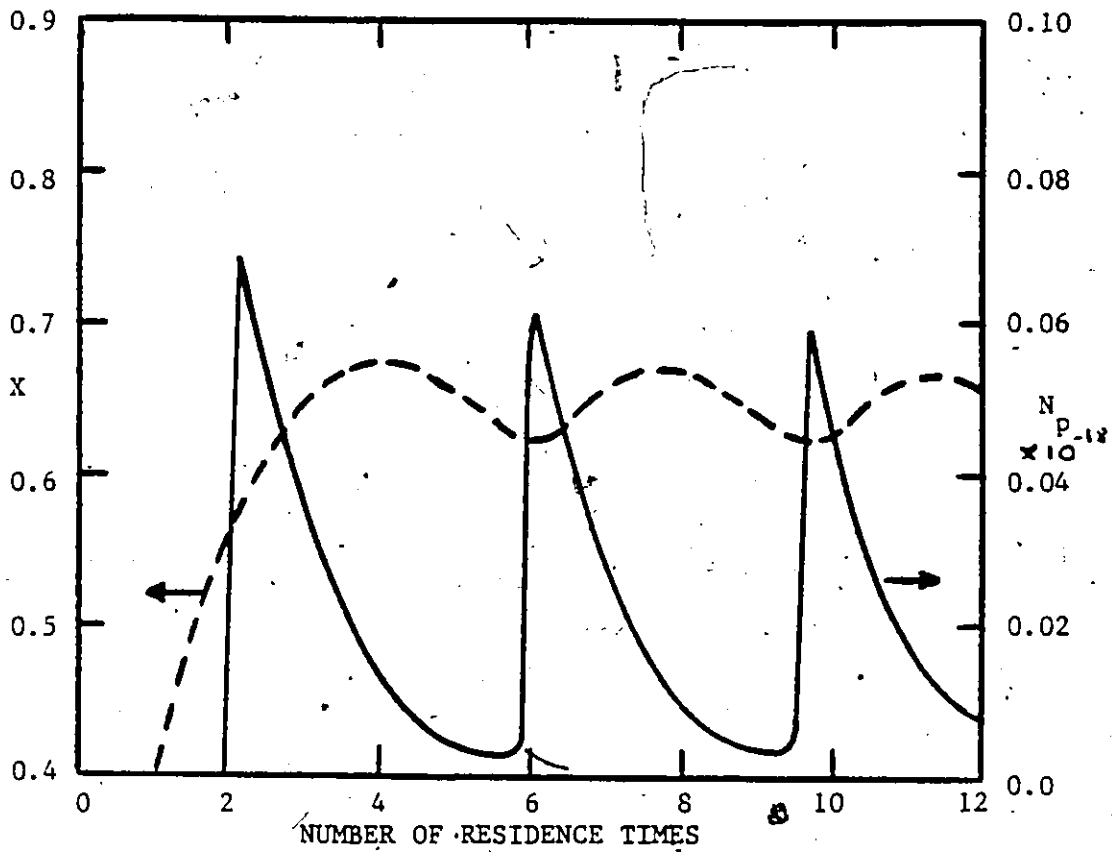
BASE CASE

FIGURE 6.2a - Graph of Conversion X and Number of Particles N_p versus Time for Base Case Reactor Configuration

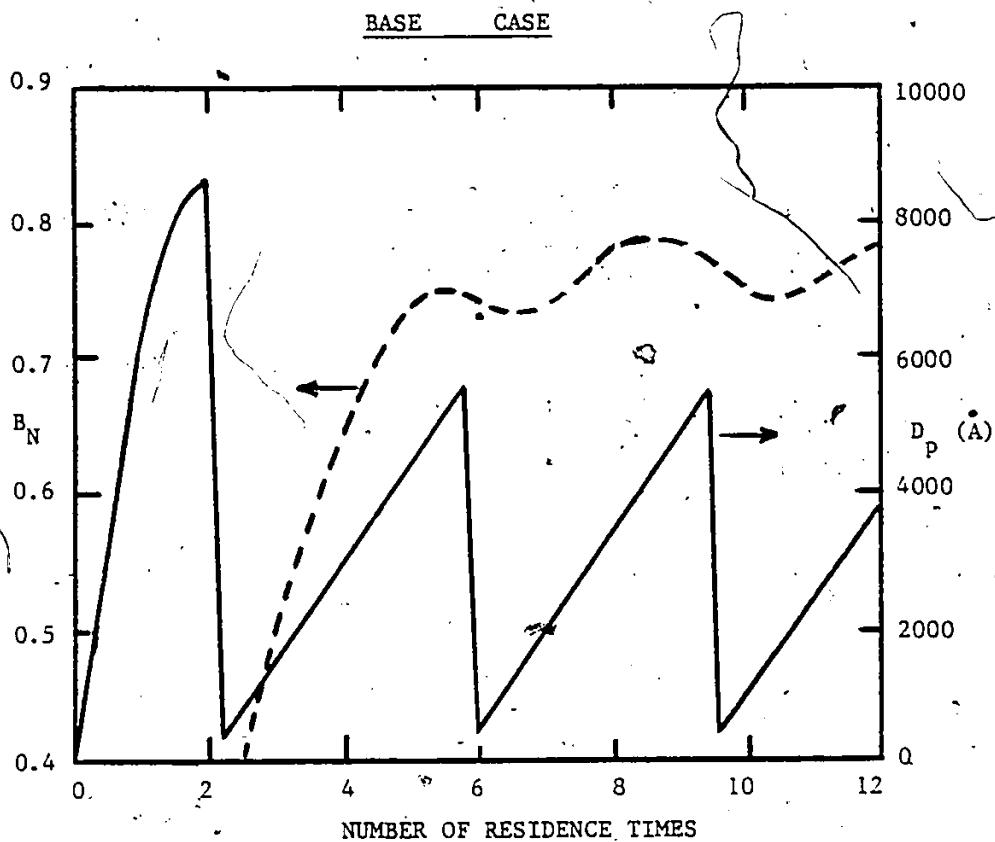


FIGURE 6.2b - Graph of Average Number of Branch Points per Polymer Molecule B_N and Number Average Particle Diameter D_p versus Time for Base Case Reactor Configuration

NEW REACTOR CONFIGURATION

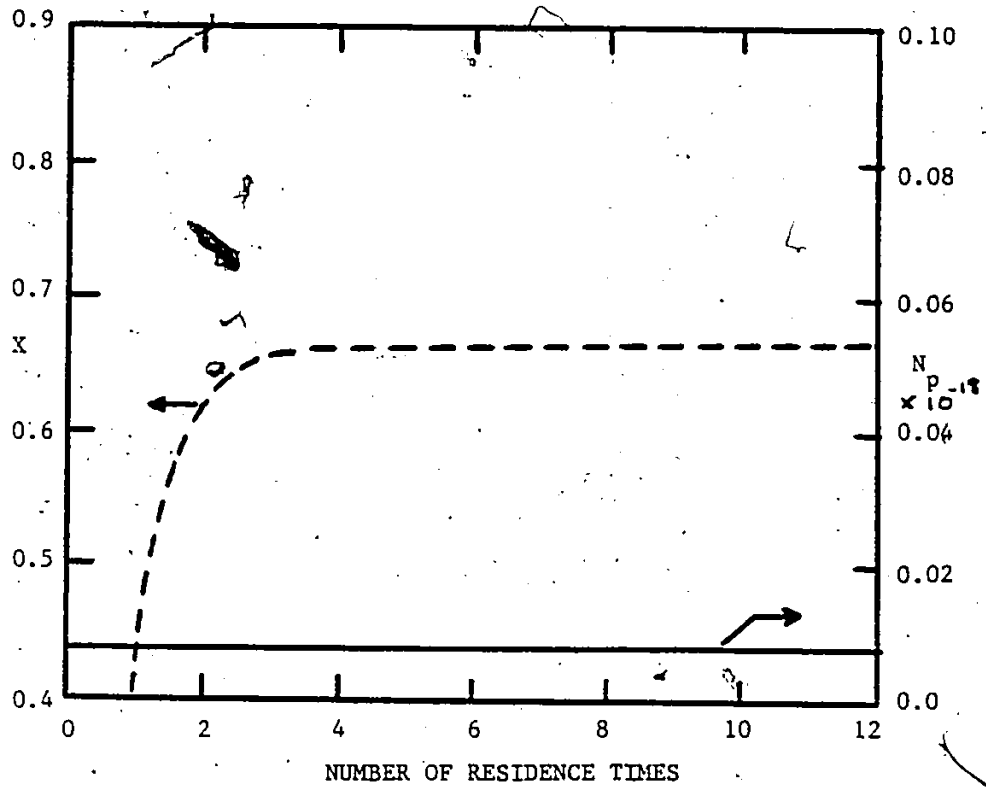


FIGURE 6.3a - Graph of Conversion X and Number of Particles N_p versus Time for Redesigned Reactor Configuration

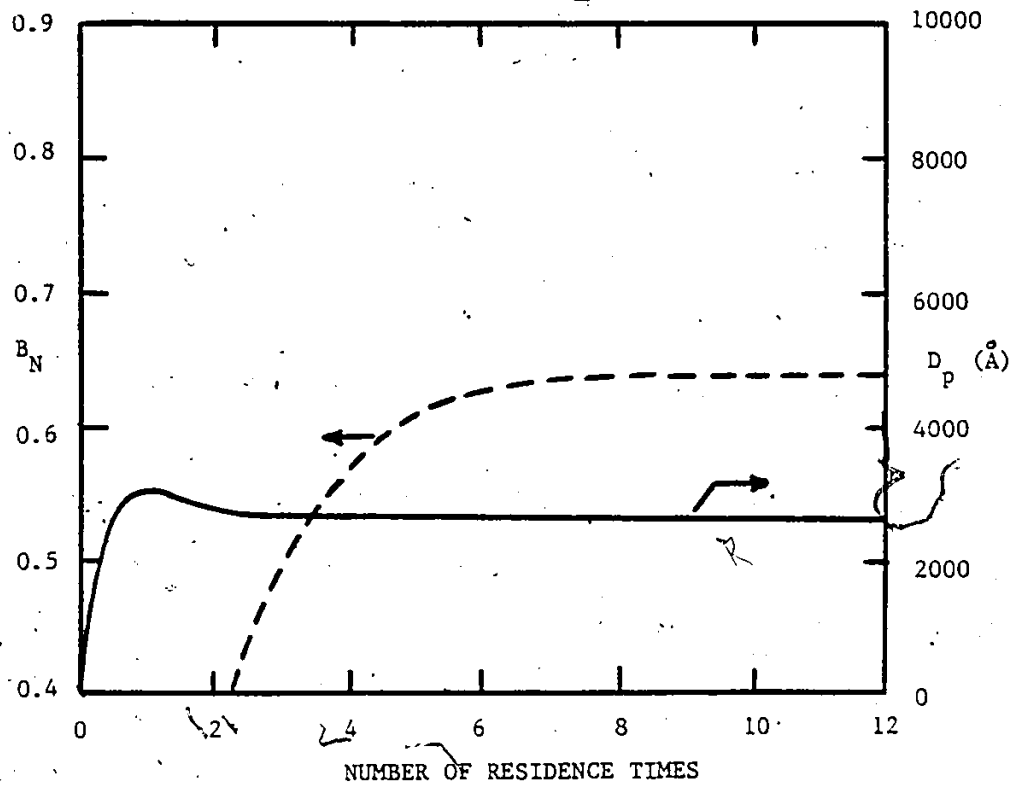
NEW REACTOR CONFIGURATION

FIGURE 6.3b - Graph of Average Number of Branch Points per Polymer Molecule B_N and Number Average Particle Diameter D_p versus Time for the Redesignated Reactor Configuration

Case II illustrates that if the same molecular weight and particle size averages are desired as for the base case operation, approximately 6% higher conversion can be obtained using less initiator and still maintain stable operation. This can represent a significant savings in terms of raw material costs plus monomer removal costs for the system.

Thus, this study demonstrated that the redesigned configuration can achieve superior performance in terms of more stable operation, lower raw material costs and either a higher conversion or more processable product when compared to a single continuous emulsion polymerization reactor on its own.

6.3.2 CHOICE OF OPERATING CONDITIONS

From previous discussion several operating parameters could be manipulated for changing operating levels of the new system. These consisted of the initiator and emulsifier concentrations, the degree of split or bypass of the feed streams, and the size of the small seed reactor. It is the purpose of this section to discuss the effects of these parameters in more detail.

To examine the space of operating parameters, each parameter was examined at 3 levels: emulsifier and initiator concentrations were run at .005, .0075 and .01 mole/L. latex, SPLIT was run at .2, .4 and .6 and the size of the seed reactor was 1/16, 1/8 and 1/5 the size of the large main reactor as discussed in section 6.3.1. A total of eighty-one simulations were then carried out using these parameters in

all combinations in order to observe parameter effects. These results are summarized in Appendix III and are too lengthy to present in detail here. Instead, the latex properties were plotted three dimensionally as a function of initiator concentration and split for constant soap and seed reactor size. The soap was not used as an independent variable since once soap concentration is decided, it is seldom changed due to its effect on downstream operations. Since seed reactors will usually be of a fixed size, plots were not carried out using seed reactor size as an independent variable as well.

These results are shown in the set of Figures 6.4 to 6.15. Results will be discussed for the different parameter effects for just one emulsifier concentration, $[S] = .01$ mole/l. The results are readily extended to the other two soap levels.

The first three figures show the effect of parameter levels on conversion. By examining and comparing these figures the following effects were noted: i) increasing initiator concentration increased conversion, ii) decreasing split increased conversion, and iii) all of the reactor sizes showed essentially identical conversion levels with the levels increasing slightly with increasing size of seed reactor. Similar studies of the figures for average diameter, number average molecular weight and number of particles were done and are summarized with the conversion results in Table 6.2.

TABLE 6.2

EFFECTS OF PARAMETER CHANGES ON
PROPERTIES AS PREDICTED BY THE MODEL

Parameter/ Property ↓	Increase in $[I]_W$ PRODUCT	Increase in SPLIT	Increase in V_1	Increase in $[S]_{PRODUCT}$
Conversion	Increase	Decrease	Slight increase	Increase
Average Diameter	Little effect	Large increase	Decrease	Large decrease
\bar{M}_n	Slight increase	Slight decrease	Decrease	Slight increase

The effect of increasing the soap concentration is also shown, though no figures are provided to illustrate this result. The effect of parameters on the number of particles is shown in the final three figures and presents some interesting results. For larger seed reactors, the number of particles decreased with increasing split and were effectively independent of changes in initiator levels. However, for the smallest size seed reactor, the number of particles first decreased and then increased with continuing increases in the degree of split which is probably due to a residence time effect becoming important at small seed reactor sizes. The structure of the system can thus cause large non-linear effects in the number of particles being generated but these non-linear effects do not seem to be important to the behavior of the other latex properties as all other

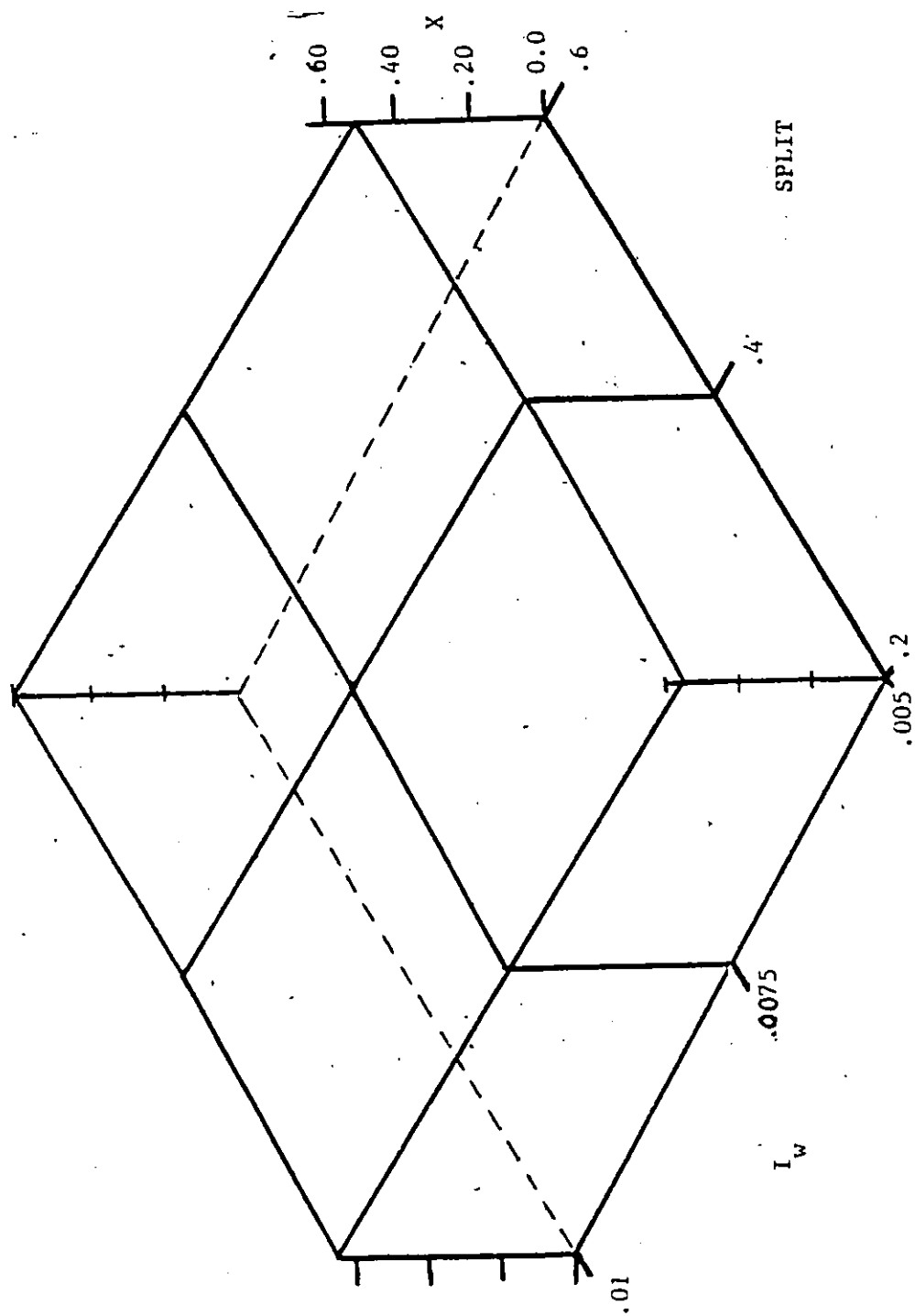


FIGURE 6.4 - Conversion X versus Concentration of Initiator in the Water
Phase I_w and Degree of Bypass SPLIT for $V_1=75$ mL, $S_T = .01$ M

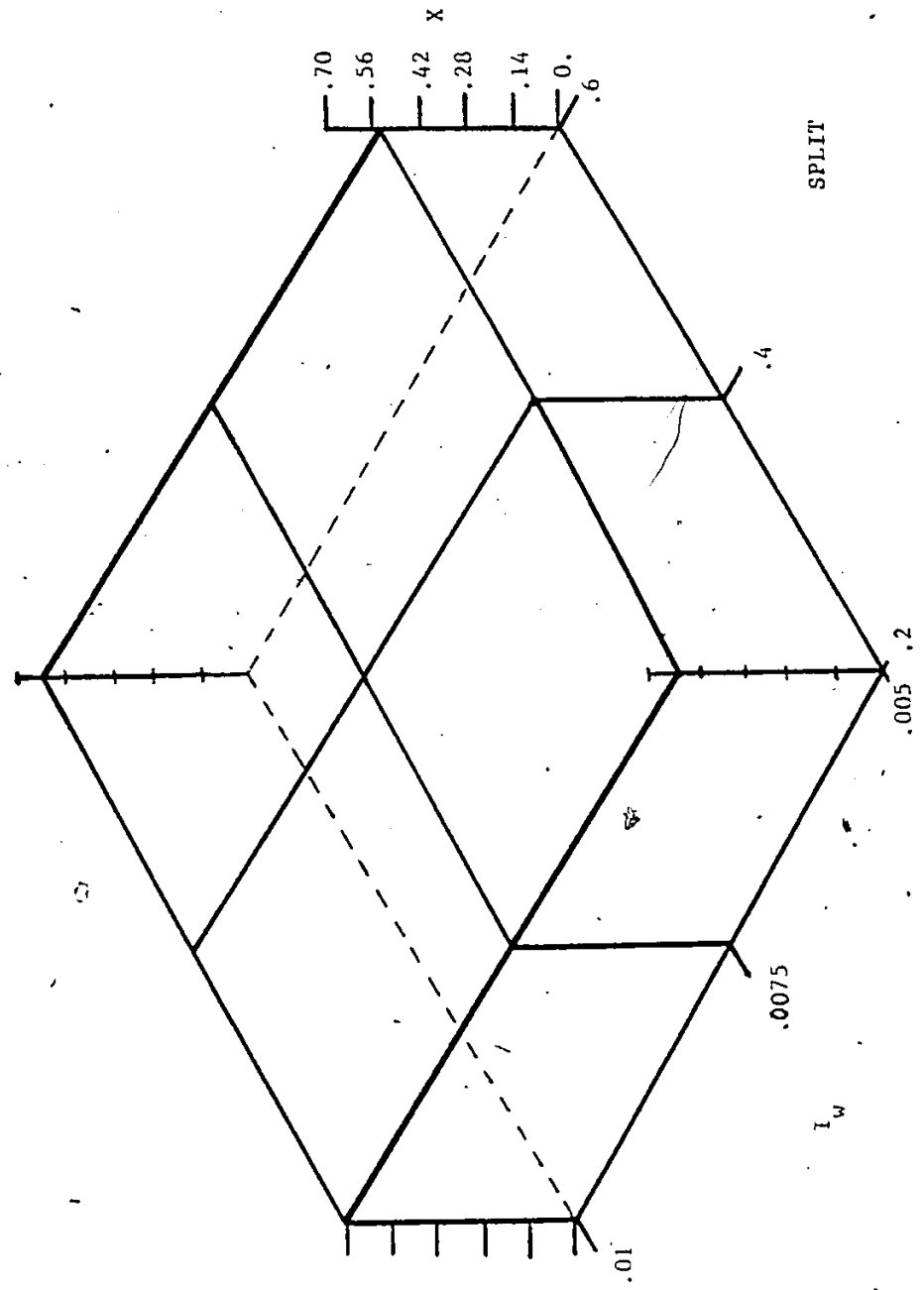


FIGURE 6.5 - Conversion X versus Concentration of Initiator in the Water
Phase I_w and Degree of Bypass SPLIT for $V_1=150$ mL., $S_T = .01$ M

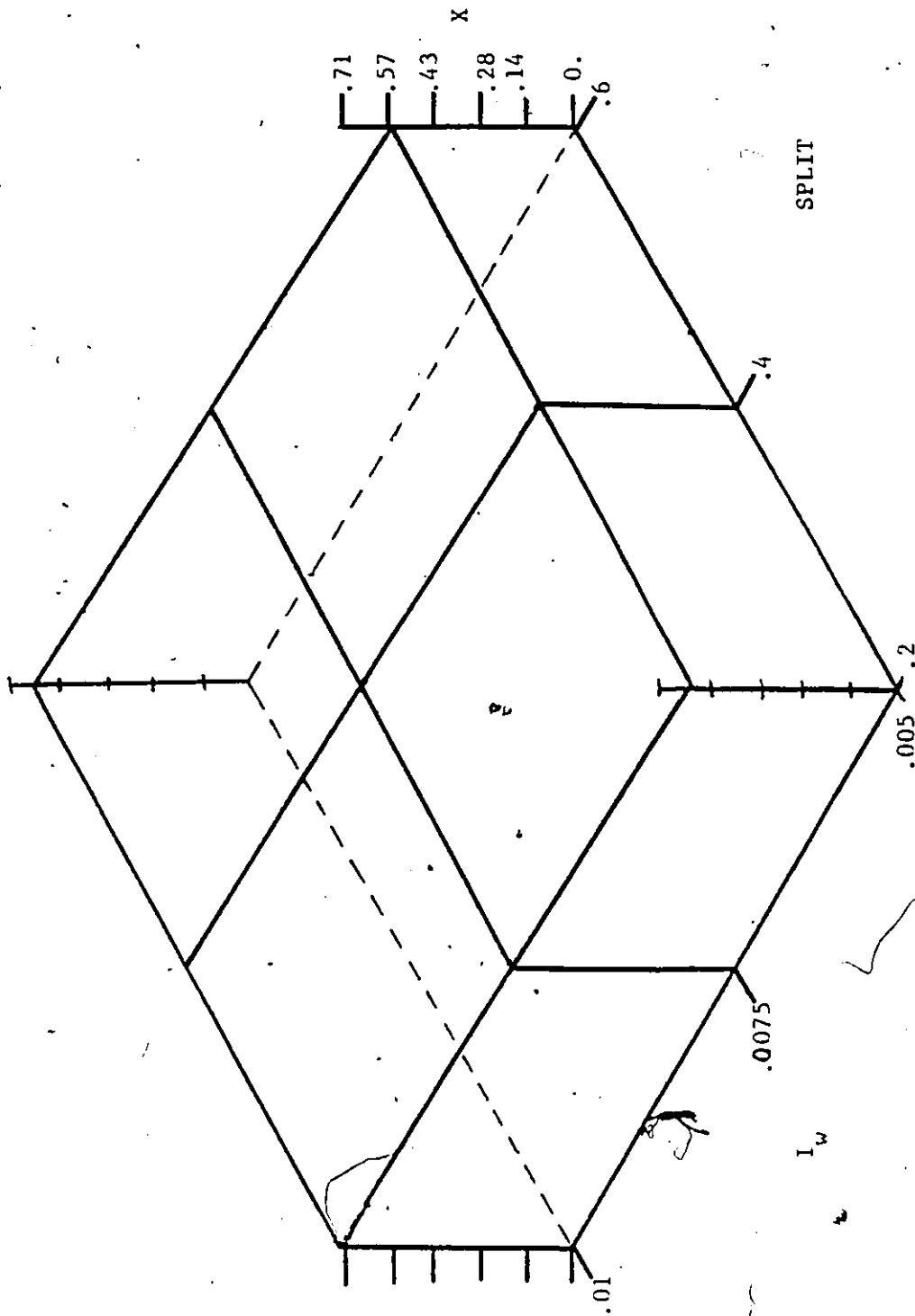


FIGURE 6.6 - Conversion X versus Initiator Concentration in the Water
Phase I_w and Degree of Bypass SPLIT for $V_1=225$ mL., $S_T = .01$ M

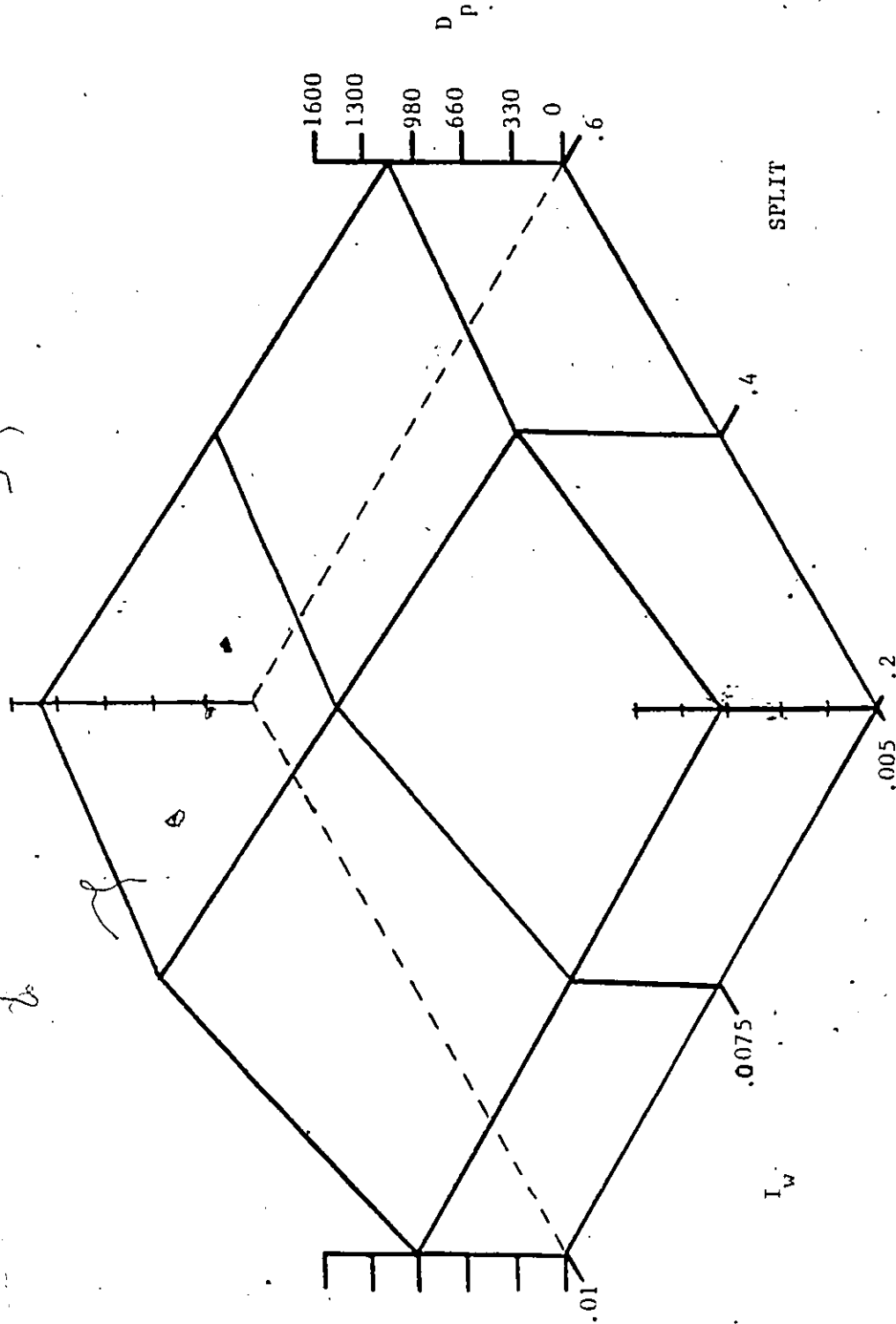


FIGURE 6.7 - Number-Average Particle Diameter D_p versus Initiator Concentration in the Water Phase I_w and Degree of Bypass SPLIT_i for $V_1=75$ mL., $S_T=.01M$

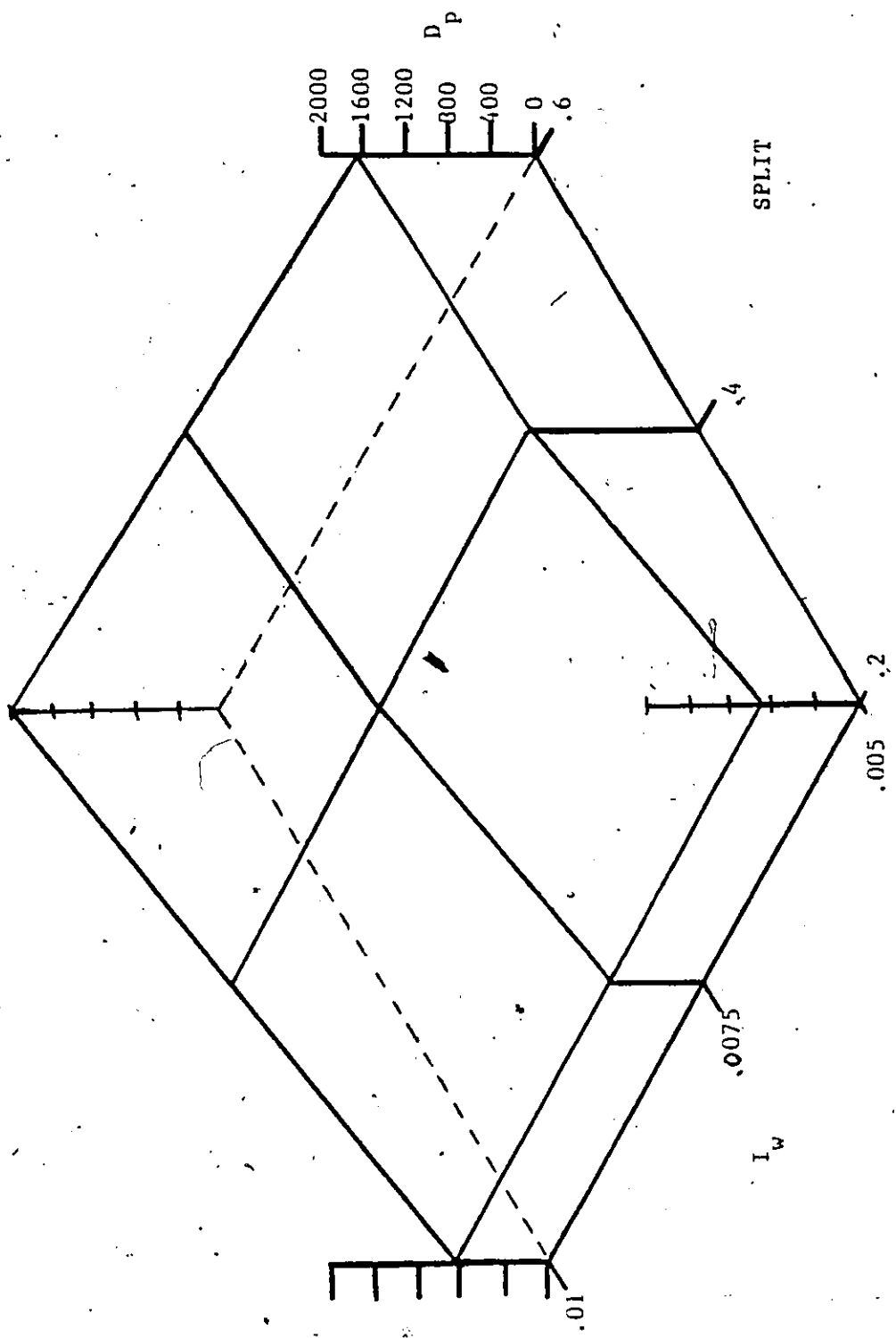


FIGURE 6.8 - Number Average Particle Diameter D_p versus Initiator Concentration in the Water Phase I_w and Degree of Bypass $SPLIT$ for $V_1 = 150$ mL., $S_T = 0.01M$

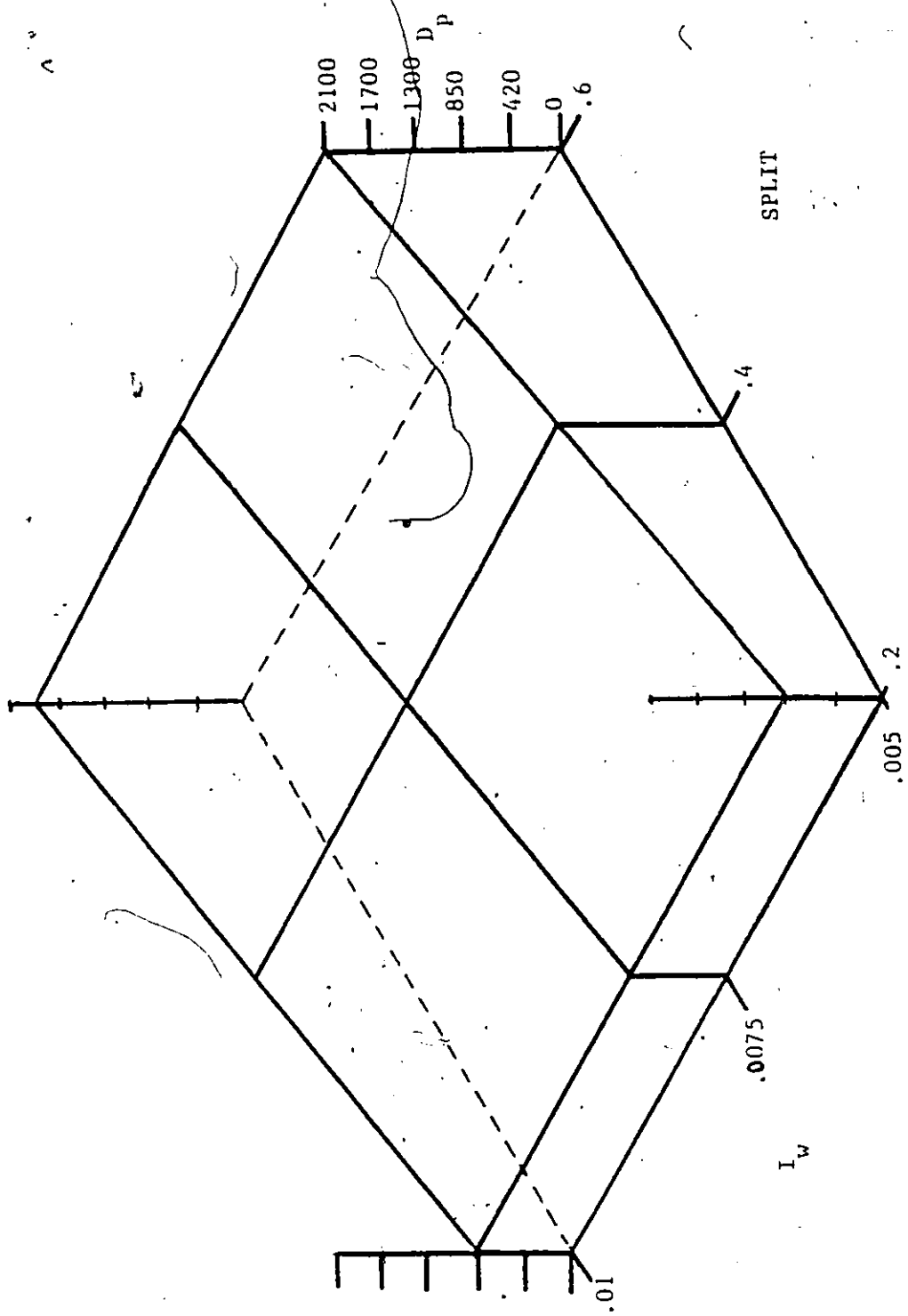


FIGURE 6.9 - Number Average Particle Diameter D_p versus Initiator Concentration S_1 in the Water Phase I_w and Degree of Bypass SPLIT for $V_1=225$ mL., $S_1=.01M$

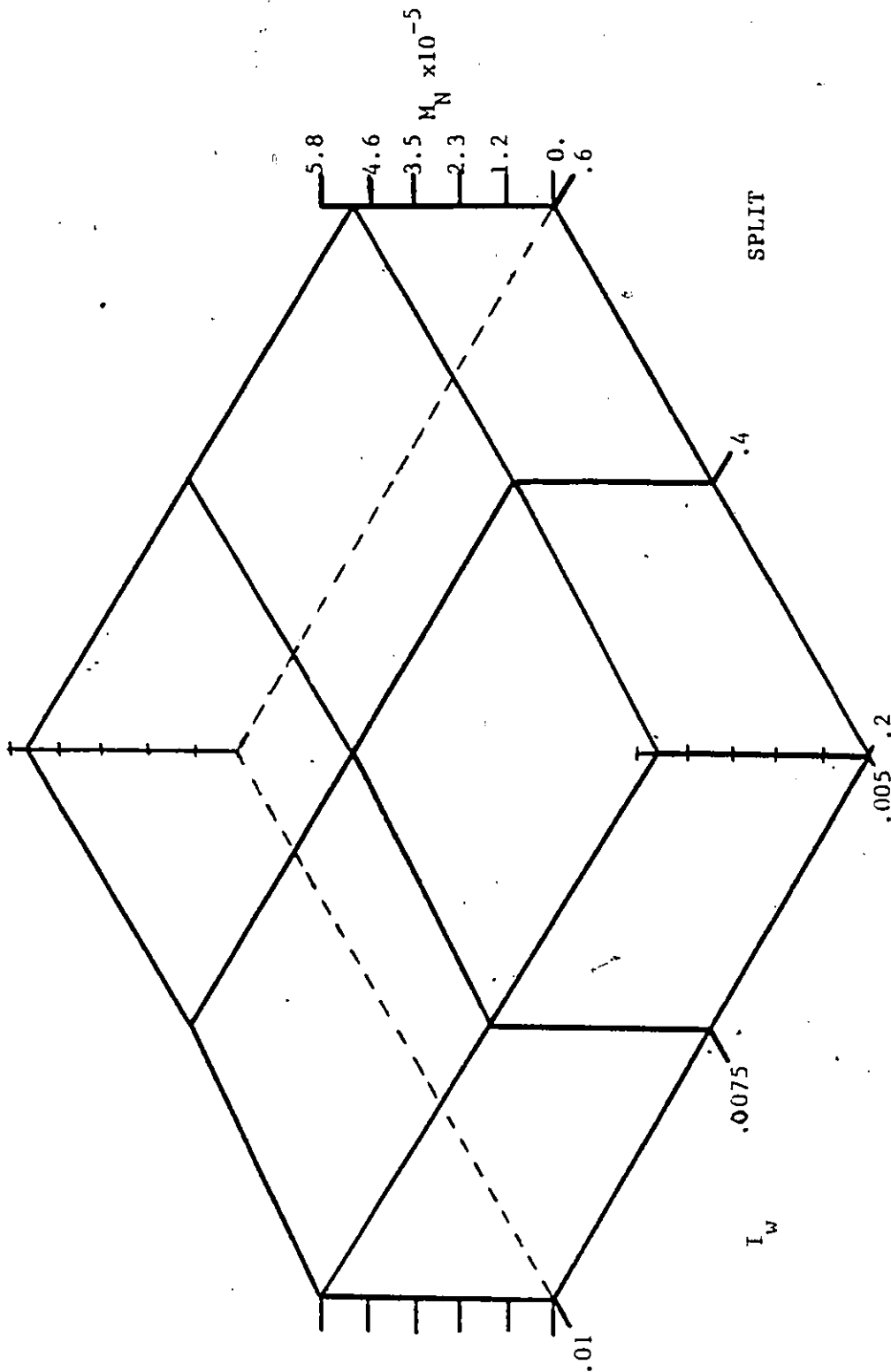


FIGURE 6.10 - Number Average Molecular Weight M_N versus Initiator Concentration in the Water Phase I_w and Degree of Bypass SPLIT for $V_I = 75$ ml., $S_T = .01$ M

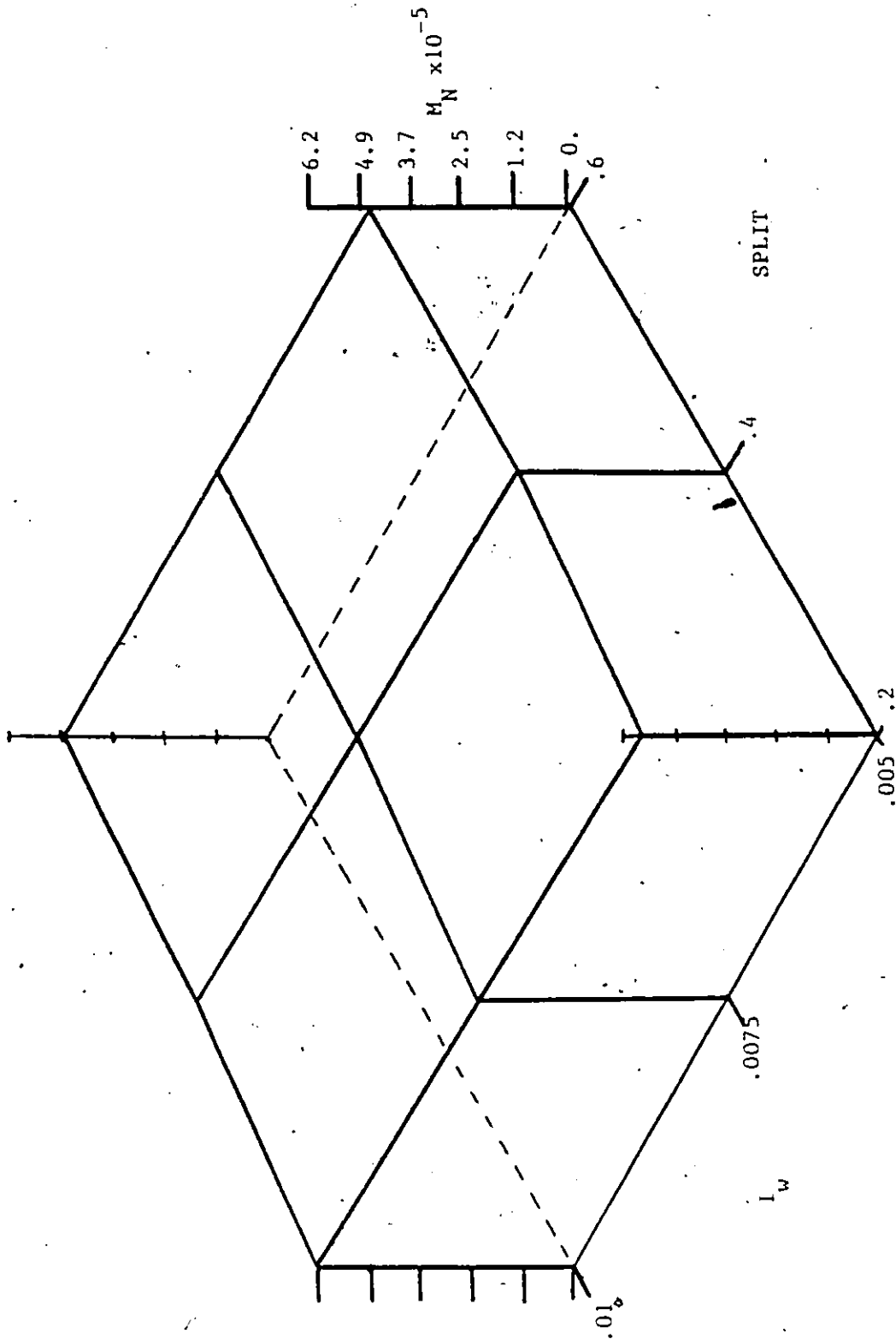


FIGURE 6.11 - Number Average Molecular Weight M_N versus Initiator Concentration in the Water Phase I_w and Degree of Bypass SPLIT for $V_1=150$ mL., $S_T=.01M$

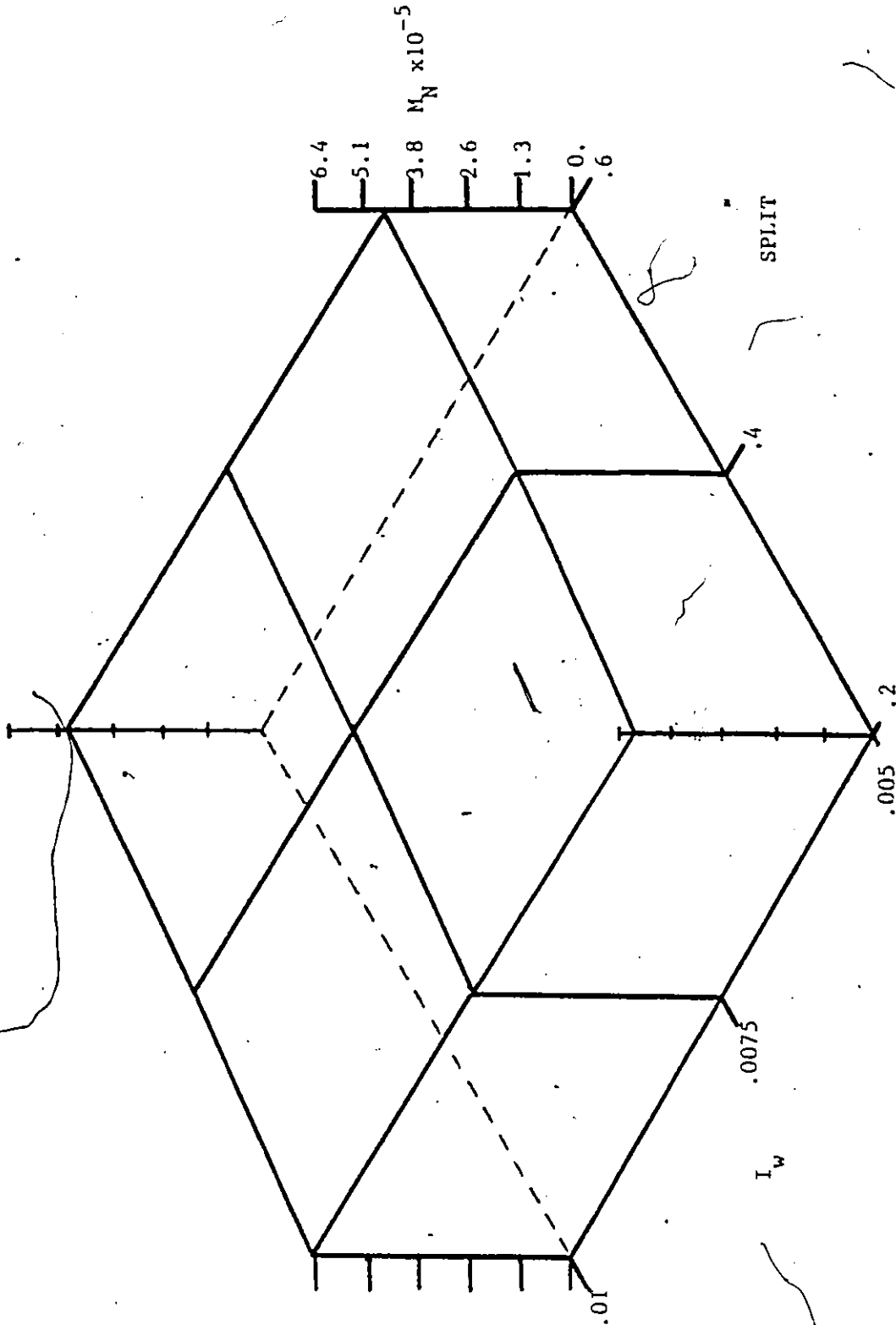


FIGURE 6.12 - Number Average Molecular Weight M_N versus Initiator Concentration in the Water Phase I_w and Degree of Bypass SPLIT for $V_1=225$ mL., $S_T=.01$ M

e

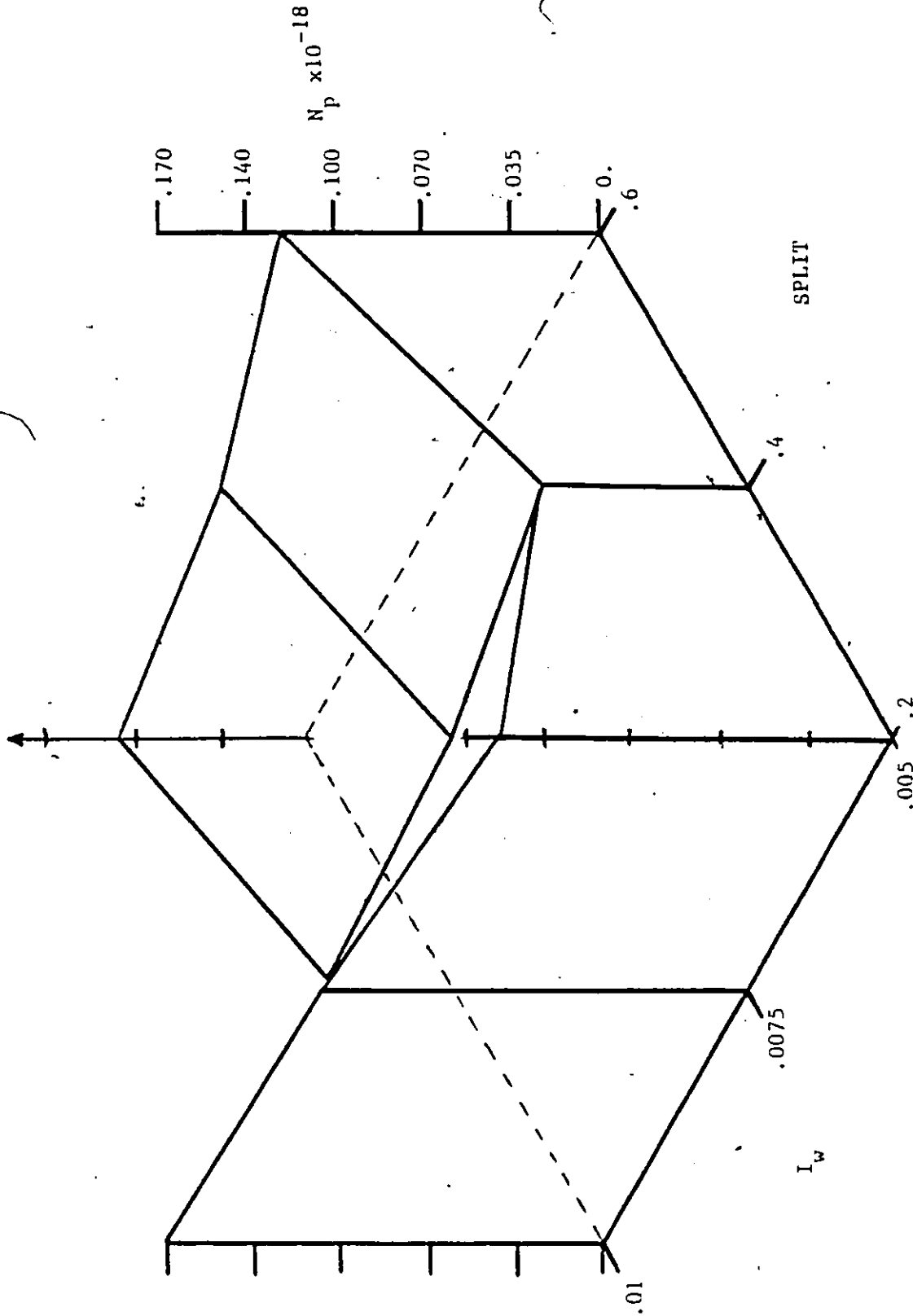


FIGURE 6.13 - Number of Particles N_p versus Initiator Concentration in the Water Phase I_w and Degree of Bypass SPLIT for $V_1 = 75$ mL., $S_T = .01$ M

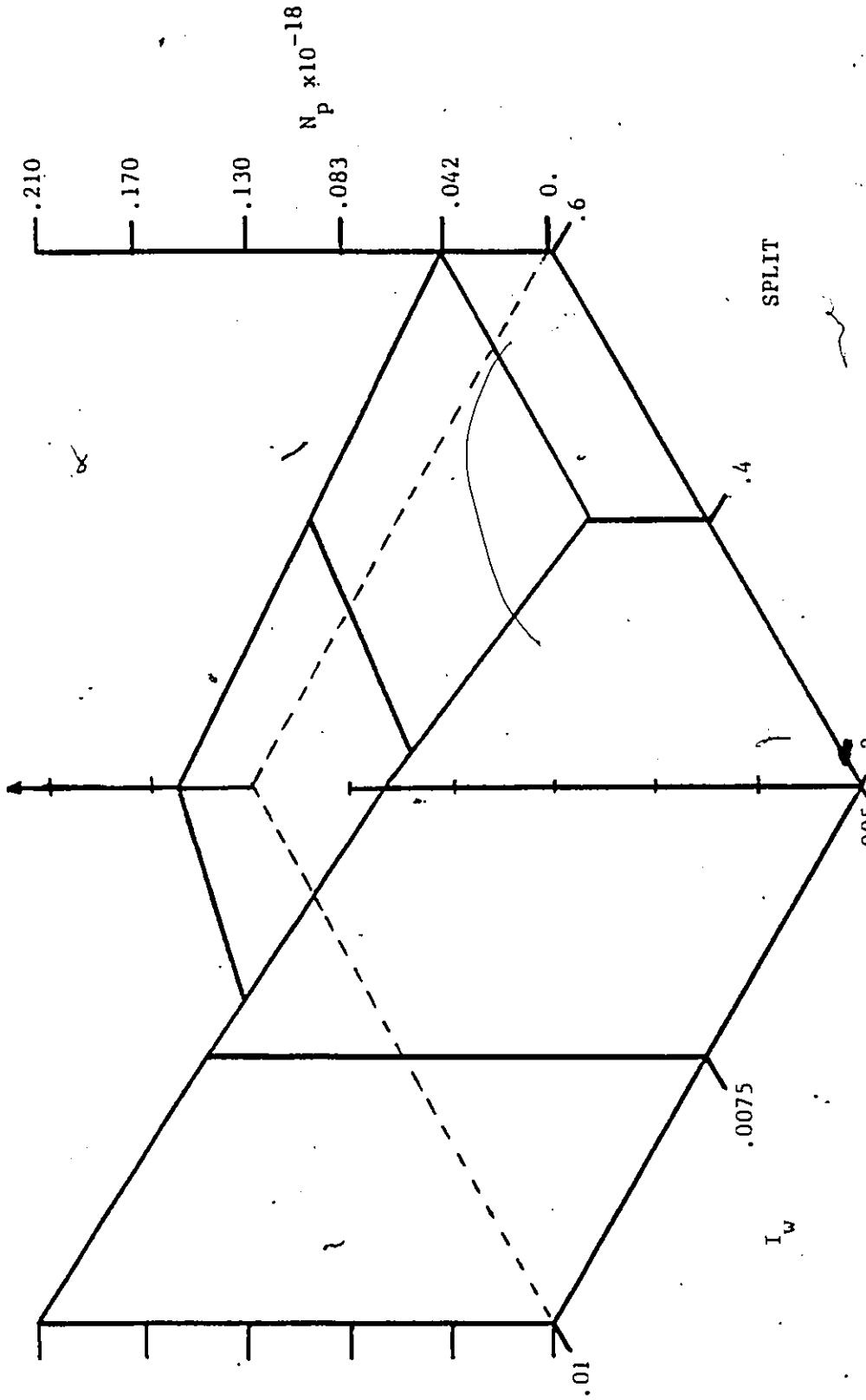


FIGURE 6.14 - Number of Particles N_p versus Initiator Concentration in the Water Phase I_w and Degree of Bypass SPLIT for $V_1 = 150$ ml., $S_T = .01$ M

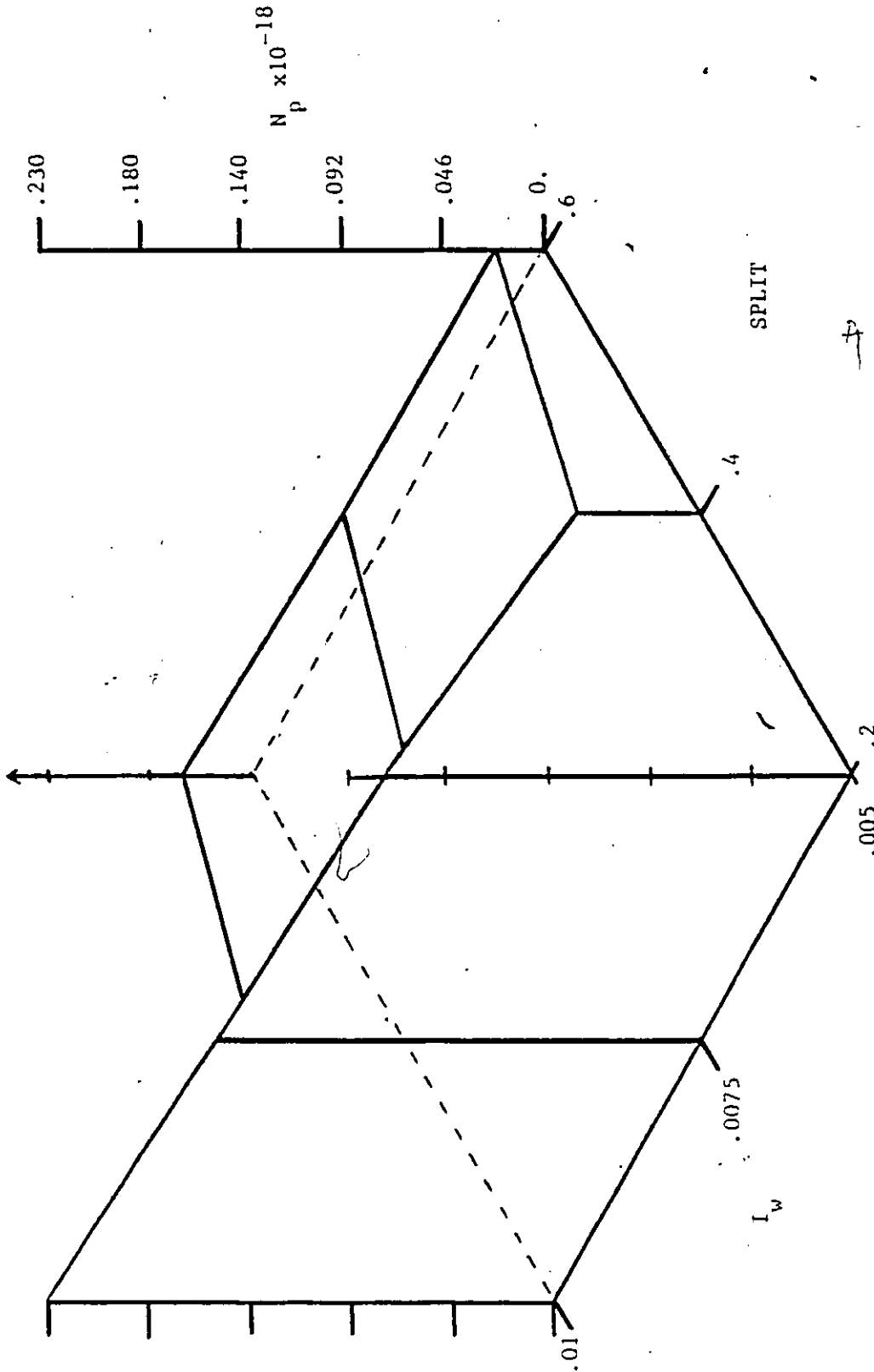


FIGURE 6.15 - Number of Particles N_p versus Initiator Concentration in the Water Phase I_w and Degree of Bypass. SPLIT for $V_1=225$ mL., $S_T = .01$ M.

properties usually show either steady decreases or increases with no real saddle shapes as appear for the number of particles.

The particle diameter appeared to be the most sensitive property to changes in operating variables so that for different operating parameters it was possible to maintain the same conversion but vary the particle size using changes in the degree of split in the system plus changes in initiator concentration. Results illustrating this fact are shown in Table 6.3. The first four rows show the effect of changing only the feed split in the system. This results in a decrease in particle size from 1200 Å down to 600 Å with a 10% increase in conversion. The amount of long chain branching and hence

TABLE 6.3

COMPARISON OF POLYMER LATEX PROPERTIES FROM REACTOR 2 WHEN USING DIFFERENT BYPASS PERCENTAGES AS CONTROL VARIABLE ($\theta_2 = 1800$ SEC., $V_1 = 75$ MLS., $[S] = .01$ MOLE/L)

Split	[I] (mole/L.)	X	D_p (Å)	N_p ($\times 10^{-18}$)	M_N ($\times 10^{-5}$)	M_W ($\times 10^{-6}$)	B_N
.4	.01	.616	1670	.047	5.06	2.40	.756
.3	.01	.637	1340	.075	5.33	3.29	.920
.2	.01	.666	980	.17	5.77	6.22	1.20
.1	.01	.702	610	.62	6.32	--	1.67
.4	.01	.616	1670	.047	5.06	2.04	.756
.3	.0085	.616	1360	.078	5.21	2.75	.833
.2	.0069	.617	1010	.16	5.49	3.73	.993
.1	.005	.618	640	.58	5.79	8.06	1.20

weight average molecular weights also increase mainly due to the increase in conversion. The final four rows of Table 6.3 show that by changing the split and decreasing the amount of initiator, the conversion was maintained constant while the particle sizes were still decreased by about the same amount. The increases in molecular weight were not so dramatic and would usually be controlled by addition of a chain transfer agent in most practical applications.

In none of the simulations using the two smallest seed reactors were any oscillations in the final latex properties observed. If the first seed reactor was increased further in size, however, as in the case of the largest seed reactor, it was possible to observe some small oscillations in the product since the largest seed reactor plus main reactor began to approach the usual industrial system of equal sized reactors where oscillations do occur.

The conclusions from this section were that the choice of a reasonably small seed reactor should prevent oscillations for all operating conditions used. In addition, operating conditions could be chosen so that a switch from one condition to another would not change the conversion but would alter the average particle size which indicated a highly flexible reactor configuration.

6.3.3 FORCED OSCILLATION FOR BROADENING OF PSD

For certain applications a lower bulk latex viscosity is desired. For constant solids, it is possible to lower the

viscosity by producing a broader particle size distribution. With the redesigned system this can be easily accomplished by cycling the degree of bypass in some manner, either sinusoidally or in a square wave pattern, for example, with the concentrations and seed reactor volume chosen to produce diameters in the desired range. The cycling behavior in this case can be controlled well and is accomplished by changing only a physical variable, the degree of split, which is easily applied in a practical sense. It is the purpose of this section to present results illustrating the technique and subsequent broadening of the distribution.

Results from several simulations are shown in Table 6.4. The simulations were run by first holding the split steady yielding stable operation and constant levels, then introducing a square wave function of a given amplitude into the split. (some small scatter of particle diameter was still apparent as shown by the non-zero standard deviation with zero amplitude). The period for the entire square wave for these simulations was 80 minutes using a 30 minute residence time for the large reactor and a seed reactor size of 1/16 of the main reactor. In this way the split was high for 40 minutes followed by low for 40 minutes where the amplitude was considered as one half the difference between high and low split levels.

Case I and II are the results comparing cycling about a split level of .4 and .5, respectively. These results illustrated that cycling increased the breadth of the particle size distribution

strongly as measured by the standard deviation of the diameter distribution. As the amplitude increased, however, the average diameter was seen to decrease yielding the wrong average diameter. Case III used a technique to eliminate the problem. Case IIIB showed the same behavior as Cases I and II with a decrease in average diameter. Case IIIC showed that by keeping the amplitude constant but increasing the average split during cycling that the average diameter decrease could be compensated for and still yield a broad distribution.

TABLE 6.4

SIMULATION RESULTS FROM SQUARE WAVE
VARIATION OF SPLIT PARAMETER

		Split	Amplitude	\bar{D}	Standard Dev. of Diameter	\bar{X}	\bar{B}_N
Case I:	A) Steady	.4	0	1640	52	.616	.756
	B) Cycling	.4	.2	1455	69	.623	.834
	C) Cycling	.4	.3	1175	165	.648	.979
Case II:	A) Steady	.5	0	1480	44	.614	.803
	B) Cycling	.5	.15	1420	83	.616	.833
	C) Cycling	.5	.3	1120	128	.639	1.01
Case III:	A) Steady	.2	0	980	40	.666	1.20
	B) Cycling	.2	.1	810	174	.690	1.30
	C) Cycling	.25	.1	1090	190	.658	1.08

By proper choice of the average split the average diameter could thus be maintained constant but a much broader distribution produced.

These results are illustrated for Case III in Figure 6.16.

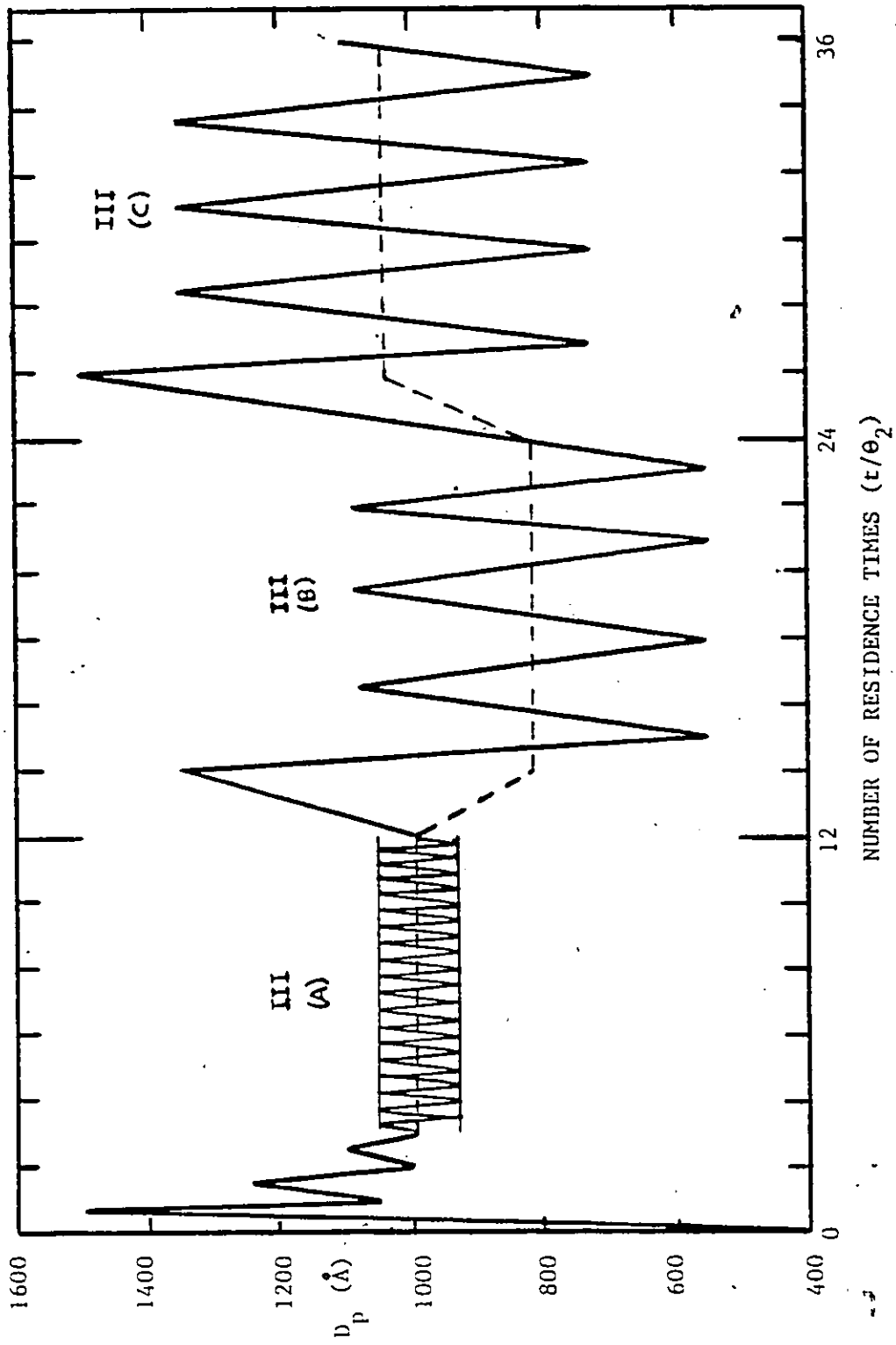


FIGURE 6.16 - Graph of Number Average Particle Diameter D_p versus Number of Residence Times showing Controlled Oscillation for Particle Size Distribution Broadening (Case III)

One other possibility to eliminate the diameter decrease during cycling is to change the type of cycle used. For example, more time spent at the high split level would bias the diameters in favor of larger sizes. By using a square wave of unequal times at the extremes the average diameter could be held constant. In effect this would be the same as shifting the time average split of the system which is the same result as occurs by the technique used in this study.

It should be noted that the extent of the diameter oscillations shown in Figure 6.16 is not as extreme as that of the single reactor of Figure 6.2b. However, the forced oscillation system is more controlled in its operation, and as shown by the results in Table 6.4 the diameters can easily be shifted from one level to another by changing a physical parameter, split, rather than emulsifier levels. The potential for tailor making a distribution by choosing an appropriate function for cycling the split thus makes this system much more flexible than a single CSTR operating on its own. While not illustrated here, larger swings in amplitude should be possible in order to produce a particle size distribution (PSD) comparable to or broader than the PSD of a single CSTR.

The final conclusion for this section is that by cycling the split in a controlled manner about a slightly increased average split level compared to the split for steady operation, a broader particle size distribution could be produced with the same average particle diameter as for steady operation.

6.4 SUMMARY AND CONCLUSIONS

The usual industrial system for the production of polymer latices by emulsion polymerization consists of a series of nearly equal sized CSTR's in which all feed streams enter the first reactor. The new reactor configuration has several advantages over this traditional design as discussed in previous sections.

The maximum amount of emulsifier required should be determined by the latex stability criteria and not by the need to produce an adequate number of particles for any reactor system. In the new configuration, by adjusting the split, the emulsifier levels in the seed reactor can be set to high concentrations to produce the required number of particles in the system. In this way the total soap added to the reactor system can be determined by latex stability since the particles have already been nucleated upon entering the main reactor train.

The new system was also highly flexible in its operation. The volume of the small seed reactor, the degree of split and the initiator can all be used as control variables in the system without changing the emulsifier levels. Using these variables it is possible to produce a wide variety of latex products as discussed in the simulation results.

The main advantage for this system is stable reactor operation. With the seed reactor present no property oscillations in the latex product are observed. Even if the seed reactor is undergoing property oscillations, the combination of dilution of the seed reactor effluent

by the bypass stream plus the large difference in residence time for the seed and main reactors damp out any seed reactor oscillations which occur. This result is illustrated more fully in the simulation section and the stable operation is demonstrated experimentally in Chapter 7.

Another advantage for the redesigned system is that purification of the feed to the seed reactors may become economical. The nucleation step for emulsion polymerization is highly sensitive to the presence of impurities. Since all nucleation occurs in the small seed reactor in the redesigned configuration, only impurities in the feeds to the seeder need to be considered. With the large bypass in the redesigned configuration, these feeds are small. Purification of these feeds may thus be feasible leading to insensitivity to feedstock changes and a higher efficiency of nucleating polymer particles. This reproducibility in the long run may be economical for an industrial situation.

For some operating conditions, lower initiator and soap may be required than for the conventional system to produce the same latex product. This represents a decrease in the raw material costs for this system.

For many applications a narrow particle size distribution is desired. However, in some instances such as when a lower bulk latex viscosity is desired a broader particle size distribution is better. The redesigned reactor configuration can produce broader particle size distributions in a controlled manner by cycling of the split for the

feed streams. Thus, tailor making of a desired particle size distribution may be possible with this system.

In conclusion, the redesigned reactor configuration offers many advantages over the conventional system, with stable operation and high flexibility being the main advantages for this system.

1/2

CHAPTER 7

EXPERIMENTAL RESULTS

7.1 INTRODUCTION

The experiments carried out for this study had two main aims. First, to prove the simulation results stating that the oscillations could be removed by the use of the split feed seed reactor design as discussed in Chapter 6. Secondly, to obtain experimental verification of the molecular weight section of the model and estimates of the important parameters in the model as discussed in Chapter 3.1.

7.2 EXPERIMENTAL PROCEDURE

7.2.1 MATERIALS

The raw materials used for this study were vinyl acetate, distilled water, sodium lauryl sulphate (SLS) as emulsifier and potassium persulphate as initiator.

The vinyl acetate was provided by the CIL research laboratories in Toronto. During the runs for checking out the design stage control scheme, the vinyl acetate was distilled once before use to remove the inhibitor and stored refrigerated in an opaque container to prevent polymerization. This was done to reduce any unreproducible effects due to monomer soluble impurities in the vinyl acetate monomer. When carrying out molecular weight determination runs as described later,

however, the vinyl acetate was used as supplied without distillation. The conversion level was the important parameter in these runs and could be measured directly. Any deviation could be compensated for by changing initiator levels and detailed predictions of all the PSD properties were not required so that impurity effects were not deemed to be as critical.

The emulsifier used was sodium lauryl sulphate as supplied by BDH Chemicals without further purification. The initiator was laboratory grade (99.7% purity) potassium persulphate as supplied by Fisher Chemicals, which also was not purified further. The high purity nitrogen used to purge the system and to provide an inert blanket over the reactors was first bubbled through a 5% pyrogallol solution in 2 N NaOH to remove oxygen traces before being used in the reactor system for purging or stirring.

7.2.2 REACTOR LAYOUT

The experimental apparatus was designed in such a way that the system could be run as a single CSTR alone, or a small seed reactor could be placed ahead of the large main reactor. By opening and closing clamps on the feed lines, interchange of feed tanks plus introduction and removal of the seed reactor were easily accomplished.

The reactor layout is shown in Figure 7.1. The large reactor was a 1.2 litre glass overflow reactor with an external jacket for heating, and 4 ports in the lid. The central port contained a variable speed stirrer which was set at 320 rpm. The other three

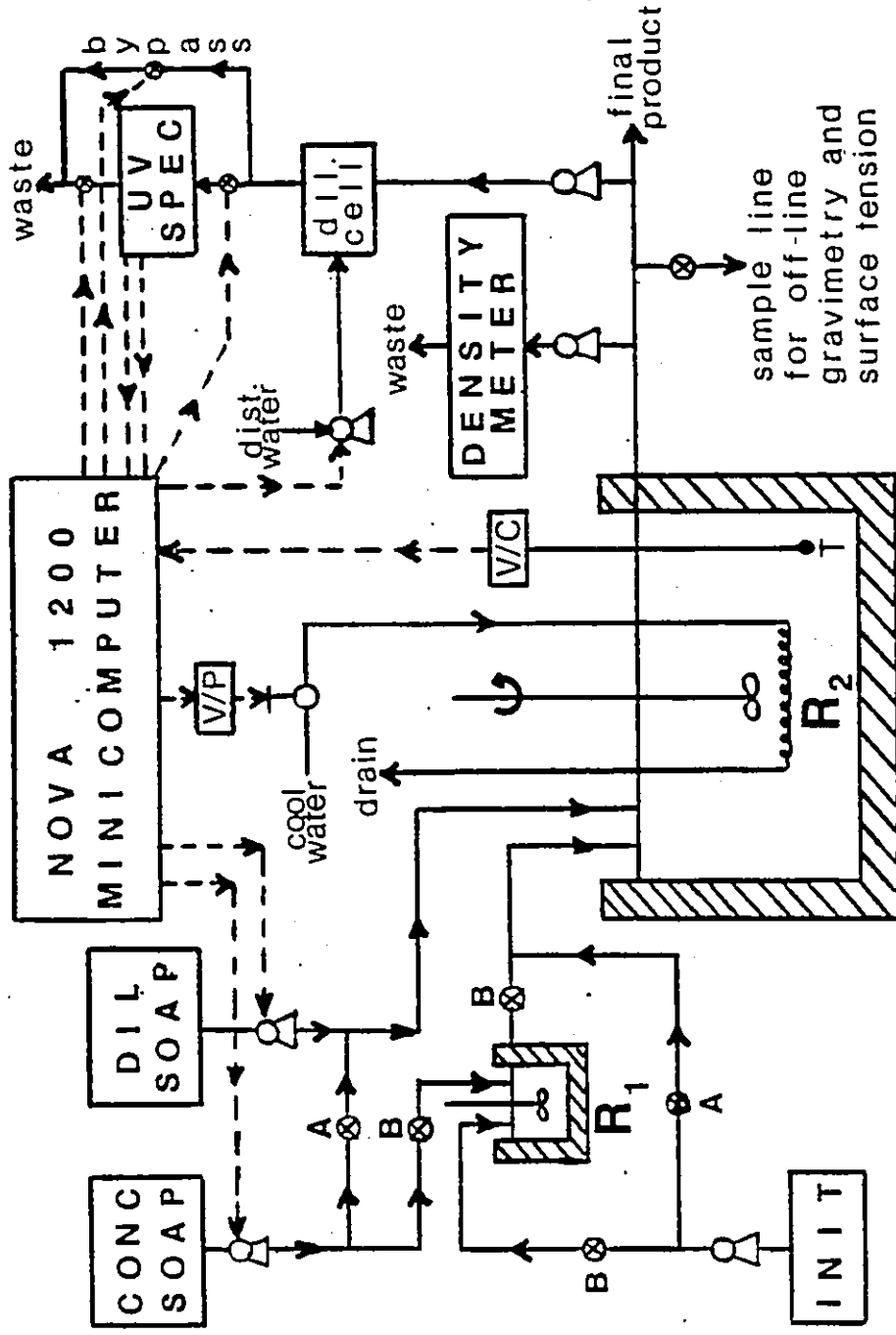


FIGURE 7.1 - Experimental Reactor System

ports were used for introduction of raw material feeds or overflow from the first reactor plus temperature sensors, leads for the cooling coil inside the reactor, and for an overhead condenser to recondense any vinyl acetate vapors.

The seed reactor was a small Erlenmeyer flask (usually of 75 mL volume when stirred) equipped with a magnetic stirrer. Feed streams to the seed reactor entered into the top along with a thermometer for temperature measurement by means of a three-holed cork with rubber cement sealant to prevent oxygen contamination. The whole seed reactor was immersed in a 50°C constant temperature bath. In order to control the temperature of the small reactor, the feed streams to the seed reactor were preheated electrically using heating tape and the temperature control was carried out manually by adjusting the power input to the tape by means of a variable transformer.

The initiator feed tank was an 8 litre polyethylene tank with a bottom take-off. The flow was regulated by a constant displacement pump with the rate being set by the stroke length, though for most applications the flow was held constant at 5 mL/min. The mixture in this tank consisted of initiator only dissolved in water (INIT in Figure 7.1).

The dilute soap feed (DIL soap in Figure 7.1) consisted of a monomer-water emulsifier mixture with just enough emulsifier to stabilize the monomer drops according to the scheme of Figure 6.1. The concentrated soap feed mixture (conc soap in Figure 7.1) also consisted of a monomer-water-emulsifier combination, but containing

the majority of soap. The amount of emulsifier in the concentrated feed tank was calculated to provide the desired concentration in the product after accounting for the small amount of emulsifier fed in with the dilute soap feed stream. The ratio of monomer to water in both soap feeds was identical, and was set to give the desired monomer concentration in the total feed to the main reactor. The dilute soap emulsion feed was held in an 18 litre polyethylene tank equipped with a flat-blade paddle for stirring and bottom take-off. The concentrated soap emulsion feed was centered in two 4 litre interchangeable glass tanks which were stirred by nitrogen bubbling in at the bottom. The flow rates from the two emulsion tanks were set by two variable speed pumps which were under direct control of the minicomputer in this system. These flowrates were adjusted to provide the desired bypass. Through a calibration curve, the appropriate flowrate for each pump yielded the mA signal (4 to 20 mA range) required for the pump. The mA signal was then sent from the minicomputer to a SECO interface box which set the pump stroke frequency to give the desired flow rates for these emulsion feeds.

The temperature control of the large reactor consisted of two parts. The outer jacket of the large reactor was used for heating. A centrifugal pump supplied water at 65°C from an external hot water bath at approximately 13 L/min to the jacket to maintain the jacket temperature constant. The cooling water was then used to control the temperature through a control loop as follows. Two chromel-alumel thermocouples inside the reactor were used to measure the latex temperature. The millivolt signal was sent to an Acromag transmitter which transmitted

a mA signal to the minicomputer where it was converted to a voltage and input using a voltage analogue to digital converter (ADC). The computer implemented a PI control algorithm to calculate a 1-9 V digital to analogue converter (DAC) output which was transmitted by cable to a voltage pressure transducer. The transducer provided a signal in the range of 3-15 psi, which opened a valve on the cooling water line to the cooling coils inside the reactor. This cooling water flow rate was the control variable used to maintain the temperature at a desired setpoint inside the reactor.

The latex product flowed out of the reactor via an overflow line. A sample was taken and fed through an on-line Anton Paar DMA-45 digital density meter for measuring the conversion using a constant displacement pump set at approximately 8 mL/min. The product was also sampled and diluted on-line at a variable ratio as determined by the minicomputer and fed to a Beckman UV spectrophotometer with the signal from the spectrophotometer being sampled and sent to the minicomputer for data collection. Minicomputer-controlled solenoid valves around the spectrophotometer provided a means of bypassing the flow around the instrument while measurements were taken. The dilution ratio was calculated by the minicomputer to keep the signal from the spectrophotometer within the range of maximum selectivity.

The remaining latex product could be either sampled for off-line analysis of conversion, soap area, etc. or was sent to a waste drum for disposal.

With this system, several safety considerations were required. First, vinyl acetate represents a potential fire hazard due to its extreme flammability. As a result, all reactors and feed tanks were placed in a fume hood. Electrical equipment such as heaters, pumps, or pump control boxes were kept outside the fume hood to minimize spark hazards. Also, the waste material from the reactor system was still active and capable of polymerizing further in the waste drum. Since the reaction is highly exothermic, hydroquinone was added to the waste drum to prevent further reaction by eliminating any remaining free radicals.

Due to the exothermic nature of the reaction, reactor runaway was also considered. In case of sensor failure, the minicomputer was instructed to turn the cooling water on full to shut down the reaction, and to stop all entering flows. If the computer failed, raw material feeds would cease, and the 65°C jacket temperature would serve to prevent a runaway condition, since the jacket would serve to cool the reaction mixture if the temperature exceeded 65°C. A hydroquinone solution was also kept handy to dampen the reaction in case of any problems in the system.

7.2.3 EXPERIMENTAL PROCEDURE

CONTROL RUNS

The emulsion recipe consisted of 1000 parts distilled water, 400 parts vinyl acetate and varying amounts of initiator (.01-.02 mole per liter latex) and emulsifier (.0075-.01 mole per liter latex). The

initiator was predissolved and purged with nitrogen. A small amount of sodium sulfite was added to the initiator in sufficient quantity to scavenge off dissolved oxygen in the reaction system.

Two monomer-soap-water feed solutions were then mixed. The first consisted of monomer and water in the appropriate ratio plus just enough soap to stabilize the monomer droplets in the tank after emulsifying. The second feed solution consisted of monomer and water in the appropriate ratio plus all remaining soap. The amount of soap added was calculated to give the desired latex product soap concentration for the degree of split under consideration. These two solutions were pre-emulsified by a high speed stirrer for an hour under a nitrogen blanket. The dilute soap emulsion was added to the 18 litre feed tank equipped with a flat-blade paddle, while the concentrated solutions were placed in the smaller 4 litre glass feed tanks with nitrogen bubbling used for mixing.

The reactor was filled with a pre-emulsified mixture of monomer, soap and water in the correct ratios and purged with nitrogen for 1 hr to remove oxygen in the reactor contents.

At this point, the main reactor was heated to 50°C by using the heating jacket. A small charge of initiator was added to the reactor and the flows of all feed streams started.

When the seed reactor was brought on-line, the initiator stream and concentrated soap MS stream were diverted to the seed reactor and overflow from this first reactor was then passed to the main reactor in place of these two streams.

Samples of approximately 10 mL were collected every 5 minutes for off-line measurements of conversion, as well as taking density readings or UV readings at these times. Every half hour, a somewhat larger sample was taken for use in measuring the surface tension. All the samples had a drop of a dilute hydroquinone solution added and were immersed immediately in ice to prevent further reaction.

In order to calibrate the density measurement for conversion, several samples were analyzed gravimetrically. This consisted of transferring 1 mL of the sample to a preweighed glass dish and drying to constant weight in a vacuum oven.

Experimental runs were carried out to examine the benefit of having a seed reactor, as well as examining the effect of the degree of split on the latex product.

MOLECULAR WEIGHT RUNS

The general preparation for the molecular weight runs followed the same scheme as the control runs but with the following differences.

Only the main reactor was used for these runs, and the soap concentration was kept high at .06 mole/liter latex. Kiparissides (1978) showed that under these conditions, a steady-state was achieved at high conversion levels.

Due to the nature of vinyl acetate emulsion polymerization, branching phenomena are most apparent at relatively high conversion. Also, as indicated by the model, the conversion level is the dominant factor in determining the various molecular weight averages. The particle size distribution does not play a part in the molecular

weight determination. As a result, the molecular weight experiments were carried out by achieving a steady-state system and varying the level of initiator to vary the level of conversion. At each initiator and conversion level, once steady-state was achieved, a sample was taken to be analyzed by low-angle laser light scattering (LALLS) off-line to determine the weight average molecular weight. The conversion at that time was obtained from the density measurement and the initiator level or temperature was then changed to a new operating condition.

The sample was first precipitated using calcium chloride and then washed well with distilled water and several washes of sodium hydroxide. The precipitated polymer was then dried for constant weight in a vacuum oven. This dried polymer was then dissolved in THF and the solution used in the off-line analysis of weight average molecular weight by LALLS.

7.3 EXPERIMENTAL ANALYSIS

7.3.1 CONVERSION

In order to measure the conversion, two experimental techniques were employed.

The first technique was off-line analysis of an emulsion sample by gravimetry. A polymer sample to be analyzed first had a drop of hydroquinone added to inhibit further polymerization followed by immersion in ice. A 1 mL aliquot was transferred to a preweighed glass dish and weighed. This was then dried to constant weight in a vacuum oven. The fraction solids (FSOL) is then given by:

$$FSOL = \frac{\text{WEIGHT (DISH+DRIED SAMPLE)} - \text{WEIGHT (DISH)}}{\text{WEIGHT (DISH+LATEX SAMPLE)} - \text{WEIGHT (DISH)}} \quad (7.1)$$

At the time of the sample, from the experimental conditions, the weight fraction of initiator FI, weight fraction emulsifier FE, and weight fraction monomer FM in the latex product is known. Thus, the conversion is obtained as:

$$X = \frac{FSOL - FI - FE}{FM} \quad (7.2)$$

The second technique for measuring conversion consisted of a vibrating glass U-tube with the sample flowing through so that on-line analysis was possible. The period of oscillation (T) of the tube depends on the square root of the mass contained within the tube, and the density is obtained by:

$$\rho = \frac{1}{A} (T^2 - B) \quad (7.3)$$

where A and B are calibration constants obtained at a given temperature by using known water and air densities to correct the instrument readings. An Anton-Paar DMA-45 digital density meter constructed on this principle was used on-line with this emulsion system by using a constant displacement pump with low flow rate to push the latex product through the U tube. Schork and Ray (1981) have shown that the technique works for estimating the conversion of poly(methyl methacrylate) produced by emulsion polymerization, and the general equation which holds is given by:

$$x = \frac{\rho - \rho_0}{\rho_{100} - \rho_0} \quad (7.4)$$

where ρ_{100} is the emulsion density at 100% conversion and ρ_0 is the density at 0% conversion. The predicted calibration curve from equation 7.4 for the emulsion polymerization of vinyl acetate is shown in Figure 7.2 along with the experimental curve found by comparison with gravimetric analysis. While close, the two curves do differ and the experimental result was used in this study.

The experimental curve was obtained by a least squares regression using .62 gravimetric measurements, yielding a correlation coefficient of .88. Since the conversion in the experimental runs rapidly increased to high values, the majority of the measurements were found in the .2 to .5 conversion range. The lack of a large number of low conversion results may be the cause of the apparent bias in the zero conversion readings due to extension of the curve beyond its best predictive range.

Gravimetric analysis, while accurate and reproducible, has several drawbacks. First, it is not adaptable to on-line analysis, creating problems if control is to be applied to the system. Second, if a large number of samples are analyzed, time delay occurs between sampling and analysis. Settling, agglomeration and some evaporation may all occur causing problems in the analysis. For this reason, the gravimetric analysis was used to examine and calibrate the vibrating U-tube density meter during the experiments whereupon the density measurements then provided the conversion measurement.

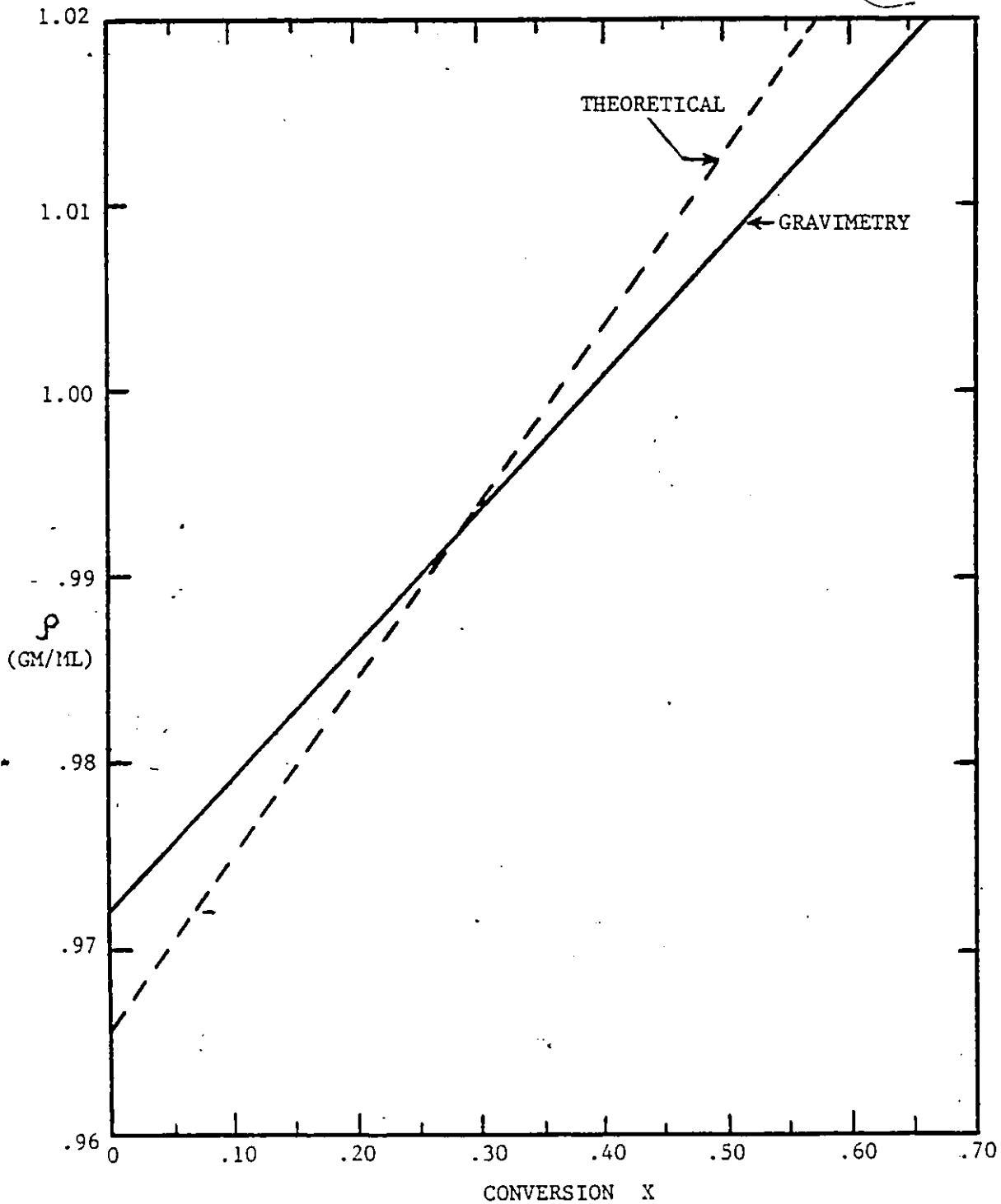


FIGURE 7.2 - Graph of Density from Anton-Paar Digital Density Meter ρ versus Conversion X as Determined Theoretically and by Comparison to Off-Line Gravimetry

7.3.2 SURFACE TENSION

Measurements of surface tension provide a way of examining whether soap micelles are present or not. A typical surface tension versus concentration curve for sodium lauryl sulphate in water is shown in Figure 7.3. If the free soap concentration is above the critical micelle concentration (CMC) in an emulsion polymerization, the surface tension will remain constant at its lowest value as shown by the horizontal line. If the free soap concentration is below the CMC, the surface tension will be somewhat higher. In this way, surface tension measurements should be able to detect oscillations in the emulsion polymerization of vinyl acetate, and possibly provide an indication of the degree of coverage of the polymer particles.

Several methods of measuring surface tension are available such as the Wilhelmy plate or du Nuoy ring. These methods can be time consuming, are best applicable to very clean systems, and present very little chance of on-line measurement as well. In this study, the equipment was a Digitec Surface Tension Meter 500, an experimental apparatus developed by Madison Kipp Corporation. It consisted of two glass tubes of different orifice sizes submerged to the same level in the sample to be tested through which bubbles were emitted with a constant frequency. A differential pressure measurement, across the two tubes, after passing through a smoothing filter, provided the estimate of the surface tension. The method was quick (approximately 30 seconds per sample), was independent of depth or contamination by dust or dirt and was highly reproducible. By using a flow-through

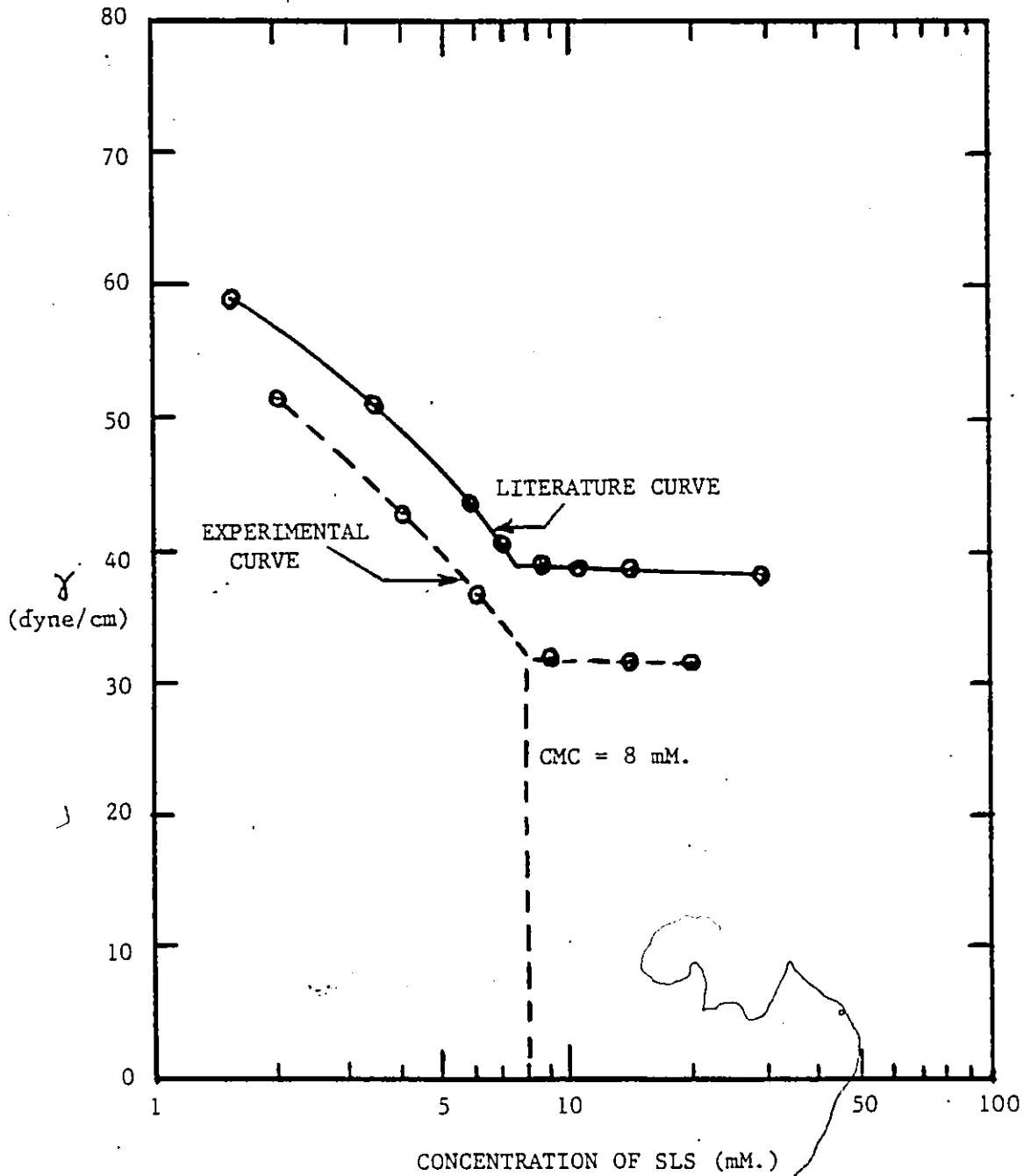


FIGURE 7.3 - Graph of Surface Tension γ versus Surfactant Concentration (Sodium Lauryl Sulfate) for Literature Values (Brady (1949)) and Experimental Data from Madison-Kipp Surface Tension Meter

cell, it would also be possible to achieve an on-line surface tension measurement.

Calibration of the equipment consisted of tuning two potentiometers to give true readings for two substances of known surface tension.

This instrument was then used in this study to track surface tension during the experimental runs.

7.3.3 WEIGHT AVERAGE MOLECULAR WEIGHT

In order to test out the molecular weight section of the model, it was necessary to have a technique for measuring the molecular weight. Several techniques are available for this purpose.

End group assay, ebullioscopy, cryoscopy and isothermal distillation are limited to polymers with low molecular weights ($< 10^4$). Osmotic pressure can provide number average molecular weight but has problems with any fraction having a molecular weight below 30,000. Also, number average molecular weight remains reasonably constant until very high conversions, even with branching so that parameter estimates will not be readily resolvable if number average molecular weight is used. Ultracentrifugation is also possible, but due to the large analysis time required due to equilibration, it is not a desired technique.

The two best methods for molecular weight analysis of second or higher moments are probably intrinsic viscosity and light scattering. They are roughly of comparable overall accuracy. However, in the

past, light scattering has involved measurements at a variety of angles and concentrations and extrapolating to zero concentration and angle, a time consuming and possibly inaccurate method. To combat this, new instrumentation in the form of low-angle light scattering systems have become more accepted. The use of the low angle allows extrapolation only in concentration, and the light scattering technique has become very quick and reproducible. As a result, a low-angle laser light scattering (LALLS) system was tried in this study for determining weight average molecular weight.

If unpolarized light is used to detect isotropic molecules, the general equation for the Rayleigh ratio is given by:

$$R_0 = r^2 \frac{I(r, \theta)}{I_i} = \left(\frac{4\pi^2}{N_A \lambda^4} \right) n^2 \left(\frac{dn}{dc} \right)^2 \left(\frac{1 + \cos^2 \theta}{2} \right) \left(\frac{C}{M_w P(\theta)} + 2A_2 C \right) \quad (7.5)$$

where $I(r, \theta)$ = intensity of scattered light at distance r , and angle θ

I_i = intensity of incident light

λ = wavelength of light in vacuo

n = refractive index of solvent

(dn/dc) = specific refractive index increment

C = concentration

M_w = weight average molecular weight

A_2 = second virial coefficient

$P(\theta)$ = particle scattering function

$$\approx 1 - \frac{1}{3} S^2 \bar{\rho}^2$$

where $S = \frac{4\pi}{\lambda'} \sin \frac{\theta}{2}$, $\bar{\rho}^2$ = mean square radius of gyration of the polymer molecule

and λ' = wavelength of light in the medium

Since small angles only are employed, the particle scattering function $P(\theta)$ is essentially 1.0. As a result, the equation used for this system is given by:

$$R_{\theta} = \left(\frac{1}{M_w} + 2A_2 C \right) \frac{K C}{\lambda'^4} \quad (7.6)$$

$$\text{where } K = \frac{2\pi^2 n^2}{N_A \lambda'^4} \frac{dn}{dc}^2 (1 + \cos^2 \theta) \quad (7.7)$$

The instrument available to measure the Rayleigh ratio was a Chromatix KMX-6 low angle laser light scattering instrument. The instrument used the following formula to determine the Rayleigh ratio.

$$R_{\theta C} = \frac{G_{\theta C}}{G_{0C}} D (\mu L)^{-1} \quad (7.8)$$

where $G_{\theta C}$ = instrument reading at angle θ and concentration C
 G_{0C} = instrument reading at angle 0 and concentration C
 D = instrumental gain depending on attenuators used
 $(\mu L)^{-1}$ = instrumental constant depending on angle and field stop used
 $R_{\theta C}$ = Rayleigh ratio at concentration C

The excess Rayleigh ratio to be used in the calculations is calculated from:

$$\bar{R}_{\theta C} = R_{\theta C} - R_{\theta 0} \quad (7.9)$$

where $\bar{R}_{\theta C}$ = excess Rayleigh ratio at concentration C. If the specific refractive index (dn/dc) is known, K can be calculated and a non-linear least squares fit for equation (7.6) can be used to estimate the weight average molecular weight.

The determination of the specific refractive index (dn/dc) was available from a Chromatrix KMX-6 laser differential refractometer for this system.

The overall estimated error for this light scattering measurement is usually in the order of 5-10%.

7.4 EXPERIMENTAL RESULTS

7.4.1 CONTROL RUNS

This series of experimental runs was carried out to verify the work of Chapter 6 on system redesign, which indicated that stable operation could be achieved using a small CSTR as a seed reactor for the main reactor. Examination of the experimental results from conversion and surface tension measurements did confirm the dramatic improvement of stability of the redesigned reactor configuration. With the seed reactor present, extended periods of time were observed with no oscillations. These periods also showed good stability when upsets to the system occurred, in the sense that the conversion quickly returned to its pre-

upset level and was again stable. Due to several equipment limitations however, total stability was not achieved. It was felt that major modification in the process equipment would have been necessary to conclusively demonstrate the stability. Some of the equipment problems and temporary solutions will now be discussed, and the results from the experimental runs presented.

Initial runs not shown here indicated several problems with the experimental apparatus. First, the dilution cell for the UV spectrophotometer was subject to settling out of the polymer causing misleading readings. In addition, other severe problems were encountered in attempts to dilute the sample accurately in these

experiments which meant that on-line measurements of turbidity were not possible with the apparatus that was available. Since Kiparissides' (1978) use of the turbidity was mainly for an estimate of conversion which was already available for this study by use of a digital density meter, detailed work using this instrument was not carried out further in this research.

Secondly, it was found that due to leaks in the equipment either at connections of tubing or through the pumps themselves, a small quantity of oxygen was entering the system. This conclusion was reached due to the fact that either little or no conversion took place in the system without the presence of sodium sulfite as an oxygen scavenger. In Figure 7.7, for example, showing conversion versus time for run A, the large initial transient shown at the beginning was due to the addition of a large quantity of sodium sulfite to the main reactor to start conversion after several hours of running yielded zero conversion. An overshoot to high conversion then occurred followed by gradual settling to the lower levels of conversion shown in the figure. Sodium sulfite was then placed in all feed streams and the reaction proceeded at reasonable levels for the remainder of the run. It was found that sodium sulfite had to be present in all runs to achieve adequate conversion levels in this system. Thus, oxygen represented an experimental problem difficult to overcome using this apparatus. el

The results from the three control experiments are shown in Figures 7.4 to 7.9. Runs A and B consisted of running the main

reactor alone without the seed reactor present for 5 and 7 hrs respectively followed by cutting in the small seed reactor for the remainder of the experiment. Run C was carried out by first running with the seed reactor present for 12 hrs followed by use of the large CSTR alone for the remainder of the run.

The results from off-line surface tension measurements taken every half hour are shown in Figures 7.4 to 7.6 for runs A to C, respectively. It can be seen that the surface tension does not vary a great deal but it was still possible to use surface tension to detect when generations had occurred. This possibility could be seen as follows. From the simulation results, it was found that the conversion showed a lag behind the number of particles in its changes. That is, if the number of particles underwent a massive nucleation, it would be around one half of a residence time before the conversion would bottom out and start to rise during property oscillations. However, the massive generation of new particles causes a large increase in surface area, hence a decrease in free soap and an increase in surface tension. Thus, it would be expected that peaks in surface tension would lead an increase in conversion by around 15 minutes or one-half residence time. The peaks in surface tension from Figures 7.4 to 7.6 are indicated by the dotted arrows on the conversion plots of Figures 7.7 to 7.9. From the locations it can be seen that peaks or surges in surface tension usually do lead the valleys of conversion by around 15 minutes or half a residence time. In the cases with the seed reactor present, the surge in surface tension was usually farther ahead since the conversion changes were

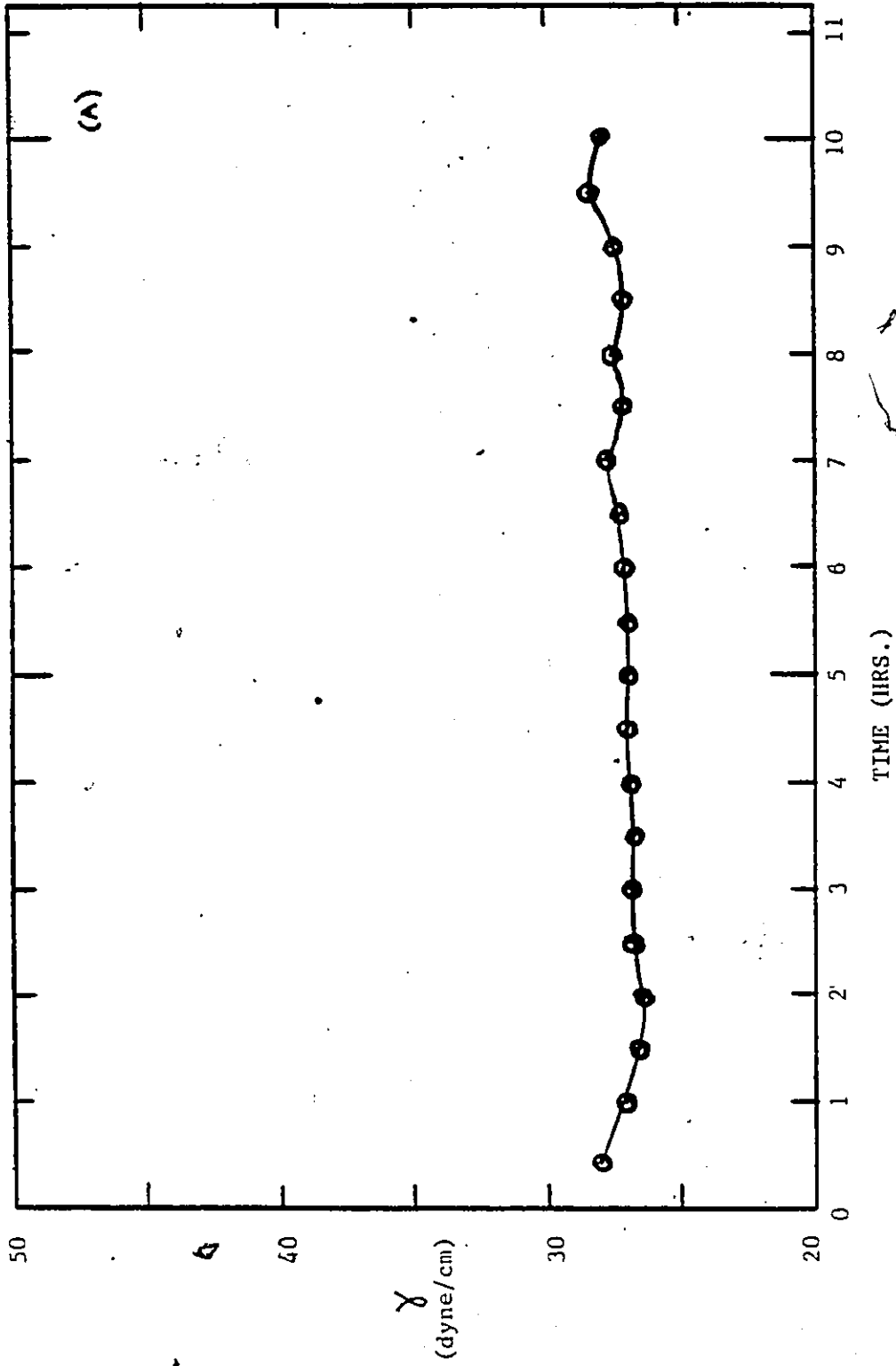


FIGURE 7.4 - Graph of Surface Tension γ versus Time for Run A at $T=50^{\circ}\text{C}$, $\theta=30$ min.

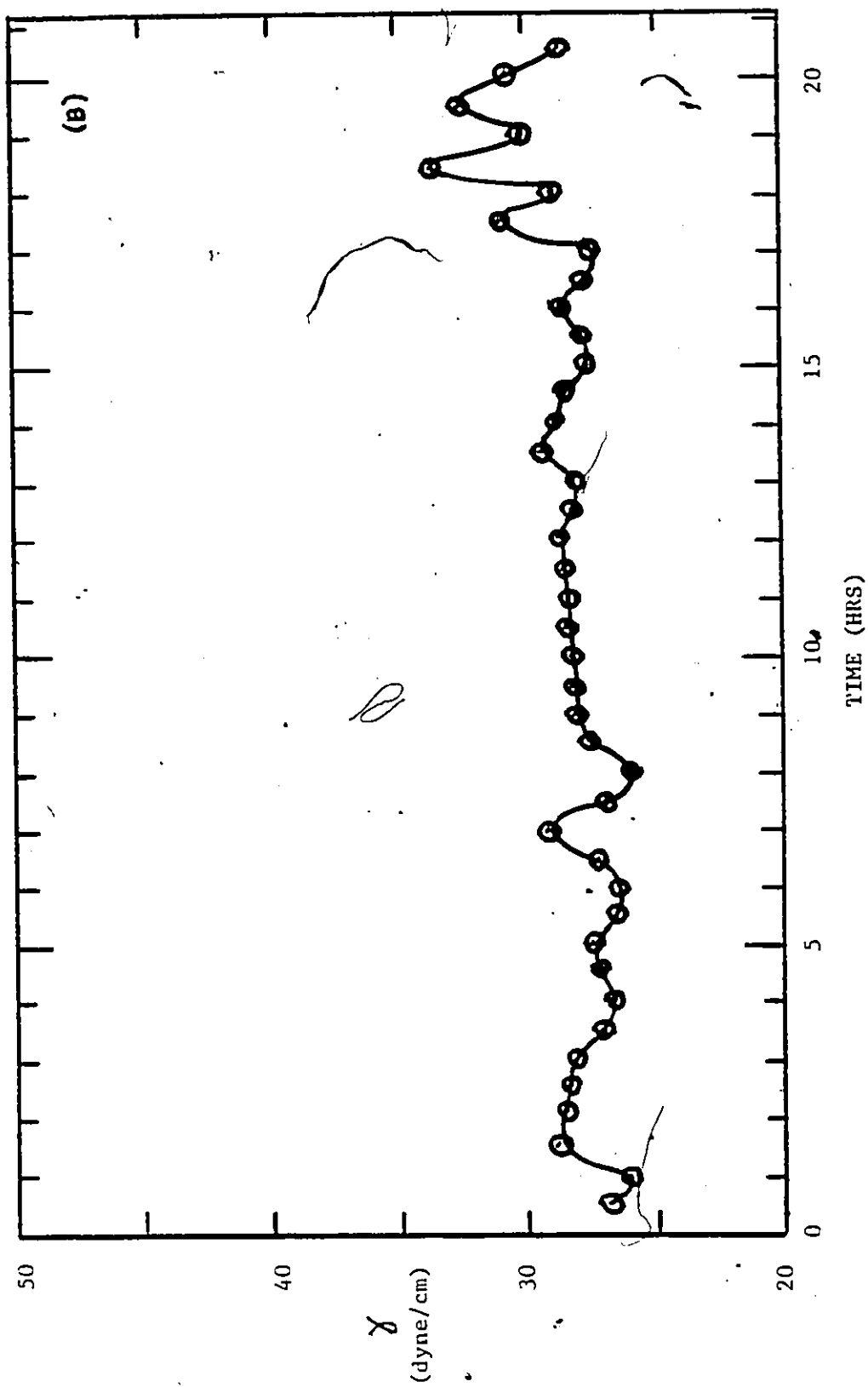


FIGURE 7.5 - Graph of Surface Tension γ versus Time for Run B at $T=50^{\circ}\text{C}$, $\theta=30$ min.

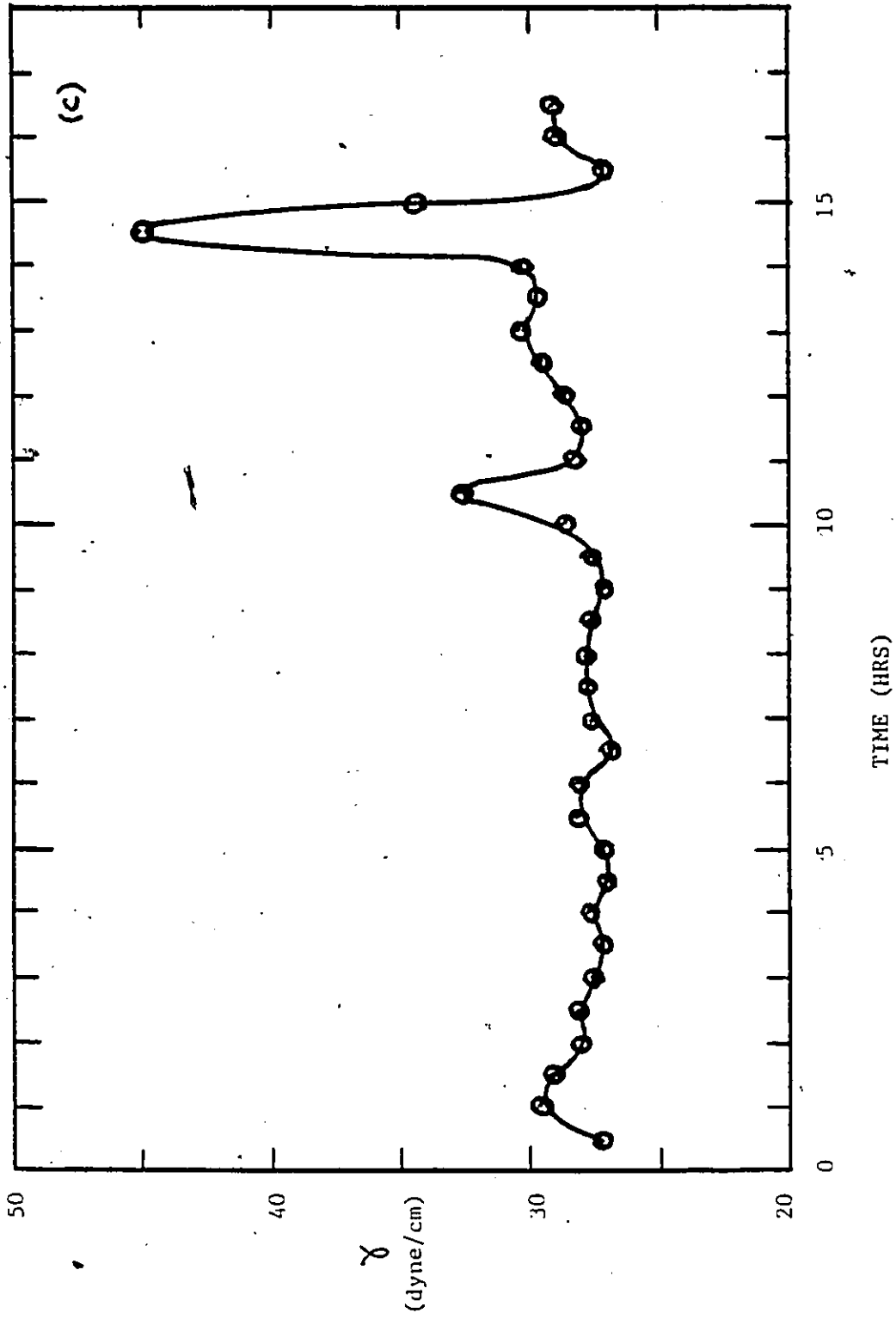


FIGURE 7.6 - Graph of Surface Tension γ versus Time for Run C at $T=50^{\circ}\text{C}$, $\theta=30$ min.

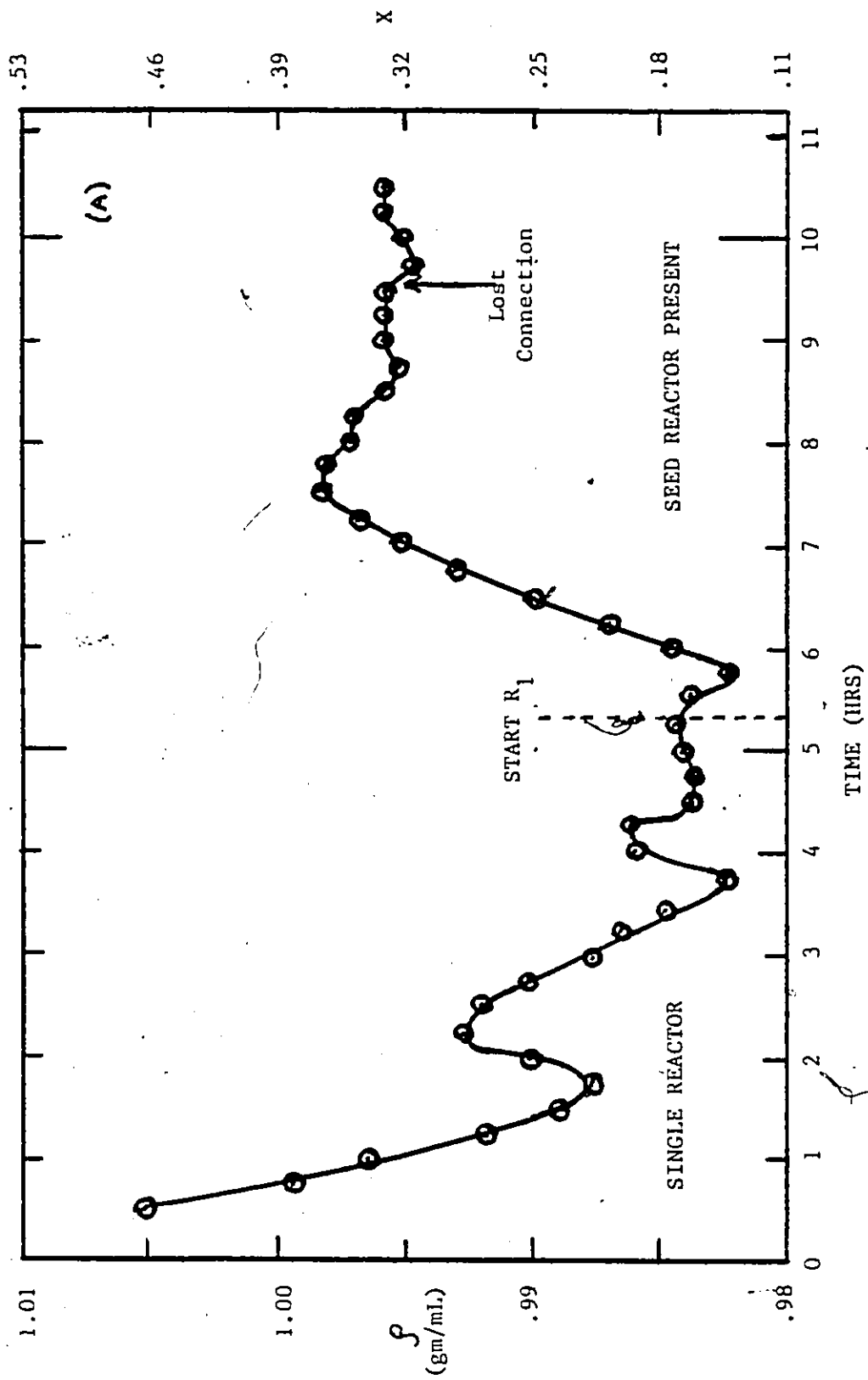


FIGURE 7.7 - Graph of Density ρ or Conversion X versus Time for Run A at $T=50^\circ\text{C}$, $\theta=30$ min.

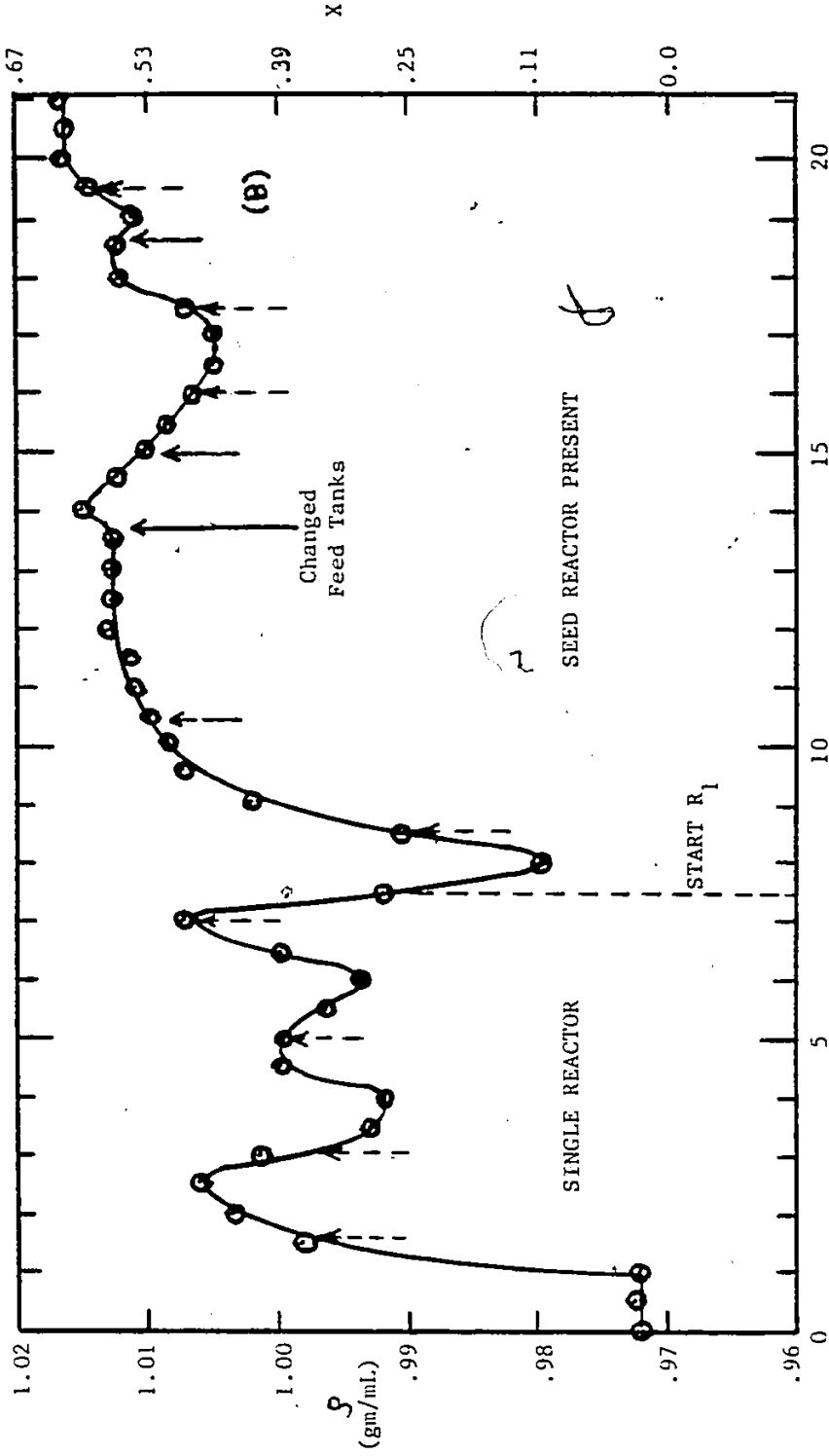


FIGURE 7.8 - Graph of Density ρ or Conversion X versus Time for Run B at $T=50^{\circ}\text{C}$, $\theta=30$ min.

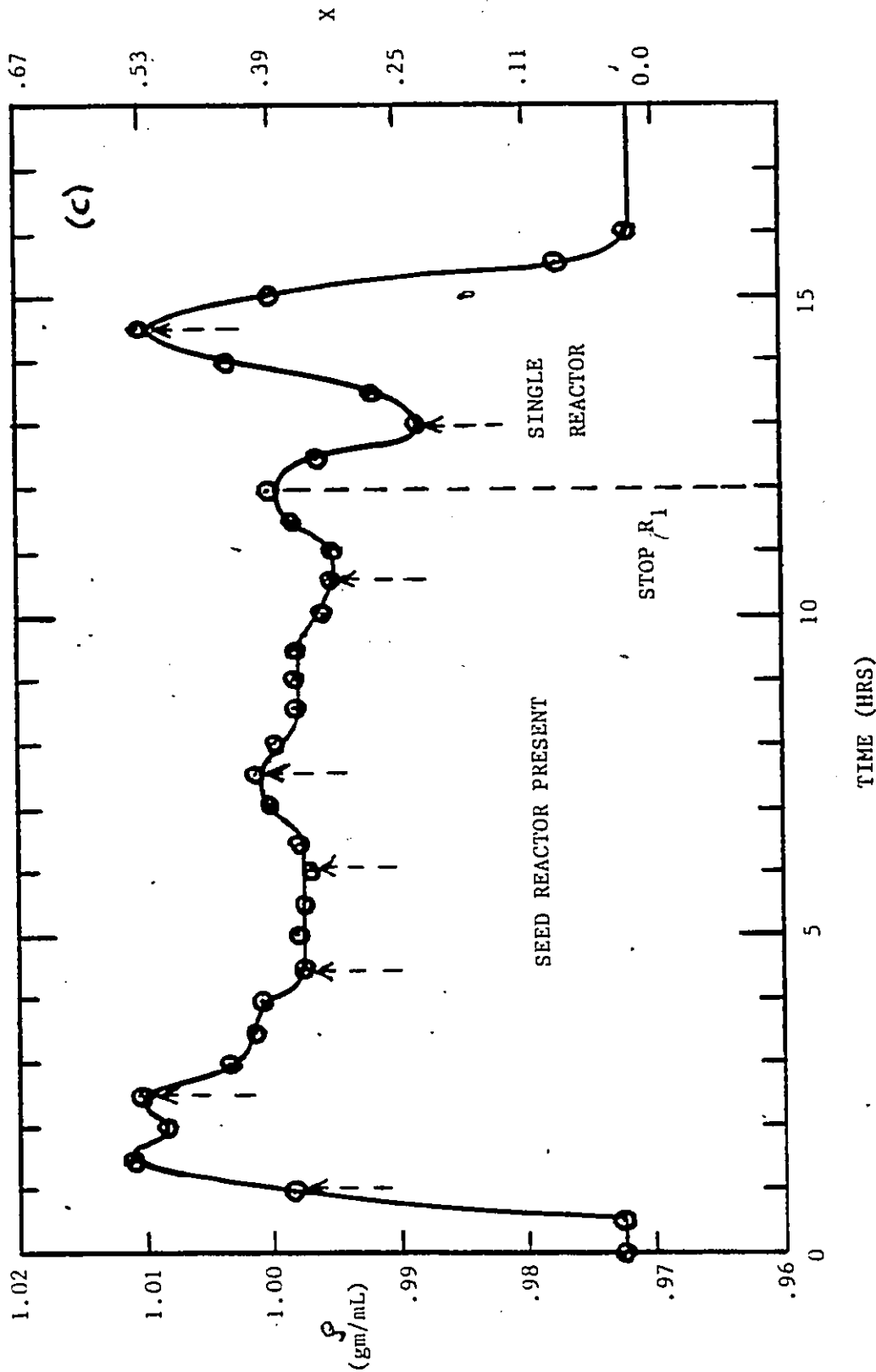


FIGURE 7.9 - Graph of Density ρ or Conversion X versus Time for Run C at $T=50^\circ\text{C}$, $\theta=30$ min.

also passing through the seed reactor. The conclusion was that even though the changes in surface tension were small, the surface tension measurements were able to forecast conversion changes and detect particle generation times in the system. It is also worth noting that for Run B, the surface tension remained very constant from 8 hrs to 13 hrs with the seed reactor present, which indicated the stability of operation during this period. Run C also showed reasonable stability at the same measurement level (29 dyne/cm) as the Run B stable level for the 2-1/2 to 10 hr period of operation during which the seed reactor was present. Again, the conclusion was that surface tension did show promise in predicting conversion swings or particle generations, and did give an indication that the system with seed reactors was more stable than the single reactor alone, despite the small variation of the measurements.

The conversion results for this system as mentioned previously are shown in Figures 7.7 to 7.9. The sections from 7-10 hrs on Run A, 10 to 13 hrs on Run B and somewhat the section of 4 to 9 hrs on Run C all showed signs of stability. The beginning of runs A and B indicated the change from oscillatory operation with one reactor to fairly stable operation with the seed reactor present. The end of Run C showed that when the seed reactor was removed, oscillatory behavior resulting in cessation of the reaction occurred.

During all experiments, unavoidable feed solution changes occurred due to the necessity of small feed tanks to allow all hazardous materials to be kept in the fume hood during experimental

operation. For this reason, all these experimental runs were subject to disturbances due to changeover of the feed tanks yielding changes in impurity levels of oxygen for example which could cause upsets to the stable system. For these reasons the experimental results were not as conclusive a test as was originally desired. However, trends are indicated quite clearly showing the stability which can be achieved using the redesigned configuration.

7.4.2 MOLECULAR WEIGHT RUNS

In order to use the simulation for the prediction of molecular weight averages and degree of long chain branching, it is first necessary to have accurate values for the parameters C_p , C_m and K_t described in section 3.4.4. These parameters represent ratios of rate constants comparing transfer to polymer, transfer to monomer or transfer agent, and terminal double bond polymerization rate constants, respectively, to the propagation rate constant.

To obtain these values more accurately for this system, several experiments were run to high conversions where branching phenomena become more important. By comparing experimental molecular weights to predicted values from the simulation, it was hoped that a non-linear estimation routine such as UWHAUS could be used to estimate these parameters more accurately, and hence provide a better means of calculating these values than was found in the literature, yielding more quantitatively accurate simulation predictions.

Using the procedure discussed previously in section 7.2.3, the single large reactor was run at high emulsifier levels (.06 mole/litre latex), two different temperatures (50°C and 60°C) and various initiator levels. Experimental data from two runs are shown in Table 7.1. These data represent values found once the reactor had reached stable operation for approximately 2 residence times as indicated by fairly steady density values.

TABLE 7.1
CONVERSION DATA FROM TWO RUNS FOR USE IN
MOLECULAR WEIGHT PARAMETER ESTIMATION

<u>Run No.</u>	<u>Sample No.</u>	<u>Density (gm/mL)</u>	<u>Conversion</u>	<u>Temp. (°C)</u>
D	1	.9912	26.7	50
	2	1.0128	56.9	60
	2-2	1.0161	61.5	60
	Final	1.0370	90.8	60
E	1	.9998	38.7	50
	2	.9965	34.1	50
	3	1.0302	81.3	60
	4	1.0300	81.0	60
	5	1.0307	82.0	60
	6	1.0267	76.4	60
	7	1.0226	70.6	60

Several experimental difficulties were encountered in running the reactor during the molecular weight runs. The major difficulty was the massive agglomeration which occurred usually after only a very few hours of operation. A typical result illustrating the complete "setting up" of the reaction during these runs is shown in Figure 7.10. Several possibilities exist for this phenomenon. The first is the broad particle size distribution which results due to the continuous

particle nucleation occurring in the single large reactor. Small particles and large particles have a greater affinity for each other than equal sized particles so that the broader particle size distributions should yield increased agglomerations. A second possibility is incorrect agitation rates with high shear often causing destabilizing of a latex, but is probably not a major problem in this case. The most likely reason was probably the high ionic strengths which occur due to the high initiator levels required for high conversion plus the necessity of adding sodium sulfite as an oxygen scavenger to allow sufficient generation of free radicals. The addition of high salt levels leading to high ion concentrations with an anionic surfactant such as sodium lauryl sulfate results in compression of the electrical double layer around the particles and a subsequent destabilization of the latex. It can be noted from the data that catastrophic agglomeration resulted at the highest conversion levels where the initiator concentration was highest, indicating that the high ionic strength is probably the most likely cause for this problem.

A second experimental problem which occurred at the high conversion levels followed from the previous problem. As the latex was pumped through the density meter, severe plugging of the tubes began to occur due to agglomeration. This necessitated shutting down the pump and rapidly flushing the tubes with distilled water. This event was usually the first indication of the onset of catastrophic agglomeration in the reactor so that in these experiments once the



FIGURE 7.10 - Experimental Example of Catastrophic Agglomeration

conversion measurement became unavailable, the reactor usually set up about five minutes later.

It was decided after these experiments to use the limited amount of experimental data shown in Table 7.1 in an attempt to obtain parameter estimates for the molecular weight model discussed in section 3.4.4 before proceeding further. The latexes were coagulated with calcium chloride and rinsed as discussed in section 7.2.3 to remove the salt. Known weights of the polymer samples were then placed in a volumetric flask containing tetrahydrofuran (THF) to provide a concentration standard at the upper end of the concentration range desired for the LALLS system (4 to 5×10^{-3} gm/mL as shown in Hamielec, Ouano and Nebenzahl (1978)). These were to be diluted to provide the range of concentrations required for the analysis.

It was at this point that the final experimental problem manifested itself. Despite the excellence of the solvent THF for poly(vinyl acetate) the polymer samples did not dissolve to any appreciable degree in the solvent. After several months, the highest conversion samples had swollen slightly but had not dissolved to any noticeable degree and remained as large pieces floating in the solution. Even the lower conversion samples did not dissolve fully but were present as small gels which could be suspended upon shaking the flask. This lack of solubility prevented any meaningful analysis of the samples and weight average molecular weights were not attainable in this research. The lack of solubility was most likely due to a high degree of crosslinking of the poly(vinyl acetate) at the higher conversion levels used.

For the reasons presented in the preceding discussion, this research was unable to provide a useful technique for estimating the molecular weight model parameters for this system. Higher quality laboratory apparatus yielding fewer oxygen problems in conjunction with a good redox catalyst system to provide high initiation rates at lower ionic strengths could possibly solve the agglomeration problem. From this point, more controlled experiments at conversion levels lower than those attempted in this research, in order to lower crosslinking, may yield a better chance of providing parameter estimates, but this study carried the work no further.

7.5 CONCLUSIONS

The use of a small seed reactor with bypass in front of the main reactor showed marked improvement in controlling the latex property oscillations of the system. Despite several experimental problems resulting mainly from equipment limitations plus the long experimental run-times required for this system, experimental results verified the stabilizing influence of the seed reactor in this system.

Attempts to use the apparatus for parameter estimation of kinetic parameters for molecular weight states were unsuccessful due to extensive crosslinking at the high conversions required. The long experimental times to obtain the samples and data would also indicate that the use of alternative methods is preferable.

CHAPTER 8

CONCLUSIONS AND FUTURE WORK

Inherent in the continuous emulsion polymerization kinetics for vinyl acetate is the possibility of sustained property oscillations over a wide range of operating conditions. The modelling and control of this phenomenon represents a challenging problem which needs to be solved before continuous emulsion polymerization reactors can be utilized on an industrial scale. The aim of this work was the development of a technique to eliminate the property oscillations while yielding a flexible reactor system in terms of latex properties which can be produced.

The first step involved the development of a detailed dynamic model which was able to describe the particle size development plus the molecular weight development of the emulsion system. In Chapter 3, the developed model was used to simulate the experimental data of Kiparissides (1978) and Greene, et al. (1976) with a high degree of success. The model was extended to simulation of the batch emulsion polymerization data of Keung (1974), and was also extended to modelling of continuous styrene emulsion polymerization to show the general applicability of the model. The model was also used to determine an optimum start-up policy for a single CSTR, corresponding for example to the first reactor in a chain of CSTR's. Inability of

the model to predict the entire particle size distribution (PSD) was shown not to be a limitation by the development of a method for predicting the current PSD based on past history of the overall latex properties.

The second step involved the use of the model in developing a control scheme for the elimination of the latex property oscillations. Advanced control theory in the form of linear quadratic stochastic optimal control was shown in Chapter 4 to be inadequate for this system due to the highly non-linear nature of the emulsion polymerization kinetics involved. Instead, the reactor configuration was redesigned using a small continuous seeding reactor with a large degree of bypass to effectively introduce control at the design stage. Simulation studies in Chapter 6 showed this to be a highly effective means of eliminating the oscillations while still yielding a flexible system capable of changing the latex property levels in a relatively easy fashion. In Chapter 7, experimental verification of the ability of the redesigned reactor system was provided with a reasonable degree of success.

A major problem with any control scheme for use with polymerization systems in general is the lack of good on-line sensors for measuring the polymer or latex properties. Chapter 5 showed that Kalman filtering theory could be used to guide the development of sensors in terms of sensor type and sensor measurement error required to yield the most information about an emulsion polymerization reactor system, using the dynamic model developed in Chapter 3.

The experimental use of a digital density meter for measuring conversion in a continuous emulsion polymerization system was illustrated in Chapter 7 with a high degree of success. Off-line measurement of surface tension was shown to yield information about particle nucleation times but further development of this technique is required. Attempts to obtain molecular weight parameters from the continuous reactor system by running at high conversions were unsuccessful due to the high degree of crosslinking which resulted.

While the application of the redesigned reactor configuration for eliminating property oscillations was shown to be successful, additional future work is needed to give a more conclusive demonstration of the improvements that should result from the process modification. Improved equipment should provide much better verification of the efficiency of the redesigned system, plus allow quantitative study of latex property changes as a result of operating parameter changes in the system.

Extension of the model to styrene kinetics achieved reasonable success in this work. Improvements to the model and extensions to copolymerization systems would be of interest.

The problems discovered in testing on-line sensors described in the experimental section, do indicate the need for further development of good on-line sensors for the latex properties. The ideas on optimum sensor choice should serve as a reasonable starting point

for future development work, both for emulsion polymerization systems and other polymerization systems as well.

Finally, although the model was mainly applied to continuous reactor systems and to continuous reactor control, it was shown that the model could be used as a starting point to study other applications, such as batch reactors, semi-batch reactors or reactor start-up in detail.

REFERENCES

- Abbey, K. J., in "Emulsion Polymers and Emulsion Polymerization" edited by D. R. Bassett, A. E. Hamielec, ACS Symp. Ser. 165, pp. 345-356, ACS, Washington, D.C., 1981
- Acres, G. J. K., Dalton, F. C., J. Poly. Sci.: Part A 1, p. 96, 1969.
- Advances in Chemistry 125, "Polymer Molecular Weight Methods" edited by Gould, R. F., Washington, 1973.
- Ahlberg, D. T., Cheyne, I., A.I.Ch.E. Symp. No. 159, 72, p. 221-229, 1972.
- Ahmad, A., Treybig, M. N., Anthony, R. G., J. Appl. Poly. Sci., 21 p. 2021-2028, 1977.
- Alexander, A. E., Napper, D. H., Progr. Poly. Sci., 3, 145, 1971.
- Alexander, A. E., Robb, I. D., Koll. Zeit. und Zeit. für Poly. 228, p. 64-65, 1967.
- Allen, P. W., J. Poly. Sci., 17, p. 156-158, 1955.
- Ambler, M. R., J. Appl. Poly. Sci., 25, p. 901-920, 1980.
- Ambler, M. R., Fetters, L. J., Kesten, Y., J. Appl. Poly. Sci., 21, p. 2439-2451, 1977.
- Amrehn, H., Automatica, 13, p. 533-545, 1977.
- Astrom, K. J., "Introduction to Stochastic Control Theory" Acad. Press, N.Y. 1970.
- Astrom, K. J., A.I.Ch.E. Symp. Ser. 159, 72, p. 184-194, 1972.
- Athans, M., IEEE Trans. on Automatic Control, AC-16(6), p. 529-552, 1971.
- Beasley, J. K., J. Am. Chem. Soc., 75, p. 6123, 1953.
- Beck, M. B., "On-Line Estimation of Nitration Dynamics", published by Int. Inst. for Applied Sys. Analysis, Research Report pp-79-3 Austria, July, 1979.

- Ben-Yosef, N., Gimo, O., Mahlab, P., Weitz, A., Sarig, S., J. Phys. Chem. 80, p. 253-255, 1976.
- Bengoust, W. I., Mellille, H. W., Proc. Roy. Soc. of London: A Math and Phys. Sci., 230, p. 429-447, 1955.
- Bergstra, T., Fong, J., Ruginis, D., fourth year undergraduate design project (course 4W4), McMaster University, Hamilton, Ontario, Canada, 1982.
- Beste, C. F., Hall, H. K., Macromol. Chem., 1, p. 121-136, 1966.
- Bly, D. D., Yau, M. W., Stoklosa, N. J., Anal. Chem., 48, p. 1256, 1976.
- Box, G. E. D., MacGregor, J. F., J. of the Roy. Stat. Soc.; Ser. C (Appl. Stat.), 23, No. 2, pp. 158-175, 1974.
- Box, G. E. D., Jenkins, G. M., MacGregor, J. F., Technometrics, 16, No. 3, pp. 391-398, 1974.
- Bradford, S. B., Vanderhoff, J. W., J. Coll. Sci., 14, pgs. 543-561, 1959.
- Brady, A. P., J. Phys. Coll. Chem., 53, p. 56, 1949.
- Brandrup, J. R.; Immergut, R. H., "Polymer Handbook", 2nd Ed., Wiley Interscience, John Wiley and Sons, New York, 1975.
- Breitenbach, J. W., Edelhauser, H., Hochraver, R., Monatshefte für Chemie, 99, pp. 625-634, 1968.
- Breitenbach, J. W., Kuchner, K., Fritze, H., Tarnowicus, H., Br. Poly. J., 2, pp. 13-17, 1970.
- Brodnyan, J. H., Brown, G. C., J. Coll. Sci., 15, pgs. 76-82, 1960.
- Brodnyan, J. G., Cala, J. A., Konnen, T., Kelley, P., J. Coll. Sci., 18, pp. 73-90, 1963.
- Brooks, B. W., Br. Poly. J., 2, pp. 197-201, 1970.
- Brooks, B. W., Br. Poly. J., 3, pp. 269-273, 1971.
- Brooks, B. W., Kropholler, H. W., Purt, S. N., Polymer, 19, p. 193, 1978.
- Burnett, G. M., Cameron, G. G., Thorat, P. C., J. Poly. Sci.: A-1, 8, pp. 3435-3442, 1978.

- Ceska, G. W., J. Appl. Poly. Sci., 18, pp. 427-437, 1974.
- Ceska, G. W., J. Appl. Poly. Sci., 18, pp. 2453-2499, 1974.
- Chan, R. K. S., Worman, C., Poly. Eng. and Sci., 12, No. 6, pp. 437-443, 1972.
- Chatterjee, A., Park, W. S., Graessley, W. W., Chem. Eng. Sci., 32, pp. 167-178, 1972.
- Chen, S. A., Jeng, W. F., Chem. Eng. Sci., 33, pp. 735-743, 1978.
- Chiang, A. S. T., Thompson, R. W., A.I.Ch.E. J., 25, p. 520, 1979.
- Chiang, A. S. T., Thompson, R. W., A.I.Ch.E. J., 25, p. 552, 1979.
- Clarke, J. T., Howard, R. O., Stockmayer, W. G., Makro. Chem., 44, pp. 427-447, 1961.
- Cohen, M. H., Turnbull, D., J. Chem. Phys., 31, No. 5, pp. 1164-1169, 1959.
- Cozewith, C., Graessley, W. W., Verstrate, G., Chem. Eng. Sci., 34, pp. 245-248, 1979.
- "C.R.C. Handbook of Chemistry and Physics" 65th Ed., C.R.C. Press, Boca Raton, Florida, 1979.
- Daoud, A. T., Chem. Eng. Sci., 31, pp. 510-511, 1976.
- Davidson, J. A., Collins, R. A., J. Coll. Interf. Sci., 29, No. 3, pp. 456-459, 1969.
- Davidson, J. A., Collins, R. A., Haller, H. S., J. Poly. Sci.: Part C, No. 35, pp. 235-255, 1971.
- Davis, J. J., Kermode, R. I., Ind. and Eng. Chem.: Proc. Des. and Dev., 14, No. 4, pp. 459-466, 1975.
- Degraaf, A. W., Poehlein, G. W., J. Poly. Sci.: A-2, 9, pp. 1955-1974, 1971.
- Dickinson, R. F., Ph.D. thesis, University of Waterloo, Waterloo, Ontario, Canada, 1976.
- Dietz, R., J. Appl. Poly. Sci., 25, pp. 951-953, 1980.
- Dill, K. A., Zimma, B. H., Macromolecules, 13, pp. 426-449, 1980.

- Dunn, A. S., Taylor, P. A., Macro. Chem., 83, pp. 207-209, 1965.
- Elgood, D. G., Gulbekian, E. V., Kinsler, D., J. Poly. Sci., : B (Poly. Lett.), 2 pp. 257-261, 1964.
- Finlayson, B. A., Scrivan, L. R., Appl. Mech. Rev., 19, No. 9, pp. 735-748, 1966.
- Fitch, R. M., in "Emulsion Polymers and Emulsion Polymerization" ed. by D. R. Bassett, A. E. Hamielec, ACS Symp. Ser. 165, pp. 1-30, ACS, Washington, D.C., 1981.
- Fitch, R. M., Tsai, C. H., in "Polymer Colloids", pp. 73-116, Plenum Press, N.Y., 1971.
- Foldes-Berezsenich, T., Szesztay, M., and Boros-Gyevi, E., J. Poly. Sci.: Poly. Chem. Ed., 18, pp. 1223-1232, 1980.
- Foss, A. S., A.I.Ch.E. J., 19, No. 2, pp. 209-214, 1973.
- Freedman, B. G., A.I.Ch.E. Symp. Ser. 159, 72, pp. 206-218, 1972.
- French, D. M., J. Poly. Sci., 32, pp. 395-411, 1958.
- Friis, N., Goosney, D., Wright, J. D., Hamielec, A. E., J. Appl. Poly. Sci., 18, p. 1297, 1974.
- Friis, N., Hamielec, A. E., J. Poly. Sci.: Poly. Chem. Ed., 11 pp. 3321-3325, 1973.
- Friis, N., Hamielec, A. E., J. Poly. Sci.: Poly. Chem. Ed., 12, pp. 251-254, 1974.
- Friis, N., Hamielec, A. E. in "Emulsion Polymerization", ed. by R. F. Gould, ACS Symp. Ser. 24, pp. 82-91, ACS, Washington, D.C., 1976.
- Friis, N., Nyhagen, L., J. Appl. Poly. Sci., 17, pp. 2311-2327, 1973.
- Gardon, J. L., J. Poly. Sci.: A-1, 6, pp. 623-641, 1968.
- Gardon, J. L., J. Poly. Sci.: A-1, 6, pp. 643-664, 1968.
- Gardon, J. L., Br. Poly. J., 2, pp. 1-12, 1970.
- Gardon, J. L., Rubber and Chem. Tech., 43, No. 7, pp. 74-94 1970.
- Gardon, J. L., J. Poly. Sci.: Chem., 11, pp. 241-251, 1973.

- Gaylor, V. F., James, H. L., Herdering, J. P., J. Poly. Sci.: Chem., 13, pp. 1575-1587, 1975.
- Gebert, W., Banderman, F., Macro. Chem., 57, pp. 153-167, 1977.
- Gerrens, H., Angew Chem., 71, No. 19, pp. 608-612, 1959.
- Gerrens, H., Fortschr. Hochpoly.-Forch. 1, pp. 234-328, 1959.
- Gerrens, H., Zeitschr. für Electroch., 64, No. 10, pp. 1199-1216, 1960.
- Gerrens, H., Drchema.-Monga. 49, pp. 53-73, 1964.
- Gerrens, H., Kolloid-Zeitschr. und Zeitschr. für Polymere, 227 (Heft. 1-2), pp. 92-107, 1968.
- Gerrens, H., J. Poly. Sci.: C 27, pp. 77-93, 1969.
- Gerrens, H., Kuchner, K., and Ley, G., Chem. Ing. Tech., 43, 12, p. 693, 1971.
- Gershberg, D. B., Longfield, J. E., 45th American Institute of Chemical Engineers Meeting, New York, Preprint No. 10, 1961.
- Ghosh, M., Forsyth, T. H., in "Emulsion Polymerization", ed. by I. Piirma, J. L. Gardon, ACS Symp. Ser. 24, pp. 367-378, ACS, Washington, D.C., 1976.
- Giddings, J. C., Anal. Chem., 39, No. 8, pp. 1027-1028, 1967.
- Goodall, A. R., Wilkinson, M. C., Hearn, J., J. Coll. Inter. Sc., 53, No. 2, pp. 327-331, 1975.
- Goosney, D. D., M. Eng. thesis, McMaster University, Hamilton, Ont., Canada, 1973.
- Gorber, D. M., Ph.D. thesis, Waterloo University, Waterloo, Ont., Canada, 1973.
- Gordon, D. L., Wiedner, K. R. in "Emulsion Polymers and Emulsion Polymerization" ed. by D. R. Bassett, A. E. Hamielec, ACS Symp. Ser. 165, pp. 505-532, ACS, Washington, D.C., 1981.
- Grancio, M. R., Williams, D. J., J. Poly. Sci.: A-1, Poly. Chem. 8, pp. 2733-2745, 1970.
- Grancio, M. R., Williams, D. J., J. Poly. Sci., 8, No. 9, p. 2617, 1970.

- Greene, R. K., Gonzalez, R. A., Poehlein, G. W., in "Emulsion Polymerization", ed. by I. Piirma and J. L. Gardon, ACS Symposium Series 24, ACS, p. 341-358, Washington, D.C., 1976.
- Gresh, G. G., Wilson, J. F., J. Appl. Poly. Sci., 5, No. 14, pp. 135-148, 1961.
- Gulbekian, B. V., J. Poly. Sci.: A-1, 6, pp. 2265-2280, 1968.
- Gulbekian, B. V., Br. Poly. J., 1, p. 96, 1969.
- Gulbekian, B. V., Quadri, B. H., Reynolds, G. E. J. Br. Poly. J., 2, p. 146, 1970.
- Guttman, C. M., DiMarzio, E. A. Macromol., 3, No. 5, p. 681, 1970.
- Hamielc, A. E., course notes for "Polymer Reaction Engineering" short course presented at McMaster University, Hamilton, Ontario, Canada, 1976.
- Hamielc, A. E., Omorodian, S. N. R., in "Size Exclusion Chromatographs (GPC)", A.C.S. Symp. Ser. 138, ed. by T. Provder, 1980.
- Hamielc, A. E., Ouano, A. C., Nebenzahl, C. I., J. Liq. Chr., 1, No. 4, pp. 527-554, 1978.
- Hamielc, A. E., Walther, G., Wright, J. D., in "Polymer Molecular Weight Methods", ACS, Symp. Ser. 125, pp. 138-147, 1973.
- Hamilton, J. C., Seborg, D. E., Fisher, D. G., A.I.Ch.E. J., 19, No. 5, pp. 901-909, 1973.
- Hansen, F. K., Ugelstad, J., J. Poly. Sci.: Chem., 16, pp. 1953-1979, 1978.
- Harada, M., Nomura, M., Eguchi, W., Nagata, S., J.Ch.E. of Jap., 4, No. 1, p. 59, 1971.
- Harkins, W. D., J. Am. Chem. Soc., 69, p. 1428, 1947.
- Harris, T., Ph.D. thesis, McMaster University, Hamilton, Ont. Canada, 1980.
- Harris, B., Hamielc, A. E., Marten, L., in "Emulsion Polymers and Emulsion Polymerization", ed. by D. R. Bassett, A. E. Hamielc, ACS Symp. Ser. 165, pp. 315-326, ACS, Washington, D.C., 1981.
- Harris, T. J., Wright, J. D., MacGregor, J. F., "Opt. Sensor Loc. with an Appl. to a Packed Bed Tub. Reactor", 1981.

- Hawkett, B. S., Napper, D. H., Gilbert, P. G., J. Poly. Sci.: Poly. Chem. Ed., 19, pp. 3173-3179, 1981.
- Hicks, J., Mohan, A., Ray, W. H., Can. J. Ch. Eng., 47, pp. 590-597, 1969.
- Hochberg, A., Low, W., J. Appl. Poly. Sci., 47, No. 3, pp. 1001-1002, 1976.
- Hoffman, T. M., "Model of Batch, Semi-Batch, and Continuous Reactors Involving Emulsion Copoly." at Polymer Course, McMaster University, 1980.
- Hoffman, R. F., Schreiber, S., Rosen, G., Ind. and Eng. Chem., 56, No. 5, pp. 51-57, 1964.
- Hoftyzer, P. J., Hoogschagen, J., Van Krevelen, A. W., 3rd European Symp. on Chem. React. Eng., pp. 247-254, Amsterdam, 1964.
- Homola, A. M., Inove, M., Robertson, A. A., report PGRL175, pub. by Pulp and Paper Research Institute of Canada, 1975.
- Huglin, M. B., "Light Scattering from Polymer Solutions", Academic Press, New York, 1972.
- Hulburt, H. M., Akiyama, T., I.E.C. Fund., 8, No. 2, pp. 319-324, 1969.
- Hulburt, H. M., Katz, S., Chem. Eng. Sci. 19, pp. 555-574, 1964.
- Husain, A., Hamielec, A. E., Vlachopoulos, J., in "Size Exclusion Chromatography (GPC)" ed. by T. Provder, A.C.S. No. 138, 1980.
- Husain, A., Hamielec, A. E., Vlachopoulos, J., J. Liq. Ch., 4, No. 3, pp. 459-482, 1981.
- Husain, A., Vlachopoulos, J., J. Liq. Ch., 4, No. 3, pp. 425-458, 1981.
- Hyun, J. C., Bankoff, S. G., Chem. Eng. Sci., 31, pp. 953-958, 1976.
- Ilahie, M. Y., M. Eng. thesis, McMaster University, Hamilton, Ont., Canada, 1982.
- Jackson, R. A., Small, R. A., Whiteley, K. S., J. Poly. Sci.: Poly. Chem., 11, pp. 1781-1829, 1973.
- Jaisinghani, R., Ray, W. D., Chem. Eng. Sci., 32, pp. 811-825, 1977.

- James, H. L., Pürma, I. in "Emulsion Polymerization", ed. by I. Piirma, J. L. Gardon, ACS Symp. Ser. 24, pp. 197-210, ACS, Washington, D.C., 1976.
- Jazwinski, A. H., "Stochastic Processes and Filtering Theory", Academic Press, N.Y., 1970.
- Jen-Yüan, C., "Determination of Molecular Weights of High Polymers", Israel Program for Scientific Translations, Jerusalem, 1963.
- Jo, J. H., Bankoff, S. G., A.I.Ch.E., 22, No. 2, pp. 361-368, 1976.
- Jutan, A., Tremblay, J. P., MacGregor, J. F., Wright, J. D., A.I.Ch.E. J., 23, No. 5, pp. 732-758, 1977.
- Kaufman, H., Berry, P., Automatica, 12, pp. 565-576, 1976.
- Keung, C. K. J., M. Eng. thesis, McMaster University, Hamilton, Ont., Canada, 1974.
- Keyes, M. A., Kennedy, J. P., Proc. 2nd Purdue Conf. on Proc. Control: Adaptive Control, pp. 89-98, 1974.
- Kiparissides, C., Ph.D. thesis, McMaster University, Hamilton, Ont., Canada, 1978.
- Kiparissides, C., Hamielec, A. E., MacGregor, J. F., J. Appl. Poly. Sci., 23, pp. 401-418, 1979.
- Kiparissides, C., Hamielec, A. E., MacGregor, J. F., Can. J. Ch. Eng., 58, p. 56, 1980.
- Kiparissides, C., Hamielec, A. E., MacGregor, J. F., Can. J. Ch. Eng., 58, p. 48, 1980.
- Kiparissides, C., MacGregor, J. F., Hamielec, A. E., A.I.Ch.E. J., 27, No. 1, p. 13, 1981.
- Kirillov, V. A., Ray, W. H., Chem. Eng. Sci., 33, pp. 1499-1506, 1978.
- Kurz, H., Iserman, R., Schumann, R., Automatica, 16, No. 2, pp. 117-134, 1980.
- Kwakernaak, H., Sivan, R., "Linear Optimal Control Systems", J. Wiley and Sons, New York, 1977.
- Kwon, Y. D., Evans, L. B., A.I.Ch.E. J., 21, No. 6, pp. 1158-1164, 1975.

- Ledwith, A., Russel, P. J., J. Poly. Sci. B: Poly. Letters, 13, pp. 109-112, 1975.
- Lee, C. K., Forsyth, T. H., in "Emulsion Polymers and Emulsion Polymerization", ed. by D. R. Bassett, A. E. Hamielec, ACS Symp. Ser. 165, pp. 567-578, ACS, Washington, D.C., 1981.
- Leffew, K. W., Deshpande, P. B. in "Emulsion Polymers and Emulsion Polymerization", ed. by D. R. Bassett, A. E. Hamielec, ACS Symp. Ser. 165, pp. 533-566, ACS, Washington, D.C., 1974.
- Ley, G., Gerrens, H., unpublished preprint, 1974.
- Lichti, G., Gilbert, R. G., Napper, D. H., J. Poly. Sci., 18, pp. 1297-1323, 1980.
- Liegeois, J. M., Angew. Mak. Chem., 56, pp. 115-170, 1976.
- Litt, M., Stannett, V., J. Poly. Sci.: A-1, 8, pp. 3607-3649, 1970.
- MacFarlane, A. G. J., A.I.Ch.E. Symp. Ser., 72, pp. 126-143, 1959.
- MacFarlane, A. G. J., Automatica, 8, pp. 455-462, 1972.
- MacGregor, J. F., Can. J. Ch. Eng., 51, pp. 468-477, 1973.
- Macoveneau, M., Nagakeuschi, U., Feldman, D., Die Angew. Makro. Chem., 64, pp. 19-28, 1977.
- Magaris, P., Control Eng., p. 98, 1981.
- Martin, A. J. P., Synge, R. C. M., Bio. Chem. J., 35, pp. 1358-1368, 1941.
- Maxim, L. D., Klein, A., Meyer, M. F., Kust, G. H., J. Poly. Sci.: C, 27, pp. 195-205, 1969.
- Mehmet, H., Roche, R. S., J. Appl. Poly. Sci., 20, No. 7, pp. 1955-1965, 1976.
- Min, K. W., Gostin, H. E., Ind. Eng. Chem.: Prod. Res. and Dev., 18, No. 4, p. 272, 1979.
- Min, K. W., Ray, W. H., J. Macromol. Sci.: Rev. Macromol. Chem.: C, 11, No. 2, pp. 177-255, 1974.
- Min, K. W., Ray, W. H. in "Emulsion Polymerization", ed. by I. Piirma, J. L. Gardon, ACS Symp. Ser. 24, pp. 359-366, ACS, Washington, D.C., 1976.

- Min, K. W., Ray, W. H., J. Appl. Poly. Sci., 22, pp. 89-112, 1978.
- Mochizoki, S., Itoh, N., Chem. Eng. Sci., 33, pp. 1401-1403, 1978.
- Mori, S., Porter, R. S., Johnson, J. F., Anal. Chem., 46, No. 11, pp. 1599-1602, 1974.
- Nagasubramanian, K., Graessley, W. W., Chem. Eng. Sci., 25, pp. 1549-1558, 1970.
- Napper, D. H., Lichti, G., Gilbert, R. G. in "Emulsion Polymers and Emulsion Polymerization", ed. by D. R. Bassett, A. E. Hamielec, ACS Symp. Ser. 165, pp. 105-120, ACS, Washington, D.C., 1981.
- Newell, R. B., Fisher, D. G., Automatica, 8, pp. 247-262, 1972.
- Nomura, M., Harada, M. in "Emulsion Polymers and Emulsion Polymerization", ed. by D. R. Bassett, A. E. Hamielec, ACS Symp. Ser. 165, pp. 121-144, ACS, Washington, D.C., 1981.
- Nomura, M., Harada, M., Eguchi, W., Nagata, S., J. Chem. Eng. of J. Appl. Poly., 4, p. 54, 1971.
- Nomura, M., Harada, M., Eguchi, W., Nagata, S. in "Emulsion Polymerization", ed. by I. Piirma, G. L. Gardon, ACS Symp. Ser. 24, pp. 102-121, ACS, Washington, D.C., 1976.
- Nomura, M., Harada, M., Nakagawara, K., Eguchi, W., Nagata, S., J. Chem. Eng. of J. Appl. Poly., 4, No. 2, pp. 160-166, 1971.
- Nomura, M., Kojima, A., Harada, M., Eguchi, W., Nagata, S., J. Appl. Poly. Sci., 15, pp. 675-691, 1970.
- Nomura, M., Sasaki, S., J. Appl. Poly. Sci., 22, pp. 1043-1060, 1978.
- Noton, A. R. M., "Introduction to Variational Methods in Chemical Engineering", Pergamon Press, New York, 1965.
- Omi, S., Ueda, T., Kubota, H., J. Chem. Eng. of Japan, 2, No. 2, pp. 183-198, 1969.
- Oho, H., Saeki, H., Br. Poly. J., 7, pp. 27-31, 1975.
- Osakada, K., Fan, L. T., J. Appl. Poly. Sci., 14, pp. 3065-3082, 1970.
- O'Toole, J. T., J. Appl. Poly. Sci., 4, pp. 1291-1297, 1965.

Ouano, A. C., Horne, D. L., Gregges, A. R., J. Poly. Sci.: Chem., 12, pp. 307-322, 1974.

Panuska, V., I.E.E.E. Trans. on Auto. Cont., AC-25, No. 2, pp. 229-234, 1980.

Pearce, S. C., M. Eng. thesis, McMaster University, Hamilton, Ont. Canada, 1967.

Pearson, J. D., J. Elect. Cont., 13, pp. 453-469, 1962.

Perry, R. H., C. H., "Chem. Eng. Handbook", 5th ed. McGraw-Hill, New York, 1973.

Poehlein, G. W., Dougherty, D. J., Rubber Chem. and Tech., 50, pp. 601-638, 1977.

Pollock, M. J., MacGregor, J. F., Hamielec, A. E., "Dynamic Modelling of Molecular Weight and Particle Size Development for Continuous Poly(Vinyl Acetate) Emulsion Polymerization Reactors and Application to Optimal Multiple Reactor System Design", presented at A.C.S. Symp., New York, August 1981.

Pollock, M. J., MacGregor, J. F., Hamielec, A. F., "The Control of Oscillations and Latex Properties on Continuous Stirred Tank Emulsion Polymerization Reactors", presented at A.I.Ch.E. Conf., New Orleans, November 1981.

Ponnuswamy, S. E., Kiparissides, C., "Application of Population Balance Equations to Latex Reactors", presented at 88th A.I.Ch.E. Conference, Philadelphia, June 1980.

Ramkrishna, P., Chem Eng. Sci., 26, pp. 1134-1136, 1971.

Ray, W. H., Can. J. Chem. Eng., 47, pp. 590-597, 1969.

Ray, W. H., Gall, S. E., Macromol., 2, No. 4, pp. 425-428, 1969.

Reimschuessel, H. K., Nagasubramanian, K., Chem. Eng. Sci., 37, pp. 1119-1123, 1972.

Rijnsdorp, J. E., Seborg, D. F., A.I.Ch.E. Symp. Ser. 159, 72, pp. 112-123, 1972.

Roe, C. P., Ind. Eng. Chem., 60, No. 20, 1968.

Roquemore, K. G., Eddy, E. E., Chem. Eng. Prog., 57, No. 9, p. 35, 1961.

Rosenbrock, H. H., Chem. Eng. Prog., 58, No. 9, pp. 43-50, 1962.

Sacks, M. E., Lee, S., Biesenburger, J. A., Chem. Eng. Sci., 28, pp. 241-257, 1973.

Schörk, F. J., Ray, W. H. in "Emulsion Polymers and Emulsion Polymerization", ed. by D. R. Bassett, A. E. Hamielec, ACS Symp. Ser. 165, pp. 505-514, ACS, Washington, D.C., 1981.

Shah, B. H., Ramkrishna, D., Burwanker, J. D., A.I.Ch.E. J., 23, No. 6, pp. 897-904, 1977.

Shastri, J. S., Fan, L. T., Erickson, L. E., J. Appl. Poly. Sci., 17, pp. 3101-3126, 1973.

Shastri, J. S., Fan, L. T., Erickson, L. E., J. Appl. Poly. Sci., 17, pp. 3127-3141, 1973.

Singh, S., M. Eng. thesis, McMaster University, Hamilton, Ont. Canada, 1977.

Singh, S., Hamielec, A. E., J. Appl. Poly. Sci., 22, 577-589, 1978.

Small, H., J. Coll. Interf. Sci., 48, No. 1, pp. 147-161, 1974.

Smith, C. L., "Digital Computer Process Control", Intext Pub., New York, 1972.

Smith, W. V., Ewart, R. H., J. Chem. Phys., 16, p. 152, 1948.

Snuparek, J., Krska, F., J. Appl. Poly. Sci., 21, pp. 2253-2260, 1977.

Stephenson, R. M., "Introduction to the Chemical Process Industries", Reinhold Publishing Co., New York, 1966.

Stevens, J. D., Funderburk, J. O., Ind. Eng. Chem.: Proc. Des. Dev. 11, No. 3, pp. 360-369, 1972.

Stockmayer, W. H., J. Poly. Sci., 24, p. 314, 1957.

Sundberg, D. C., Hsieh, J. Y., Soh, S. K., Baldus, R. F. in "Emulsion Polymers and Emulsion Polymerization", ed. by D. R. Bassett, A. E. Hamielec, ACS Symp. Ser. 165, pp. 327-344, ACS, Washington, D.C., 1981.

Sutton, T. L., MacGregor, J. F., Can. J. Ch.E., 55, pp. 609-613, 1977.

- Thompson, R. W., Stevens, J. D., Chem. Eng. Sci. 32, pp. 311-322, 1977.
- Trevathan, V. L., A.I.Ch.E. Symp. Ser. 159, 72, pp. 40-49, 1972.
- Tse, E., A.I.Ch.E. Symp. Ser. 159, 72, pp. 195-205, 1972.
- Ueda, T., Omi, S., Kubota, H., J. Ch. Eng. of Japan, 4, No. 1, p. 50, 1971.
- Ugelstad, J., Hansen, F. K., Rubber Chem. and Tech., 43, No. 7, pp. 79-94, 1970.
- Ugelstad, J., Hansen, F. K., Rubber Chem. and Tech., 49, pp. 536-609, 1976.
- Ugelstad, J., Mörk, P. C., Aasen, J. O., J. Poly. Sci.: A-1, 5, p. 2281, 1967.
- Wahba, G., I.E.E.E. Trans. on Auto. Control, AC-25 No. 2, pp. 235-238, 1980.
- Weber, A. P. J., Lapidus, L., A.I.Ch.E. J., 17, No. 3, pp. 641-658, 1971.
- Wessling, R. A., J. Appl. Poly. Sci., 12, pp. 309-319, 1968.
- Whitney, R. S., Burchard, W., Makromol. Chemie., 181, pp. 869-890, 1980.
- Wismer, D. A., I.E.E.E. Trans. Auto Control, 10, No. 4, pg. 455, 1965.
- Woods, D. R., "Surfaces, Colloids, and Unit Operations", McMaster University, Hamilton, Ont., Canada, 1980.
- Wright, J. D., private communication, 1980.

APPENDIX I

LIST OF SYMBOLS

- a - ratio of radical production to termination, Chapter 2
 a_s - surface coverage per emulsifier molecule, dm^2 , Chapter 2
 A - $(n \times n)$ dynamic state matrix
 A - density meter calibration constant
 A_d - total surface area of monomer drops, dm^2/L latex.
 A_m - total micellar surface area, dm^2/L latex.
 $a_n(t, T)$ - total surface area of the class of particles $n(t, T)dT$, dm^2/L latex
 $A_p(t, T)$ - surface area of a particle of class $n(t, T)dT$, dm^2
 $A_p(t)$ - total surface area of polymer particles, dm^2/L latex
 A_1, A_2, A_3 - sub-matrices of partitioned A matrix
 b - ratio of desorption to termination, Chapter 2
 B - $(n \times r)$ coefficient matrix for control variables
 B - density meter calibration constant
 B_N - average number of branch points per polymer molecule
 C - constant in monomer volume fraction equation, Chapter 3
 C - constant in light scattering theory, Chapter 7
 C - $(n \times (n+1))$ coefficient matrix in control theory, Chapter 4
 CI - initiator concentration in initiator stream, mole/L stream
 CIC - initiator concentration in control initiator stream, mole/L stream

- C_M - ratio of rate constant for transfer to monomer over propagation rate constant, k_{fm}/k_p
- C_p - ratio of rate constant for transfer to polymer over propagation rate constant, k_{fp}/k_p
- C_S - emulsifier concentration in emulsifier-monomer-water-stream, mole/L stream, Chapter 4
- C_{SC} - emulsifier concentration in control emulsifier-water stream, mole/L stream, Chapter 4
- D - light scattering instrument coefficient
- D - $(n \times (n + \nu + \mu))$ coefficient matrix, Chapter 4
- $d(t, T)$ - diameter of a particle of class $n(t, T)dT$, dm
- d_m - density of monomer, gm/L
- d_N - number average particle diameter, dm
- d_p - polymer density, gm/L
- $D_p(t)$ - sum of particle diameters over all classes at time t , dm/L latex
- DP_{max} - maximum degree of polymerization
- d_s - surface average particle diameter, dm
- d_v - volume average particle diameter, dm
- D_w - diffusion coefficient of monomer in the water phase, dm^2/sec
- E - expectation operator
- F - $(r \times (n + \nu + \mu))$ coefficient matrix, Chapter 4
- $f(t)$ - particle nucleation rate, #/sec
- f_{eff} - initiation rate coefficient to denote fraction of initiator radicals which succeed in initiating a polymer chain
- $f_{GEN}(t, T)$ - generation rate of new particles of class $n(t, T)dT$ in a reactor due to inflow of particles at time T

- $f_{IN}(t,T)$ - generation rate of new particles of class $n(t,T)dT$ in a reactor due to inflow of particles at time T
- $f_{NUCL}(t,T)$ - equivalent to $f(t)$
- FE - fraction of emulsifier in gravimetric sample, Chapter 7
- FI - fraction of initiator in gravimetric sample
- FI - flow rate of initiator stream, mL/min, Chapter 4
- FIC - flow rate of control initiator stream, mL/min, Chapter 4
- FM - fraction of monomer in gravimetric sample, both as polymer and free monomer
- FMS - flow rate of monomer-soap-water stream, mL/min, Chapter 4
- FSC - flow rate of control emulsifier stream, mL/min, Chapter 4
- FSOL - fraction solids in gravimetric sample
- $g(T)$ - general function of T
- $g_{ij}()$ - general function in (i,j) position of A matrix
- $G_{\theta c}$ - light scattering instrument reading at angle θ and concentration c
- $h(x,t)$ - non-linear measurement matrix, Chapter 4
- I - identity matrix, Chapter 4,5
- $I(r,\theta)$ - intensity of scattered light at angle θ , distance r , Chapter 7
- I_i - intensity of incident light, Chapter 7
- $[I]_F$ - concentration of initiator in feed stream, mole/L stream
- $[I]_W$ - concentration of initiator in water phase, mole/L latex
- K - vector of parameters, Chapter 4
- K - ratio of rate constant for terminal double bond polymerization to propagation rate constant, k_p^*/k_p
- K - light scattering constant

- K_{K+1} - Kalman gain matrix
 k_{ab} - rate constant for radical capture by polymer particles, dm/sec
 k_d - rate constant for initiator decomposition, sec^{-1}
 $k_{de}(t,T)$ - rate constant for radical desorption from polymer particles of the class $n(t,T)dT$, L/mole-sec
 k_{fm} - rate constant for transfer to monomer, L/mole-sec
 k_{fp} - rate constant for transfer to polymer, L/mole-sec
 k_{ft} - rate constant for transfer to chain transfer agent, L/mole-sec
 k_h - rate constant for homogeneous nucleation, sec^{-1}
 k_m - rate constant for micellar nucleation, dm/sec
 k_p - propagation rate constant, L/mole-sec
 k_p^* - rate constant for terminal double bond polymerization, L/mole-sec
 k_{tw} - rate constant for radical termination in the water phase
 k_v - L latex/L aqueous phase
 L - Einstein diffusion length, dm
 L_k $rx(n+\mathcal{N}+\mu)$ linear feedback matrix
 m - partition coefficient of monomeric radicals between water and particle phase
 M - (mxn) linear measurement matrix
 M^* - $(mx(n+\mathcal{N}+\mu))$ augmented M matrix
 M_1 - submatrix of partitioned M matrix, Chapter 5
 $[M]_F$ - concentration of monomer in feed stream, mole/L
 $[M]_{MON}$ - concentration of free monomer, mole/L
 $[M]_p$ - concentration of monomer in the polymer phase

- $[M]_{TOT}$ - concentration of total monomer units existing in free monomer and as units in polymer chains
 $[M]_W$ - concentration of monomer in the water phase
 M_N - number average molecular weight
 M_W - weight average molecular weight
 $M_{W,MON}$ - molecular weight of the monomer
 n - number of states in control theory
 $n(t,T)$ - number of particles in class $n(t,T)dT$ at time t
 $n_{GEN}(t,T)$ - number of particles in class $n(t,T)dT$ due to nucleation
 $n_{IN}(t,T)$ - number of particles in class $n(t,T)dT$ present due to inflow
 N_A - Avagadro's number
 $N_p(t)$ - total number of particles at time t , #/L latex
 P - observability matrix, Chapter 5
 $P(t)$ - general macroproperty at time t
 $P(\theta)$ - particle scattering function
 $P_{GEN}(t,T)$ - property of a class of particles $n_{GEN}(t,T)dT$ due to nucleation
 $P_{IN}(t,T)$ - property of a class of particles $n_{IN}(t,T)dT$ due to inflow
 $P_{ik}(\cdot)$ - general function in (i,k) position of \mathcal{B} matrix
 $P_{k/k}$ - covariance matrix of the states (after measurements available)
 $P_{K+1/K}$ - covariance matrix of the state estimates
 $q(t,T)$ - average number of radicals per polymer particle of class $n(t,T)dT$
 Q - $(n \times n)$ penalty matrix on state deviations
 Q_1 - $(n + \nu + \mu) \times (n + \nu + \mu)$ augmented penalty matrix
 $Q_n(t,T)$ - total number of radicals in class $n(t,T)dT$

- Q_{rT} - sum of rth polymer moments over all classes
 r - number of control variables
 r_c - critical chain length for precipitation of polymer radicals
 r_{VP} - regression coefficient of V on P where V = variable = E or δ^1 and P = property = I or S concentration
 R - (rxr) penalty matrix on control deviations from setpoint
 R_p - total rate of polymerization, mole/sec-L latex
 $R_{P\text{POLY}}$ - rate of polymerization in polymer phase, mole/sec-L latex
 R_{PAQ} - rate of polymerization in aqueous phase, mole/sec-L latex
 R_V - (rxr) measurement covariance matrix
 R_W - (nxn) state covariance matrix
 $[R^\bullet]_W$ - concentration of radicals in the water phase in the reactor, #/L latex
 $[R^\bullet]_{W_F}$ - water phase radicals present in the feed stream, #/L stream
 $R_{\theta c}$ - excess Rayleigh ratio at angle θ , concentration c
 S - light scattering function
 $[S]_{CMC}$ - critical micelle concentration for the soap, mole/L water
 $[S]_F$ - soap concentration in the feed, mole/L stream
 $[S]_T$ - total soap concentration, free plus adsorbed plus micellar, mole/L latex
 S_K - $(n+2+\mu) \times (n+2+\mu)$ matrix in control theory
 S_p - surface area of the polymer particles stabilized by end groups, dm^2/L latex
 S_∞ - surface coverage per emulsifier molecule, dm^2
 t - time, sec

- t_f - micellar disappearance time, sec
 T - birth time (same as τ)
 T - period of one discrete time step, sec
 T - period of oscillation of density meter
 T_{IND} - induction time, sec
 $[Tr]$ - concentration of chain transfer agent, mole/L latex
 u_k - (nx1) vector of control actions at step k
 u_d - vector of desired control levels
 V - (rx(n+ τ + μ)) matrix in control theory
 $v(t,T)$ - volume of polymer in a particle of class $n(t,T)dT$, dm^3
 v_k - (nx1) vector of white noise measurement errors at time k
 $v_p(t,T)$ - volume of particle of class $n(t,T)dT$, dm^3
 $V_p(t)$ - total volume of polymer particles at time t, dm^3/L latex
 V_1, V_2 - $|P_{k+1/k}|^{1/2}$, $|P_{k/k}|^{1/2}$ respectively
 V_1, V_2 - $|P_{k+1/k}|^{1/2}PSD$, $|P_{k/k}|^{1/2}PSD$ respectively
 w_k - (nx1) vector of white noise errors in state at time k
 w_k - (n+ τ + μ)x1 augmented state noise vector
 x - conversion
 x_c - critical conversion
 x_d - vector of desired states in control theory
 x_k - (nx1) vector of states in control/estimation theory at time k
 \dot{x}_k - (nx1) vector of state derivatives of time k
 x_{MWD} - vector of molecular weight states

- x_{PSD} - vector of particle size states
 $\hat{x}_{k/k}$ - vector of state estimates given a measurement at time k
 $\hat{x}_{k+1/k}$ - vector of forecast of state estimates one step ahead
 y_k - $(m \times 1)$ vector of measurements at time k
 $y_n(t, T)$ - number of polymer radicals in a class $n(t, T) dT$
 $Y_{OT}(t)$ - total number of polymer radicals, $\#/L$ latex
 $Y(t)$ - average number of polymer radicals per polymer particle at time t
 Z - vector of properties, Chapter 3
 Z $((n + \nu + \mu) \times 1)$ augmented state vector in control theory
 θ - light scattering angle
 θ - residence time, sec
 ρ - number of desired control levels
 ρ_A - radical capture rate
 ρ_x - density at conversion x , gm/mL
 $\rho(t)$ - radical generation rate, $\#/L$ latex-sec
 ρ_{des} - rate of radical desorption from polymer particles, $mole/L$ latex-sec
 ρ_i - rate of initiation, $mole/L$ latex-sec
 ρ_f - coalescence rate
 $\bar{\rho}^2$ - mean square radius of gyration of polymer
 ϵ - k_{ab}/k_m
 μ - k_{ho}/k_m
 μ - number of desired state levels, Chapter 4
 μ - volume growth rate of polymer particles, Chapter 2
 τ - birth time (same as T)

- ∇ - difference operator
- $\delta(t-T)$ - Kronecker delta function
- δ^l - D_w
- δ - lumped diffusion coefficient = $(1+D_w/mD_p)^{-1}$
- λ - constant in particle growth equations, vinyl acetate
- λ' - constant in styrene particle growth equations
- λ - wavelength of light in VACUO
- λ' - wavelength of light in medium
- $\xi(t)$ - time varying function in particle growth equations, vinyl acetate
- $\xi'(t)$ - $\xi(t)(1-\phi(t))$
- $\xi''(t)$ - time varying function in styrene particle growth equations
- $\eta(t)$ - function in particle size differential equations
- n - refractive index of solvent
- $d\eta/dc$ - specific refractive index increment
- n - number of desired state levels
- ϕ - monomer volume fraction in polymer phase
- ϕ_k - $(n \times n)$ state coefficient matrix at interval k
- ϕ^* - augmented $(n+n_\mu) \times (n+n_\mu)$ state coefficient matrix
- γ - surface tension, dyne/cm
- $(\mu L)^{-1}$ - light scattering instrument parameter
- Δ - $(n \times r)$ coefficient matrix for control variables
- Δ^* - $((n+n_\mu) \times r)$ augmented control coefficient matrix
- β - area growth rate based on volume growth rate μ

APPENDIX II

DETAILED SIMULATION RESULTS

Run No.	OPERATING CONDITIONS			RESULTS						
	[I] (mole/L. latex)	[S] (mole/L. latex)	Split	V_l (mL.)	x	D_p (A)	M_N ($\times 10^{-5}$)	M_w ($\times 10^{-6}$)	B_N	$N_p \times 10^{18}$
1	.100E-01	.100E-01	.600E+00	.750E+02	.613E+00	.613E+00	.522E+01	.285E+01	.846E+00	.766E-01
2	.100E-01	.100E-01	.400E+00	.750E+02	.616E+00	.164E+04	.506E+01	.244E+01	.757E+00	.467E-01
3	.100E-01	.100E-01	.200E+00	.750E+02	.666E+00	.979E+03	.577E+01	.576E+01	.120E+01	.174E+00
4	.750E-02	.100E-01	.200E+00	.750E+02	.628E+00	.995E+03	.555E+01	.431E+01	.104E+01	.168E+00
5	.750E-02	.100E-01	.400E+00	.750E+02	.581E+00	.151E+04	.500E+01	.228E+01	.711E+00	.588E-01
6	.750E-02	.100E-01	.600E+00	.750E+02	.577E+00	.128E+04	.514E+01	.256E+01	.784E+00	.929E-01
7	.500E-02	.100E-01	.600E+00	.750E+02	.530E+00	.115E+04	.501E+01	.217E+01	.700E+00	.127E+00
8	.500E-02	.100E-01	.400E+00	.750E+02	.530E+00	.135E+04	.490E+01	.198E+01	.643E+00	.804E-01
9	.500E-02	.100E-01	.200E+00	.750E+02	.571E+00	.103E+00	.625E+01	.271E+01	.838E+00	.155E+00
10	.500E-02	.750E-02	.200E+00	.750E+02	.524E+00	.144E+04	.604E+01	.219E+01	.707E+00	.576E-01
11	.500E-02	.750E-02	.400E+00	.750E+02	.492E+00	.168E+04	.482E+01	.182E+01	.590E+00	.405E-01
12	.500E-02	.750E-02	.600E+00	.750E+02	.495E+00	.141E+04	.491E+01	.197E+01	.639E+00	.649E-01
13	.750E-02	.750E-02	.600E+00	.750E+02	.543E+00	.157E+04	.505E+01	.226E+01	.722E+00	.483E-01
14	.750E-02	.750E-02	.400E+00	.750E+02	.543E+00	.187E+04	.493E+01	.204E+01	.660E+00	.302E-01
15	.750E-02	.750E-02	.200E+00	.750E+02	.584E+00	.139E+04	.532E+01	.292E+01	.879E+00	.626E-01
16	.100E-01	.750E-02	.200E+00	.750E+02	.624E+00	.137E+04	.553E+01	.395E+01	.102E+01	.646E-01
17	.100E-01	.750E-02	.400E+00	.750E+02	.579E+00	.201E+04	.500E+01	.265E+01	.709E+00	.524E-01
18	.100E-01	.750E-02	.600E+00	.750E+02	.575E+00	.172E+04	.514E+01	.254E+01	.781E+00	.377E-01
19	.100E-01	.500E-02	.600E+00	.750E+02	.519E+00	.244E+04	.498E+01	.209E+01	.679E+00	.129E-01
20	.100E-01	.500E-02	.400E+00	.750E+02	.518E+00	.286E+04	.488E+01	.193E+01	.628E+00	.824E-02
21	.100E-01	.500E-02	.200E+00	.750E+02	.562E+00	.233E+04	.516E+01	.246E+01	.783E+00	.133E-01
22	.750E-02	.500E-02	.200E+00	.750E+02	.511E+00	.237E+04	.497E+01	.205E+01	.671E+00	.128E-01
23	.750E-02	.500E-02	.400E+00	.750E+02	.484E+00	.263E+04	.478E+01	.178E+01	.579E+00	.105E-01
24	.750E-02	.500E-02	.600E+00	.750E+02	.485E+00	.224E+04	.488E+01	.191E+01	.622E+00	.160E-01
25	.500E-02	.500E-02	.600E+00	.750E+02	.438E+00	.202E+04	.474E+01	.167E+01	.540E+00	.212E-01
26	.500E-02	.500E-02	.400E+00	.750E+02	.434E+00	.238E+04	.466E+01	.158E+01	.505E+00	.135E-01
27	.500E-02	.500E-02	.200E+00	.750E+02	.450E+00	.248E+04	.472E+01	.165E+01	.536E+00	.155E-01
28	.750E-02	.100E-01	.200E+00	.150E+03	.659E+00	.908E+03	.593E+01	.791E+01	.131E+01	.203E+00
29	.750E-02	.100E-01	.400E+00	.150E+03	.614E+00	.155E+04	.512E+01	.248E+01	.776E+00	.505E-01
30	.750E-02	.100E-01	.600E+00	.150E+03	.590E+00	.184E+04	.481E+01	.186E+01	.610E+00	.344E-01
31	.100E-01	.100E-01	.600E+00	.150E+03	.527E+00	.202E+04	.485E+01	.276E+01	.196E+01	.264E-01
32	.100E-01	.100E-01	.400E+00	.150E+03	.599E+00	.149E+04	.531E+01	.304E+01	.912E+00	.563E-01
33	.500E-02	.100E-01	.600E+00	.150E+03	.581E+00	.168E+04	.475E+01	.171E+01	.562E+00	.439E-01
34	.500E-02	.100E-01	.400E+00	.150E+03	.554E+00	.160E+04	.487E+01	.188E+01	.626E+00	.477E-01
35	.500E-02	.100E-01	.200E+00	.150E+03	.606E+00	.930E+03	.561E+01	.422E+01	.106E+01	.193E+00
36	.500E-02	.750E-02	.200E+00	.150E+03	.559E+00	.132E+04	.537E+01	.313E+01	.898E+00	.683E-01
37	.500E-02	.750E-02	.400E+00	.150E+03	.506E+00	.221E+04	.470E+01	.163E+01	.530E+00	.183E-01
38	.500E-02	.750E-02	.600E+00	.150E+03	.490E+00	.208E+04	.468E+01	.161E+01	.523E+00	.222E-01
39	.750E-02	.750E-02	.600E+00	.150E+03	.547E+00	.230E+04	.477E+01	.175E+01	.567E+00	.172E-01
40	.750E-02	.750E-02	.400E+00	.150E+03	.567E+00	.215E+04	.493E+01	.199E+01	.659E+00	.192E-01
41	.750E-02	.750E-02	.200E+00	.150E+03	.618E+00	.127E+04	.568E+01	.472E+01	.111E+01	.754E-01
42	.100E-01	.750E-02	.200E+00	.150E+03	.656E+00	.124E+04	.591E+01	.799E+01	.129E+01	.802E-01
43	.100E-01	.750E-02	.400E+00	.150E+03	.615E+00	.206E+04	.512E+01	.255E+01	.779E+00	.219E-01
44	.100E-01	.750E-02	.600E+00	.150E+03	.580E+00	.257E+04	.480E+01	.184E+01	.602E+00	.123E-01
45	.750E-02	.500E-02	.200E+00	.150E+03	.545E+00	.223E+04	.528E+01	.274E+01	.844E+00	.146E-01
46	.750E-02	.500E-02	.400E+00	.150E+03	.490E+00	.373E+04	.464E+01	.155E+01	.500E+00	.885E-02
47	.750E-02	.500E-02	.600E+00	.150E+03	.486E+00	.323E+04	.468E+01	.161E+01	.520E+00	.611E-02
48	.100E-01	.500E-02	.600E+00	.150E+03	.525E+00	.347E+04	.474E+01	.171E+01	.558E+00	.505E-02
49	.100E-01	.500E-02	.400E+00	.150E+03	.540E+00	.353E+04	.482E+01	.180E+01	.598E+00	.452E-02
50	.100E-01	.500E-02	.200E+00	.150E+03	.586E+00	.218E+04	.550E+01	.363E+01	.987E+00	.154E-01
51	.500E-02	.500E-02	.600E+00	.150E+03	.427E+00	.298E+04	.456E+01	.145E+01	.457E+00	.731E-02
52	.500E-02	.500E-02	.400E+00	.150E+03	.437E+00	.354E+04	.450E+01	.139E+01	.427E+00	.463E-02
53	.500E-02	.500E-02	.200E+00	.150E+03	.488E+00	.221E+04	.501E+01	.209E+01	.687E+00	.148E-01
54	.100E-01	.100E-01	.600E+00	.225E+03	.658E+00	.191E+04	.498E+01	.215E+01	.717E+00	.287E-01
55	.100E-01	.100E-01	.400E+00	.225E+03	.688E+00	.138E+04	.558E+01	.404E+01	.108E+01	.652E-01
56	.750E-02	.100E-01	.600E+00	.225E+03	.608E+00	.205E+04	.481E+01	.189E+01	.610E+00	.239E-01
57	.500E-02	.100E-01	.600E+00	.225E+03	.544E+00	.212E+04	.461E+01	.153E+01	.493E+00	.225E-01
58	.500E-02	.100E-01	.400E+00	.225E+03	.585E+00	.148E+04	.507E+01	.222E+01	.738E+00	.555E-01
59	.500E-02	.750E-02	.200E+00	.225E+03	.581E+00	.124E+04	.562E+01	.643E+01	.107E+01	.779E-01
60	.500E-02	.750E-02	.400E+00	.225E+03	.538E+00	.210E+04	.488E+01	.190E+01	.626E+00	.207E-01
61	.500E-02	.750E-02	.600E+00	.225E+03	.480E+00	.290E+04	.453E+01	.142E+01	.444E+01	.817E-02
62	.750E-02	.750E-02	.600E+00	.225E+03	.562E+00	.280E+04	.466E+01	.159E+01	.521E+00	.968E-02
63	.750E-02	.750E-02	.400E+00	.225E+03	.598E+00	.203E+04	.513E+01	.234E+01	.773E+00	.217E-01
64	.100E-01	.750E-02	.400E+00	.225E+03	.642E+00	.198E+04	.534E+01	.198E+01	.910E+00	.228E-01
65	.100E-01	.750E-02	.600E+00	.225E+03	.604E+00	.285E+04	.480E+01	.183E+01	.605E+00	.909E-02
66	.100E-01	.500E-02	.600E+00	.225E+03	.533E+00	.457E+04	.459E+01	.150E+01	.482E+00	.233E-02
67	.500E-01	.500E-02	.400E+00	.225E+03	.565E+00	.349E+04	.499E+01	.204E+01	.685E+00	.458E-02
68	.100E-01	.500E-02	.200E+00	.225E+03	.605E+00	.204E+04	.575E+01	.685E+01	.117E+01	.178E-01
69	.750E-02	.500E-02	.200E+00	.225E+03	.568E+00	.208E+04	.555E+01	.498E+01	.102E+01	.177E-01
70	.750E-02	.500E-02	.400E+00	.225E+03	.522E+00	.353E+04	.481E+01	.178E+01	.588E+00	.447E-02
71	.750E-02	.500E-02	.600E+00	.225E+03	.499E+00	.406E+04	.454E+01	.144E+01	.453E+00	.325E-02
72	.500E-02	.500E-02	.600E+00	.225E+03	.437E+00	.376E+04	.447E+01	.135E+01	.413E+00	.399E-02
73	.500E-02	.500E-02	.400E+00	.225E+03	.455E+00	.374E+04	.458E+01	.146E+01	.455E+00	.375E-02
74	.500E-02	.500E-02	.200E+00	.225E+03	.510E+00	.223E+04	.525E+01	.284E+01	.824E+00	.154E-01
75	.100E-01	.100E-01	.200E+00	.150E+03	.695E+00	.897E+03	.616E+01	.151E+01	.209E+00	.209E+00

APPENDIX III

DATA FOR VINYL ACETATE MODEL

USE: VA in H₂O, SLS, K₂S₂O₈

$$D_M = 930 \text{ gm/L}$$

$$D_p = 1150 \text{ gm/L}$$

$$D_p(t,t) = 50.E-09 \text{ DM} = 50 \text{ A}$$

$$k_{fm} = .716 \text{ L/mole-sec @ } 50^\circ\text{C}$$

$$k_p = 2924 \text{ L/mole-sec @ } 50^\circ\text{C}$$

$$L = 8.E-05 \text{ dm @ } 50^\circ\text{C}$$

$$m_0 = 27.1$$

$$S_a = 5.E-17 \text{ dm}^2/\text{molecule}$$

$$\delta = .5$$

$$x_c = .2$$

$$MW = 86$$

$$\mu = .55$$

$$fk_d = 5.046 \times 10^{-6} \text{ sec}^{-1}$$

$$S_{cmc} = 3.2E-03/1.4 \text{ mole/L latex}$$

$$k_p^* = 1700. - 169.59*x - 479.92*x^2 - 1014.3*x^3$$

$$k_t = 9.36E+07 [\exp(-.4407x + 6.753x^2 + .3495x^3)]$$

$$D_w = .77E-07$$

$$E = 24.4$$

$$C_m = 2.45E-04$$

$$*C_p = 50E-04$$

$$K = .5$$

*C_p reduced to prevent numerical runaway of M_w and B_N.

APPENDIX IV
DATA FOR STYRENE MODEL

Physical Data

MW_n = 104. Solubility: small

$\rho_{\text{mon}} = .9 @ 60^{\circ}\text{C}, \text{ gm./mL.}$

$\rho_{\text{poly}} = 1.04 @ 60^{\circ}\text{C}, \text{ gm./mL.}$

Polymerization Data

$k_p = 385 \text{ L/mole-sec. @ } 60^{\circ}\text{C}$
 $= 125 \text{ L/mole-sec. @ } 50^{\circ}\text{C}$

$x_c = .27$

$f_{kd} = 1.0 \times 10^{-6} @ 50^{\circ}\text{C (ammonium persulfate)sec}^{-1}$

$a_s = 61 \text{ \AA}^2/\text{molecule SLS}$